INTEGRATED APPROACH FOR PM CHARACTERIZATION: A COMPARATIVE ANALYSES BETWEEN ICP-MSMS AND PIXE, SOURCE LOCATION, SOURCE APPORTIONMENT AND PROBABILISTIC HEALTH RISK ASSESSMENT

Abdallah M. A. DAWOOD

Ph.D. THESIS

Department of Environmental Engineering

Supervisor: Assoc. Prof. Dr. Eftade E. GAGA

Anadolu University, Eskisehir

Graduate School of Sciences

June 2018

This thesis was supported by the Scientific Research Project, BAP (project no. 1306F272) of Anadolu University and TÜBİTAK (project no. 112Y305).

FINAL APPROVAL FOR THESIS

This thesis titled **Integrated Approach for PM Characterization: A Comparative Analyses between ICP-MSMS and PIXE, Source Location, Source Apportionment and Probabilistic Health Risk Assessment** has been prepared and submitted by **Abdallah M. A. Dawood** in partial fullfillment of the requirements in "Anadolu University Directive on Graduate Education and Examination" for the Degree of Doctor of Philosophy(PhD) in **Environmental Engineering Department** has been examined and approved on …../…../……..

Committee Members	**Title Name Surname**	**Signature**
Member (Supervisor)	: Assoc. Prof. Dr. Eftade E. Gaga	.....
Member	: Prof. Dr. Gülen GÜLLÜ	.....
Member	: Prof. Dr. Berrin BOZAN	.....
Member	: Prof. Dr. Tuncay DÖĞEROĞLU	.....
Member	: Prof. Dr. Duran KARAKAŞ	.....

Prof.Dr. Ersin YÜCEL

Director of Graduate School of Sciences

ABSTRACT

INTEGRATED APPROACH FOR PM CHARACTERIZATION: A COMPARATIVE ANALYSES BETWEEN ICP-MSMS AND PIXE, SOURCE LOCATION, SOURCE APPORTIONMENT AND PROBABILISTIC HEALTH RISK ASSESSMENT

Abdallah M. A. DAWOOD

Department of Environmental Engineering

Anadolu Universıty,

Graduate School of Sciences,

June 2018

Supervisor: Assoc. Prof. Dr. Eftade E. GAGA

Particle Induced X-ray Emission (PIXE) and Inductively Coupled Plasma Mass Spectrometer (ICP-MSMS) were used to characterize $PM_{2.5}$ and $PM_{2.5-10}$ from rural and urban backgrounds. This was followed by a site-specific comparative analysis between PIXE and ICP-MSMS based on their resolving potentials for PM metal constituents. Geoaccumulation index (Igeo) and positive matrix factorization (PMF) model were together used to apportion and profile PM metal sources measured by PIXE. HYSPLIT model, dust model, mineral dust tracers as well as satellite images were used as a combined methodology to locate the potential origin of PM sources intercepted at the receptor locations of this study. Finally, using Monte Carlo's probabilistic approach health risk assessment of exposure to fine PM ($PM_{2.5}$) was conducted.21 resolved elements including Na, Mg, Al, S, Ca, Ti, V, Cr, Mn, Fe, Ni, Cu, Zn, As, Se, Br, Rb, Sr, Zr, Mo and Pb by the two methods shows: Percent below detection limit (%BDL) for PIXE, varied between 0% (for Zn) and 83% (for Mo) with important markers such as Ca, S, K, Cl and Na being 4%, 8%, 11%, 12% and 21% respectively. For ICP-MS, %BDL varied between 0% (for Mg) and 98% (for Se) while important markers such as Na, Al, Ca, Cr, V and S were between 0% and 1% below detection. Both regression analysis and absolute relative difference showed a very good positive relationship between the two methods especially for crustal species. Back trajectories of the air masses traced pollutants intercepted at the receptors to countries including Bulgaria, Greece, Azerbaijan and Georgia. Daily exposure doses via ingestion was found to be the highest followed by inhalation and lastly dermal absorption. Ingestion contributed 85% of the dose in the adult age group and 94%, in the child age group. Estimated risk i.e. incremental lifetime cancer risk (ILCR) for all the metals were below the cancer threshold value of 10^{-6}. Based on sensitivity analysis, the least and highest impacting parameters on cancer risk in both children and adult age groups were averaging time (AT) and exposure duration (ED), respectively.

Keywords: Air Particulate Matter, Particle Induced X-ray Emission, Inductively Coupled Plasma Mass Spectrometer, Positive Matrix Factorization, Health Risk Assessment.

ÖZET

PM KARAKTERİZAYONU İÇİN ENTEGRE YAKLAŞIM: ICP-MSMS VE PIXE ARASINDAKİ KARŞILAŞTIRMALI ANALIZLER, KAYNAK YERİ, KAYNAK PAYLAŞIMI VE OLASILIKSAL SAĞLIK RİSKİ DEĞERLENDİRMESİ

Abdallah M. A. DAWOOD

Çevre Mühendisliği Bölümü

Anadolu Üniversitesi, Fen Bilimleri, Haziran 2018

Tez Danışmanı: Doç. Dr. Eftade E. GAGA

Parçacık Kaynaklı X-ışını Emisyonu (PIXE) ve İndüktif Olarak Birleştirilmiş Plazma Kütle Spektrometresi (ICP-MSMS), kırsal ve kentsel alanlardan $PM_{2.5}$ ve $PM_{2.5-10}$'u karakterize etmek için kullanılmıştır. Bunu, PIXE ve ICP-MSMS arasında PM metal bileşenleri için çözüm potansiyellerine dayalı olarak sahaya özgü karşılaştırmalı analizler izledi. Coğrafi birikim indeksi (Igeo) ve pozitif matriks faktorizasyon (PMF) modeli PIXE ile ölçülen PM metal kaynaklarının paylaştırılması ve profili için birlikte kullanılmıştır. HYSPLIT modeli, toz modeli, mineral toz izleyicileri ve uydu görüntüleri, bu çalışmanın alıcı yerlerinde yakalanan hava partiküllerinin potansiyel kaynaklarını / kaynağını bulmak için birleşik bir metodoloji olarak kullanılmıştır. Son olarak, Monte Carlo'nun olasılıksal yaklaşımını kullanarak, iyi PM'ye maruz kalmanın sağlık riski değerlendirmesi gerçekleştirilmiştir ($PM_{2.5}$). İki yöntemle Na, Mg, Al, S, Ca, Ti, V, Cr, Mn, Fe, Ni, Cu, Zn, As, Se, Br, Rb, Sr, Zr, Mo ve Pb içeren 21 çözülmüş eleman gösterilmektedir. : PIXE için algılama yüzdesinin (% BDL) altındaki yüzde,% 0 (Zn için) ve% 83 (Mo için) arasında, Ca, S, K, Cl ve Na gibi önemli işaretleyicilerle% 4,% 8,% 11 arasında değişmiştir. Sırasıyla, % 12 ve% 21. ICP-MS için, % BDL, % 0 (Mg için) ve% 98 (Se için) arasında değişirken Na, Al, Ca, Cr, V ve S gibi önemli belirteçler, saptamaların% 0 ila% 1'i arasındaydı. Hem regresyon analizi hem de mutlak bağıl fark, özellikle kabuklu türler için iki yöntem arasında çok iyi bir pozitif ilişki gösterdi. Hava kütlelerinin geri yörüngeleri, reseptörlere Bulgaristan, Yunanistan, Azerbaycan ve Gürcistan gibi ülkelere karışan kirleticiler izledi. Yeme içme yoluyla günlük maruziyet dozları en yüksek, en sonunda inhalasyon ve son olarak da dermal emilimdir. Yeme içme, erişkin yaş grubundaki dozun% 85'ine ve çocuk yaş grubunda% 94'üne katkıda bulunmuştur. Tahmini risk, yani tüm metaller için artan yaşam boyu kanser riski (ILCR), 10^{-6}'nın kanser eşik değerinin altındaydı. Duyarlılık analizine dayanarak, hem çocuklarda hem de yetişkin yaş gruplarında kanser riski üzerindeki en az ve en yüksek çarpma parametreleri sırasıyla ortalama (AT) ve maruz kalma süreleri (ED) idi.

Anahtar Kelimeler: Hava Partikül Maddesi, Parçacık Kaynaklı X-ışını Emisyonu, İndüktif Eşleşmiş Plazma Kütle Spektrometresi, Pozitif Matriks Faktorizasyonu, Sağlık Riski Değerlendirmesi.

ACKNOWLEDGMENT

I would like to express my sincere appreciation to my advisor Assoc. Prof. Dr. Eftade E. Gaga for her insightful guidance, unlimited patience and encouragement throughout the years. She is one of the finest professors; technically inclined with fore-sightedness. I am very glad to have worked with her and hope to apply all I have learned from her.

I am very grateful to the Turkish government for offering me full scholarship for this program. I owe Prof. Dr. Tuncay Dogeroglu a debt of gratitude for volunteering out of her busy schedules to be my supervisor for a period of one academic year when my actual supervisor went on a Scientific Visit to Canada. She was dedicative and instrumental in my BAP-sponsored trip to Florence, Italy to analyze my samples. To all members of my thesis committee, a very big thank you to you for your time and important critiques and inputs that has led to this success.

My profound gratitude also goes to the entire lecturers of my department for their thoughtfulness and motivation for me. Special emphasis on the Air Quality Research Group members –Dr. Hicran Altug, Dr. Ozlem Ozden Uzmez, Dr. Akif Ari, Mr. Emre Can, Pelin Ozturk-Ari and Gulzade Artun. It would not have been the same without them.

My appreciation also goes to the research unit, BAP, of Anadolu University for sponsoring my trip to Florence, Italy to analyze my samples at the INFN-LABEC laboratory. To this end my endless gratitude goes to all the research members of the INFN-LABEC laboratory, especially, Prof. Franco Lucarelli, Dr. Silvia Nava, Dr. Massimo Chiari and Dr. Giulia Carzolai.

The support, friendship and motivation of my friends and co-research fellows at Anadolu University and Ghana Atomic Energy Commission are greatly acknowledged; Masoud Derakhshandeh, Phanindra Prasad, Doreen Smith, Lilian Agyeman, Paul Essel, Emmanuel Atule Aberikae, Evans Ameho, Emmanuel Boafo and Maruf Abubakar.

I cannot thank my parents and siblings enough for their understanding and encouragement in diverse ways.

Finally, I would like to thank my wife, Rahmat and kids, Hikmah, Rayann and Hanan for their prayers, patience and support. For urging me on even though my absence in the house was a great worry to them.

And all praises belong to Allah, the Lord of Glory and Honor.

Abdallah M.A. DAWOOD

29/06/2018

STATEMENT OF COMPLIANCE WITH ETHICAL PRINCIPLES AND RULES

I hereby truthfully declare that this thesis is an original work prepared by me; that Ihave behaved in accordance with the scientific ethical principles and rules throughout the stages of preparation, data collection, analysis and presentation of my work; that I have cited the sources of all the data and information that could be obtained within the scope of this study, and included these sources in the references section; and that this study has been scanned for plagiarism with "scientific plagiarism detection program" used by Anadolu University, and that "it does not have any plagiarism" whatsoever. I also declare that, if a case contrary to my declaration is detected in my work at any time, I hereby express my consent to all the ethical and legal consequences that are involved.

Abdallah M. A. DAWOOD

To my entire family especially: Ramy, Hiki, Naa and Hanan.

TABLE OF CONTENT

LIST OF TABLES

LIST OF FIGURES

LIST OFABREVIATIONS AND ACRONYMS

AERONET	:	Aerosol Robotic Network
AOD	:	Aerosol Optical Depth
ARL	:	Air Resources Laboratory
BDL	:	Below Detection Limit
BSC	:	Barcelona Supercomputing Center
CCN	:	Cloud Condensation Nuclei
CMB	:	Chemical Mass Balance
CSF	:	Cancer Slope Factor
DL	:	Detection Limit
DREAM8b	:	Dust Regional Atmospheric Model
ED	:	Exposure Duration
EF	:	Enrichment Factor
EEA	:	European Environment Agency
EMEP	:	European Monitoring and Evaluation Programme
EPA	:	Environmental Protection Agency
HYSPLIT	:	Hybrid Single Particle Lagrangian Integrated Trajectory
ICP-MS	:	Inductively Coupled Plasma – Mass Spectrometer
ICP-OES	:	Inductively Coupled Plasma - Optical Emission Spectrometry
Igeo	:	Geoaccumulation Index
IARC	:	International Agency for Research on Cancer
IN	:	Ice Nuclei
INFN	:	National Institute of Nuclear Physics
IPCC	:	Intergovernmental Panel on Climate Change
CPF	:	Conditional Probability Function
LOD	:	Limit of Detection

LOQ	:	Limit of Quantification
MDL	:	Method Detection Limit
MDM	:	Minimum Detection Mass
NCEP	:	National Centers for Environmental Prediction
NMMB	:	Non-hydrostatic Multiscale Model
NRT	:	Near Real Time
PCA	:	Principal Component Analysis
PIXE	:	Particle-Induced X-Ray Emission
PM	:	Particulate Matter
PMF	:	Positive Matrix Factorization
READY	:	Real-time Environmental Applications and Display sYstem
SFU	:	Stacked Filter Unit
SRM	:	Standard Reference Material
XRF	:	X-ray Fluorescence
TÜBİTAK	:	The Scientific and Technological Research Council of Turkey
WHO	:	World Health Organization

1. INTRODUCTION

1.1. Study Background

Interactions of particulate matter (PM) with atmospheric radiation have impacted strongly on the global climate dynamics which has triggered a new challenge in atmospheric science (Adams, Seinfeld, and Koch 1999; Ban-Weiss and Collins 2014). Dynamic equilibrium that exist between the solid, liquid and gas phases of the atmosphere; the inter-relationship between aerosol-liquid and gas phases and their transformation make atmospheric aerosols a complex air pollution phenomenon (Haywood 2003; Pöschl, 2005) and therefore a holistic approach should be adopted for PM characterization.

Emission and formation of air particulate matter in the atmosphere has caught global attention now than ever before. This is obviously due to its increasing impact on climate and health consequences. Aerosol studies conducted across the globe have implicated air particulate matter and its metal constituents as being deleterious to human health and the environment at large. They do not only reduce visibility and contribute to climate change (Peng et al., 2017) but also are carcinogenic (IARC, 2016). Epidemiological studies have reported a link between exposure to air particulates and decreased lung function, aggravation of respiratory illnesses and increased hospitalization admissions for the elderly (Di Ciaula 2012; Francine Laden et al. 2000; Manousakas, Eleftheriadis, and Papaefthymiou 2013). It is reported in a recent study that pollution-triggered diseases are responsible for an estimated 9 million premature deaths in 2015 alone(International Energy Agency 2016) and that 7 million premature deaths annually linked to air pollution (Organization, 2014). Such unpalatable truths make research in air pollution a worthwhile consideration. There is therefore the need for continuous research to inform policy and strategy aimed at controlling, mitigating/remediating air pollution in general and toxic PM metal constituents.

A key and essential factor required for policies aimed at mitigating and controlling particulate air pollutants and their attending health and climatic hazards is to identify the location/origin of the source regions of their chemical constituents, to unravelthe physicochemical nature of the aerosols and the likely atmospheric interactions,

transformation and fate of their metal constituents. Previous studies (Dall'Osto et al., 2013) have indicated the effects of source regions on the chemical make-up of PM.

Since air masses pick up pollutants on their transport path to a receptor location, back trajectory information can be related to observed concentrations of air particulate species.Trajectory analysis is an application for determining the origin of air masses and to establish source-receptor relationships (Fleming, Monks, and Manning, 2012).The technique is frequently used to point out the direction and sources of air pollution at a receptor site (San José et al., 2005; Y. Q. Wang, Zhang, and Draxler, 2009). Furthermore, the chemical constituents of atmospheric aerosols acts as a signature of the sources of direct particle emissions into the atmosphere as well as that of the conversion of gaseous molecules into particulate-phase species (J. H. Seinfeld, 2014).

Meteorological parameters are important factors that strongly affect the formation and composition of atmospheric aerosols.A study report had indicated that $PM_{2.5}$ inEurope appears to be more sensitive to temperature changes compared to other meteorological and gaseous parameters in all seasons (Megaritis et al., 2014). Several studies including (See, Balasubramanian, and Wang, 2006), have widely reported about seasonal variation of $PM_{2.5}$ mass and its chemical composition in the Asian region. Variations in emission strength, transport pathways and local meteorological conditions are reported to cause episodes in trace element dataset (Koçak, Kubilay, and Mihalopoulos 2004; Koçak, Mihalopoulos, and Kubilay, 2007). The impact of local meteorology on PM metals concentrations have therefore been investigated in this study.

To protect people from the harmful effects of toxic substances in the atmosphere, several criteria have been established based on guides and standards to determine air quality. The International Agency for Research on Cancer (IARC), has classified PM as a major component of air pollution and carcinogenic to humans (Group1), based on sufficient evidence that exposure is associated with an increased risk of lung cancer (IARC 2016; IARC Working Group on the Evaluation of Carcinogenic Risks to Humans 2012). This study therefore delves into the realm of health risk assessment using a probabilistic approach of the Crystal Ball model which in turn is based on the robust Monte Carlo simulation model.

PIXE being a quantitative technique, allows for obtaining further proof of Saharan origin by observing the inter-elemental ratios whose values are different for the desert on one hand and local dust on the other hand (Nava et al.,2010); this is obviously due to its excellent exploits for Saharan (Al, Ca, Ti, Fe, Sr and, in particular, Si) aerosols. Elemental ratios that show the most significant differences between Saharan and non-Saharan days are those involving Fe or Ca (Traversi et al. 2014).

Iron and Ca enrichment of local dust with respect to the Saharan dust has been reported in other studies including Nava et al; 2012, (Giuntini, Massi, and Calusi, 2007; Massi et al., 2002). In this regard, dust intrusion to the study area, general trend of dust flow and mineral dust episodes have also been studied using dust model together with a near real time (NRT) base station's observations and dust-to-non-dust day ratios of dust tracers.

1.1.1. Aim and objectives of study

Atmosperic PM samples collected within the sampling program of two projects ((BAP (1306F272) and TÜBİTAK (112Y305) projects)) were first analyzed by Inductively Coupled Plasma Mass Spectrometer (ICP-MSMS) and later on by Particle Induced X-ray Emission (PIXE). By this approach the two methods were evaluated and subjected to a site-specific comparative analysis. Geoaccumulation index (Igeo) and PMF model were together used to apportion the PM sources based on the PIXE measurementand subsequently HYSPLIT model, dust model, mineral dust tracers and satellite images of these models were used as a combined methodology to identify the potential location/origin of the PM sources intercepted at the receptor locations of this study. Finally, using Monte Carlo's probabilistic approach, health risk assessment of daily exposure and cancer risk due to trace metals of PM were determined. Details of samples analyzed by PIXE is given in sections 3.2 and 3.5.1.

Specific objectives include:

i. To determine the trace metal constituents of PM and their concentrations, from the two study backgrounds by PIXE.

ii. To compare PIXE and ICP-MSMS based on their resolving potentials for the identified PM metals.

iii. To resolve PM sources and their contributions to measured concentrations using Geoaccumulation index and Positive Matrix Factorization model.

iv. To determine the potential source locations/origin of PM species.

v. To determine the impact of Saharan dust intrusion on the region of receptor location.

vi. To perform health risk assessment and sensitivity test using probabilistic approach of the Monte Carlo model.

2. LITERATURE REVIEW

2.1. PM in the Atmosphere – Origin and Size Distribution

Particulate matter (PM) originates from the condensation of gases and by the action of the wind on the Earth's surface. PM can also be emitted or formed when emissions of nitrogen oxides (NOx), sulfur oxides (SOx), ammonia (NH_4), organic compounds and other gases react in the atmosphere (EPA 2006; World Health Organization (WHO) 2000). Regulation and control mechanism of PM is based on the particle size(J. Y. Kim and Sansalone, 2008) and therefore size distribution is fundamental to any facet of PM analysis. For these reasons the examination of heavy and trace metals concentration size distribution is a useful approach for the characterization and apportionment of the sources of urban air particulate matter (Kemp 2002; Vallius et al., 2003).

Particulate air pollution is a mixture of solid, liquid or solid and liquid particles suspended in the air (Dockery et al. 1993; F Laden et al., 2000; Francine Laden et al., 2000). These suspended particles vary in size, composition and origin. Whereas fine aerosols originate almost exclusively from condensation of precursor gases such as Sulfuric acid (H_2SO_4), coarse aerosols originate from the mechanical action of the wind on the Earth's surface emitting sea salt, soil dust, and vegetation debris into the atmosphere (Jacob and Winner, 2009; J H Seinfeld and Pandis, 1998; John H Seinfeld and Pandis, 2006). It is thus, convenient to classify air particulates based on their aerodynamic properties (WHO, 2003; World Health Organization, 2006), which is the most important factor that govern their transport and removal from the atmosphere (Lippmann and Schlesinger 2000; Quincey and Butterfield 2009); their deposition within the respiratory system (Radojević and Harrison, 1992) and association with the chemical composition as well as sources of the particles.

It is also documented that mass and composition of airborne particulate matter tend to divide them into fine and coarse particulates in which the coarse particles are defined as being larger than 2.5 μm but less than 10 μm in aerodynamic diameter;usually containing earth crust materials and fugitive dust from roads and industries (Dockery et al., 1993; World Health Organization (WHO) 2000). Fine particles by definition are smaller than 2.5 μm in aerodynamic diameter; formed mainly from gas-to-particle

conversion, combustion of fuel and recondensed organic and metal vapours; theyare also known to contains most of the acidity (hydrogen ion) and mutagenic activityof particulate matter, although in fog some coarse acid droplets are also present (Radojević and Harrison 1992). Airborne particles are either biological contaminants, particulate contaminants, gaseous contaminants, or dust (Wikipedia, Air Particulate; Accessed online, April 2016). Figure 2.1, shows the types and size distribution of atmospheric particulate matter, their sources and biological contaminants whilst in Figure 2.2, a schematic illustration of the size distribution of particulate matter in ambient air is given.

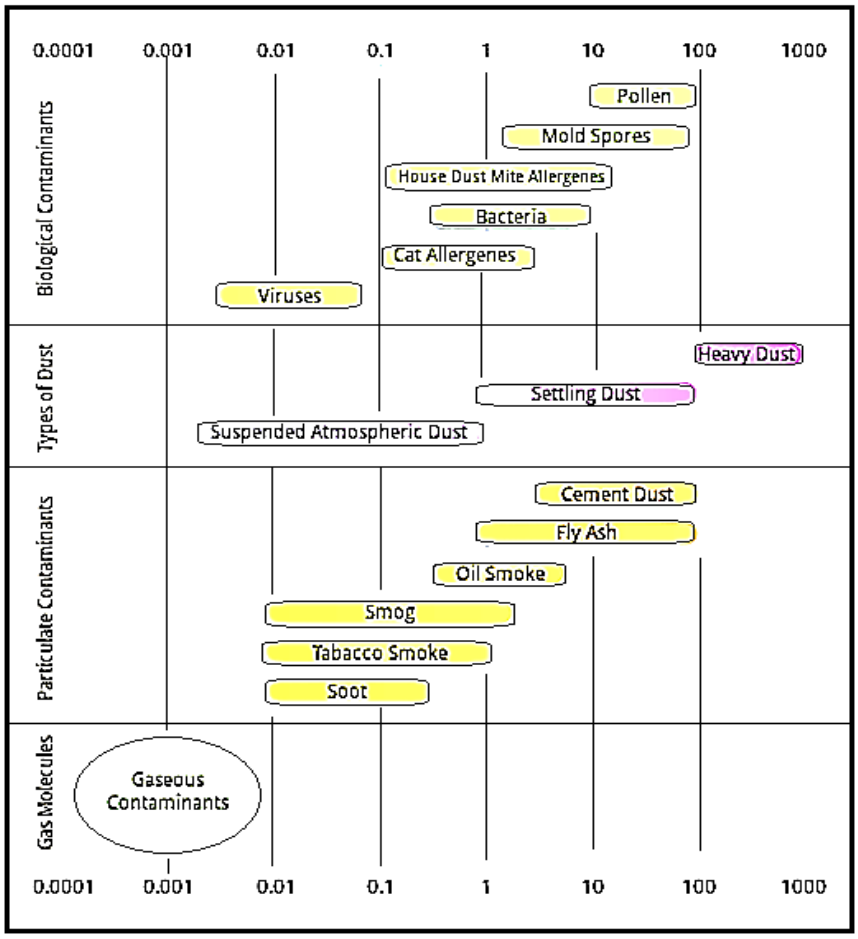

Figure 2.1. *Types and size distribution (in micrometres) of atmospheric particulate matter, their sources and biological contaminants. (http://www.balkanoglasi.com/Particulates)*

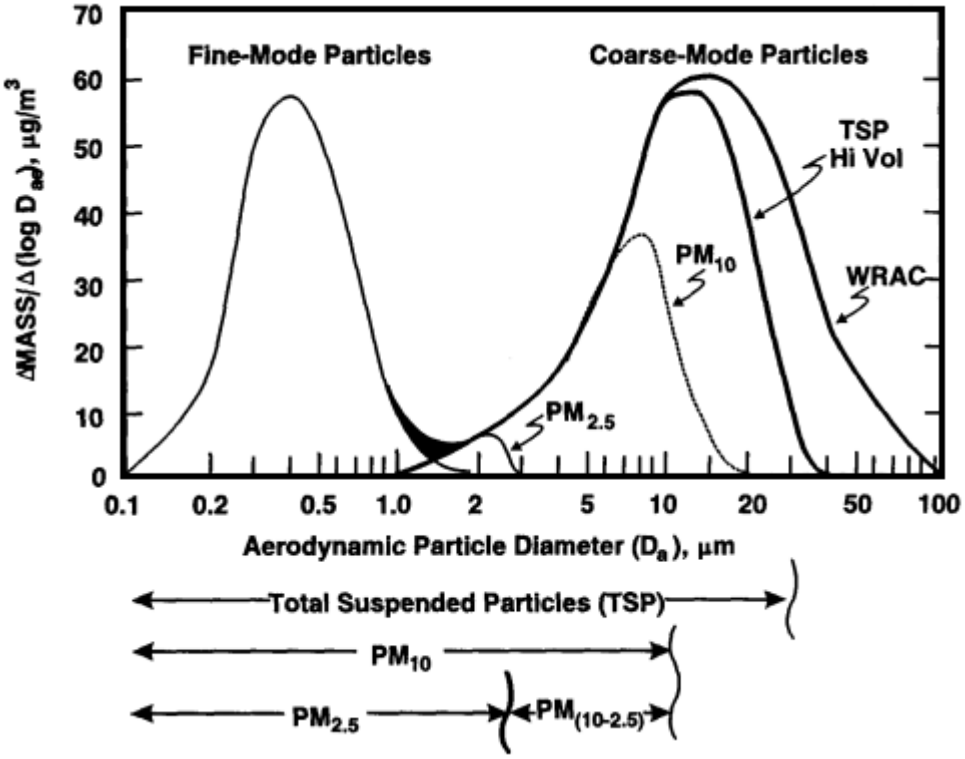

Figure 2.2. *Schematic illustration of the size distribution of particulate matter in ambient air (Wilson and Suh, 1997)*

In aerosol studies, PM fractions are usually in the fine, ultra-fine and coarse modes. Fine PMs are aerosols (PM < 2.5 μm) are produced mainly from combustion processes, forest fires and transformations of gaseous species (J. Y. Kim and Sansalone, 2008; Ohlström et al., 2000). They are produced by particles emitted directly into the atmosphere and from the chemical transformation of gaseous pollutants in the atmosphere. $PM_{2.5}$ usually have low levels of soil particle components with its main anthropogenic source being a product of the combustion of fossil fuels (Ohlström et al., 2000). Particles finer than 1 mm are difficult to generate mechanically because their large area-to-volume ratios make their surface tension per unit aerosol volume high. Atmospheric residence time of $PM_{2.5}$ has also been reported to be in the order of days (James Haywood and Boucher 2000) to weeks and has been shown to travel hundreds to thousands of kilometers thereby prolonging their exposure and increased health problems (Bell, Samet, and Dominici 2004; Engel-Cox et al., 2013). On the contrary, particles coarser than 10 mm are not easily lifted by the wind and therefore tend to have shorter atmospheric lifetimes because of their large sedimentation velocities (Jacob, 1999).

Mineral dust which arises from uplifting of soil particles by winds and suspension of them in the air is another natural source of aerosols. The Sahara-Sahel region of northern Africa and central Asia are the largest global mineral dust sources (Chin et al., 2007; Engelstaedter, Tegen, and Washington 2006; Rodríguez et al., 2011). Crustal species such as Fe, Ca, Si, Al and Ti are documented as being the major species of soil dust. Mineral dust contribution estimates are highly uncertain and ranges from 1000-3000 Tg per year to the global aerosol mass (Chin et al., 2007; Engelstaedter, Tegen, and Washington, 2006). H_2SO_4 is a key precursor gasproduced in the atmosphere by oxidation of SO_2 emitted from fossil fuel combustion, volcanoes, and other sources. Sulfate aerosol composition can be modified by condensation of other gases with low vapor pressure including NH_3, HNO_3, and organic compounds(Jacob, 1999). As can be seen in Figure 2.3, organic carbon mainly from condensation of large hydrocarbons of biogenic and anthropogenic origin represents a major fraction of the fine aerosol. Another important component of the fine aerosol is soot produced by condensation of gases during combustion. Soot as commonly defined includes both elemental carbon and black organic aggregates (Heintzenberg 1989; Jacob, 1999).

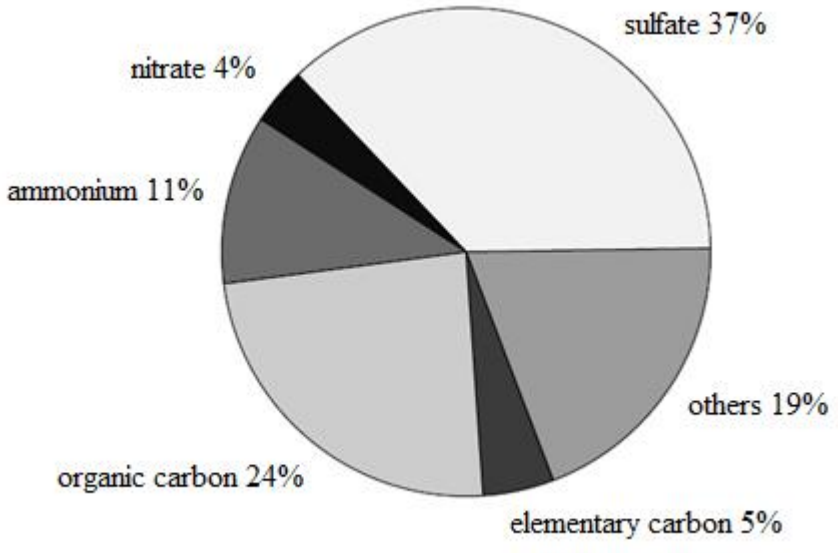

Figure 2.3. *Typical composition of fine continental aerosol*
(Heintzenberg, J., Tellus, 41B, 149-160, 1989)

2.2. Precursors of Particulate Matter

Sulfuric acid (H_2SO_4) is a key precursor gas produced in the atmosphere by oxidation of sulfur dioxide (SO_2) emitted from both natural and anthropogenic sources. Because of its low vapor pressure over H_2SO_4-H_2O solutions it condenses under all atmospheric conditions to form aqueous sulphate particles (Jacobson 2013; J H Seinfeld and Pandis 1998; John H Seinfeld and Pandis, 2006).

Nitrogen oxides, sulphur dioxide, ammonia and volatile organic compounds are all precursors of secondary aerosols; they are reflective and therefore they naturally scatter solar radiation back to space and thereby causing a negative (cooling) radiative forcing of climate (Adams, Seinfeld, and Koch, 1999; Department for Environment Food and Rural Affairs (DEFRA) 2010). They also influence the radiative properties of clouds and thus, their reduction in the atmosphere will likely cause an increases in temperatures; evidence that the cooling effects of sulphate aerosol may have partly masked the warming effects of greenhouse gaseshave been reported (Department for Environment Food and Rural Affairs (DEFRA) 2010).

Black carbon absorbs solar radiation and black carbon aerosols, or mixtures of aerosols containing a relatively large fraction of black carbon, exert a positive (warming) radiative forcing. Their effect is especially marked when the black carbon aerosol is located above reflective surfaces such as clouds or snow and ice(Department for Environment Food and Rural Affairs (DEFRA) 2010).

The most important gas phase reaction that leads to the oxidation of SO_2 is the reaction with $HO^{\cdot}$ radical (Calvert et al., 1978; Stockwell, 1994); all others including oxidation by O_3 is a very slow process but quite significant in water droplets. It is a known fact that the gas-phase oxidation for SO_2 is primarily through its reaction with the OH radical and therefore on sunny days when there is excess production of OH radicalan enhanced gas-phase oxidation of $SO_2$is produced(Liang and Jacobson, 1999; Srivastava, Jozewicz, and Singer, 2001).Similarly, the gas-phase oxidation of NO_X by OH is favored by high temperatures. However, oxidation of NO_X by OH about 10 times faster than that for SO_2, therefore on sunny days the gas-phase oxidation for NO_X is significantly higher than its SO_2 counterpart.

Ozone is a precursor for NO in the troposphere. Thus, the formation of NO_2 in the atmosphere can be influenced by O_3. Photochemical reactions occurring in the atmosphere also play a significant role in ozone formation and depletion; with maximum concentrations generally occurring downwind of the source areas of the precursor pollutants (Demirel et al., 2014; Lefohn et al., 1997). Ozone also makes a significant contribution to the radiative balance of the upper troposphere and lower stratosphere, such that changes in the distribution of ozone in these atmospheric regions will affect the radiative forcing of climate (Munro et al., 1998) and also serve as a source of the hydroxyl radical which controls the abundance and distribution of many atmospheric constituents, including greenhouse gases such as methane and hydro-chlorofluorocarbons.

Various natural and anthropogenic sources such as volcanic eruption, fossil fuel combustion, biomass burning, industrial processes and agricultural activities emit precursor gases into the atmosphere(Jacob, 1999); a major fraction of ambient PM arises from atmospheric gas-to-particle conversion such as in the formation of ozone and photochemical smog by the reaction between organic pollutants and nitrogen oxides shown in the following reaction, 1-6 (Jacob, 1999):

$$NO_2 + 2O_2 + hv \rightarrow NO_2 + O_3 \quad (1)$$

$$NO_2 + hv \rightarrow NO + O \quad (2)$$

$$O + O_2 + M \rightarrow O_3 + M \quad (3)$$

$$NO + HC + O_2 + hv \rightarrow NO_2 + O_3 \quad (4)$$

$$NO + VOC \rightarrow SMOG \quad (5)$$

$$2NO + O_2 + VOC \rightarrow RCHO + 2NO_2 + H_2O \quad (6)$$

M is an energetic unreactive species, RCHO, an organic product, HC, a hydrocarbon.

2.3. Trace Metals of Particulate Matter

Trace metals also known as trace elements are constituents of organic and inorganic species present in small but measurable amounts in nature. Common trace metals encountered in the atmosphere through soil, plant tissues, and water sediments include iron (Fe), magnesium (Mg), lithium (Li), zinc (Zn), copper (Cu), chromium (Cr), nickel (Ni), cobalt (Co), vanadium (V), arsenic (As), molybdenum (Mo), manganese Mn, selenium (Se) and Lead (Pb)(Nriagu 1979; Pacyna and Pacyna, 2001). Though they are needed by the human body, animals and plants for some specific functions, ingestion of, or exposure to excessive quantities can be harmful.

Air particulates and their trace metal constituents have been linked to both acute and chronic adverse health and deaths. Respiratory illnesses, lung cancer and cardio-pulmonary effects are among the major health problems associated with air pollution (Adamson, Prieditis, and Vincent, 1999; Prieditis and Adamson 2002; Aprajita Singh et al. 2015). Arsenic, Be, Cl, Cr, Cd, Co, Hg, Mn, Ni, Pb, Sb and Se have been defined as being carcinogenic or agents of carcinogen hazardous to humans (Hazardous Air Pollutants (HAPs) (Cogliano et al., 2010; Ward et al. 2010; Wogan et al., 2004); Scientists have therefore become increasingly interested in the fate of toxic or potential toxic trace elements from major anthropogenic sources like coal-fired power plants.

In the coal combustion process, there are three streams of general tendencies in the distribution of trace elements: Solid waste, fly ash and waste gas which are influenced by the properties of trace compounds and the efficiency of dust control systems (Chen et al., 2015). Other studies including (Mohr et al., 1996) reported that, among the trace elements that are emitted in power plants, the fly ash formed during coal combustion processes is characterized by Cr, Cu, Mn, Ni, Pb and Zn. Other earlier studies (Quiterio et al., 2004; Shah et al. 2006; Shah and Shaheen 2010; Watson 2002), have cited road dust, motor vehicles, coal and oil combustion and incineration as the major sources of inorganic trace metals and compounds in ambient air. Extractive metallurgy (metal smelting), exhaust and non-exhaust vehicular emissions are other anthropogenic sources of trace elements in the atmosphere. Lead for instance is associated with the use of leaded gasoline; Cu, Zn and Cd are traced to tyre abrasion, lubricants, industrial and incinerator emissions (Pöschl 2005; Signorell and Bertram, 2009; Thorpe and Harrison, 2008;

Wilcke et al., 2006). Ni and Cr are associated with road dust, corrosion of vehicular parts and chrome plating of motor vehicle parts (Al-Shayeb and Seaward 2001; Salim Akhter and Madany, 1993). Common PM metal constituents encountered in the atmosphere and their sources are given in Table 2.1.

Table 2.1. *Sources of major trace elements*

Source	Element
Soil	Al, Sc, Mn, Fe, Rare Earth Elements, Th, U
Sea Particles	Na, CI
Coal Burn	As, Se, Hg, Be, Co, Mo, Sb
Oil Burning	V, La, La/Sm
Refinery	Rare Earth Elements
Motor Vehicles	Br, Zn, Sb
Wood Burning	K
Insulator	Na, K, Cl, In, Hg
Chlorine Alkali Facilities	Cl, Hg
Aluminum Plant	Al, Mg
Urban Industrial Zone	V, Zn, As, Se, Br, Sb
Iron and Steel Facilities	Fe, Zn, Se, Mo, Sb
Zn, Cd, Pb Castings	In, Zn, Cd, Pb, Zn
Ni, Cu Castings	Ni, Cu, Hg, As, As/Se

Source: Gone, Olmez and Ames, 1999, page 136

Trace metals are proven to be useful tracers. As a result, they have become a target by the emission reduction policies and being used extensively to identify sources of emissions (Córdoba et al., 2012; Dall'Osto et al., 2013) making monitoring of elemental composition of PM a crucial part of air quality programs in many countries around the world.

2.4. Health and Environmental Effects of Particulate Matter

Airborne particulates and their trace metal constituents have been linked to both acute and chronic adverse health problems such as respiratory illnesses, lung cancer and cardio-pulmonary effects (Adamson, Prieditis, and Vincent ,1999; Prieditis and Adamson 2002; See, Balasubramanian, and Wang, 2006).Their contribution to climate change and

poor visibility are well documented in the literature (Haywood 2003; Ward et al. 2010; World Health Organization, 2006). Epidemiological studies have reported a positive relationship between exposure to air particulates and decreased lung function; aggravation of respiratory illnesses and increased hospitalization admissions for the elderly (Di Ciaula, 2012; Francine Laden et al., 2000; Manousakas, Eleftheriadis, and Papaefthymiou, 2013). In recent years, research in chemical compositions, source identification and environmental impacts of atmospheric aerosols have been conducted inseparably (Chio et al., 2014; See, Balasubramanian, and Wang, 2006). The epidemiologicalstudies of the human health outcomes have investigated, especially for cancer incidence among occupational and non-occupational populations. However, the issue of the adverse health effectscaused directly but not epidemiologically by atmospheric aerosols israrely addressed (See, Balasubramanian, and Wang, 2006).

A Chinese study reports a statistically and substantively significant adverse relationship between birth weight and maternal exposure to total suspended PM (X. Zhu et al. 2015). According to the study there is some evidence suggesting that both pre- and post-natal exposure to ambient PM affects birth-weight and mortality. In other studies infant mortality have been identified with excess exposure to PM (Lave and Seskin 1972; Lipfert, Zhang, and Wyzga 2000; Woodruff, Grillo, and Schoendorf, 1997; Woodruff, Parker, and Schoendorf, 2006). Woodruff et al., 1997 in particular links PM_{10} exposure to an increased incidence of sudden infant death syndrome whilst the finer particles originating from sulphates, nitrates and black smoke have been found to be associated with total mortality (See, Balasubramanian, and Wang, 2006), although the relationship may well not be causal.

New evidence on exposure-risk information and improved global exposure estimates (Brauer et al., 2012; Burnett et al., 2014) suggest higher exposure to ambient particulate matter (PM) than previously estimated. An important fraction of the exposure leading to those health impacts occurs in cities, due to the higher density of human activities and their emissions to the air.

Though regulated as un-speciated mass, atmospheric particulate matter (PM) exerts most effects on vegetation and ecosystems by virtue of the mass loading of its chemical constituents (Grantz, Garner, and Johnson, 2003); their deposition on vegetated

surfaces depends on the size distribution of the particles and, to a lesser extent, on the chemistry.

Lighter carbon-free particles reflect solar radiation, making the air and earth surface below them a bit cooler than they will otherwise be (Jim Haywood 2003; World Health Organization (WHO) 2000). On the contrary, particles containing substantial amounts of black carbon (e. g. soot), warm their surroundings by absorbing solar radiation before they reach the ground.

Ground level ozone is a secondary air pollutant formed by chemical reactions between oxides of nitrogen (NOx) and volatile organic compounds (VOC) in the presence of sunlight (Demirel et al. 2014; EPA, 2006). Emission sources of ozone and its precursors include industrial facilities, electric utilities, motor vehicle exhaust, gasoline vapors, and chemical solvents. Breathing ozone can trigger several health problems, particularly in children, the elderly, and people who have lung diseases. Ground level ozone can also have harmful effects on sensitive vegetation and ecosystems (Jacob and Winner, 2009; Francine Laden et al., 2000).

2.5. Removal of PM and its Precursors from the Atmosphere

Atmospheric deposition is a process that removes pollutants from the atmosphere and considered an important source of nutrients and contaminants for ecosystems. Trace elements especially toxic metals deposited on plants, in soil or water, can cause substantial damage to the environment and human health due to their transfer and accumulation in food chains (Pan and Wang, 2015).

The removal of pollutants from the atmosphere by wet deposition is often considered an important natural mediating factor in cleansing the atmosphere (Qu et al., 2012). In contrast to the episodic nature of wet deposition, however, dry deposition is a continuous and dependable process involved in atmospheric cleansing (Grantz, Garner, and Johnson, 2003). In regions with low precipitation, such as the Mediterranean climate area (Muezzinoglu and Cizmecioglu, 2006), dry deposition as a scavenging mechanism is more important than wet deposition on an annual basis.

While dry deposition is a continuous process for scavenging gaseous and suspended particulates, wet scavenging can only be attained in the presence of precipitation (Anderson and Downing 2006; Sehmel 1980; Zhang et al., 2001). Despite the dry process being slower than the wet deposition, the accumulated removal quantity of a pollutant could be more important in case of dry deposition. Both the dry and wet depositions depend on the properties of the gases or particles and removal processes are governed by several environmental factors including near-surface concentration, weather condition and precipitation (E. Kim, Kalman, and Larson 2000; S. A. Slinn and Slinn 1980; W. G. N. Slinn, 1982).

There have been only a few studies that have considered the dry deposition of coarse particles even though recent work has shown that coarse particles are responsible for the majority of the atmospheric dry deposition (Davidson et al. 1985; E. Kim, Kalman, and Larson 2000; Lestari, Oskouie, and Noll 2003; Lin, Noll, and Holsen, 1994).

Although natural deposition cleanses the atmosphere, the ultimate result is transfer of nutrients such as reactive nitrogen species and heavy metalcontaminants from air into water and soil (Andersen and Hovmand 1999; Larssen, Duan, and Mulder 2011). Therefore in the absence of simultaneous measurements of wet and dry deposition processes, their relative and combined contributions to the total deposition remain unclear; and debatable whether dry deposition is the major cleansing mechanism(Pan and Wang 2015).

Figure 2.4 illustrates the different processes involved in the production, growth, and eventual removal of atmospheric aerosol particles. Typically, the size range of gas molecules is in the order of 10^{-4}-10^{-3} mm and their clustering or nucleation often produces ultrafine aerosols in the size range of 10^{-3}-10^{-2} mm (Jacob, 1999).

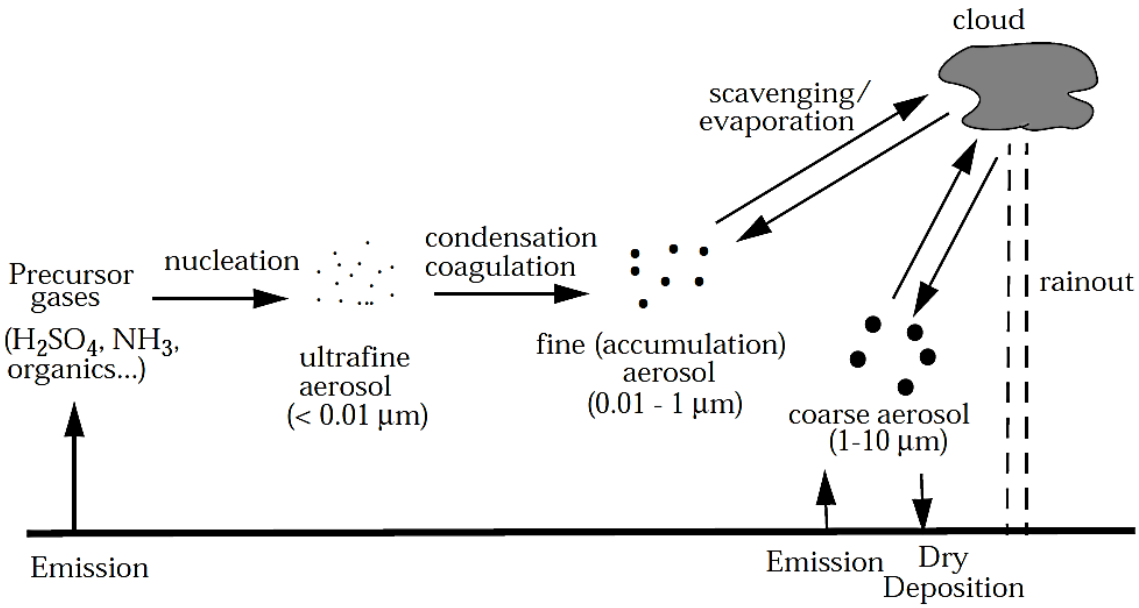

Figure 2.4. *Different processes involved in the production, growth, and eventual removal of atmospheric aerosol particles from the atmosphere (Jacob, 1999)*

Aerosol particles originating from condensation of gases accumulate in the size range 0.01-1 µm, often called the accumulation mode as opposed to the ultrafine or the coarse modes. These particles are too small to sediment at a significant rate, and are therefore removed from theatmosphere mainly by scavenging by cloud droplets and subsequent rainout or direct scavenging by raindrops (John H Seinfeld and Pandis, 2006).

In the context of dry deposition, there is not yet a reliable method to measure directly the dry deposition of the full size range of aerosol particles to a water surface (Arimoto et al., 2003). Therefore, dry deposition of aerosols is often estimated using the dry deposition velocity, v_d. For dry deposition, the flux is then given by Eq. 2.1:

$$F_d = v_d . C_a \tag{2.1}$$

Where F_d is the dry deposition flux (e.g., in $gm^{-2}s^{-1}$), v_d is the dry deposition velocity (e.g., in ms^{-1}), and $C_a$is the concentration of the substance on the aerosol particles in the atmosphere (e.g., in gm^{-3}). In this formulation v_d incorporates all the processes of dry

deposition, including diffusion, impaction, and gravitational settling of the particles to a water surface.

The removal of pollutants from the atmosphere by wet deposition is often considered an important natural mediating factor in cleansing the atmosphere (Qu et al., 2012). Long-term studies show that on average the wet deposition rates of many species are related to their concentrations in the atmospheric aerosol and to rainfall rates (Huang, Zhang, and Prospero 2009; Prospero and Arimoto, 2009). This relationship is expressed in terms of a dimensionless scavenging ratio, *S*expressed in Eq.2.2: it should be noted, however, that wet deposition rates depend on the vertical distribution of PM and the type of precipitation event (e.g., frontal, cumulus, and stratus). In practice, comprehensive, long-term, aerosol data are only available from surface sites; consequently, one must assume that over the longer term the PM concentrations in surface-level air are correlated with their vertical distributions. Therefore, *S* is appropriately calculated only when data have been obtained over periods of a year or more (Prospero and Arimoto, 2009).

$$S = C_p \, \rho C_a - 1 \tag{2.2}$$

Where C_p is the concentration of the substance in precipitation (g kg^{-1}), ρ the density of air (~1.2 kg m^{-3}), and C_a the aerosol concentration of the species of interest (g m^{-3}).

Gases and vapors in the atmosphere can be removed by dissolving into raindrops (Hemond and Fechner, 2015; Shukla et al., 2008). At equilibrium, the chemical concentration in the raindrops is given by Henry's law expressed in Eq 2.3:

$$C_{water} = \ C_{air}/H \tag{2.3}$$

Where C_{water} is the concentration of the chemical dissolved in the raindrops [M/L^3], C_{air} is the concentration of the chemical in the air [M/L^3], and H is the Henry's law constant (dimensionless). This expression, however, favors the wet deposition of more polar substances, which tend to have lower Henry's law constants because they partition more readily into water (Hemond and Fechner 2015).

Chemical equilibrium may generally be assumed if the rain forms in contact with the air (rainout) or travels through at least several tens of meters in contact with an air mass (washout). In the context of wet deposition, the ratio C_{water}/C_{air}, which is equal to the reciprocal of the dimensionless Henry's law constant, is sometimes called the *washout ratio*, W_r. For a given rainfall rate, expressed as depth of precipitation per time, the flux density of dissolved gas or vapor associated with the falling rain is given as Eq. 2.4, (Hemond and Fechner 2015).

$$J = C_{water}.I = C_{air}.1H.I = C_{air}.Wr.I \quad (2.4)$$

Where J is the flux density of dissolved gas or vapor [M/L^2T], I is the rainfall rate [L/T], and W_r is the washout ratio (dimensionless).

SO_2 emission is proportional to the Sulfur content of the fuel, although regarding coal a proportion, usually less than 10% is retained in the ash. Therefore, one of the simplest ways to reduce the amount of SO_2 released from the combustion process can be achieved by switching to a fuel that has lower Sulfur content (Department for Environment Food and Rural Affairs (DEFRA) 2010).

SO_2 emissions can significantly be reduced in 3 major processes: removal before, during and after combustion. Inorganic Sulfur in the form of pyrite (FeS_2) can be removed from coal relatively easily by simply washing the coal. This method can result in a reduction of 10 - 50% of total Sulfur content(Department for Environment Food and Rural Affairs (DEFRA) 2010). Removal during combustioncan be achieved through a process known as fluidized bed combustion (FBC). Emissions of SO_2 generated during the combustion of fossil fuels can be reduced by treating the flue gases before they are emitted into the atmosphere via the stack; this is termed flue gas desulfurization (FGD),(Air et al. 2012; Department for Environment Food and Rural Affairs (DEFRA) 2010).

2.6. Health Risk Assessment of PM Metals

Human health risk assessment is a widely used process of identifying and estimating the nature and probability of harmful health effects due to human exposure to pollutants and also forms the basis of decision making in health policies associated with environmental pollution (Qu et al., 2012). The most effective way to study the impacts of atmospheric air pollutant on human health is through a mechanistic modeling(Chio et al., 2014)because of its capability of resolvinguncertainties and limitations associated with deterministic statistical techniques.

Embedded in atmospheric PM are toxic metal species that can be injurious to human health; they are known to possess environmental and health risks effects (Cao et al., 2012). Chromium for example occurs usually in two oxidation states, Cr^{3+} and Cr^{6+}. Whilst Cr^{3+} is an essential nutrient for humans in amounts of 50-200 μg/day, a small concentration of Cr^{6+} is reported to be harmful to human (Duruibe, Ogwuegbu, and Egwurugwu, 2007). Exposure to the compoundsof both Cr^{3+} and Cr^{6+} cause allergic responses in sensitive individuals (Duruibe, Ogwuegbu, and Egwurugwu, 2007). Other effects include irritating respiratory effects, effects on stomach and blood, liver and kidney effects and increased risk of death from lung cancer (EU 2008; European Parliament and Council of the European Union, 2008). Also, Pb, Cd and Hg have no importance to biological, chemical and physiological needs of humans and therefore their accumulation in the human body can be injurious to the extent of causing kidney damage and also bone effects and fracture (Duruibe, Ogwuegbu, and Egwurugwu, 2007).

Hazard quotients (HQ) and hazard indexes (HI) formulated by the US Environmental Protection Agency (USEPA), are often used to characterize the non-cancer and cancer risks, respectively posed by pollutants (Granero and Domingo 2002). However, due to uncertainty inherently associated with risk assessment (J. Li et al., 2006; Nieto-Morote and Ruz-Vila, 2011), Monte Carlo simulation in human health risk assessment is therefore a preferred choice due to its capability of adequately quantifying uncertainty (J. Li et al., 2006).

Major pathways of toxic metals of air particulates into the human system as reported in the literature include: ingestion (through food and water), inhalation (through

the mouth and nose) and dermal absorption (adhesion to exposed skin)(EPA 2006; K. 2016; Widziewicz and Loska, 2016).

Carcinogenic risk is the probability of an individual developing any type of cancer from lifetime exposure to carcinogenic hazards. The acceptable risk for regulatory purposes is in the range $10^{-6} – 10^{-4}$ (EPA 2006; Ferreira-Baptista and De Miguel 2005; World Health Organization (WHO) 2000). Arsenic, Be, Cl, Cr, Cd, Co, Hg, Mn, Ni, Pb, Sb and Se have been defined as being carcinogenic or agents of carcinogen and/or hazardous to humans (IARC 2016; Manousakas, Eleftheriadis, and Papaefthymiou, 2013). Main Components of risk assessment are hazard identification, dose response assessment and exposure assessment. Hazard identification is referred to the potential harm caused by contaminant to the human and/or environmental health (IARC Working Group on the Evaluation of Carcinogenic Risks to Humans, 2012; Anita Singh et al., 2010). A dose-response relationship describes how the likelihood and severity of adverse health effects are related to the amount and condition of exposure to a receptor (EPA, 2006).

2.6.1. Uncertainty in risk assessment

Any event involving measurement is associated with some uncertainties, i.e. the possibility of loss; over or under-estimation of observations.The nature of uncertainties and the manner of dealing with them has been a topic of discussion by statisticians, engineers and other specialists for a long time (Paté-Cornell, 1996), Vrouwenvelder 2003, Faber, 2005). Typically, uncertainties are borne out of lack of measurement points, over-calibration, inaccurate expert judgment and subjective interpretation of available data or information (Dutta 2015; Dutta and Ali, 2012).

Uncertainties are generally categorized into two: aleatory and epistemic uncertainties (Dutta, 2015). Aleatory uncertainty often associated with ‘variability’ arises due to inherent variability, natural stochasticity, environmental or structural variation across space and time and variety of other sources of randomness (Dutta, 2015), it can be resolved by traditional probability theory. Epistemic uncertainty on the other hand arises due to lack of full knowledge about things. Sources of epistemic uncertainty include measurement uncertainty, small sample size, detection limits and data censoring,

ignorance about the details of the physical mechanisms and processes involved and other imperfection in scientific understanding (Dutta, 2015).

Efforts have been made by various researchers to deal with all forms of uncertainties in scientific research; (Arunraj, Mandal, and Maiti, 2013), proposed an integrated approach with fuzzy set theory and Monte Carlo simulation for uncertainty modeling in risk assessment; (Pastoor et al., 2014), studied roadmap for human health risk assessment in 21st century, (Dutta and Ali, 2012) discussed modeling uncertainty in risk assessment using Double Monte Carlo method, and proposed a hybrid method to deal with aleatory and epistemic uncertainty in risk assessment. Propagation of aleatory and epistemic uncertainties were studied by Pedroni et al and Flage et al. (Ferrario, Pedroni, and Zio, 2014; Flage et al., 2013; Pedroni et al., 2012), in which probabilistic and possibilistic treatment of epistemic uncertainties have been discussed.

Uncertainty surrounding health risk assessment using a probabilistic approach of the Crystal Ball model which in turn is based on the robust Monte Carlo model is gaining popularity in recent times (Coffee, 2005) and (Oracle, accessed online, April 2018: https://www.oracle.com/applications/crystalball/). Monte Carlo method involves many calculations of the intake rate rather than a single calculation; for each calculation, the input parameter values are randomly selected from the probability distribution function (PDF) for that variable.

An important advantage of Monte Carlo method in environmental risk assessment is that its outputs give more information than deterministic point estimates (Susan R. Poulter, 1998). The probability distributions created by Monte Carlo methods display the location of any risk estimate within the range of risk, making it possible to determine risk or exposure level at the 50th, 90th, 95th percentile or any other percentile level of risk (Susan R. Poulter, 1998). Monte Carlo technique considers the variability of the risk parameters under consideration in the risk assessment simulation and determination of effects.

2.7. Source Apportionment

In air quality studies, the fundamental problem is to resolve the identities and contributions of components in an unknown mixture (Viana et al., 2008). Receptor modeling measures atmospheric concentrations of chemically speciated particles to infer

the sources responsible for their emission or the pathways of formation of secondary particles(Wagstrom and Pandis, 2011). This process of resolving the identities and contributions of components in an unknown mixture is referred to as source apportionment. It involves identification of the various sources and determination of how much each contributes to a given pollutant material. Model tools such as chemical mass balance (CMB), (Begum, Biswas, and Hopke, 2007), Factor analysis (FA) (Knafl and Grey, 2007) and positive matrix factorization (PMF) (Paatero and Tapper, 1994) are commonly used to identify PM sources and quantify their contributions to atmospheric pollution in urban and industrial areas.

Enrichment factor (EF) is a double normalization procedure used for determining the presence as well as the amount of pollutant species relative to their parent/reference sources (Feng et al. 2011; Tessier, Campbell, and Bisson, 1979). It is often used as a preliminary source apportionment method for aerosol species in the atmosphere. Crustal and marine species are the most abundant species in the atmosphere and therefore widely used as reference sources in enrichment factor calculation (Reimann and De Caritat 2005). The calculated EF is known as crustal enrichment factor (EFc) if crust is used as the reference source and if marine source is used as the reference source, EF in this case is referred to as marine EF (EFm). Sodium for example is commonly used as reference element For EFm whilst for EFc, either of Al, Fe, Li, Sc, Zr, Mn or Ti which are enriched in crustal materials and do not have sources other than soil can be used as the reference element (Reimann and De Caritat, 2005).

Geoaccumulation index (Igeo) is a method like enrichment factor analysis used to preliminarily apportion components of soil origin or species associated with aerosols(Barbieri 2016; Peng et al. 2017; Tessier, Campbell, and Bisson, 1979). A positive Igeo value is an indication of significant anthropogenic contribution to the metal concentration while a negative value indicates a negligible or no contribution, Müller G., 1982; (Müller, 1985). Seven classes of Geoaccumulation Index as shown in Table 2.2 was defined by Müller G., 1982. In this classification, Igeo value ranged from class 0 (Igeo = 0; unpolluted) to Class 6 (Igeo $\geq$ 5; extremely polluted) with the highest class (Class 6) reflecting at least a 100-fold enrichment factor above background values. Although it is often difficult to obtain pre-industrial soil data, Geoaccumulation index (Igeo) relative to pre-industrial soil (‘background’) data from the same environment has

been used and recommended by researchers to evaluate pollution of metals in solid matrices (Rubio et al., 2000; Wei and Yang, 2010; Atiemo et al., 2012; Tang et al., 2015a).

Table 2.2. *Geoaccumulation index (Igeo) classification*

Class	Value	Soil dust quality
0	Igeo≤0	Uncontaminated
1	0< Igeo <1	Uncontaminated to moderately contaminated
2	1< Igeo <2	Moderately contaminated
3	2< Igeo <3	Moderately to heavily contaminated
4	3< Igeo <4	Heavily contaminated
5	4< Igeo <5	Heavily to extremely contaminated
6	Igeo≥5	Extremely contaminated

Source: Müller G., (1982)

Positive Matrix Factorization (PMF) is a receptor model developed by Paatero and Tapper (Paatero and Tapper, 1994) has become a major tool for development and review of air and water quality standards, exposure research and environmental forensics. PMF model is based on the idea that time dependency of a chemical species measured at a given receptor is the same for species from the same source. Therefore, species of similar variability are grouped together in a minimum number of factors (sources) that explain the variability of the data set. It is assumed that each factor is associated with a source or source type (Chueinta, Hopke, and Paatero, 2000).

2.7.1. Source location

Several studies including (Dall'Osto et al., 2013; Traversi et al., 2014) have reported the effects of source regions on the chemical make-up of PM. Reddington et al., 2011, stressed on the need to understand the relative contribution of primary and secondary particles in regional and global aerosol so that models can attribute aerosol radiative forcing to different sources.

Since air masses pick up pollutants on their transport path to a receptor location, back trajectory information can be related to observed concentrations of air particulate species (Fleming, Monks, and Manning, 2012). Back trajectory of air masses is frequently used to study the sources and paths traversed by airborne pollutants before reaching a receptor site. HYSPLIT – HYbrid Single-Particle Lagrangian Integrated Trajectory (Draxler and Hess, 1998) is the most commonly used model for studying air mass back trajectories as well as atmospheric transport and dispersion (Draxler and Hess, 1998; Fleming, Monks, and Manning, 2012). The application allows for determining the origin of air masses and establish relationship between sources and receptors. Trajectories reaching the receptor during whole measurement period are divided mainly into two groups, as "polluted" and "clean" trajectories. Polluted trajectories are those corresponding to high concentrations of the test species at the receptor while clean trajectories are the ones corresponding to low concentrations of the test species when they arrive at the receptor (San José et al., 2005).

2.7.2. Saharan dust intrusion and mineral dust episode

The Sahara and its margins are the largest and most continuous dust sources in the world. It is a major component of aerosols on the global scale and its intrusion and impact on both regional and global atmosphere is a well-documented phenomenon (Cuesta et al., 2010). The Saharan climate is modulated by the influence of the monsoon during summer and the westerly winds during the rest of the year (Cuesta et al., 2010). In July and August easterly winds, moist air masses and scarce rainfall are the prevailing weather conditions in the Saharan region.

Transport of dust from the Sahara to the Eastern Mediterranean is maximized in the months of April and May, (Alpert and Ziv, 1989). Rodriguez, studied on the impact of African dust in the Mediterranean region. They underscored that increasing PM_{10} values from north to south and from west to east across the basin almost corresponds to the PM_{10} African dust load patterns (Rodríguez et al., 2011).

Diffusion models and satellite observations are effective techniques for studying dust intrusion over an area. Several satellite and ground based observation analyses have led to identifying the base of the Ahaggar and Tibesti mountains and the Bodélé

Depression as the major sources in this area (Ginoux et al., 2001, 2012; Goudie and Middleton, 2001). They are however, not suitable for precise quantification analysis. Satellite observation for instance gives the contribution on the whole air column although advection of air masses from the Sahara does not necessarily imply high PM concentration at the ground level due to ability of dust confining in the high troposphere.

Most of the naturally emitted mineral dust released to the atmosphere is from arid or semi-arid areas and that major dust source areas relevant for the European Union (EU) are located along the west coast of North Africa(Léon and Legrand 2003; Prasad and Singh, 2007). It is reported (EEA Technical report, 2012) that dust intrusions moving from the African continent are derived from different sources and therefore contain different mixtures of mineral particulate matter.

Dust models mainly predict dust emission, transport within the atmosphere and deposition(Pérez et al., 2011). Dust forecast models such as the regional BSC-DREAM (San José et al., 2005), SKIRON (Kallos et al., 2006) and the global NAAPS model (Westphal et al., 2009) have focused on the accurate representation of the short-term variability of the dust to provide air quality/visibility forecasts up to 3 to 5 days.

It was suggested in recent studies that inclusion of mineral dust radiative effects can improve the radiative balance of short and medium-range forecast models and thus can increase the overall accuracy of the weather prediction itself (Perez et al., 2006b; Helmert et al., 2007). Global models have also assumed varying degrees of simplification in the dust emission schemes as a function of the availability and accuracy of the input data (e.g., Ginoux et al., 2001; Tegen et al., 2002; Zender et al., 2003a; Miller et al., 2006).

The NMMB/BSC Dust model is a new online multi-scale atmospheric dust model designed and developed at the Barcelona Supercomputing Center (BSC) in collaboration with NOAA/National Centers for Environmental Prediction (NCEP), NASA Goddard Institute for Space Studies and the International Research Institute for Climate and Society (IRI) (Pérez et al., 2011). The dust model is embedded into the Non-hydrostatic Multiscale Model NMMB developed at NCEP (Haustein et al. 2012; Pérez et al., 2011).

NMMB/BSC-Dust model has been evaluated at regional and global scales toprovide short to mediumrange weather and dust forecasts from regional to global scales and represents a first step towards the development of a unified chemical-weather model

(Haustein et al. 2012; Pérez et al., 2011). At the global scale, the model lies within the top range of AEROCOM dust models in terms of performance statistics for surface concentration, deposition and aerosol optical depth (AOD). At regional scale, the model reproduces significantly well the daily variability and seasonal spatial distribution of the dust optical depth over Northern Africa, Middle East and Europe.

Aerosol optical depth is the measure of aerosols distributed within a column of air from the Earth's surface to the top of the atmosphere (Eck et al. 1999; Holben et al., 1998). The measurement includes variables such as urban haze, smoke, particles, desert dust, sea salt etc. This parameter gives us an insight on the visual outlook of the atmosphere. For example, an optical depth of less than 0.1 is an indication of a crystal-clear sky with maximum visibility, whereas an optical depth value of 1 or greater indicates a very hazy conditions (NASA Earth Observation).

Transport of dust and its loading over an ‘area’ is reported comprehensively as being responsible for cooling in that ‘area” (Haywood 2003; Z. Li et al. 2017; C. Luo 2003; A. Zhu et al., 2007). Lau K.M. and Kim K.M., 2007, examined the possible relationships between Saharan dust and Atlantic sea surface temperature. Their results showed that the estimated anomalous cooling pattern of the Atlantic during June 2006 relative to June 2005 due to attenuation of surface solar radiation by Saharan dust remarkably resemble observations, accounting for approximately 30-40% of the observed change in sea surface temperature.

Mineral, dust tracers such as Al, Fe, Ca and Ti; air mass back trajectories and satellite aerosol images can together be used to investigate and identify Saharan/mineral dust episodes as well as the dust flow system (Barnaba and Gobbi, 2004, Borbely-Kiss et al., 2004, Papadimas et al., 2009, Rodriguez et al., 2001).

2.8. PM Characterization Methods

There are several analytical methods being used for the determination of chemical composition of particulate matter. Notable among them include Inductively Coupled Plasma Mass Spectrometry (ICPMS) (Tanimizu et al., 2013; H. Wang et al., 2017). Atomic Absorption Spectrometry (AAS) (Headridge, 1980; Dickson, 2012), Proton-

Induced X-Ray Emission Spectrometry (PIXE) (S. A. E. Johansson 1989; S. Johansson, Campbell, and Malmqvist 1997; Nejedlý et al. 1997); Artaxo et al., 1992; Smolik et al., 2003; Begum et al., 2005), Instrumental Neutron Activation Analyser (INAA) (IAEA, 2017; Werner et al., 1967) and X-Ray Fluorescence (XRF) (Onat et al., 2013).

In recent years, microwave digestion of aerosols followed by chemical analysis by ICP-MS has gained huge popularity for determining trace elements in aerosol samples(Pekney and Davidson, 2005; Sandroni et al., 2007). The method is reported to have high efficiency, sensitivity and low detection limit for aerosol measurement (Sandroni et al., 2007). By using the appropriate extraction conditions (extracting solution composition, pH, temperature, pressure, contact time) the metal fraction which is more ‘‘available” for the natural systems is obtained and in this way it is possible to evaluate better the impact of heavy metals on the environment and the human health (Traversi et al., 2014).

Elements including phosphorus (P), sulfur (S), silicon (Si), and chlorine (Cl) continue to be a great challenge to be analyzed by ICP-MS due to intense interferences from polyatomic ions based on carbon, nitrogen and oxygen, which are difficult to completely remove (Tanimizu et al., 2013); Agilent Application Note, 2012); at low concentrations Chlorine is difficult to analyze using ICP-MS because it is a common contaminant often present in reagents used in the laboratory environment. Also, the first ionization potential of Cl (12.967 eV) is higher than that of any other commonly measured element, making its sensitivity low and poorly ionized (Perkin Elmer, 2001; Pröfrock and Prange, 2012). Chloride has several serious interferences by ICP-MS making its determination difficult. The ^{35}Cl line is often interfered with by $^{16}O^{18}O^{1}H$ and $^{34}S^{1}H$; and the ^{37}Cl line is interfered with by $^{36}Ar^{1}H$, and $^{36}S^{1}H$. (Inorganic Ventures, 2017; Accessed online: April 2018).

PIXE is reported to have a high sensitivity for all the crustal elements including Si which is not easily detected by ICP (Traversi et al., 2014). Since PIXE is a quantitative technique, it enables determination of a further proof of the Saharan origin aerosols by observing the inter-elemental ratios, whose values are different for the desert and the local dust (Lucarelli et al., 2011; Nava et al., 2010). Suitability of PIXE for analyzing aerosol samples attributed to its ability to measure samples on filter surfaces without the need for

solubilization of the samples thereby shortening the analysis time and reducing sample contamination risk (Lucarelli et al., 2011).

Ion Beam Analysis (IBA) are a suite of analytical techniques that exploit the interactions of rapid (~MeV) charged particles with matter to determine the elemental composition and structure of the surface regions of solids from ~0 to 100 micrometers (Lucarelli et al., 2011; Traversi et al., 2014). PIXE is one of the most relevant IBA techniques due to its exploits for aerosol analysis and its non-destructive nature. It can detect all elements heavier than Na including important anthropogenic elements (S, V, Ni, Cu, Zn, As and Pb) and crustal elements (Al, Si, K, Ca, Ti, Mn and Fe), (D'Alessandro et al., 2003; Lucarelli et al. 2011; Traversi et al., 2014). Integration of particle induced x-ray emission (PIXE) and other complementary measuring techniques have been reported as useful approach for a complete aerosol analysis (Artaxo et al., 1999).

In charged particle induced X-ray emission studies, the characteristic X-rays are superimposed on a continuous background of electromagnetic radiation. This background is a significant source of uncertainty when charged particle induced X-ray emission is used for analytical purposes(Renan, 1980). Continuum background up to 6 keV can be observed in a typical PIXE spectra(Ishii et al., 2005). This background is the result of different processes that occur during the interaction between the projectile and the target. The contributions to the continuous background in this case are from bremsstrahlung that results from the deceleration process of the primary protons, and from bremsstrahlung emitted by electrons inside the specimen itself (Ishii et al., 2005; Murozono et al., 1999). Another contribution that can sometimes be seen in PIXE spectra at higher energies is from gamma rays emitted by nuclear reactions inside the specimen if it contains elements such as sodium or fluorine (Murozono et al. 1999; Renan, 1980).

Another uncertainty that may arise in PIXE analysis is the need to increase the energy of the proton beam to increase the X-ray emission cross section of mid to high energy atomic number elements on one hand and the need to decrease the energy in order to reduce the extent and intensity of the background due to secondary electron bremsstrahlung (D'Alessandro et al., 2003) and (M. Chiari et al., 2005). In atmospheric aerosol analysis, however, there is no need to increase the proton beam energy to increase the probed depth into the sample since they are thin targets (Massimo Chiari et al., 2015; Shao, Wang, and Nastasi, 2006).

3. MATERIALS AND METHODS

3.1. Study area

The study was conducted in Kütahya, a Province in the Aegean region of Western Turkey. The Province has a population of 571,554. Its topography is characterized not only with mountains and hills but also lowlands lying to the Northwest and Southeast. The 11.875 km^2 of the Province is composed of 57.5% mountains, 31.5% plateaus and 11% plains (Kütahya Valiligi, 2005); and has generally a Mediterranean climate (Akan, 1995).

Main pollution sources in the region are traffic, residential heating and industry (especially power plants and mining). Coal is the most commonly used fuel for residential heating and industrial activities due to its abundance as well as proximity of the lignite reserves around the region. The region is referred as a thermal power plant region due to the presence of three thermal power plants: Seyitömer Thermal Power Plant (600 MW), Tunçbilek Thermal Power Plant (365 MW) and Orhaneli Thermal Power Plant (210 MW), which are 20 km, 50 km and 105 km, respectively from the city center (Artun et al., 2016). Among these plants, Tunçbilek and Seyitömer power plants are located within the study area. Other potential industrial pollution sources located in the Province include a sugar factory, ceramic factory, food plants, transportation, boron mining and magnesite industries.

This study had two monitoring stations; a rural and urban stations as shown in in Figure 3.1. The selections of these sites were based on several factors including population, traffic and industrialization. The urban station which was close to the urban center of Kütahya is characterized by heavy vehicular activities (vehicular density of about 167.094 per day), several industrial operations and a population of 260,776 (Kütahya Valiligi, 2013). The rural station is located at proximity (1.5 km) to the Tunçbilek power plant. It has a lower traffic density and population of about 6000 (Kütahya Valiligi, 2013). There are three major highways in the city: Kütahya-Bilecik, Kütahya-Afyon, and Kütahya-Balıkesir. Kütahya-Bilecik highway has the most negative air pollution effect on the city (Tuna et al., 2015). The details of sampling site selection can be found elsewhere (Hacıoğlu et al. 2016).

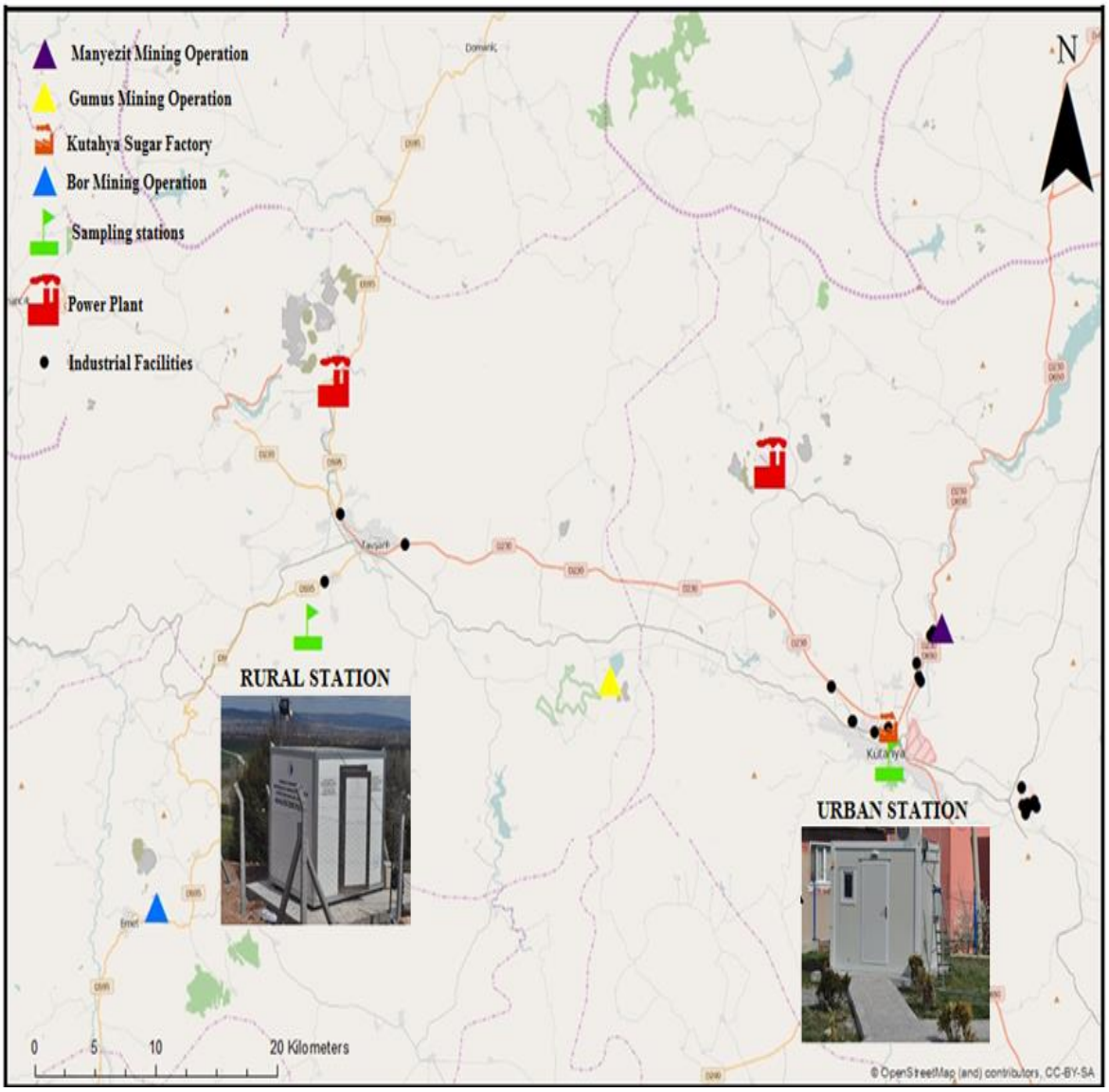

Figure 3.1. *Map of study area showing the two monitoring stations and major industrial facilities in the Province (Air Quality in Kutahya Project, 2014)*

3.1.1. Sampling

To be able to measure both inhalable and respirable fractions of particles in air; a pre-collector with a sampling filter is a basic required tool. The filter is used as a surface upon which the particles are collected for measurement. Two alternative size-selective criteria for atmospheric monitoring i.e. PM_{10} and $PM_{2.5}$were used in this study. PM_{10} is defined by ISO as particles which pass through a size-selective inlet with a 50% efficiency cut-off at 10 μm aerodynamic diameter and $PM_{2.5}$ as particles which pass through a size-selective inlet with a 50% efficiency cut-off at 2.5 μm aerodynamic diameter.

Different types of size-segregated, high and low volume PM samplers including Andersen, RespiCon, DustTrak, SidePak and Stacked-filter Unit are some commonly used samplers available on the market for air sampling.

PM sampling in this study was conducted between March 9, 2014 and April 10, 2015. During this period, 334 urban and 325 rural samples were collected by means of a stacked-filter unit (SFU) sampler on a 47mm nucleopore (polycarbonate) filter membrane. The SFU sampler (shown in Figure 3.2) consists of a pump, a two-stage filter, and a pre-impulse to remove particles larger than 10 microns as in the case of Hopke et al., 1997. It has a low volume air sampler and the air flow rate of 16.7 L/min. The choice of using SFU sampler was mainly because of its sequential size-segregation ability, collection efficiency and reproducibility particularly for nucleopore filters. The use of nucleopore filters as opposed to Teflon (CF_2) filters was to avoid gamma-ray emissions from the Fluorine in the teflon filters causing high resonance in $^{19}F(P, P' \gamma)^{19}F$ inelastic reaction producing 110 and 197 keV gamma-rays which in turn causes an increase in the continuous background of the PIXE spectra (Shao, Wang, and Nastasi, 2006).

The first filter holder of the cassette (holder facing the air intake) was loaded with the coarse filter whilst the second filter holder was loaded with the fine filter. Both the fineandcoarse filters had their shiny sides up (facing the air intake). The filter area for both fine and coarse filters exposed to the air flow during sampling was 12.88 cm^2. The sampler was installed at a height of 2 m above ground. When the air flow started, the fine particles

were collected on a filter of 0.4 μm pore size with diameter of 47 mm whereas the coarse were collected on 8 μm pore size filter with diameter of 47 mm.

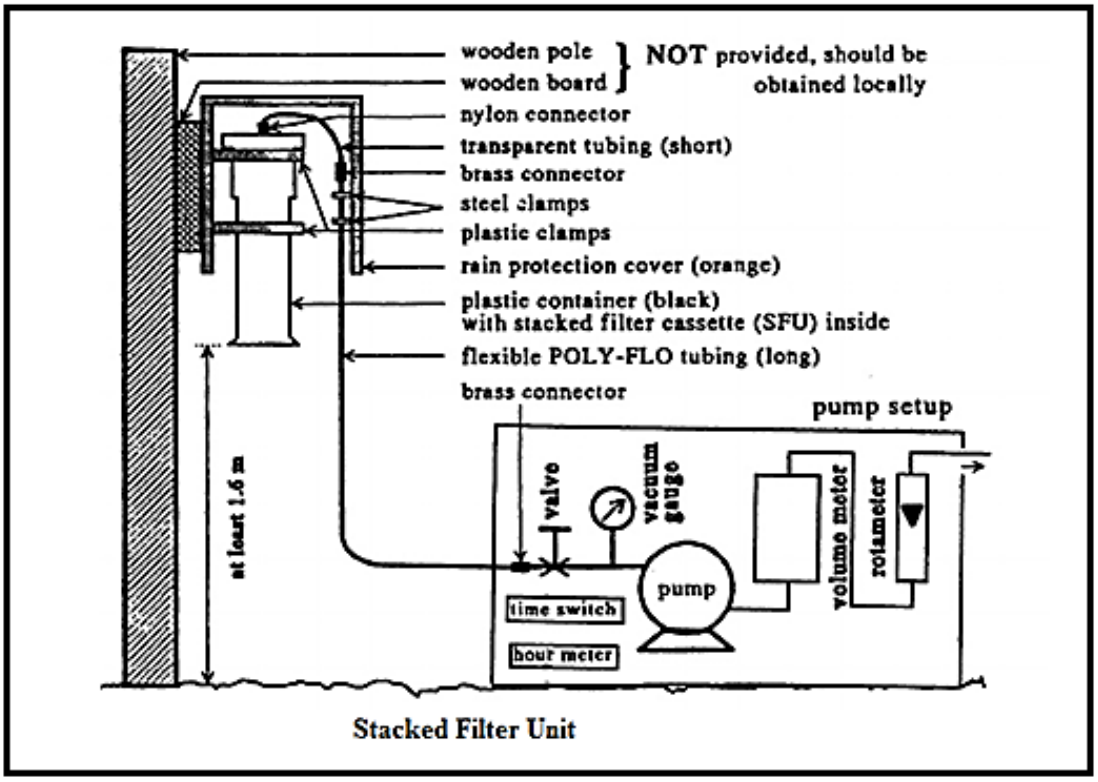

Figure 3.2. *Schematic diagram of the stacked-filter unit (SFU) sampler (Maenhaut et al., 1996)*

3.1.2. Analytical techniques (instrumentation)

PIXE analysis was performed using 3MeV protons (3MV Tandetron accelerator) at the LABEC laboratory; National Institute of Nuclear Physics (INFN), Florence, Italy. The set-up was an external ion beam, 30 – 80 nA. The beam scanned the streak in steps corresponding to 1 hr. of aerosol sampling and each spot irradiated for about 180 s. PIXE spectra were fitted using the GUPIX software and elemental concentrations obtained through a calibration curve from a set of thin standards of known areal density. The accuracy of hourly elemental concentrations was determined by the sum of independent uncertainties on:

standard samples thickness (5 %), aerosol deposition area (2 %), air flow (2 %) and X-rays counting statistics (2–20 %). Detection limits were about 10 ng/m^3 for low-Z elements and 1 ng/m^3 for medium to high Z elements. The use of silicon drift detector (SDD) as opposed to Si(Li) detector was to improve the minimum detection limits of the aerosol samples analysis. SDD has detector thickness one order of magnitude less (0.5 mm) compared to 3-5 mm for Si(Li). The use of SDD leads to a significant reduction in the gamma-ray Compton background without affecting the efficiency in the range of 10-20 keV (D'Alessandro et al. 2003; Schmidt and Wetzig 2013).

3.1.2.1. Operating principle of PIXE

PIXE is an X-ray spectrographic technique. The X-ray spectrum is initiated by energetic protons exciting the inner shell electrons in the target atoms (illustrated in Figure 3.3). The expulsion of these inner shell electrons results in the production of X-rays. The energies of the X-rays, which are emitted when the created vacancies are filled, have a unique characteristic of the elements from which they originate, and the number of X-rays emitted is proportional to the mass of that corresponding element in the sample being analyzed. The generation of X-rays in a sample is very strongly influenced by the bombarding proton.

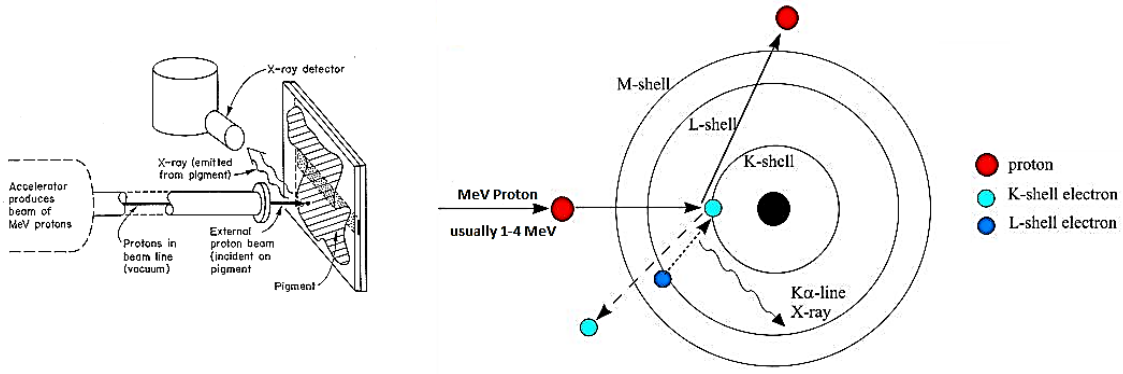

Figure 3.3. *Typical PIXE setup (right) and energetic proton interaction with target material (left)*

The probability of X-ray production depends upon both the total number of incident protons and the proton energy (measured in mega/million electron volts (MeV)). The total

number of incident protons can be expressed as proton current (measured in micro amps); the greater the proton current, the greater the probability for X-ray production (Giuntini, et al., 2007). As proton energy changes, so does the probability for X-ray production. For a quantitative analysis to be accomplished, both factors must accurately be known. The process is basically to assign observed X-ray peaks (energies) to appropriate elements (qualitative) and convert observed X-ray peaks (areas) into elemental concentrations (quantitative) based on the Eq. 3.1–3. The deposit area of the filter is very important; it is based upon which, the areal concentration/areal density (μg/cm^2), $\rho t_{Z,\,sample}$ of the elementin the sample is calculated as follows:

$$\rho t_{Z,sample} = \frac{\left(\frac{AX_Z}{Q}\right)_{sample} * \rho t_{Z,std}}{\left(\frac{AX_Z}{Q}\right)_{std}} \quad (3.1)$$

Where $\rho t_{Z,std,}$ is the areal concentration of the element Z in the standard in μg/cm^2, $(AX_Z/Q)_{sample}$ is the ratio of the net X-ray peak area for the element Z, corrected for the fraction of counts lost due to acquisition dead time and pile-up effects and $(AX_Z/Q)_{std}$,is the ratio of the net X-ray peak area for the element Z, also corrected for the fraction of counts lost due to dead time and pile-up to the total collected proton beam charge (Q) from the measurement on the standard.

The pileup correction (pu_{corr}) can be obtained by:

$$pu_{corr} = \frac{tot_b + pu_b}{tot_b} \quad (3.2)$$

Where tot_b and pu_b are the total dead time of big detector and pileup of big detector, respectively. The element concentration in μg/m^3 for instance can be obtained by multiplying the areal concentration (Eq. 3.3.1) by the surface area (cm^2) and divide by the sampling volume (m^3):

$$\rho t_Z = \frac{\rho t_{Z\,(\mu g/cm^2)} * S(cm^2)}{V(m^3)} \tag{3.3}$$

For homogeneous samples in air particulate analysis, measurement of any part of it gives directly the elemental areal density; in the case of inhomogeneous samples the beam is scanned over an area larger than the deposit area. The largest possible area is analyzed and averaged to obtain the possible sampling/collection inhomogeneities (Schmidt et al., 1995; Nastasi et al., 2014). This is achieved by using a collimated or focused beam and mechanically scanning the sample (S. Johansson, Campbell, and Malmqvist, 1997; Mkoma et al., 2009). Shown in Figure 3.4, is an illustration of a typical homogeneous and inhomogeneous filter samples. The total mass of the element is obtained by the product of the areal density (ρt) and the scanned/aerosol deposit area (A) in the case of inhomogeneous sample and for homogeneous sample the product of areal density and aerosol deposit area (S) as given in Eq. 3.4 and 3.5. Elemental concentration is finally determined by dividing the elemental mass (obtained in Eq. 3.4 and 3.5) by the sampled volume as given in Eq. 3.6.

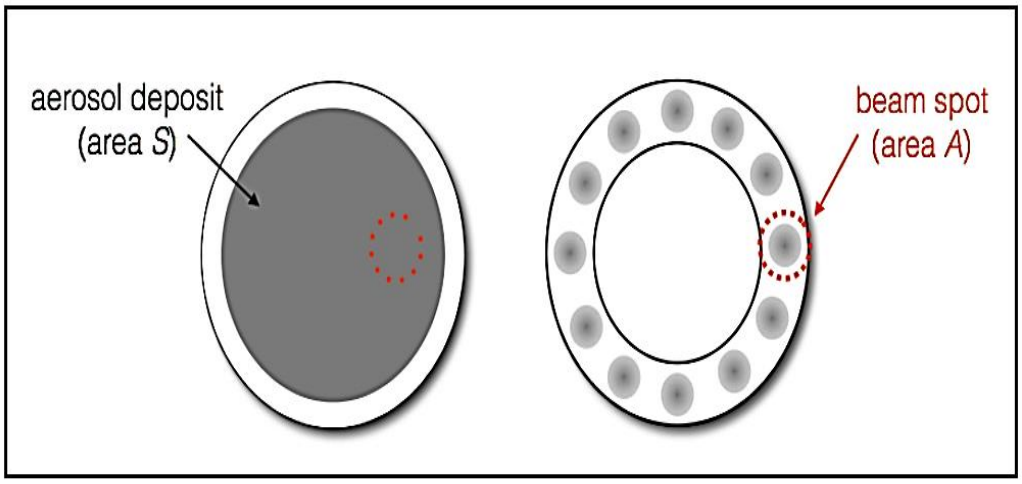

Figure 3.4. *Aerosol deposit area for homogeneous and inhomogeneous filter samples*

$$m_z = (\rho t)_z \, . A \tag{3.4}$$

$$m_z = (\rho t)_z \, . S \tag{3.5}$$

$$C = \frac{\rho t \left(\mu \frac{\mathrm{g}}{\mathrm{m}^3}\right) . S(cm^2)}{V(m^3)} \tag{3.6}$$

Where m_z, *A, S and V* are elemental mass, aerosol deposit area for homogeneous sample, beam spot area and sampled volume, respectively.

3.1.2.2. PIXE peak analysis

Analysis of the X-ray spectra from which the concentrations of the PM metal constituents were determined was done using the GUPIXWIN software. GUPIXWIN is a versatile software package for fitting PIXE spectra from thin, thick, intermediate and layered samples. It extracts peak intensities and converts these to concentrations via the H-value standardization method (Campbell et al., 2010; IAEA, 2003). The PIXE routine (GUPIX) consists of two separate sections, a data input section (PIX) coupled to a fitting section (PIXMFT). The fitting routine uses the method of non-linear least squares developed by Marquardt (Bevington 1969), followed by an iterated linear least squares procedure which allows the user to fit a PIXE spectrum of up to MXCH channels containing the x-ray peaks of a maximum of MXNEL elements (GUPIXWIN User Guide, V2.1, 2008). Many of the parameters defining vector lengths are contained in an inclusion file AP0PAR.INC. In addition to fitting for elements in a known matrix, it is possible to iterate a fitting of the major elements to provide the matrix composition in an unknown matrix; this can be done when one or more of the major elements are "invisible" (their x-rays are not in the fit region), or even for multi-layered targets whose layer thicknesses can also be iterated (Campbell et al., 2010).

3.1.3. Quality control-quality assurance

3.1.3.1. Quality control-quality assurance for PIXE

The X-ray spectrum was preliminarily calibrated in energy using the position of peaks from sample targets of known composition. For the low energy region of the X-ray spectrum, a 2-point calibration was accomplished from the measurement of a thin NaCl standard using the positions of the Na Kα peak at 1.04 keV and the Cl Kα peak at 2.62 keV. Alternatively, for the higher energy spectrum, a 3-point calibration was accomplished from the measurement of a thin CuSx standard using the positions of the Cu Lα peak at 0.93 keV, the S Kα peak at 2.31 keV and the Cu Kα peak at 8.04 keV. Analyzing the NIST SRM 2783 (Air Particulate on Filter Media) standard offered the possibility to choose among four relatively intense X-ray peaks, according to the specific range of detected energies: Si Kα peak at 1.74 keV, Fe Kα peak at 6.40 keV, Zn Kα at 8.63 keV or Pb Lα at 10.55 keV. MicroMatter standards were measured to obtain the sensitivity curve once per measurement run. Furthermore, the analysis of the NIST SRM 2783 was repeated each measurement day to control and to compensate possible systematic deviations of the experimental parameters (such as detector geometry, beam charge integration etc.).

Standards calibration was carried out under same conditions as samples so that each element has a spectrum in each position. A normalized linear combination of the two detector positions for the standards allows for extrapolation to any desired combination of irradiation times for unknown targets. The calibration is carried out by irradiating each standard with and without the filter in front of the detector for a preset charge collection. The standards are then fit into the gravimetric mass and the relative intensities for all of the X-ray lines are established and stored in a library. The certified elemental areal concentrations for the NIST SRM 2783 standard, together with the quoted uncertainties, are shown in Table 3.4.1. In Figure 3.4.1 is a typical PIXE spectra of NIST standard collected with 18 two-SDD device.

Table 3.1. *Certified elemental areal concentrations for the NIST SRM 2783 standard. For the elements marked with the asterisk (*) the concentrations are reference values only*

Element	Areal concentration (µg/cm2)	Uncertainty (µg/cm2)
Na	0.19	0.01
Mg	0.87	0.05
Al	2.33	0.05
Si (*)	5.9	0.2
S (*)	0.11	0.03
K	0.53	0.05
Ca	1.3	0.2
Sc (*)	0.00036	0.00003
Ti	0.15	0.02
V	0.0049	0.0006
Cr	0.014	0.003
Mn	0.032	0.001
Fe	2.7	0.2
Co	0.0008	0.0001
Ni	0.007	0.001
Cu	0.041	0.004
Zn	0.18	0.01
As	0.0012	0.0001
Rb (*)	0.0024	0.0006
Sb	0.0072	0.0003
Ba	0.034	0.005

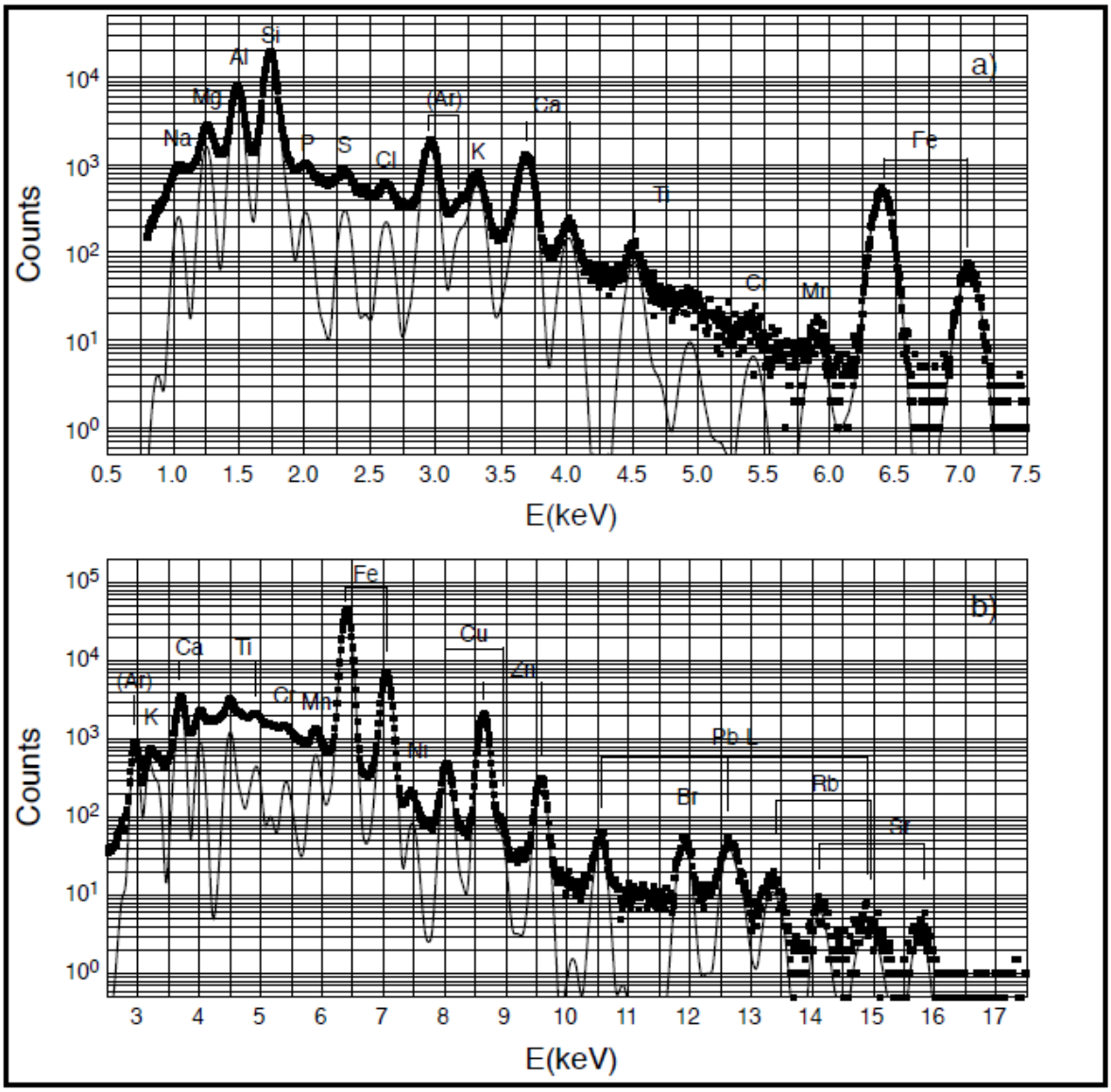

Figure 3.5. *PIXE spectra of the NIST SRM 2783 standard: panel a) low-Z elements; panel b) high-Z elements)*

Calibration curves in units of counts/(μg/cm^2/μCoulomb) are established using a least squares polynomial fit of the standards. This procedure is justified because the probability for X-ray production is a smooth continuous function of the atomic number, for a given proton energy. In this manner, small errors in the gravimetric analysis are smoothed over and obvious bad points become clear. Once these curves are established, for both the K and L-

line X-ray groups, they are stored and combined with the library of X-ray lines and intensities, to become the calibration for the system.

3.1.3.2. Quality control-quality assurance for ICP-MSMS

All reagents used in the analysis were analytical or higher grade. Hydrochloric acid (37% w/w), nitric acid (69% w/w) and hydrofluoric acid (48% w/w) were purchased from Merck (Germany). All acids were re-distilled (before digestions) to eliminate any interferences using an infrared acid distillation unit (Berghof Distill acid BSB 939, Germany). Deionized water obtained from Millipore (Milli Q) water purification system with resistivity of 18.2 MΩ was used throughout the experiments.

Due to high sensitivity of the ICP-MSMS, extreme precautions were taken to avoid contamination before and during sampling; digestion and analysis. For each batch of digestion, an acid blank was always prepared. All blanks were prepared and analyzed in the same manner as the field samples. Field blank samples were digested by the same acid mixture and analyzed together with samples.

Accuracy of the analytical technique was assessed by analyzing standard reference material (SRM 1648a, urban dust) purchased from NIST, (Gaithersberg, MD, USA). SRM 1648a was digested and analyzed by the same method described previously. Prior to analysis of the samples, ICP-QQQ-MS was calibrated for six levels (0, 25, 50, 100, 250 and 500 μg/L) by diluting the freshly prepared stock solutions with 20% HNO_3 same with acid concentration in the samples. Only Hg was calibrated for lower levels (0, 0.25, 0.5, 1, 2.5 and 5 μg/L) because of the very low levels in PM samples. Known amount of calibration standards were also analyzed several times with the real samples in each batch and ICP-QQQ-MS was re-calibrated if the deviations exceeded 10% within the same batch. Fresh calibration standards were prepared daily.

Prior to each batch of analysis, ICP-QQQ-MS was tuned with a tuning solution containing the masses of 7 (Li), 89 (Y) and 205 (Tl). Parameters such as torch position, sample depth, extraction, ion focus lenses voltages, omega lenses voltages, quadrupole

settings, electron multiplier settings, oxide and doubly charge ratios were optimized by tune operation. Oxides and doubly charge ratios were always kept below 1% and 2%, respectively.

In Table 3.2, are given the values of acid mixture blank samples, field blank samples and averages of sample-to-blank ratios. It should be noted that, sample-to-blank ratio was not subtracted from the data set, however, this was considered in the results evaluation.

Table 3.2. *Acid mixture blank samples, field blank samples and averages of sample-to-blank ratios of ICP–MSMS*

Element	**Acid Mixture Blank (ng/ml)**	**Field Blank (ng/ml)**	**Sample/Blank (Urban $PM_{2,5}$)**	**Sample/Blank (Urban $PM_{2,5-10}$)**	**Sample/Blank (Rural $PM_{2,5}$)**	**Sample/Blank (Rural $PM_{2,5-10}$)**
Li	0,14	0,12	1,6	2,0	1,2	3,4
B	1,63	1,19	9,7	4,7	11	1,6
Na	1,40	1,26	55	29	113	56
Mg	6,42	6,77	15	50	4,0	14
Al	4,77	4,03	19	76	14	106
K	0	0				
Ca	25	24	6,1	40	3,6	8
Sc	0,004	0,005	2,3		4,5	
Ti	1,15	1,14	5,1	25	5,5	12
S	11	22	21	65	7,1	15
V	0,22	0,22	6,6	11	3,4	3,6
Cr	1,12	4,10	4,1	2,9	2,6	3,8
Mn	0,27	0,19	8,8	34	9,3	15
Fe	10	10	7,8	38	8,1	14
Co	0,003	0,002	42		13	66
Ni	0,458	0,416	3,5	7,3	5,5	3,8
Cu	0,015	0				
Zn	1,245	1,076	9,7	395	6,4	3,4
Ga	0,035	0,013	19		16	
Ge	0,004	0,003	18			9,3
As	0,044	0,039	14	24	14	11
Se	0,002	0				
Br	1,518	1,239	2,0	1,4	3,1	
Rb	0,018	0,010	20	278	20	19

Table 3.2 (continued). *Acid mixture blank samples, field blank samples and averages of sample-to-blank ratios of ICP-MSMS*

Element	Acid Mixture Blank (ng/ml)	Field Blank (ng/ml)	Sample/Blank (Urban $PM_{2,5}$)	Sample/Blank (Urban $PM_{2,5-10}$)	Sample/Blank (Rural $PM_{2,5}$)	Sample/Blank (Rural $PM_{2,5-10}$)
Sr	0,086	0,083	11	21	11	14
Zr	0,056	0,476	1,8	16	1,3	20
Nb	0,062	0,027	4,9	4,6	9,8	17
Mo	0,033	0,015	7,2	11	7,0	4,8
Ag	0,131	0,002			26399	1870
Cd	0,004	0,003	247		56	31
Sn	0,025	0,007	68	2764	43	18
Sb	0,030	0,022	8,4	31	88	8,9
Te	0,009	0,001			85	65
Cs	0,004	0,002	41	62	11	15,3
Ba	0,066	0,039	13,1		24	
La	0,001	0,001			12	
Ce	0,004	0,001	24			
Nd	0,003	0,001	228		12	
Sm	0,001	0,0003			12	
Ho	0,0005	0,00003			49	
Lu	0,0005	0,00003			36	
Ir	0,027	0,001		504	7,1	
Pt	0,003	0,0001		106		22
Au	0,306	0,143	4,6	1,0	4,4	1,8
Hg	0,019	0,009	86	5,2	13	101
Tl	0,018	0,002			3,6	
Pb	0	0				
Bi	0,009	0,006	26		4,5	3,3
Th	0,002	0,0005	413		14	626
U	0,002	0,001	89,9		101	20

3.1.3.3. Acid-mixture digestion program

A Milestone Start D (Sorisole, Italy) microwave digestion system with HPR-1000/10S rotor and PTFE vessels was used for the digestion of the filter samples. The digestion procedure is described as follows:

Nucleopore filters were divided into 2 equal parts using a clean ceramic scissors. One half of the filters were placed into the Teflon (TFM) bottles after which high purity 7 mL of

nitric acid (HNO_3, Merck Suprapur, 65% purity), 1 mL hydrochloric acid (HCl, Merck Suprapur, 37% purity) and 0.5 mL hydrofluoric (HF, Merck Suprapur, 48% purity) were added in that order. (Perhaps this was the most crucial step in the digestion process i.e. finding a suitable acid mixture for the digestion). The Teflon vessels were then tight-covered and placed in the Milestone Start D microwave extractor for digestion. Ten samples one of which was a blank were prepared for dissolution in each batch of digestion. The digestion program was in two stages. In the first stage, the temperature was set to rise to 180 ° C in 15 minutes, and in the second stage it was made to stay for 10 minutes at this temperature. After this, the samples were allowed to cool to room temperature, taken up into a contamination-free polyethylene (PE) vessels and diluted to 20 mL by addition of ultrapure water (18.2 MΩ / cm). Samples were stored in the refrigerator at 4 ° C until ICP-MSMS analysis

At the end of the digestion, the Teflon containers together with their covers were cleansed using the cleaning program of the microwave extractor – a mixture of 5 mL HNO_3 and 5 mL ultrapure water was put into each of the 10 vessels and placed in the microwave. The cleaning program was equally of 2 stages; the temperature rose to 180 °C in the first 15 minutes and in the next stage it was made to stay at this temperature for 5 minutes. After the containers have cooled down, they were washed again with ultrapure water and brought back into service. The analytical vessels in which the samples were stored were left to stay in a solution containing 20% HNO_3 for 24 hours, and then cleansed with ultrapure water. Figure 3.6 shows a typicalMilestone Start D microwave digestion system used in this study.

Figure 3.6. *A Milestone Start D (Sorisole, Italy) microwave digestion system*

3.1.5. Method detection limit (MDL)

3.1.5.1. *Method detection limits by PIXE and ICP-MSMS*

Previously, MDL was determined as the minimum concentration of a substance that can be measured and reported with 99% confidence that the analyte concentration is greater than zero from analysis of a sample in a given matrix containing the analyte (USEPA 2003, 2004a, 2004c). The latest procedure for determining MDLs, however, relies on the use of method blanks where MDL is defined as the minimum measured concentration of a substance that can be reported with 99% confidence that the measured concentration is distinguishable from method blank results. In a typical ion beam system like PIXE, MDL was calculated in terms of areal density (μg/cm^2) using Eq. 3.7; and subsequently converted to μg/m^3 for PMF and other analyses.Generally, an X-ray peak is considered detectable if its intensity exceeds a three-standard deviation fluctuation of the underlying background (Minimum Detection Limit, MDL), which maycomprise contributions from Bremsstrahlung, nuclear reaction gamma-rays and overlapping X-rays (Calzolai et al., 2008; S. A. E. Johansson, 1989).The continuous background in PIXE spectra is mainly due to secondary electron Bremsstrahlung

radiation (from the filter more than from the aerosol sample) for energies typically below 10 keV (Folkmann et al., 1984).

$$MDL = 3.\frac{\sqrt{N_B}}{\eta_Z . Q} \quad (3.7)$$

Where $N_B$is the number of counts integrated in a region of the background under the peak, η_Z is the corresponding sensitivity value for the specific element and Q is thebeam charge during the measurement.

For ICP-MSMS, MDL was calculated as a function of the standard deviation of the signal and the gradient of the calibration curve using Eq. 3.8(Skoog, Holler, and Nieman, 1997). It should be noted that MDLs for the two methods were originally calculated in units of ng/ml for ICP-MS and μg/cm^2 for PIXE. For convenience of comparison, they were converted to the sample mass in ng.

For both methods, limit of quantification, LOQ, was calculated as 10 times the MDL, Eq. 3.9. In Table 3.3-4 are typical MDLsreported in the literature for some species of PM by PIXE and ICP-MSMS. Full list of calculated MDLs and LOQs by this study are given and discussed in section 4.4.3 of this thesis.

$$MDL = \frac{Stadard\ deviation\ of\ signal}{Calibration\ curve\ gradien} * 3 \quad (3.8)$$

$$LOQ = MDL * 10 \quad (3.9)$$

Table 3.3. *Typical detection limits and experimental uncertainties for IBA analysis of aerosol samples measured by 3 MeV protons and 5-10 nA proton beam intensity at the INFN-LABEC laboratory*

Element	IBA technique	Typical detection limit ($\mu g/cm^2$)	Typical detection limit (ng/m^3)[a]	Total uncertainty
Na-V	PIXE	0.05	10	5-20%
Cr-Pb	PIXE	0.01	2	5-20%

Source: INFN-LABEC laboratory. ***a.*** *for a 47 mm filter for a 24 hr. sampling at 2.3 m^3/hr.*

Table 3.4. *Typical MDLfor some metal species in ambient air by ICP-MS*

Element	Recommended analytical mass	Estimated Method Detection Limits (MDLs)	
		µg/L	ng/m3
Aluminum	27	0.05	0.01
Antimony	121	0.08	0.01
Arsenic	75	0.9	0.30
Barium	137	0.5	0.10
Beryllium	9	0.1	0.02
Cadmium	111	0.1	0.02
Chromium	52	0.07	0.01
Cobalt	59	0.03	0.01
Copper	63	0.03	0.01
Lead	206,207,208	0.08	0.01
Manganese	55	0.1	0.02
Molybdenum	98	0.1	0.02
Nickel	60	0.2	0.02
Selenium	82	5	1.10
Silver	107	0.05	0.01
Thallium	205	0.09	0.01
Thorium	232	0.03	0.01
Uranium	238	0.02	0.01
Vanadium	51	0.02	0.01
Zinc	66	0.2	0.04

Source: EPA /625/R-96/010a. MDL based upon sampling rate of 1.13 m3 /min for 24-h for a total sample volume of 1,627.2 m^3, factor of 9 for partial filter analysis; digestion of 0.040 L/filter.

3.1.6. Sample preparation and analyses

3.1.6.1. *PIXE analysis*

One half of the 47 mm nucleopore filter samples were analyzed by ICP-MSMS and the other halves prepared for PIXE analysis. It is important to mention that, the number of samples available for PIXE analysis were about a third less than the number of samples analyzed by ICP-MSMS. This is partly due to re-analysis of samples by ICP-MSMS to replace errors in the previous measurements and partly due to lost of the samples (by falling off the sample holder) during PIXE analysis.

Although the PM samples for PIXE analysis do not need dissolution or pre-concentration, it was necessary to condition the samples to a constant weight in a cabinet type desiccator between 25 ◦C and 35 ◦C and relative humidity of 25% - 35% for more than 24 h to avoid risks of contamination and loss of samples during this process. Filters were weighed on an analytical balance (Sartorius CP124S) with a precision of 1 µg and then transferred into clean petri dishes, labeled, sealed and stored in a dark cupboard until analysis.

Nucleopore filter samples were prepped on a clean bench environment and immediately transferred to the target chamber for analysis. Sample preparation consists of simply coding the filters and placing them into a wheel/carousel made to hold filters of different dimensions as shown in Figure 3.7.

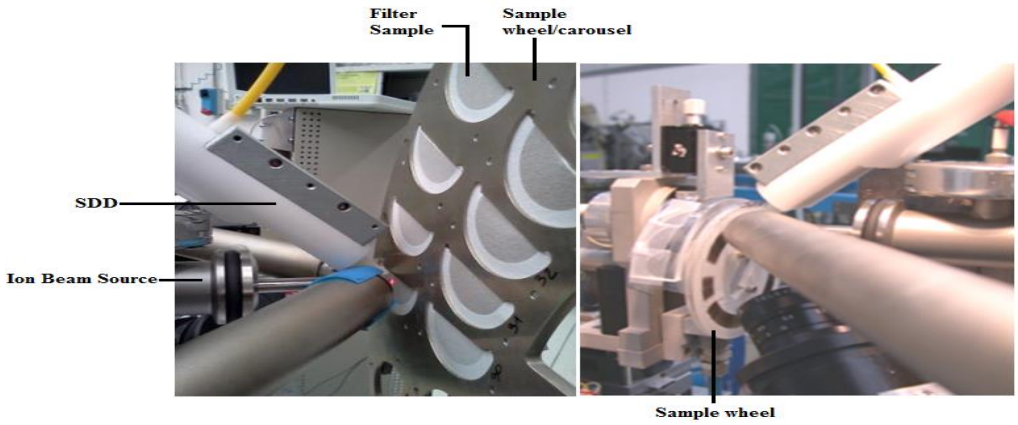

Figure 3.7. *A mounted aerosol samples ready for analysis by PXE*

The analysis of both fine ($PM_{2.5}$) and coarse ($PM_{2.5-10}$) nucleopore samples were done by an external ion beam PIXE setup at the National Institute of Nuclear Physics (INFN-LABEC) laboratory in Florence, Italy. The sample wheel (on which the target/samples are placed) was mounted in its position and placed perpendicular at about 1 cm from the window of the ion beam (the exit nozzle) and the Silicon Drift Detector (SDD) at 45 º to the target as shown in Figure 3.7. SDDs are now routinely employed in high resolution X-ray spectroscopy (Lucarelli et al., 2014, Calzolai et al., 2015) because of the low capacitance of the collecting electrode (0.5-1 pF/cm^2) and the low leakage current (1-2 nA/cm^2 at room temperature) resulting in an improved energy resolution yet at short shaping times and also sustained high count rates. Because the set-up was an external type (as oppose to vacuum type), constant flow of Helium (He) gas was very essential. Helium flow reduces both the beam energy loss and energy straggling (scattered energy) along the path in the atmosphere and the absorption of the low-energy X-rays.

To obtain a good average of sampling/collection inhomogeneity, the largest area possible of the sample must be analyzed and this can be accomplished in two possible ways: using a broad beam (typically 8-10 mm diameter) or a more collimated/focused beam (beam spot of about few mm^2) and mechanically scanning the sample. In this study, the collimated beam with sample scanning method was adopted since it is much more technically feasible and cost effective with an external beam set-up which does not require vacuum actuators.

3.1.7. ICP-MSMS analysis

PM samples characterization was done following the microwave assisted digestion described earlier. Shown in Figure 3.8, is a schematic diagram of the ICP-MSMS and its major components.

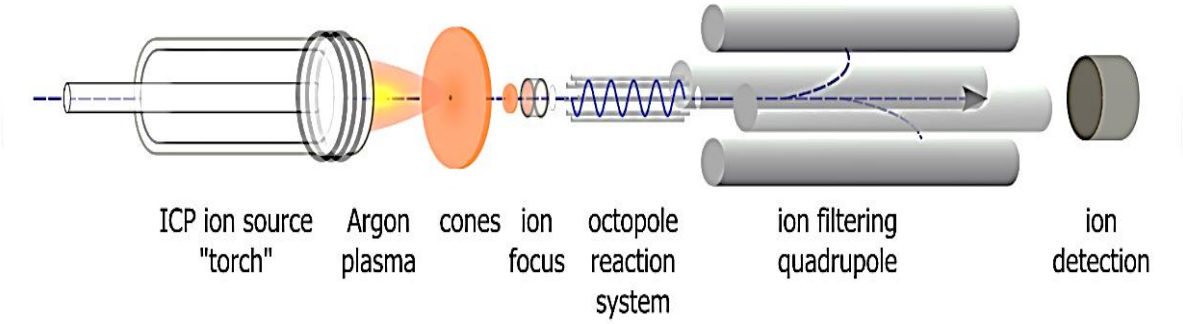

Figure 3.8. *Schematic diagram of ICP-MSMS, showing major components of the instrument*

The combined technology of the Triple Cone Interface (TCI) and Quadrupole Ion Deflector (QID) causes drift minimization and reduce contamination of the interface region. Sample introduction system made up of auto-sampler, peristaltic pump, nebulizer, spray chamber, and quartz injector are together responsible for getting the analyte into the instrument. The spray chamber removes larger particles from the analyte mist prior to injection and the injector delivers sample to the ICP torch.

The torch comprises two concentric quartz tubes through which argon flows at nonequivalent rates. The argon feeding the plasma flows through a gap between the quartz middle and outer tubes, which is surrounded by a RF coil near its end. Plasma formation occurs inside the outer quartz tube where it is surrounded by the coil. After the sample is injected, the plasma's extreme temperature causes the sample to separate into individual atoms (atomization). Next, the plasma ionizes these atoms ($M \rightarrow M^+ + e^-$) so that they can be detected by the mass spectrometer. Most elements ionize very efficiently (> 90%) in the hot plasma consisting of a small metal plate placed in the center of the ion beam, which reflects the photons away from the detector.

The skimmer and sampler cones are responsible for narrowing the ion beam. The vacuum system is made up of Turbo and Rotary pumps. The Turbo pump depressurizes the region behind the skimmer cone, holding the ion optics and mass filter systems in place. The Rotary pump on the other hand is responsible for pumping away majority of the gas stream from the plasma torch region.

The mass spectrometer also known as quadrupole mass filter comprises four parallel electrically conducting rods responsible for m/z selection of the analyte ion. Upon exiting the mass spectrometer, ions strike the first dynode of an electron multiplier, which serves as a detector. The impact of the ions releases a cascade of electrons, which are amplified until they become a measureable pulse. A software compares the intensities of the measured pulses to those from standards which make up the calibration curve to determine the concentration of the element.

3.2. Source Apportionment

Three methods: Enrichment factors (EF), Geoaccumulation index (Igeo) and positive matrix factorization (PMF) areusually employed in identifying and apportioning PM sources. In this study, Igeo was used to preliminarily apportion the PM sources whilst PMF model was used for a more comprehensive PM source apportionment and profiling.

3.2.1. Igeo calculation

Geoaccumulation Index (Igeo) was determined for each element using Eq. 3.10. Unlike enrichment factor (EF) analysis, Igeo is not based on double normalization procedure. Rather, a constant factor of 1.5 (Barbieri, 2016), is used to allow for analysis of natural fluctuations in the content of a given substance in the environment and to detect very small anthropogenic influence. It is a factor compensating the background data (correction factor) due to lithogenic effects.

$$Igeo = \ln {C_n}/{1.5} * B_n \qquad (3.10)$$

Where Cn is the measured concentration of the element in re-suspended soil dust sample and Bn is the geochemical background (reference) value of the element under investigation.

Enrichment factor, EF, is a double normalization procedure often used as a preliminary source apportionment. Based on Chester and Stoner, 1973, Zoller et al., 1974, the EF is calculated using Eq. 3.11.

$$EF = \frac{\left(\frac{C_X}{C_R}\right)_{aerosol}}{\left(\frac{C_X}{C_R}\right)_{Reference}} \quad (3.11)$$

Where C_x represents the concentration of the target element and C_R represents the concentration of the reference element which can be used as a marker of its source. The ratio of the C_x to C_R in aerosol sample to that in the reference source constitutes the double normalization in the EF determination method.

3.2.2. PMF analysis

The model primarily reduces the large number of variables in complex analytical data sets to combinations of species called 'source types' and 'source contributions'. The source types are identified by comparing them to measured profiles while the source contributions are used to determine how much each source contributed to a sample. The model assumes that there are p sources, source types (or factors) impacting a receptor and linear combinations of the impacts from the p factors give rise to the observed concentrations of the various species. Mathematical representation of PMF model is given in Eq. 3.12, in which X_{ij} is the concentration of j^{th} species on the i^{th} day at a receptor, g_{ik} is the contribution of the k^{th} factor to the receptor on the i^{th} day, f_{kj} is the fraction of the k^{th} factor for j^{th}species, e_{ij} is the residual for the j^{th} species on the i^{th} day.

$$X_{ij} = \sum_{k=1}^{p} g_{ik} f_{kj} + e_{ij} \quad (3.12)$$

The goal in the above expression is to estimate the contributions, g_{ik} and the fractions or profiles, $f_{kj}$to the concentration, x_{ij}. Both the contributions ($g_{ik} \geq 0$) and mass fractions ($f_{kj} \geq 0$) are non-negative. This implies sources cannot have negative species concentration and sample cannot have a negative source contribution in PMF analysis. This is the most important advantage of PMF over conventional FA in which source contributions can be negative.

Data below detection can be retained for use in the model; associated uncertainty must however, be adjusted so these data points have less influence on the solution than measurements above the detection limit. Factor contributions and profiles are derived by the PMF model, minimizing the objective function, *Q*, expressed in Eq. 3.13. Q should be approximately equal to the number of data points in the concentration data set if the uncertainties specified are truly reflective of the uncertainties in the data (EPA, 2008); this makes the model appropriate for the data.

$$Q = \sum_{i=1}^{n}\sum_{j=1}^{m}\left|\frac{X_{ij} - \sum_{k=1}^{p} g_{ik}f_{kj}}{u_{ij}}\right|^2 \qquad (3.13)$$

An important step in the analyses of PMF model's output is identification of physical meaning of factors of which there is no well-established methodology. While some factors can simply and straightforwardly be identified, others are quite complicated and difficult to identify. For example, a factor containing high concentrations of litophilic elements can easily be identified as crustal or soil source because there are no many sources that can emit such elements in high concentrations. Similarly, a factor consisting primarily of Na and Cl^- can also be easily identified as marine source. However, identification of factors representing anthropogenic sources is not straightforward. This is because many pollution-driven elements usually have multiple sources; their chemical interactions and transformations during their transport from source to the receptor make their identification quite problematic.

In the PMF model operation, the input data via the Concentration/Uncertainty, Concentration Scatter Plot, Concentration Time Series, and Data Exceptions screens are analyzed carefully before running the Base Model Runs and obtaining Base Model Results. This is necessary to obtain reasonable results (EPA PMF User Guide 5).

The parameter Fpeak was used to control the rotation problem and find the optimal solution for the explained factors. Based on the G score correlations between the factors Fpeak range is set. Flow chart summarizing result evaluation in PMF is given in Figure 3.9.

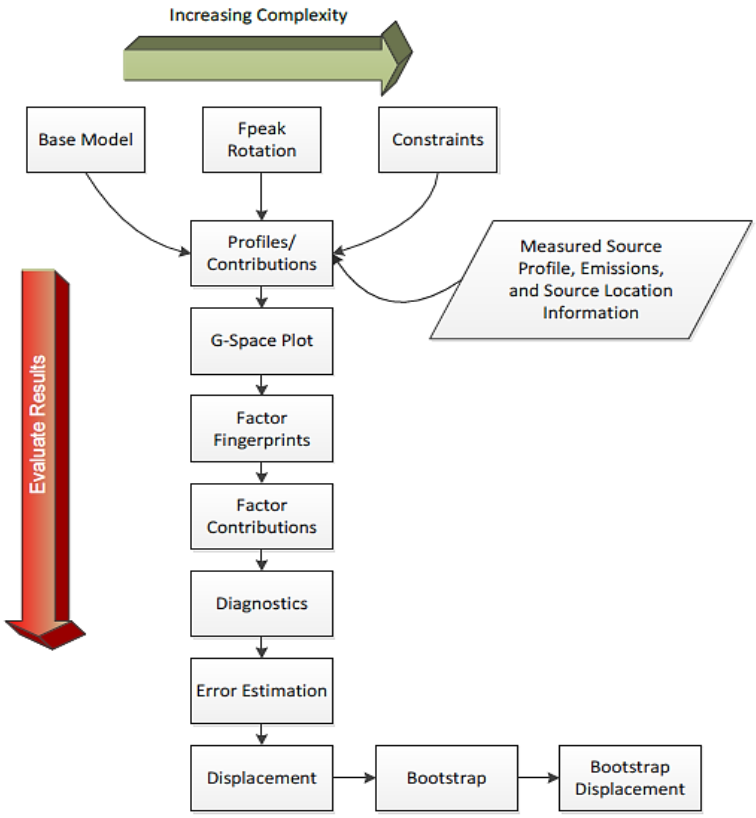

Figure 3.9. *PMF results evaluation process (chart from EPA, PMF User Guide)*

3.3. Potential Source Location

3.3.1. HYSPLIT model (back trajectory analysis)

Back trajectories of the air masses arriving at the two receptor locations were obtained for each day of the campaign from 06:00 UTC 09 Mar 14 to 19:00 UTC 28 Feb 15. Five-day archived back trajectories were run using HYSPLIT model modulated by the on-lineReal-time Environmental Applications and Display sYstem, (READY). The primary application of READY is running HYSPLITfor trajectory analysis. Airparcel trajectories that follow the movement of the wind patterns defined by the meteorological models can be produced (READY, 2017).

The model calculation method is a hybrid between the Lagrangian approach, using a moving frame of reference for the advection and diffusion calculations as the trajectories or air parcels move from their initial location, and the Eulerian methodology, which uses a fixed three-dimensional grid as a frame of reference to compute pollutant air concentrations (The model name, no longer meant as an acronym, originally reflected this hybrid computational approach). The model was run interactively on the Web through the ARL-READY system through the following steps:

1. Selecting/choosing the number of trajectory starting location
2. Selecting/choosing the type of trajectory e.g. Normal, Matrix, Ensemble or Frequency trajectories.
3. Selecting/inputting meteorology and starting receptor locations
4. Selecting/choosing meteorological forecast cycle
5. Selecting/choosing the direction of trajectory i.e. forward or backward
6. Selecting motion type e.g. vertical velocity, isobaric or isentropic
7. Setting the model's total run time and date based on the study period
8. Select display option and run model.

3.3.2. Mineral dust tracers

To identify an episode as dust event, at least one of the three back trajectories computed for that day must have either a North African, Central Asian or Middle Eastern origin. These regions are documented as the global sources of mineral dust species such as Fe, Ca, Si, Al and Ti, (Brauer et al., 2012; Haustein et al., 2012; Zender, 2003).

In this study; Al, Fe, Ti, Siand Ca were used as indicators of dust episode by computing and plotting the ratios of their median concentrations in dust days to non-dust days on one hand and by assessing their concentrations along with Saharan dust loadings and dust surface concentrations in the selected months of March, July, August and November of 2014 on the other hand.

3.4. Saharan Dust Intrusion and Mineral Dust Episode

Intrusion of Saharan dust to the Eastern Mediterranean is well documented in the literature. It was therefore necessary this study undertakes dust flow analysis to unravel the dust flow pattern and its impact on our receptor locations.

In this study, the Barcelona Dust Forecast Center's dust model, NMMB/BSC was used to assess: daily and monthly averages of dust surface Concentration (DSC), aerosol optical depth (AOD) and dust loadings (DL) for the entire sampling campaign period from March 9, 2014 to February 28, 2015. The months of March, July, August and November which represent the coldest but mostly wet and the warmest but mostly dry periods in Turkey were selected as representative months for the dust flow investigation.

In dust intrusion forecasting, an important consideration is to perform a near-real-time (NRT) evaluation aimed at assessing how the dust model behaves relative to the NRT AERONET's observations. In this regard, Angstrom Exponent (AE) and dust optical depth (DOD) as well as aerosol optical depth (AOD) were observed each day of the representative months using a Saharan Aerosol Network Station (IMS-METU-ERDEMLI) based in Turkey.

The NMMB/BSC-Dust model:

The NMMB/BSC-Dust (Pérez et al., 2011; Haustein et al., 2012) is an online multi-scale atmospheric dust model designed and developed at the Barcelona Supercomputing Center (BSC-CNS) in collaboration with the NOAA's National Centers for Environmental Prediction (NCEP), the NASA's Goddard Institute for Space Studies and the International Research Institute for Climate and Society (IRI). The dust model is fully embedded into the Non-hydrostatic Multiscale Model NMMB developed at NCEP (Chen et al., 2007; Haustein et al. 2012; Pérez et al., 2011)and is intended to provide short to medium-range dust forecasts for both regional and global domains.At regional scale, the model reproduces significantly well the daily variability and seasonal spatial distribution of the dust optical depth over Northern Africa, Middle East and Europe.

3.6. Health Risk Assessment

Health risk assessment procedure in this study is summarized in a flow diagram shown in Figure 3.10. Variables/parameters of interest and steps taken to arrive at the cancer risk estimation are herein explained.

Though this study investigated both rural and urban PM samples; health assessment was focused only on the urban $PM_{2.5}$, because of the varying and/or multiple emission sources coupled with high population density of the urban area than the rural area and due to the respirable nature of $PM_{2.5}$. According to the report of the World Health Organization (WHO, 2012) an important fraction of the exposure leading to those health impacts occurs in the cities, due to the higher density of human activities and their emissions to the air.

Exposure to selected trace metals including Cu, Pb, Zn, Co, Cr, Mn, Ni, V and Asof the urban fine PM fraction were determined in this assessment. Three exposure pathways – inhalation, ingestion and dermal absorption were considered and the relationship between exposure and risk was assessed based on a probabilistic distribution function (PDF). Using the Monte Carlo method, cancer riskdue to exposure to these metals was estimated as incremental lifetime cancer risk (ILCR) for both children (between 2 and 20) and adults

(between 21 and 76) year groups. Physiological parameters like age and body weight were set based on Turkish standard values. From (Neyzi et al., 2006; Neyzi, Saka, and Kurtoğlu, 2013) and Turkish Statistical Institute, children between the ages of 5 and 11 have average weight of 31 Kg and between 12 and 18 have average weight of 49 Kg. In the design of this study, children between 2 and 11yr. were lumped together with those between 12 and 21yr. as child age group category whilst those from 22 up to 76yr. were categorized as adult age group. The average body weight was finally set at 16.8 and 68.2 Kg, respectively for the child and adult age groups of the entire population.

In the health risk assessment, body weight, exposure duration, exposure frequency, average time etc. were used together with the observed species concentration to estimate exposure dose and subsequently, cancer risk was estimated by product of exposure dose and cancer slope factor and other parameters as explained later in this thesis.

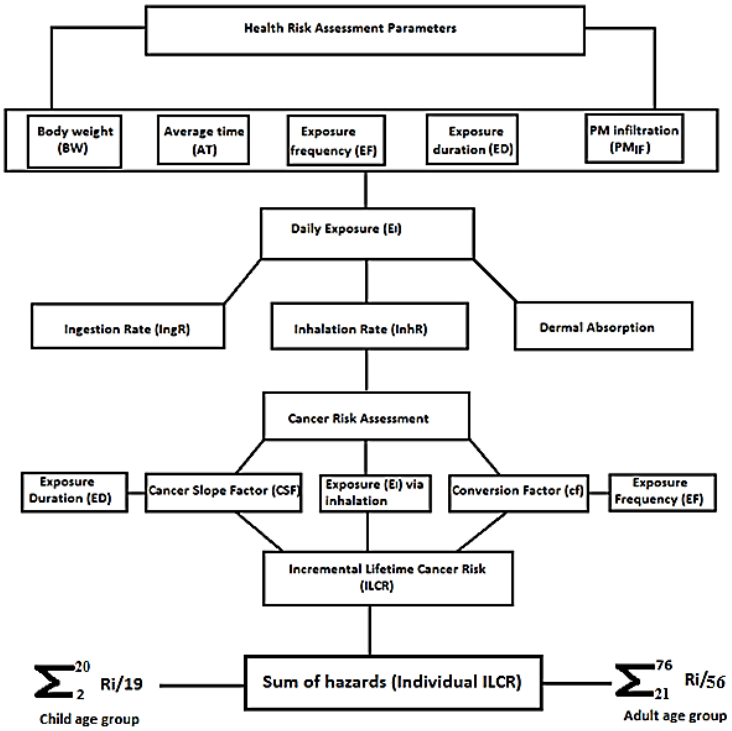

Figure 3.10. *Health risk assessment flow diagram*

3.6.1. Monte Carlo simulation

Monte Carlo method is recognized by EPA as a means of quantifying variability and uncertainty in risk assessments partly due to the degree of conservatism associated with the assumptions employed in a typical deterministic risk assessment methodology (US EPA, 2009). As stated earlier, Monte Carlo method involves many calculations of the intake rate/exposed dose rather than a single calculation; for each calculation, the input parameter values are randomly selected from the PDF for that variable. Monte Carlo technique takes into account the variability of the risk parameters under consideration in the risk assessment simulation and determination of effects. Generally, environmental data tends to be quite vague and imprecise and therefore liable to uncertainty. Uncertainty and sensitivity analyses which are crucial in health risk assessment are better dealt with by a probabilistic approach (USEPA, 2004b).

Chemical intakes are calculated using equations that include variables for chemical concentration, exposure dose, exposure frequency, exposure duration, body weight, and exposure averaging time (Demirel et al., 2014; USEPA 2004b). Intake rates and particle emission factors can be approximated by those developed for the soil, relevant exposure parameters of children and adults in the observed areas are similar to those of reference populations, the total non-carcinogenic risk for each metal (Cu, Pb, Zn, Co, Cr, Mn, Ni, V and As) and the overall carcinogenic risk canbe calculated by summing the individual risks (sum of hazards), (Ferreira-Baptista and De Miguel, 2005). In using Monte Carlo's model for risk assessment, equations were developed for the above-mentioned variables where each variable was modeled as a specific probability distribution (PDFs).

3.6.2. Daily exposure doses

Daily exposure doses to each of the metals were estimated considering diurnal variability of the metal concentration. As a result, it was necessary to apportion time based on typical day's activity of adults and children as shown in Table 3.5 obtained from questionnaires from the study area. It was evident from the time activity of both adults and children that about 83% (20 hr.) of the day was spent indoor and therefore risk was estimated

for indoor with the assumption that indoor air quality is affected by the quality of air outdoor. There is little information regarding exchange rate of particulates between indoor and outdoor environments and therefore PM infiltration factors (PM_{IF}), derived from (Xu et al., 2015) was used to determine the differences in exposure level between indoor and outdoor environment. Exposure dose contacted through each of the three intake paths was calculated following (Widziewicz and Loska, 2016)as follows Eq. 3.14-16:

Dose via ingestion (mg/kg/day)

$$E_{Ing} = \sum_{j=1}^{2} (PM_{IF} * D_i * C) . \left(\frac{R_{tij}}{24}\right) . IngR \quad (3.14)$$

Dose via inhalation (mg/kg/day)

$$E_{Inh} = \sum_{j=1}^{2} (PM_{IF} * D_i * C) . \left(\frac{R_{tij}}{24}\right) . InhR \quad (3.15)$$

Dose via dermal contact (mg/kg/day)

$$D_{derm} = C * \frac{SA * AD * ABS * EF * ED}{BW * AT} * 10^{-6} \quad (3.16)$$

Where *C* is the exposure-point concentration (mg/kg) of the metal; IngR, ingestion rate, is 200 mg/day for children and 100 mg/day for adults (USEPA, 2001). InhR, inhalation rate, is 7.6 m^3/day for children and 20 m^3/day for adults (Van Den Berg et al., 1998). PM_{IF}, is particulate matter infiltration into indoor environment; PM_{IF} = 0.58 for $PM_{2.5}$ and 0.39 for $PM_{2.5-10}$ (Widziewicz and Loska, 2016), j, is time intervals (hr.) between daily activities, Rt_{ij}, is residence time at j time interval. Di, is particle deposition efficiency in the respiratory tract

for each age group. Di value used in this model was adopted from Widziewicz et al., 2016; 0.4 and 0.3 for children and adults, respectively for $PM_{2.5}$.

Other parameters are EF, exposure frequency, given as 334 days/year, ED, exposure duration, given as 6 years for children and 24 years for adults (USEPA, 2001), SA, exposed skin area, given as 2800 cm^2 for children and 5700 cm^2 for adults; AD, skin adherence factor, given as 0.2 mg/cm^2/day for children and 0.07 mg/cm^2/day for adults (USEPA, 2001 and Zheng et al., 2006). ABS is dermal absorption factor, given as 0.001 for all metals (Man et al., 2010, Ferreira-Baptista, et al., 2005). BW, average body weight (kg) is 16.2 kg for children and 61.8 kg for adults, AT, averaging time, ED x 365 days for non-carcinogens and 72 x 365 = 26,280 days for carcinogens (X. S. Luo et al., 2012; USEPA, 2004b).

Table 3.5. *Time apportionment based on daily activities by age groups*

Denotation	**Adults (working class + aged)**		**Children (pre-school + school going age)**	
	Activity	Apportioned time (hr.)	Activity	Apportioned time (hr.)
J1	Working time, indoor	8	School time	8
J2	Sleeping time at night	7	Sleeping time at night	9
J3	Outdoor, other than working (past time)	4	Outdoor/break/play time	1
J4	Home indoor other than sleeping	5	Home indoor other than sleeping	2

3.6.3. Cancer risk estimates

Given in Table 3.6-7 are the reference doses of the metals of interest and parameters with their reference values used in the health risk assessment, respectively.

Table 3.6. *Reference dose (RfD, mg/kg/day) of metals of interest in health risk assessment (Ferreira-Baptista et al., 2005, Peng et al., 2017, USEPA, 2017)*

Element	As	Co	Cr	Cu	Mn	Ni	Pb	V	Zn
RfD_{inh}	1.50E-5	5.71E-6	1.00E-4	4.02E-2	5.00E-5	5.00E-5	3.52E-3	7.00E-3	3.00E-1
RfD_{ing}	3.00E-4	2.00E-2	3.00E-3	4.00E-2	1.40E-1	5.00E-2	3.50E-3	7.00E-3	3.00E-1
RfD_{derm}	6.65E-07	1.60E-02	2.50E-2	1.20E-02	1.84E-3	4.00E-2	5.25E-4	7.00E-5	6.00E-2

Table 3.7. *Parameters used to calculate exposure doses and risk factors*

Factor	Symbol	Unit	Reference Value				Reference
			Adult	Child	Indoor	outdoor	
Average body weight	BW	Kg	68.2*	16.8*	-	-	Luo et al., 2012
Exposure duration	ED	Year	24	6	25	25	USEPA, 2001
Exposure frequency	EF	Day/year	350	350	305	305	USEPA, 2001, ICMR, 2000
Average time for CR	AT	Days	24258	24258	24258	24258	USEPA, 2002
Average time for NCR	AT*	Days	8760	2190	25550	25550	Cao et al., 2012
Conversion factor	cf	Kg/mg	10^{-6}	10^{-6}	10^{-6}	10^{-6}	Cao et al., 2012
Dermal absorption factor for CR	ABS	mg/cm^2	0.03	0.03	0.03	0.03	Xu et al., 2008
Dermal absorption factor for NCR	ABS*	mg/cm^2	0.001	0.001	0.001	0.001	Xu et al., 2008
Inhalation rate	InhR	m^3/day	20	7.6			Berg et al., 1995
Ingestion rate	IngR	m^3/day	100	200			USEPA, 2001
Particle emission factor	PEF	m^3/day	1.36E09	1.36E09	1.36E09	1.36E09	Cao et al., 2012, USEPA, 2001

Table 3.7. (Continued). *Parameters used to calculate exposure doses and risk factors*

Factor	Symbol	Unit	Reference Value				Reference
Particle deposition efficiency in the respiratory tract	Di	-	0.3	0.4	-	-	Widziewicz et al., 2016
Skin adherence factor	AD_{soil}	mg/cm^2	0.07	0.2	0.2	-	Cao et al., 2012, USEPA, 2001
Surface area of skin contact point	SA	cm^2/event	5700	2800	3300	3300	Cao et al., 2012, USEPA, 2001
Retention time	Rt_{if}	hr.	20**	20**	20**	20**	This study
Inhalation unit risk for cancer	IUR	$(\mu g/m3)^{-1}$	4.3E-3	4.3E-3			EPA-IRIS,1988
Cancer slope factor	CSF	$(mg/kg/day)^{-1}$	13.29	9.17			Calculated based on *RAGS, 1989*

*CR = cancer risk, NCR = non-cancer risk, * based on Turkish Standard, ** based on indoor time per 24 hr. day. Particulate matter infiltration into indoor, PM_{IF} = 0.58 ($PM_{2.5}$), 0.39 ($PM_{2.5-10}$).*

Cancer risk was initially computed as a product of the cancer slope factor (CSF) and exposure due to inhalation (E_I) giving rise to what is known as incremental lifetime cancer risk for individual as expressed in Eq. 3.17. Following Eq. 3.17, incremental lifetime cancer risk (ILCR) was determined as the sum of hazards for specific metal under consideration for each of the age groups expressed in Eq. 3.18 and 3.19 (GUS, 2013).

Finally, using the Crystal Ball's Monte Carlo model, random variables (of the estimated ILCR median value obtained from Eq. 3.6.3.2 and 3.6.3.3) were generated to simulate the model. The number of simulation runs was initially set at, 1000; it wassubsequently increased to 1500 and finally to 2000 independent iterations to ensure numerical stability of the model's output.

$$R = \frac{E_I * EF * ED \left(CSF_i \left({}^{BW}/_{76} \right)^{\frac{1}{3}} \right) . cf}{BW * AT} \qquad (3.17)$$

$$ILCR_{child} = \sum_{i=2}^{20} \frac{R_i}{19} \quad (3.18)$$

$$ILCR_{adult} = \sum_{i=21}^{76} \frac{R_i}{56} \quad (3.19)$$

Where R_i, represents the individual lifetime cancer risk for specific metal dose of the i^{th} species, E_I, is exposure dose via inhalation, CSFi, is carcinogenic slope factor for the ith element (mg/kg/day), cf, is conversion factor (10^{-6}) (mg/ng). Based on risk assessment guidance for superfund (RAGS) of the USEPA, inhalation unit risk (IUR) multiplication was done to convert IUR to CSF $(mg/kg/d)^{-1}$ (RAGS, 1989): IUR $(mg/m^3)^{-1}$ * 1000 (µg/mg) * (BW (kg)/IR (m^3/day)).

In crystal Ball model, uncertainty associated with variables are dealt with by mathematically defining a cell in a spreadsheet with a range or set of values rather than a single value. Ambiguity associated with determination of factors that drive results in sensitivity analysis by deterministic approach is eliminated by Crystal Ball simulation. Moreover, there is no need of creating several spreadsheets to analyze multiple scenarios. Parameters of interest including metals concentrations and their infiltration into indoor environment; exposure duration, exposure frequency and body weights were modeled as random variables in Crystal Ball. Estimated risk, ILCR, was compared to the threshold value of 10^{-6}. ILCR values > 10^{-6} constitute a potential cancer risk to human.

4. RESULTS AND DISCUSSION

4.1. Overview

PM Constituents were identified and quantified by PIXE at the National Institute of Nuclear Physics (INFN), Florence, Italy and by ICP-MSMS at the Environmental Engineering laboratory of the Anadolu University, Eskisehir, Turkey. With regards to PIXE, Analyses of the X-ray spectra from which the concentrations of the PM metal constituents were determined was done using GUPIXWIN; a versatile software package for fitting PIXE spectra. It extracts peak intensities and converts them to concentrations via the H-value standardization method.

4.1.1. Data distribution

Atmospheric pollutants are controlled or influenced by many different factors, naturally and humanly. Also, because environmental data are obtained as time series, they tend to have relatively high standard deviations and skewed distributions. It was necessary therefore to find the distribution of the dataset obtained by PIXE analysis to inform the type of statistical analysis to undertake.

Normality of the datasets was tested using Shapiro–Wilk (SW) test. The SW statistic is reported to be very sensitive (B. W. Yap & C. H. Sim, 2011) and its significance in SPSS was calculated by linearly interpolating within the range of simulated critical values (Shapiro and M.B. Wilk, analysis of variance test for normality, biometrika 52 (1965), pp. 591–611). The test results based on skewness and kurtosis (z-values $\pm$ 1.96 and $p < 0.05$) implied the species were not normally distributed. The skewness and kurtosis z-values of all the species ranged between 2 and 23. Except for Phosphorus, all the species had skewness and kurtosis z-values greater than 2. Few elements including S, Cl, Cr, As, and Pb had relatively low kurtotic z-values, (between 3 and 11). Skewed distributed datasets are best analyzed by the median value which is quite insensitive to extreme values and have a measure of central tendency for chemical species. Reference is made to the mean values only for purposes of comparing this study's results with other studies. Species distribution charts (histograms) for

selected crustal and anthropogenic elements based on PIXE measurements are given in Figure 4.1-4.

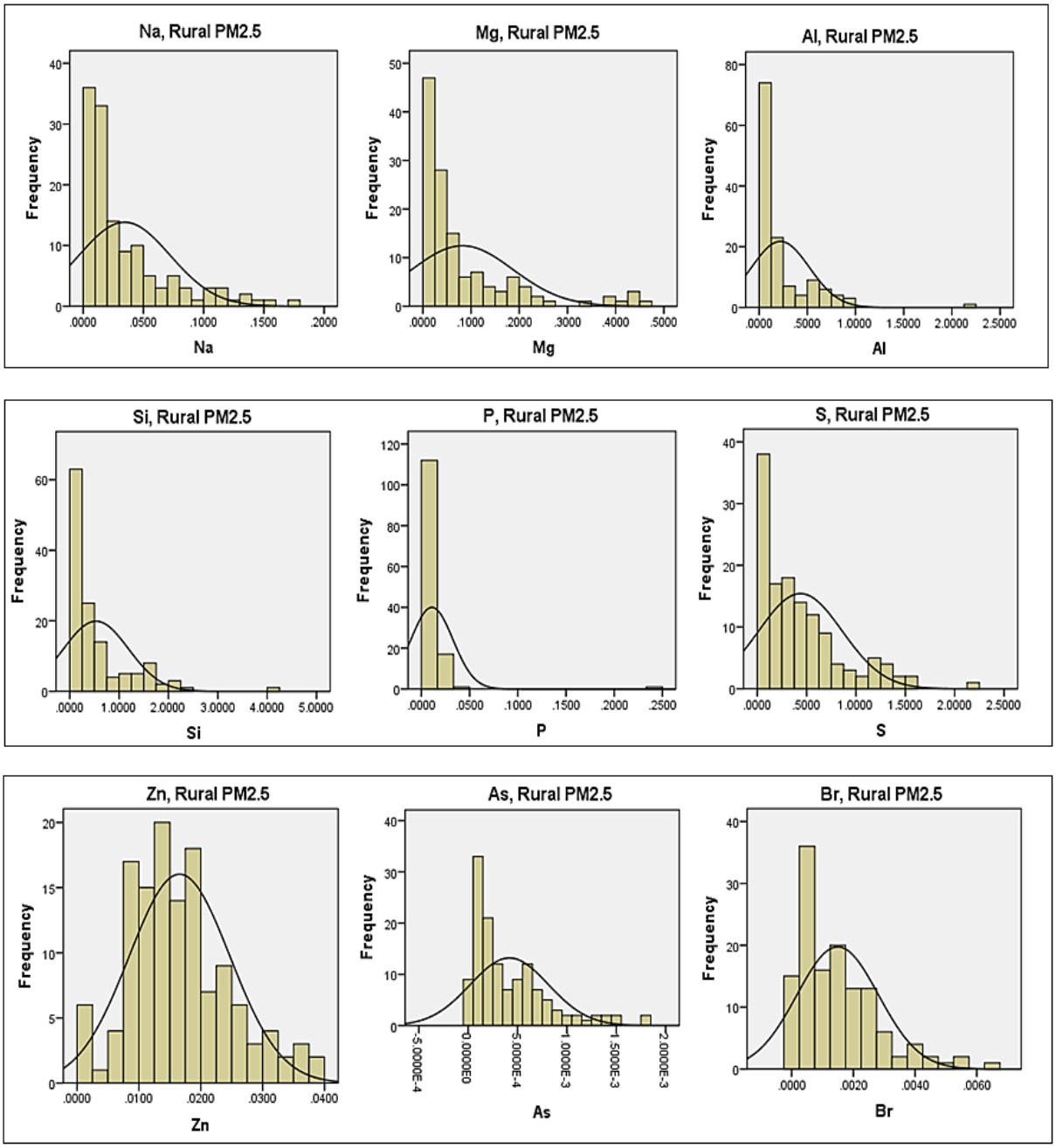

Figure 4.1. *Distribution of selected crustal and anthropogenic source elements in rural-fine PM*

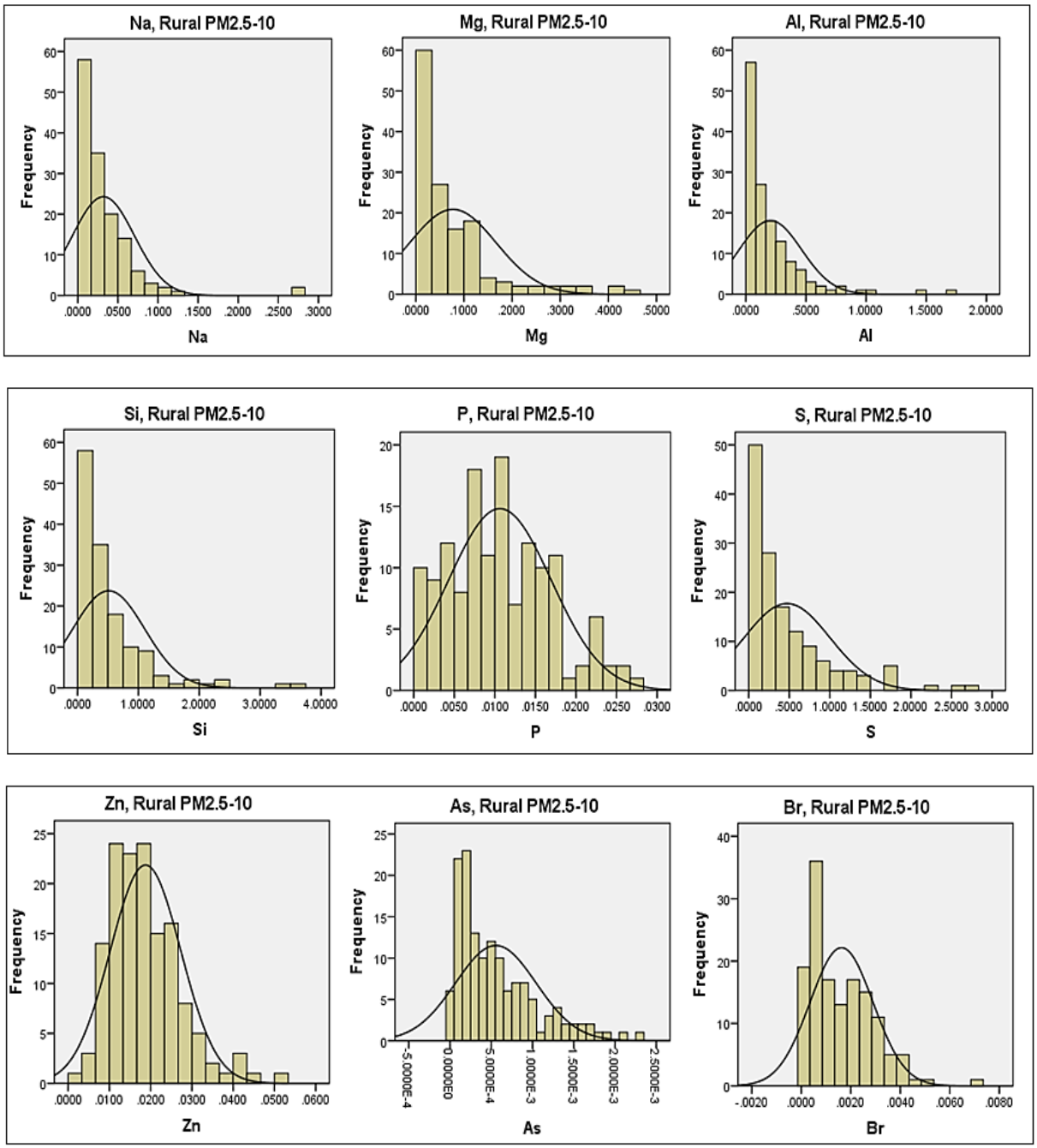

Figure 4.2. *Distribution of selected crustal and anthropogenic source elements in rural-coarse PM*

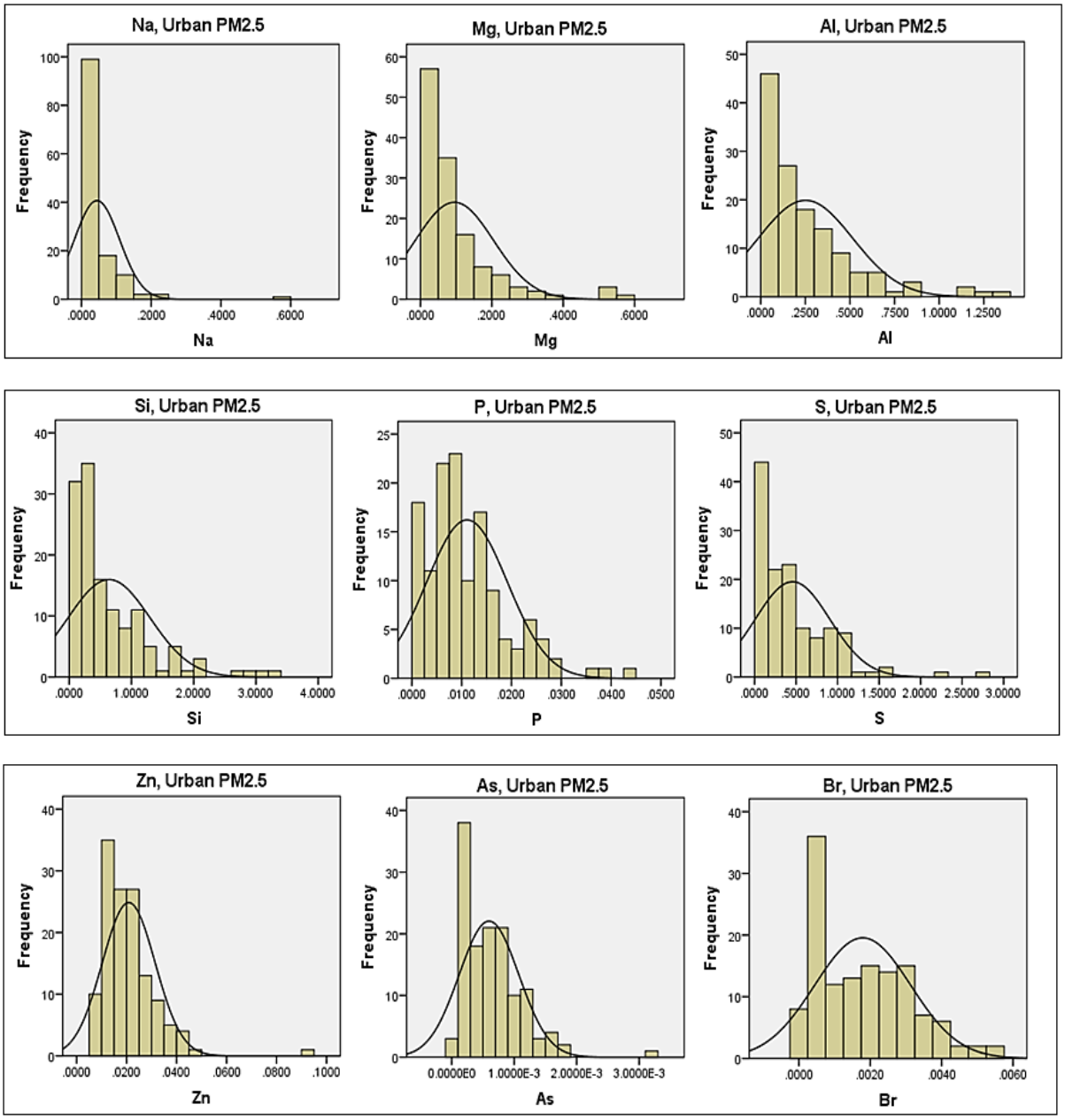

Figure 4.3. *Distribution of selected crustal and anthropogenic source elements in urban-fine PM*

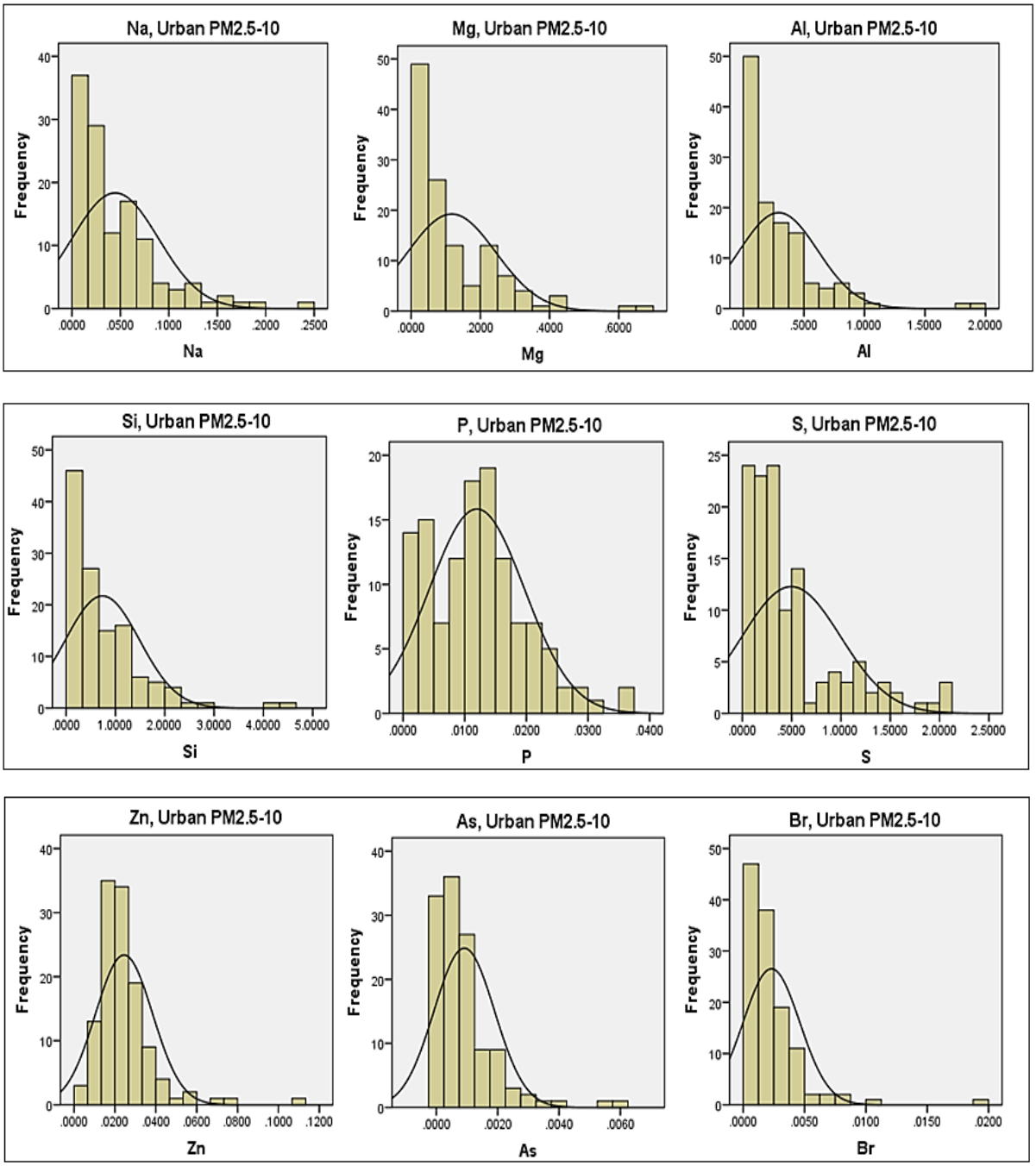

Figure 4.4. *Distribution of selected crustal and anthropogenic source elements in urban-coarse PM*

4.1.2. Descriptive statistics: metal concentration by PIXE

Concentrations of the urban and rural PM metals including, Na, Mg, Al, K, Ca, Ti, S, V, Cr, Mn, Fe, Ni, Cu, Zn, As, Se, Br, Rb, Sr, Y, Zr, Mo and Pb in both fine ($PM_{2.5}$) and coarse ($PM_{2.5-10}$) fractions measured by PIXE are herein discussed. A total of 600 samples comprising, 150 each of the fractions from the two monitoring stations were analyzed by PIXE. Concentration of species are given in ng/m^3 and in µg/m^3 for comparison purposes.

Calculation of percent below detection limit (%BDL) revealed that, not all identified species were present in all the samples. Detection ranged between 12-23 % for Mo and 100% for Zn in both $PM_{2.5}$ and $PM_{2.5-10}$. Seventeen elements (Na, Sr, P, Mg, Fe, Al, Cl, V, K, Si, S, Mn, Cu, Ni, Ca, Ti and Zn) were detected between 75% and 100%; five elements (Br, As, Pb, Rb and Zr) were between 50% and 65 % and four elements (Mo, Se, Y and Cr) were between 19% and 40%. Species below 60% of detection were excluded for detailed statistical analysis; they were however, maintained for enhancement of general statistical evaluations.

The descriptive statistics of all measured elements are given in Tables 4.1-2. The total PM mass for the rural, fine and coarse fractions were 45.70 µg and 50.94 µg respectively. The lowest concentration of 0.0023 µg/m^{3}was recorded by Pb in the rural fine samples while the highest concentration in same fraction was recorded by S (0.67 µg/m^3). In the coarse fraction, the lowest concentration (0.0017 µg/m^3) was again recorded by Pb and the highest concentration (0.59 µg/m^3) by Ca.

At the urban station, PM mass for the fine and coarse fractions were 58.91 µg and 78.33 µg respectively. The lowest and highest concentrations in the fine fraction were recorded forPb (0.006 µg/m^3) and S (0.59 µg/m^3), respectively. The lowest and highest measured concentrations in the coarse fraction were obtained for Pb (0.006 µg/m^3) and Ca (1.92 µg/m^3), respectively.

There are no annual limits for fine and coarse (i.e. $PM_{2.5}$ and $PM_{2.5-10}$) in Turkey. The measured annual average for $PM_{2.5-10}$ concentrations from the rural and urban stations,5.80 µg/m^3 and 8.80 µg/m^3, respectively summing up to be 14.6 µg/m3 as PM_{10} is below Turkey's annual limit of 50 µg/m^{3}set for total PM fraction i.e. PM_{10}. Also, the observed annual concentrations for$PM_{2.5}$from the rural and urban station, 5.33 µg/m^{3}and 6.75 µg/m^3,

respectively were below the annual $PM_{2.5}$ limit of 10 µg/m^3recommended by the World Health Organization (WHO). Adverse health effects have been reported for a long-term exposure of PM of 10 mg/m^3 (WHO, 2000), a value much higher than those measured in this study.

As can be seen, Mg, Al, Si, S, K, Ca and Fe are predominant in both the fine and coarse fractions of PM than the other elements. The median values of all the measured species except As, Se, Rb, Sr, Y, Zr and Mo were higher at the urban site than the rural site. These species are those with higher %BDL – i.e. between 35% and 88%. We can certainly conclude most of these species are almost not present.

The urban-to-rural ratio (urban/rural) values varied between 0.95 for Ni and 3.36 for Pb while the PM fractional ratio (coarse/fine) varied between 0.46 and 5.80 for the urban station dataset and 0.19 and 4.46 for the rural station dataset. Vanadium, Cu, As, Se and Br all of which are anthropogenic species had urban-to-rural ratio values of 2 – signifying a much polluted urban than the rural area by these species. These results were not surprising due to the high-density population of the urban area coupled with varied emission sources such as vehicular and other industrial activities such as mineral mining etc. Median concentrations of species and PM fractional ratios are illustrated graphically in Figure 4.5. Coarse-to-fine ratio values in both the urban and rural datasets were generally high compared to anthropogenic and mixed-source species. Species like Mg, Al, Si, Ca, Ti and Fe had coarse-to-fine ratios between 2 and 4.5 while mixed-source species like V, Cr and Cu recorded values between 1 and 1.5. Anthropogenic species including S, As, Se, Br, Zn and Pb had values between 0 and 1.

Table 4.1. *Descriptive statistics of rural station*

	Fine Fraction – $PM_{2.5}$ (N = 150)						Coarse Fraction – $PM_{2.5-10}$ (N = 150)					
Element	Mean ng/m^3	Mean µg/m^3	Std. Dev.	Median µg/m^3	Range µg/m^3	% BDL	Mean ng/m^3	Mean µg/m^3	Std. Dev	Median µg/m^3	Range µg/m^3	% BDL
$PM_{2.5}$	2157.9	2.1579	0.0120	0.0120	0.0011±0.0893		2350.9	2.3509	0.0156	0.0123	0.0005±0.1346	
Na	22.3	0.0223	0.0243	0.0146	0.0002±0.1334	22	37.6	0.0376	0.0643	0.0162	0.0001±0.5897	22
Mg	38.3	0.0383	0.0562	0.0244	0.0001±0.4316	16	73.6	0.0736	0.0704	0.0524	0.0001±0.3885	13
Al	146.2	0.1462	0.2742	0.0601	0.0001±2.1744	9	211.9	0.2119	0.2410	0.1203	0.0001±1.5275	11
Si	344.4	0.3444	0.5472	0.1865	0.0001±4.2079	6	534.6	0.5346	0.5541	0.3336	0.0001±3.4598	9
P	8.9	0.0089	0.0061	0.0086	0.0002±0.0254	21	8.6	0.0086	0.0067	0.0076	0.0001±0.0479	20
S	665.8	0.6658	0.5816	0.5508	0.0001±2.8227	6	128.4	0.1284	0.1163	0.0963	0.0001±0.6733	9
Cl	15.1	0.0151	0.0096	0.0149	0.0001±0.0595	10	67.4	0.0674	0.1392	0.0293	0.0002±1.1028	10
K	84.2	0.0842	0.0998	0.0565	0.0002±0.7298	9	97.6	0.0976	0.1031	0.0652	0.0002±0.6094	9
Ca	180.4	0.1804	0.2531	0.1103	0.0013±1.6949	3	588.6	0.5886	0.5343	0.4312	0.0016±2.5782	5
Ti	13	0.0130	0.0190	0.0064	0.0001±0.1444	1	23.4	0.0234	0.0220	0.0164	0.0001±0.1225	1
V	1.1	0.0011	0.0009	0.0008	0.0001±0.0055	19	1.3	0.0013	0.0012	0.0009	0.0001±0.0060	10
Cr	2.4	0.0024	0.0015	0.0022	0.0001±0.0084	61	3.8	0.0038	0.0028	0.0033	0.0001±0.0136	60
Mn	4.4	0.0044	0.0077	0.0022	0.0001±0.0629	11	5.6	0.0056	0.0066	0.0041	0.0001±0.0515	9
Fe	151.4	0.1514	0.1774	0.0915	0.0004±1.2624	20	267.1	0.2671	0.2318	0.2074	0.0004±1.1132	12
Ni	2.7	0.0027	0.0022	0.0020	0.0001±0.0123	4	4.5	0.0045	0.0048	0.0030	0.0000±0.0228	8
Cu	1.1	0.0011	0.0007	0.0010	0.0001±0.0041	5	1.4	0.0014	0.0043	0.0009	0.0000±0.0524	9
Zn	18.7	0.0187	0.0101	0.0176	0.0003±0.0925	0	14.6	0.0146	0.0088	0.0129	0.0009±0.0509	0

N = number of samples

Table 4.1 (Continued). *Descriptive statistics of rural station*

	Fine Fraction – $PM_{2.5}$ (N = 150)							Coarse Fraction – $PM_{2.5-10}$ (N = 150)					
Element	Mean ng/m^3	Mean µg/m^3	Std. Dev.	Median µg/m^3	Range µg/m^3	% BDL		Mean ng/m^3	Mean µg/m^3	Std. Dev	Median µg/m^3	Minimum µg/m^3	% BDL
As	0.5	0.0005	0.0005	0.0003	0.0001±0.0023	30		0.4	0.0004	0.0004	0.0002	0.0001±0.0017	44
Se	0.2	0.0002	0.0002	0.0002	0.0000±0.0009	49		0.1	0.0001	0.0001	0.0001	0.0000±0.0005	80
Br	2	0.0020	0.0013	0.0020	0.0000±0.0074	6		0.5	0.0005	0.0005	0.0004	0.0000±0.0034	47
Rb	0.3	0.0003	0.0004	0.0001	0.0000±0.0028	56		0.6	0.0006	0.0008	0.0003	0.0000±0.0059	35
Sr	0.6	0.0006	0.0008	0.0003	0.0000±0.0060	35		1	0.0010	0.0011	0.0006	0.0000±0.0061	21
Y	0.2	0.0002	0.0001	0.0001	0.0000±0.0008	82		0.2	0.0002	0.0001	0.0001	0.0000±0.0009	75
Zr	0.4	0.0004	0.0004	0.0003	0.0000±0.0019	45		0.6	0.0006	0.0006	0.0005	0.0000±0.0032	35
Mo	0.1	0.0001	0.0001	0.0001	0.0000±0.0004	88		0.2	0.0002	0.0001	0.0001	0.0000±0.0005	81
Pb	2.3	0.0023	0.0022	0.0016	0.0001±0.0110	30		1.7	0.0017	0.0020	0.0008	0.0001±0.0110	42

N = number of samples

Table 4.2. *Descriptive statistics of urban station*

	Fine Fraction – $PM_{2.5}$ (N = 150)						Coarse Fraction – $PM_{2.5-10}$ (N = 150)					
Element	Mean ng/m^3	Mean µg/m^3	Std. Dev.	Median µg/m^3	Range µg/m^3	% BDL	Mean ng/m^3	Mean µg/m^3	Std. Dev	Median µg/m^3	Range µg/m^3	% BDL
$PM_{2.5}$	2753.5	2.7535	0.0134	0.0151	0.0014±0.1166		3566.6	3.5666	0.0133	0.0233	0.0002±0.0804	
Na	25.3	0.0253	0.0259	0.0206	0.0001±0.1262	26	54.4	0.0544	0.0544	0.0406	0.0001±0.2454	20
Mg	45.9	0.0459	0.0526	0.0301	0.0003±0.2874	17	170.9	0.1709	0.1709	0.1319	0.0001±0.6833	17
Al	125.7	0.1257	0.1523	0.0819	0.0001±0.9851	11	380.2	0.3802	0.3802	0.3112	0.0001±1.9786	15
Si	302	0.3020	0.3332	0.2023	0.0001±2.0334	10	972.1	0.9721	0.9721	0.8347	0.0002±4.5339	14
P	7.7	0.0077	0.0065	0.0067	0.0003±0.0288	27	14.7	0.0147	0.0147	0.0132	0.0003±0.2440	27
S	586.9	0.5869	0.5395	0.4543	0.0001±2.7153	10	275.1	0.2751	0.2751	0.2566	0.0004±1.3231	16
Cl	19	0.0190	0.0325	0.0159	0.0002±0.3738	14	110.1	0.1101	0.1101	0.0814	0.0003±1.5128	15
K	92	0.0920	0.0915	0.0727	0.0002±0.5171	13	204.8	0.2048	0.2048	0.1812	0.0003±0.8567	17
Ca	381.7	0.3817	0.3429	0.3426	0.0013±2.7601	4	1920.1	1.9201	1.9201	1.7343	0.0009±7.2117	9
Ti	12.5	0.0125	0.0134	0.0102	0.0001±0.0814	1	36.3	0.0363	0.0363	0.0314	0.0000±0.1888	7
V	2.1	0.0021	0.0021	0.0014	0.0001±0.0117	15	3.6	0.0036	0.0036	0.0024	0.0001±0.0328	16
Cr	2.1	0.0021	0.0012	0.0020	0.0001±0.0089	43	3.9	0.0039	0.0039	0.0037	0.0000±0.0103	43
Mn	2.9	0.0029	0.0025	0.0026	0.0000±0.0119	13	7.8	0.0078	0.0078	0.0067	0.0000±0.0338	15
Fe	138.4	0.1384	0.1322	0.1214	0.0003±0.6828	19	388.4	0.3884	0.3884	0.3255	0.0001±1.8379	17
Ni	2.1	0.0021	0.0015	0.0020	0.0000±0.0106	7	4.1	0.0041	0.0041	0.0040	0.0000±0.0145	13
Cu	1.6	0.0016	0.0010	0.0016	0.0001±0.0068	9	2.8	0.0028	0.0028	0.0025	0.0001±0.0241	10

Table 4.2 (Continued). *Descriptive statistics of urban station*

	Fine Fraction – $PM_{2.5}$ (N = 150)							Coarse Fraction – $PM_{2.5-10}$ (N = 150)					
Element	Mean ng/m^3	Mean µg/m^3	Std. Dev.	Median µg/m^3	Range µg/m^3	% BDL		Mean ng/m^3	Mean µg/m^3	Std. Dev	Median µg/m^3	Range µg/m^3	% BDL
Zn	18.5	0.0185	0.0111	0.0175	0.0011±0.0765	0		22.6	0.0226	0.0226	0.0214	0.0010±0.1075	0
As	0.7	0.0007	0.0008	0.0005	0.0001±0.0058	29		0.6	0.0006	0.0006	0.0004	0.0001±0.0041	40
Se	0.4	0.0004	0.0003	0.0003	0.0000±0.0016	31		0.2	0.0002	0.0002	0.0002	0.0000±0.0011	61
Br	2.6	0.0026	0.0017	0.0025	0.0000±0.0103	10		1.4	0.0014	0.0014	0.0010	0.0000±0.0189	21
Rb	0.4	0.0004	0.0005	0.0002	0.0000±0.0034	48		0.7	0.0007	0.0007	0.0005	0.0000±0.0031	33
Sr	0.6	0.0006	0.0006	0.0005	0.0000±0.0043	27		2	0.0020	0.0020	0.0017	0.0000±0.0090	19
Y	0.2	0.0002	0.0002	0.0001	0.0000±0.0022	74		0.4	0.0004	0.0004	0.0003	0.0000±0.0017	61
Zr	0.7	0.0007	0.0008	0.0005	0.0000±0.0062	31		1.2	0.0012	0.0012	0.0010	0.0001±0.0046	29
Mo	0.2	0.0002	0.0003	0.0001	0.0001±0.0037	83		0.2	0.0002	0.0002	0.0002	0.0000±0.0006	77
Pb	6	0.0060	0.0115	0.0034	0.0001±0.1006	17		6	0.0060	0.0060	0.0035	0.0001±0.1176	23

N = number of samples.

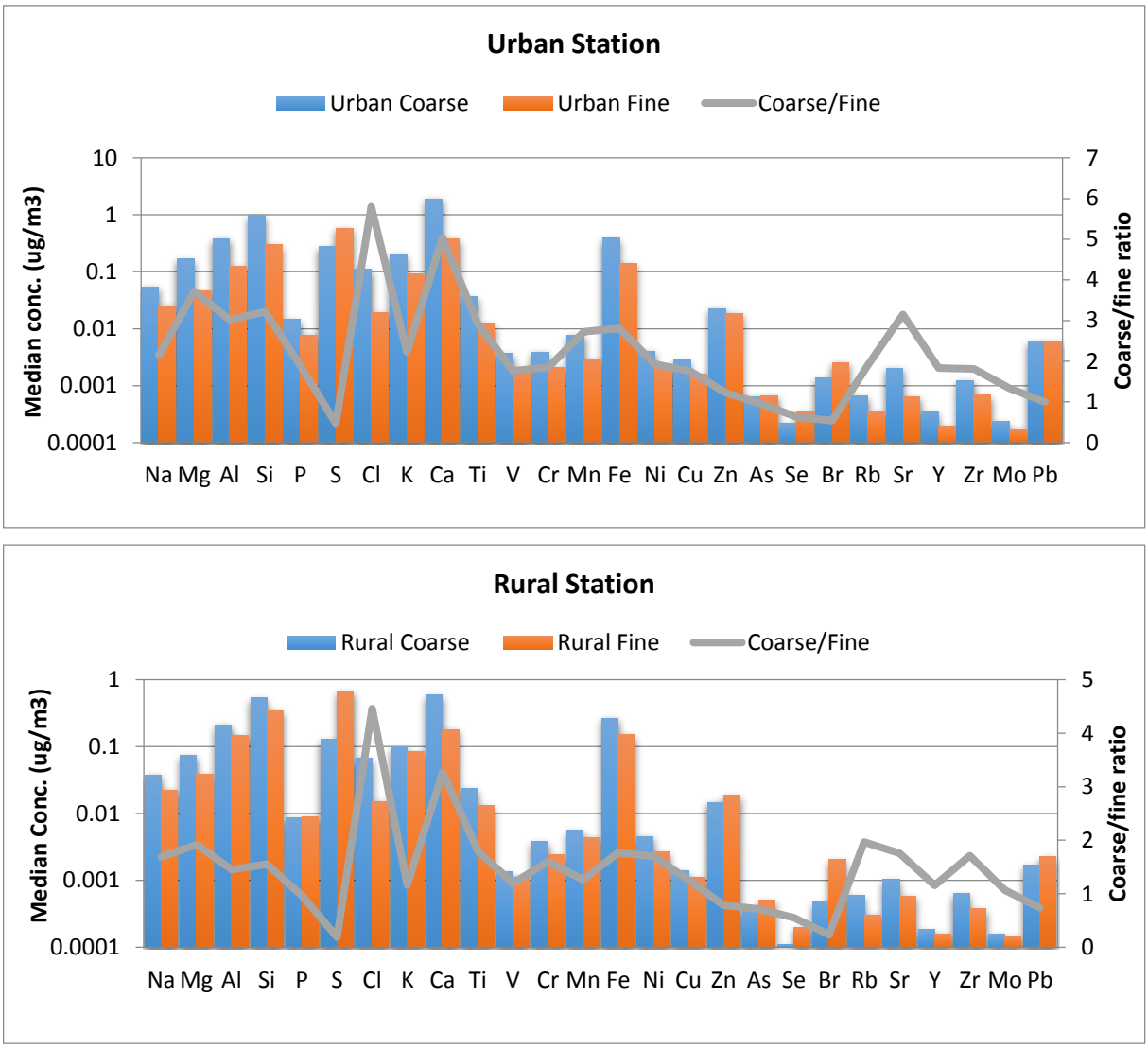

Figure 4.5. *Median concentrations of species and PM mode ratios (coarse-to-fine)*

Vanadium and Niare highly abundant in fly ash, a by-product of heavy oil combustion (Swaine, 1980; WHO, 2000); and are frequently used as fingerprint markers for petroleum-derived hydrocarbons (Laden et al., 2000; Thurston and Spengler, 1985). High Ni/V ratio is a good indication of fossil fuel combustion source for these trace elements. The Ni/V ratiofor oil combustion has been reported to be around 3 (Pacyna and Pacyna, 2001) and that of gas and diesel ranges from 0.3 to 0.5 (Rodriguez-Navarroand Sebastian, 1996). In this study, the Ni/V ratio values for fine and coarse urban aerosols were found to be 1.4 and 1.7, respectively and that of the rural aerosols were 2.5 and 3.4, respectively. These ratio values are indications

that Ni and V in both the rural and urban monitoring stations are of fossil fuel combustion source which in turn is an indicative of the impact and proximity of the coal-fired power plant to the rural area of Kutahya than the urban area. The urban area is, however, more affected by traffic (Artun et al., 2017). Also, Ni and V are both water soluble and hence their bioavailability and abundance in anthropogenic fine aerosols.

A common phenomenon of soil and dust re-suspension especially during the summer season accounts for the high concentrations of crustal and litophilic species in the atmosphere. Studies of Al-Momani et al., 1998; Güllü et al., 1998; Kubilay and Saydam, 1995, indicated that, concentrations of crustal ions Ca, Na, Mg; and soil related elements observed in most of the aerosols studies in the Mediterranean region are higher in summer season. Also, soil in most part of Turkey is known to be calcareous and therefore enriched in these elements (Kaya and Tuncel, 1997; Al-Momani et al., 1998 and Güllü et al., 1998). Slezakova et al., 2007, observed that, the elements S, Mn, Zn, Pb, P, K and Cr originated mostly from anthropogenic activities and they were predominantly present in the fine fraction while Mg, Al, Si and Ca mostly originated from crustal sources and were predominantly present in the coarse fraction.

Sulfur is a major product of coal combustion and therefore not surprising of its dominance in the fine fraction at the two monitoring stations. As stated earlier, the study area is characterized as a power plant region with three functional coal-fired power plants. Combustion of coal and petroleum accounts for 90% of the total Sulfur emitted by anthropogenic sources, the only other large source being the smelting of copper ores, (Cullis et al., 1980). Previous source apportionment studies have confirmed the mixed anthropogenic sources of zinc – non-exhaust vehicular emissions, industrial and biomass burning are the major reported sources.

Concentration of other anthropogenic trace elements like Cr, Ni, Cu and Pb measured by this study though very small, they were found comparable with values reported in other studies including Smolik et al., 2003; Artaxo et al., 1992; Zoller et al., 1974; Wagengach et al., 1988 and Tuncel et al., 1989. In a recent study in Istanbul (Sahin et al., 2010) it was observed that, V and Cu concentrations were between; 0.0020 µg/m^3 – 0.0036 µg/m3 and

0.0046 µg/m^3–0.0236 µg/m^3, respectively at a sampling station close to traffic. These values are very similar to the values observed by this study, especially the urban station measurements.

4.1.3. Methods evaluation

4.1.3.1. Regression analysis

The two methods (PIXE and ICP-MSMS) were evaluated using regression analysis at the 95% CL based onelemental concentrations. Linear regression (and itsassociatedslope, intercept and coefficient of determination R^2) is a commonly used method for analytical methods evaluation even though it is challenged by outlier effect (Yatkin et al., 2015).

As can be seen in Figure 4.6, there was a good positive relationship between PIXE and ICP-MSMS for both fine ($PM_{2.5}$) and coarse ($PM_{2.5-10}$) PM fractions; a positive relationship with R^2 value ranging from 0.5 to 0.9 was obtained for all elements. The varying R^2 value is obviously an indication of much stronger relationship between the two methods for some elements than others. Elements Ca, Ti and As showed over 80% positive relationship; Al, Mn and Mg showed over 70% positive relationship; Ni, Cr, V, Fe and Pb showed over 60% relationship whilst Na, S and Zn showed the weakest relationship with R^2 value of 30% for each of S and Zn and 40% for Na. Despite the scarcity of comparative studies in the literature, the few available studies have underscored similar relationships. Menzel et al., 2002, for instance compared the determination of metals (Ca, Mg, Fe, Al, Ni, Cu, Ti, Pb, K, Zn, Mn, Cr, Co) and non-metals (Si, P, S, Cl, Br) using both PIXE and ICP-AES on total suspended particulate samples. The study reported a good agreement (10–15%) between the PIXE and ICP-AES data for all the elements. Niu et al. (2010) also reported comparable results from EDXRF and ICP-MS for Fe, Mn, Cu, Zn and Pb, which show similar trend with the findings of this study. Okuda et al. (2015) reported comparable EDXRF and ICP-MS results on the diesel exhaust samples for Mg, S, Ca, Fe, Ni, Cu, and Zn.

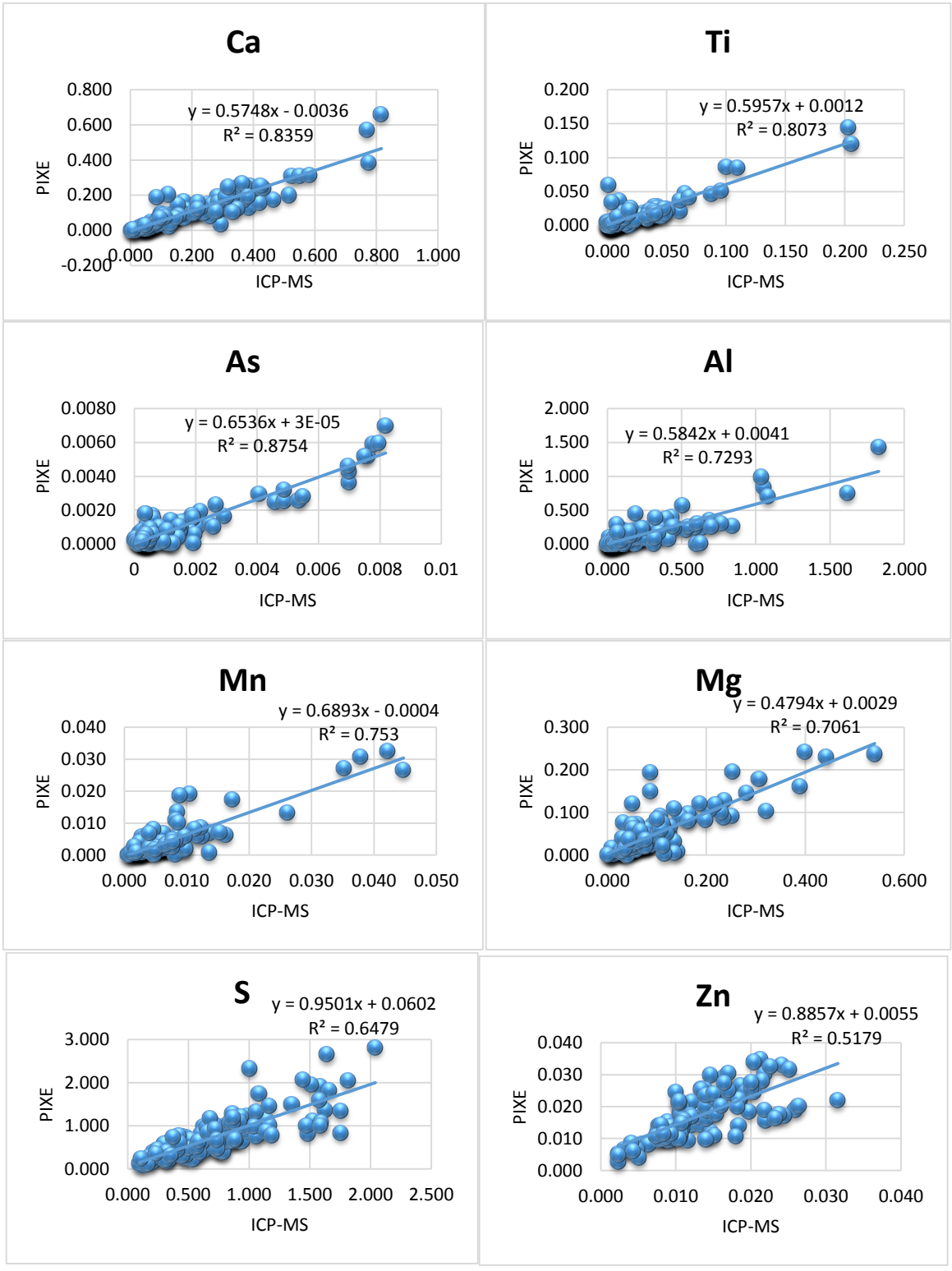

Figure 4.6. *Relationship between PIXE and ICP-MSMS based on elemental analysis*

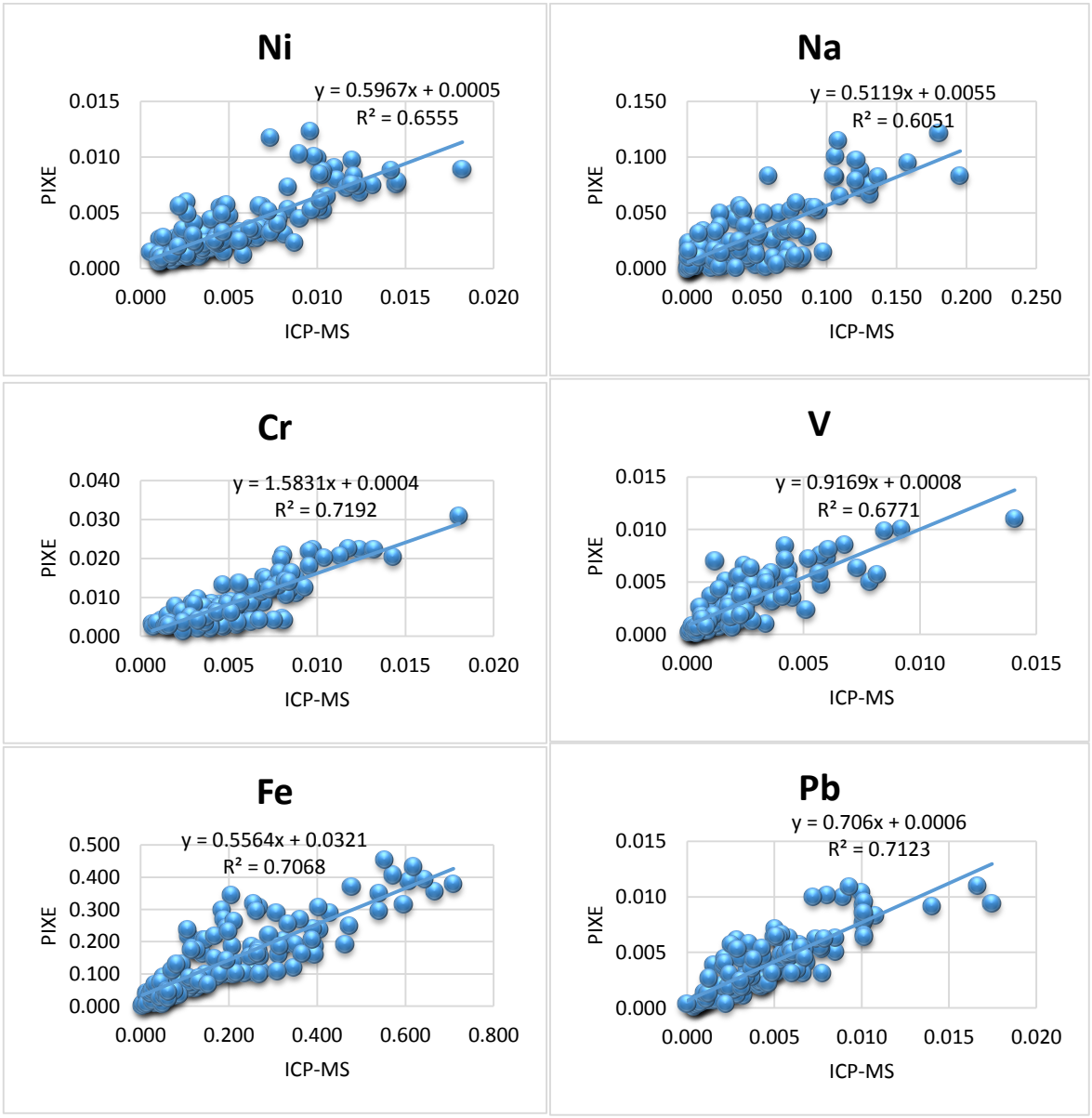

Figure 4.6 (Continued). *Relationship between PIXE and ICP-MSMS based on elemental analysis*

4.1.3.2. Absolute relative difference

Due to outlier effect in regression analysis, absolute relative difference (ARD) was also applied in evaluation of the two methods. ARD calculates the relative difference between the results of the two methods species by species (Yatkin et al., 2015). In thismethod, however, there are no standardized criteria on the acceptance of good agreement and therefore this study adopted the criteria set by Yatkin et al., 2015 in which ARD less than

20% was used as criteria for "good agreement". Presented in Table 4.7are the calculated results of the ARDsbetween PIXE and ICP-MSMS.

Table 4.3. *Calculated absolute relative difference (ARD), average and percent difference of ARD for PIXE and ICP-MSMS*

	No. SAMP	AVG	ARD_{ICPMS}	ARD_{PIXE}	ARD_{ICPMS}	ARD_{PIXE}	% Difference
Na	140	0.036 ± 0.011	98.78	74.22	0.988	0.742	25
Mg	140	0.072 ± 0.033	98.68	91.33	0.987	0.913	7
Al	140	0.19 ± 0.067	98.75	90.25	0.987	0.902	9
Ca	140	0.155 ± 0.063	98.71	88.28	0.987	0.883	10
Ti	140	0.019 ± 0.006	89.79	99.22	0.898	0.992	9
Fe	140	0.174 ± 0.041	98.83	86.17	0.988	0.862	13
S	140	0.762 ± 0.016	76.01	98.98	0.760	0.990	23
V	140	0.003 ± 0.001	99.24	78.02	0.992	0.780	21
Cr	140	0.007 ± 0.002	99.24	90.75	0.992	0.908	8
Mn	140	0.006 ± 0.002	98.82	92.26	0.988	0.923	7
Ni	140	0.005 ± 0.001	77.91	99.25	0.779	0.992	21
Zn	140	0.015 ± 0.003	75.14	98.87	0.751	0.989	24
As	140	0.001 ± 0.000	98.61	93.06	0.986	0.931	6
Pb	140	0.004 ± 0.001	89.80	98.99	0.898	0.990	9

Percent difference between ARD_{PIXE} and ARD_{ICPMS} represents the criterion for good agreement between PIXE and ICPMSMS. The criterion level set for this study is 20%.

The results as can be seen Figure 4.7, based on the agreement criteria of 20% set by this study, indicate generally a very good agreement between the two methods for most elements except Na (25%), S (23%) and Zn (24%). Slightly above the criterion level are V and Ni whose levels were 21% each. Like the regression analysis and other evaluation methods earlier discussed ARD method of evaluation also reveals a very good relationship between PIXE and ICP-MSMS for mostly crustal and/or litophilic species (Mg, Al, Ca, Ti, Fe, Cr and Mn) in particular.

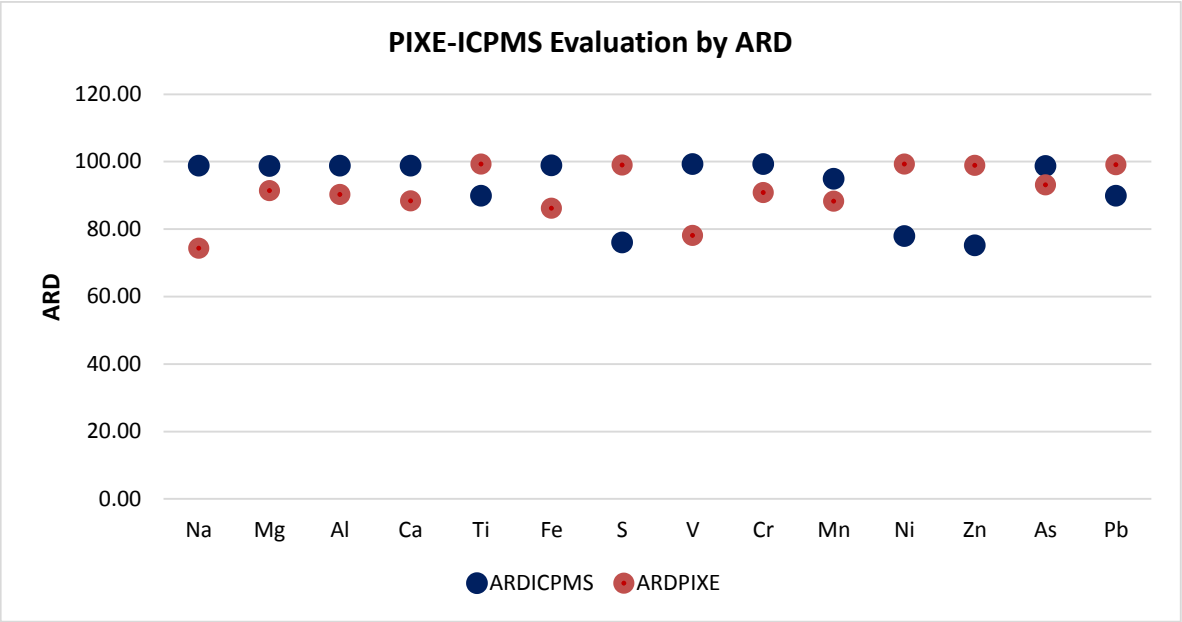

Figure 4.7. *PIXE-ICP-MSMS relationship by absolute relative difference, element by element*

In the literature, there are few studies reporting on PIXE and ICP-MSMS comparison. Few available literature reports of good relationship between EDXRF and ICP-MS for Fe, Mn, Cu and Pb (Niu et al., 2010); Fe, Mn, Cu, Pb and Zn (Yatkin et al., 2016) and Mg, Ca, Fe, Cu and Ni (Okuda et al., 2015). The findings of all three studies are very much comparable to the findings of this study. It should be noted, however, that analytical method evaluation can be affected by several factors including sample loadings, sampling approach and contamination. Also, since there are no standard criteria for good agreement between methods under evaluation, it leaves room for uncertainty especially for values close to the accepted criterion. It is important to note that, S continues to be a challenge for traditional ICP-MS analysis and thus, measurement of S was possible using the MS MS mode of ICP.

4.1.4. Species recovery, %BDL and measured concentration: PIXE vs. ICP-MSMS

Summary statistics obtained for PIXE and ICP-MSMS, their ratios and percent below detection limit (%BDL) for species in the fine and coarse fractions of PM are given in Table

4.4-5. The resolving potentials of the two techniques are discussed based on measured concentrations, detection limit and their ratio values asshown in Figure 4.8.

Based on the measured concentrations, a comparable resolving potential was found for all elements except Na by the two techniques. With respect to Na, the ICP-MSMS values were about 7 times higher in the fine and 10 times higher in the coarse fraction than the values measured by PIXE. Concentration of other elements including Mg, Al and Ca measured by the two techniques were about 1.5 – 2 times higher by the ICP-MSMS than PIXE.

All the measured elements except Na, Mg, Al, Br and Zr had ratio value (ICP-MSMS/PIXE) approximately 1 – suggesting a good relationship between the two techniques. An important observation by this study was that, the elements Ti, V, Cr, Mn, Fe, As, Se, Br, Rb, Sr, Zn, Mo and Pb yielded almost the same concentration amounts by the two techniques even though their %BDL varied in both the fine and coarse fractions. It can therefore be said that the two techniques are competitive for analysis of these elements; PIXE, however, seem to have added advantage for the fact that: it does not require sample pre-treatment which may be a source of contamination; it requires shorter time for analysis of standard daily samples than required by ICP-MSMS analysis. Moreover, PIXE has the capability of analyzing very low mass samples (Lucarelli et al., 2010) and therefore low concentrated elements such as Cr and Ni are better measured by PIXE.

There was a full recovery (90-100 %) for the elements Ca, Si, Ti, Cu, Zn, S and Cl by PIXE. Other elements including Na, K, Ni, V, Mg, Al, Fe, Mn and Pb were also recovered to a good extent (between 77% and 89%) by PIXE. Full recovery (between 99% and 100%) was realized by ICP-MSMS for the elements, Na, Mg, Al, S, Ca, Ti, V, Cr, Mn, Fe, Ni and As. To a very good extent, Cu (74%), Pb (74) and Zn (98%) were also recovered by ICP-MS. These outputs were found to be similar to that of Saitoh et al., 2001, in which urban particulate reference matter (NIST SRM 1648) was analyzed by PIXE, ICP-MS and ICP-AES where they found full recovery for anthropic metals, including Pb, As, Ni and Cu (107%, 120%, 96% and 93%, respectively), while metals with mixed anthropic-crustal origin like Al (83%), Fe (86%) and Mn (86%) were very well recovered by same method.

For PIXE, the %BDL varied between 0% for Zn and 83% for Mo; important markers such as Ca, S, K, Cl and Na were 4%, 8%, 11%, 12% and 21%, respectively below detection limit. The %BDL values for PIXE were higher compared to ICP-MSMS and this can be attributed to attenuation of low energy x-rays from lighter elements andpeak overlap, continuous background due to bremsstrahlung. Also, PIXEisaffectedbymatrixfactors which decreases the limit of detection of the element and consequently affect the observed concentration. For ICP-MS, %BDL varied between 0% for Mg, Ca, V, Cr, Mn and Fe; and 98% for Se. It is important to mention that, %BDL obtained for most elements including important markers such as Na, Mg, Al, Ca, Cr, V and S were between 0% and 1% for ICP-MS, making it a robust and highly sensitive technique for measuring these elements. On the basis of these, recovery of species was found to be generally better (~30%) by ICP-MSMS than PIXE.

Six elements including Ti, Cu, Zn, Se, Br and Zr were the only elements whose %BDL were relatively higher in the ICP-MSMS than the PIXE. Thus, the detection of these elements was better with PIXE than ICP-MSMS. Zirconium, Br and Se are quite interesting elements in the sense that, they are very rare marker elements whose characterization are useful for toxicological and exposure analyses. Bromine for example is a rare maker of biomass burning aside K. While Na and Cl give indication of sea salt spray, Br gives indication of seawater–fresh water mixing and has been cited as a marker of environmental changes driven by Grand Solar Minima and Anthropogenic activity (Moreno et al., 2014). Selenium is an important marker in medicine, its usefulness as a diagnostic marker selection for control examinations in surveillance and as a marker of cancer risk is reported in the literature (Lener et al., 2015). Zirconium is used as a catalyst for internal combustion reactions in automobile engines and can therefore serve as a good marker for automobile combustion. It is also used as a resistive heating element and as an electrolyte in solid oxide fuel cells. In medicine, Zr is used as a biomarker to visualize and characterize tumor lesions.

ICP-MSMS is found to be more robust, with lower detection and quantification limits than PIXE for most PM metals. It however, requiresa higher sample mass and sample dissolutionby a strong acid mixturedigestion prior to analysis. A process that is not only tedious but also exposes the process to serious contamination. PIXE on the other hand is

rapid and sensitive analytical method (Saitoh et al., 2002), which when combined with other components of IBA such as Particle Induced Gamma-ray Emission (PIGE), ElasticBackscattering Spectrometry (EBS) and Particle Elastic Scattering Analysis (PESA)can analyzeelements of the Periodic Table (from H to U). Unlike PIXE, ICP-MSMS is easily accessible and can be operated in any normal/standard laboratory environment. PIXE must necessarily be in an accelerator facility commonly operated by nuclear institutions.

Table 4.4. *Comparison: descriptive statistics of PIXE and ICP-MSMS – urban station dataset*

	Urban $PM_{2.5}$						**Urban $PM_{2.5-10}$**					
Element	**Mean µg/m³**		**Median µg/m³**		**% Element BDL**		**Mean µg/m³**		**Median µg/m³**		**% Element BDL**	
	PIXE (N = 141)	ICP-MS (N = 300)	PIXE (N = 141)	ICP-MS (N = 300)	PIXE (N = 141)	ICP-MS (N = 300)	PIXE (N = 141)	ICP-MS (N = 300)	PIXE (N = 141)	ICP-MS (N = 300)	PIXE (N = 141)	ICP-MS (N = 300)
Na	0.0253 ± 0.0259	0.664 ± 0.0505	0.0206	0.0564	21	9	0.0544 ± 0.0544	0.1164 ± 0.1001	0.0406	0.0895	17	1
Mg	0.0459 ± 0.0526	0.1038 ± 0.0869	0.0301	0.0827	17	2	0.1709 ± 0.1709	0.3776 ± 0.2667	0.1319	0.3216	14	0
Al	0.1257 ± 0.1523	0.1931 ± 0.2352	0.0819	0.1319	9	1	0.3802 ± 0.3802	0.5257 ± 0.4178	0.3112	0.422	13	0.3
Si	0.3020 ± 0.3332		0.2023		8		0.9721 ± 0.9721		0.8347		12	
P	0.0077 ± 0.0065		0.0067		25		0.0147 ± 0.0147		0.0132		24	
S	0.5869 ± 0.5395	0.7421 ± 0.6249	0.4543	0.6025	8	1	0.2751 ± 0.2751	0.3896 ± 0.3112	0.2566	0.2929	14	0.3
Cl	0.0190 ± 0.0325		0.0159		12		0.1101 ± 0.1101		0.0814		13	
K	0.0920 ± 0.0915	0.1031 ± 0.0798	0.0727	0.0927	11	8	0.2048 ± 0.2048	0.1433 ± 0.1286	0.1812	0.1065	15	7
Ca	0.3817 ± 0.3429	0.2614 ± 0.3041	0.3426	0.2105	4	2	1.9201 ± 1.9201	1.2765 ± 0.9839	1.7343	1.0392	8	0
Ti	0.0125 ± 0.0134	0.0112 ± 0.0124	0.0102	0.00792	1	9	0.0363 ± 0.0363	0.0303 ± 0.0226	0.0314	0.0244	7	0.3
V	0.0021 ± 0.0021	0.0022 ± 0.0020	0.0014	0.00164	13	0.3	0.0036 ± 0.0036	0.0035 ± 0.0032	0.0024	0.00269	14	0
Cr	0.0021 ± 0.0012	0.0045 ± 0.0045	0.0020	0.00329	41	0.3	0.0039 ± 0.0039	0.0042 ± 0.0020	0.0037	0.0039	43	0
Mn	0.0029 ± 0.0025	0.0031 ± 0.0027	0.0026	0.00237	11	1	0.0078 ± 0.0078	0.0073 ± 0.0055	0.0067	0.00599	13	0
Fe	0.1384 ± 0.1322	0.1564 ± 0.1384	0.1214	0.1192	17	1	0.3884 ± 0.3884	0.3595 ± 0.2567	0.3255	0.3081	16	0

N = number of samples

BDL = below detection limit

Table 4.4 (Continued). *Comparison: descriptive statistics of PIXE and ICP-MSMS – urban station dataset*

	Urban $PM_{2.5}$						Urban $PM_{2.5-10}$					
Element	Mean $\mu g/m^3$		Median $\mu g/m^3$		% Element BDL		Mean $\mu g/m^3$		Median $\mu g/m^3$		% Element BDL	
	PIXE (N = 141)	ICP-MS (N = 300)	PIXE (N = 141)	ICP-MS (N = 300)	PIXE (N = 141)	ICP-MS (N = 300)	PIXE (N = 141)	ICP-MS (N = 300)	PIXE (N = 141)	ICP-MS (N = 300)	PIXE (N = 141)	ICP-MS (N = 300)
Ni	0.0021 ± 0.0015	0.0021 ± 0.0023	0.0020	0.0015	6	1	0.0041 ± 0.0041	0.0035 ± 0.0042	0.004	0.0029	12	1
Cu	0.0016 ± 0.0010	0.0016 ± 0.0022	0.0016	0.0011	6	35	0.0028 ± 0.0028	0.0024 ± 0.0046	0.0025	0.0015	8	26
Zn	0.0185 ± 0.0111	0.0175 ± 0.0182	0.0175	0.0131	0	2	0.0226 ± 0.0226	0.0141 ± 0.0129	0.0214	0.0104	0	2
As	0.0007 ± 0.0008	0.0015 ± 0.0016	0.0005	0.0011	29	1	0.0006 ± 0.0006	0.0013 ± 0.0013	0.0004	0.0009	40	1
Se	0.0004 ± 0.0003	0.0003 ± 0.0004	0.0003	0.0003	29	34	0.0002 ± 0.0002	0.0002 ± 0.0002	0.0002	0.0001	58	89
Br	0.0026 ± 0.0017	0.0031 ± 0.0045	0.0025	0.0017	10	59	0.0014 ± 0.0014	0.0057 ± 0.0076	0.001	0.0039	19	60
Rb	0.0004 ± 0.0005	0.0004 ± 0.0004	0.0002	0.0004	46	2	0.0007 ± 0.0007	0.0009 ± 0.0006	0.0005	0.0007	31	0
Sr	0.0006 ± 0.0006	0.0014 ± 0.0016	0.0005	0.0009	24	2	0.0020 ± 0.0020	0.0037 ± 0.0030	0.0017	0.0029	19	0.3
Y	0.0002 ± 0.0002		0.0001		72		0.0004 ± 0.0004		0.0003		61	
Zr	0.0007 ± 0.0008	0.0020 ± 0.0037	0.0005	0.0009	31	33	0.0012 ± 0.0012	0.0022 ± 0.0024	0.001	0.0018	29	1
Mo	0.0002 ± 0.0003	0.0002 ± 0.0002	0.0001	0.0002	83	4	0.0002 ± 0.0002	0.0002 ± 0.0001	0.0002	0.0002	77	7
Pb	0.0060 ± 0.0115	0.0093 ± 0.03545	0.0034	0.0039	17	4	0.0060 ± 0.0060	0.0082 ± 0.0210	0.0035	0.0023	23	26

N = number of samples
BDL = below detection limit

Table 4.5. *Comparison: descriptive statistics of PIXE and ICP-MSMS – rural station dataset*

	Rural $PM_{2.5}$						**Rural $PM_{2.5-10}$**					
Element	**Mean µg/m³ (Std. Dev.)**		**Median µg/m³**		**% Element BDL**		**Mean µg/m³ (Std. Dev.)**		**Median µg/m³**		**% Element BDL**	
	PIXE (N = 150)	ICP-MS (N = 300)	PIXE (N = 150)	ICP-MS (N = 300)	PIXE (N = 150)	ICP-MS (N = 300)	PIXE (N = 150)	ICP-MS (N = 300)	PIXE (N = 150)	ICP-MS (N = 300)	PIXE (N = 150)	ICP-MS (N = 300)
Na	0.0223 ± 0.0243	0.0524 ± 0.0624	0.0146	0.0362	22	12	0.0376 ± 0.0643	0.1109 ± 0.1115	0.0406	0.0759	22	5
Mg	0.0383 ± 0.0562	0.075 ± 0.1038	0.0244	0.05	16	6	0.0736 ± 0.0704	0.2174 ± 0.1748	0.1319	0.1828	13	1
Al	0.1462 ± 0.2742	0.1739 ± 0.2642	0.0601	0.0984	9	1	0.2119 ± 0.2410	0.4042 ± 0.4215	0.3112	0.2706	11	1
Si	0.3444 ± 0.5472	0.0658 ± 0.0722	0.1865		6		0.5346 ± 0.5541		0.8347		9	
P	0.0089 ± 0.0061		0.0086		21		0.0086 ± 0.0067		0.0132		20	
S	0.6658 ± 0.5816	0.6824 ± 0.5656	0.5508	0.0477	6	22	0.1284 ± 0.1163	0.1809 ± 0.1367	0.2566	0.1442	9	0.3
Cl	0.0151 ± 0.0096		0.0149		10		0.0674 ± 0.1392		0.0814		10	
K	0.0842 ± 0.0998		0.0565	0.0697	9		0.0976 ± 0.1031	0.1017 ± 0.1114	0.1812	0.0718	9	24
Ca	0.1804 ± 0.2531	0.1208 ± 0.1642	0.1103	0.00694	3	2	0.5886 ± 0.5343	0.3666 ± 0.3456	1.7343	0.2753	5	2
Ti	0.0130 ± 0.0190	0.0118 ± 0.0165	0.0064	0.5586	1	12	0.0234 ± 0.0220	0.0242 ± 0.0246	0.0314	0.0168	1	3
V	0.0011 ± 0.0009	0.0009 ± 0.0007	0.0008	0.00066	19	14	0.0013 ± 0.0012	0.00128 ± 0.0009	0.0024	0.0010	10	0
Cr	0.0024 ± 0.0015	0.0047 ± 0.0069	0.0022	0.00374	61	2	0.0038 ± 0.0028	0.00605 ± 0.0046	0.0037	0.0049	60	15
Mn	0.0044 ± 0.0077	0.0031 ± 0.0045	0.0022	0.00192	11	2	0.0056 ± 0.0066	0.00574 ± 0.0049	0.0067	0.0043	9	1
Fe	0.1514 ± 0.1774	0.1378 ± 0.1592	0.0915	0.0929	20	1	0.2671 ± 0.2318	0.2986 ± 0.2695	0.3255	0.2263	12	1

N = number of samples

BDL = below detection limit

Table 4.5 (Continued). *Comparison: descriptive statistics of PIXE and ICP-MSMS – rural station dataset*

	Rural $PM_{2.5}$						**Rural $PM_{2.5-10}$**					
Element	**Mean µg/m³**		**Median µg/m³**		**% Element BDL**		**Mean µg/m³**		**Median µg/m³**		**% Element BDL**	
	PIXE (N = 150)	ICP-MS (N = 300)	PIXE (N = 150)	ICP-MS (N = 300)	PIXE (N = 150)	ICP-MS (N = 300)	PIXE (N = 150)	ICP-MS (N = 300)	PIXE (N = 150)	ICP-MS (N = 300)	PIXE (N = 150)	ICP-MS (N = 300)
Ni	0.0027 ± 0.0022	0.0024 ± 0.0022	0.0020	0.00167	4	16	0.0045 ± 0.0048	0.0043 ± 0.0049	0.0040	0.00267	8	14
Cu	0.0011 ± 0.0007	0.0031 ± 0.0163	0.0010	0.00081	5	67	0.0014 ± 0.0043	0.0021 ± 0.0082	0.0025	0.00047	9	81
Zn	0.0187 ± 0.0101	0.0155 ± 0.0494	0.0176	0.00712	0	31	0.0146 ± 0.0088	0.0086 ± 0.0215	0.0214	0.00503	0	14
As	0.0005 ± 0.0005	0.0008 ± 0.0007	0.0003	0.00057	30	2	0.0004 ± 0.0004	0.0007 ± 0.0006	0.0004	0.0005	44	1
Se	0.0002 ± 0.0002	0.0001 ± 0.0001	0.0002	0.00011	49	59	0.0001 ± 0.0001	0.0004 ± 0.0003	0.0002	0.00013	80	98
Br	0.0020 ± 0.0013	0.0048 ± 0.0037	0.0020	0.00388	6	53	0.0005 ± 0.0005	0.0043 ± 0.0136	0.0010	0.00147	47	78
Rb	0.0003 ± 0.0004	0.0003 ± 0.0003	0.0001	0.00017	56	4	0.0006 ± 0.0008	0.0005 ± 0.0005	0.0005	0.00036	35	2
Sr	0.0006 ± 0.0008	0.0010 ± 0.0015	0.0003	0.00059	35	1	0.0010 ± 0.0011	0.0023 ± 0.0026	0.0017	0.00157	21	1
Y	0.0002 ± 0.0001		0.0001		82		0.0002 ± 0.0001		0.0003		75	
Zr	0.0004 ± 0.0004	0.0025 ± 0.0031	0.0003	0.0016	45	55	0.0006 ± 0.0006	0.0017 ± 0.0019	0.0010	0.00106	35	12
Mo	0.0001 ± 0.0001	0.0001 ± 0.0001	0.0001	0.000095	88	35	0.0002 ± 0.0001	0.0002 ± 0.0005	0.0002	0.00009	81	14
Pb	0.0023 ± 0.0022	0.0020 ± 0.0038	0.0146	0.00135	30	23	0.0017 ± 0.0020	0.0019 ± 0.0053	0.0035	0.00065	42	78

N = number of samples

BDL = below detection limit

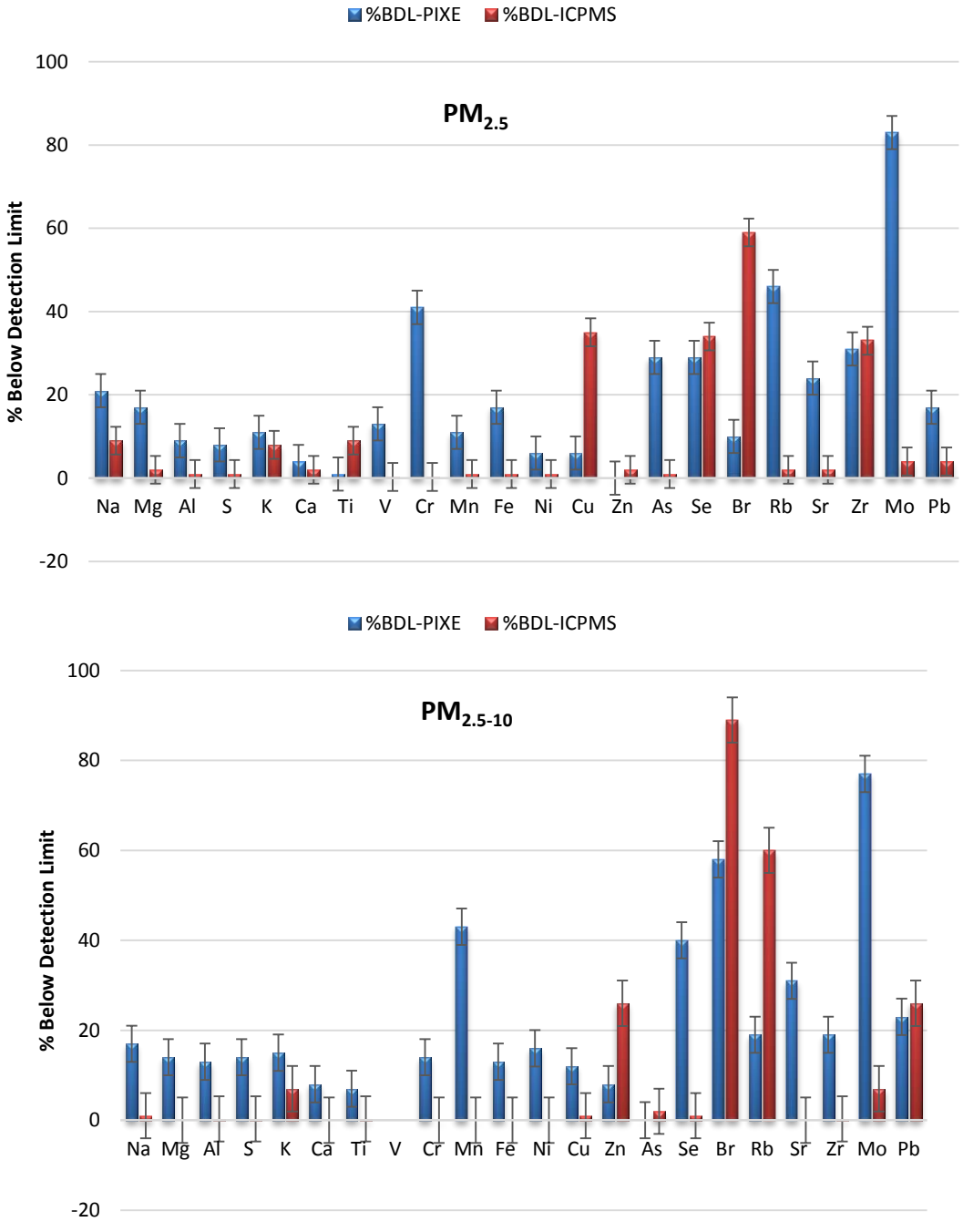

Figure 4.8. *%BDL of PM fractions by PIXE and ICP-MSMS*

4.1.5. Method detection limits: PIXE vs. ICP-MSMS

Given in Table 4.15 are the calculated MDLs with their LOQs and minimum detection mass (MDM) for PIXE and ICP-MSMS. For better graphical resolution and scaling, the mass unit of MDLs for PIXE were converted from µg to ng. MDM for PIXE and ICP-MS was calculated by multiplying their MDLs by the sample collection area in cm^2 and the sampling volume in ml, respectively.

Generally, as can be seen in both Table and Figure 4.9, MDL values for PIXE were about 2-5 orders of magnitude greater than those of ICP-MSMS. For PIXE, it was observed that the low-Z elements which are mainly crustal species including Na, Mg, Al, Fe, K, Ti and Ca recorded the high MDL values ranging between 30.0 and 50.0 ng/cm^2 corresponding to MDM of 124 – 693 ng. Mo and Pb recorded MDL values of 15.0 and 20.0 ng/cm^2, respectively which correspond to 208 and 277 ng MDM. Anthropogenic species like Ni, As, Mn and Cr recorded between 1.0 and 8.0 ng/cm^2corresponding to 14 - 69 ng MDM. The lowest MDL for PIXE was recorded by mainly mixed-source species including Zn, Cu, Se and Br; having MDL values between 0.7 and 0.9 ng/cm^2 which corresponded to 11 – 12 ng MDM.

For ICP-MSMS, K, Na and Ca recorded MDL values of 2.8, 1.88 and 1.37 ng/ml, respectively; being the highest MDLs for the method. These values correspond to 70, 47 and 34 ng MDM, respectively. The next highest was recorded by Al, Mg and Br in the rage of 0.18 – 0.6 ng/ml, corresponding to 4.5 – 15 ng MDM.

The lowest MDL for ICP-MS was recorded by mainly anthropogenic, mixed-source species including Zn, Cu, Ni, Cr, Sr, Rb, Mn and Pb. These species recorded MDL values between 0.004 and 0.011 ng/ml which corresponded to 11 – 12 ng MDM. It is obvious from these results that, ICP-MSMS had generally demonstrated better sesitivity and thus, better recovery than PIXE in terms detection limits. It is quite clear also that both methods have comparable potential for Na, K, and Ca even though their MDL values vary. Whilst Mg, Al and Fe falls in the highest MDL range for PIXE, these same species were in the second highest category for ICP-MSMS.

Table 4.6. *Calculated MDL, LOQ and MDM values for PIXE and ICP-MSMS*

Element	MDL_{PIXE} µg/cm^2	LOQ_{PIXE} µg/cm^2	MDL_{PIXE} ng/cm^2	MDL_{ICPMS} ng/ml	LOQ_{ICPMS} ng/ml	MDM_{PIXE} (ng)	MDM_{ICPMS} (ng)
Na	0.05	0.5	50.0	1.88	18.81	692.50	47
Mg	0.04	0.4	40.0	0.18	1.82	554.00	4.5
Al	0.03	0.3	30.0	0.20	2.04	415.50	5
K	0.04	0.4	40.0	2.80	28.03	554.00	70
Ca	0.04	0.4	40.0	1.37	13.66	554.00	34.25
Ti	0.009	0.09	9.0	0.071	0.71	124.65	1.775
V	0.008	0.08	8.0	0.0042	0.042	110.80	0.105
Cr	0.005	0.05	5.0	0.015	0.15	69.25	0.375
Mn	0.004	0.04	4.0	0.0076	0.076	55.40	0.19
Fe	0.003	0.03	3.0	0.083	0.83	41.55	2.075
Ni	0.001	0.01	1.0	0.011	0.11	13.85	0.275
Cu	0.0009	0.009	0.9	0.093	0.93	12.47	2.325
Zn	0.0008	0.008	0.8	0.088	0.88	11.08	2.2
As	0.002	0.02	2.0	0.017	0.17	27.70	0.425
Se	0.0009	0.009	0.9	0.049	0.49	12.47	1.225
Br	0.0008	0.008	0.8	0.63	6.26	11.08	15.75
Rb	0.004	0.04	4.0	0.0044	0.044	55.40	0.11
Sr	0.002	0.02	2.0	0.0078	0.078	27.70	0.195
Mo	0.015	0.15	15.0	0.011	0.11	207.75	0.275
Pb	0.02	0.2	20.0	0.011	0.11	277.00	0.275

MDM: minimum detection mass (ng).

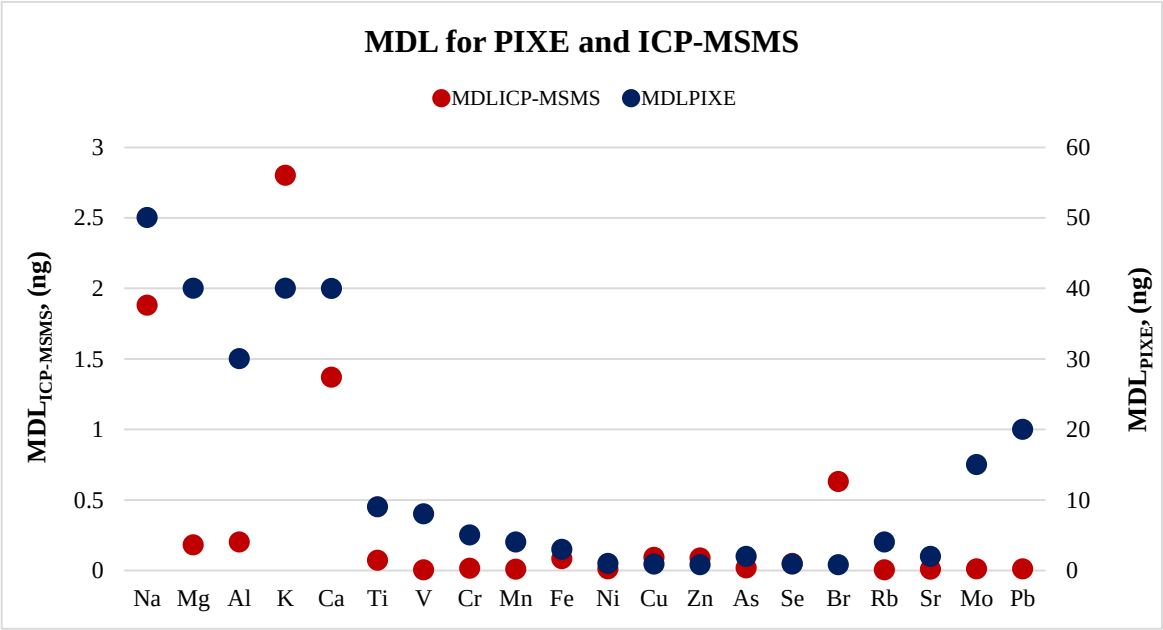

Figure 4.9. *Variation between PIXE and ICP-MSMS for PM species based on their MDLs*

4.1.6. Comparison with Literature

Results of this study obtained by PIXE measurement was compared with results of other studies using similar or same methodology; to corroborate results of this study and assess the level of pollution in the study area compared to the others. The following studies in literature have been selected for comparison purposes only: Kocak et al., 2007b; Theodosi et al., 2010a; Tecer et al., 2012; Onat et al., 2013; Artaxo et al., 1992; Smolik et al., 2003; Begum et al., 2005; Rogula-Kozlowska et al., 2013 and Balcilar et al., 2014. Given in Table 4.7, is the summary of some selected studies in the literature compared to this study. In Turkey, major aerosol analyses conducted in the past include, Özturk et al., 2012 (rural, Antalya); Kocak et al., 2007b (rural, Mersin); Theodosi et al., 2010a (urban, Istanbul); Tacer et al., 2012 (urban, Zonguldak) and Balcilar et al., 2014.

Concentration of Pb measured in these studies (Özturk et al., 2012; Kocak et al., 2007b; Theodosi et al., 2010a and Tacer et al., 2012) varied between 0.02 µg/m^3 and 0.07 µg/m^3; about 10 – 35 times higher than values recorded by the current study. It should be

noted that, leaded gasoline in motor vehicles was banned in Turkey since 2006 and therefore its ambient concentration is expected to be reducing over the years.

For crustal species like Al, Ca and Fe the four studies above recorded higher values than the current study: 0.6610 µg/m^3, 1.4220 µg/m^3 and 0.4000 µg/m^3, respectively by Özturk et al; 0.7400 µg/m^3, 2.8400 µg/m^3 and 0.7000 µg/m^3, respectively by Theodosi et al; 0.5900 µg/m^3, 1.1900 µg/m^3 and 0.4800 µg/m^3, respectively by Tecer et al., as compared to 0.2119 µg/m^3, 0.5886 µg/m^3 and 0.2671 µg/m^3, respectively by the current study. There was no recording for Al by Kocak et al., 2007b, however, it recorded 1.8900 µg/m^3 and 0.3500 µg/m^3 for Ca and Fe, respectively.

Table 4.7. *Observed concentrations of this study for selected crustal, anthropogenic and marine source species compared with other studies in the literature*

Reference	Measured Species ± SD (μg/m^3)									PM Fraction	Method	Study Background
	Al	Fe	Ca	Si	Pb	S	Ni	Na	Cl			
This Study	0.1257± 0.1523	0.1384± 0.1322	0.3817± 0.3429	0.3020± 0.3332	0.0060± 0.0115	0.5869± 0.5395	0.0021± 0.0015	0.0253± 0.0259	0.0190± 0.0325	$PM_{2.5}$	PIXE	Urban, Turkey
This Study	0.1462± 0.2742	0.1514± 0.1774	0.1804± 0.2531	0.3444± 0.5472	0.0023± 0.0220	0.6659± 0.5816	0.0027± 0.0022	0.0223± 0.0243	0.0151± 0.0096	$PM_{2.5}$	PIXE	Rural, Turkey
Onat et al., 2013	0.6020± 0.1915	0.1173± 0.0438	0.4375± 0.1727	5.4410± 1.9010		0.1105± 0.0494		0.4295± 0.1738	0.0735± 0.0399	$PM_{2.5}$	EDXRF	Urban, Turkey
[a]Smolik et al., 2003	0.0872± 0.0910	0.0377± 0.0522	0.0354± 0.0433	0.2190± 0.2560	0.0092± 0.0055	1.990± 0.7300	0.0016± 0.0007		0.0019± 0.0025	$PM_{1.0}$	PIXE	Coastal, Greece
Tecer et al., 2012	0.0940± 0.2580	0.1300	0.1970± 0.3120	0.2000± 0.5000	0.0119± 0.0070	2.7600± 1.4700	0.0030± 0.0012			$PM_{2.5}$	XRF	Urban, Turkey
Balcilar et al., 2014	0.3373± 0.3470	1.1265± 1.6879	0.5509± 0.7818	0.6307± 1.0810	0.0131± 0.0090	1.8095± 2.5090	0.0086± 0.0051	0.0367± 0.0307		$PM_{2.5}$	EDXRF	Rural (coastal) Turkey
Begum et al., 2005	1.0160± 0.4200	0.3870± 0.4180	0.3010± 0.2270	1.5820± 0.9900	0.2540± 0.4240	2.4640± 1.1720	0.0072± 0.0043	1.0070± 0.3970	0.2190± 0.1040	$PM_{2.2}$	PIXE	Urban, Bangladesh
D'Alessandro et al., 2003	0.156± 0.087	0.771± 0.370	0.651± 0.420	0.466± 0.262	0.130± 0.076	1.282± 0.524	0.007± 0.004	0.232± 0.090	0.120± 0.036	$PM_{2.5}$	PIXE	Urban, Italy
Artaxo et al., 1992	0.0029	0.0002	0.0167	0.0199	0.0007	0.0897	0.0002	0.6688	1.101	$PM_{2.0}$	PIXE	Antartic, Brazil

a. Summer values of the study

An aerosol monitoring study was conducted to measure fine particulate matter ($PM_{2.5}$ and PM_1) concentrations and composition in the urban area of Istanbul, in the north–west of Turkey by Onat et al., 2013. The quantitative analyses of Na, Mg, Al, Si, P, S, Cl, K, Ca, Ti, V, Cr, Mn, Fe, Co, Cu, Zn, As, Rb, Sr, Y, Mo and Ba were performed by Energy Dispersive X–Ray Fluorescence (ED–XRF) spectrometer. Values measured for Al (0.6021 $\mu g/m^3$) and Si (5.411 $\mu g/m^3$), were quite higher than those of the current study which were 0.1257 $\mu g/m^3$ and 0.3020 $\mu g/m^3$, respectively. Al was 5 times higher and Si, 18 times higher. However, values for Ca (0.4375 $\mu g/m^3$) and Fe (0.1173 $\mu g/m^3$) were quite comparable to values measured by this study; 0.3817 $\mu g/m^3$ and 0.1384 $\mu g/m^3$ respectively.

In the study of Artaxo et al., 1992, however, fine (dp< 2.0 μm) and coarse (2.0 μm < dp < 15 μm) atmospheric aerosols were sampled at a Brazilian Antarctic Station using SFU sampler. Concentration of elements Na, Mg, Al, Si, P, S, Cl, K, Ca, Ti, V, Cr, Fe, Ni, Cu, Zn, Se, Br, Rb, Sr, Zr and Pb were measured by Particle Induced X-ray Emission analysis. The report of the study indicates the dominance of sea-salt elements (Na and Cl) in both fine and coarse fractions with average values 0.2884 μg/m3 and 0.5332 $\mu g/m^3$, respectively. These values are 11 and 28 times higher than what were recorded by these 2 species in the current study; of course, the study location is a very important factor; the study area of the current study is very far from the coast and therefore little or no influence by marine sources. Crustal species were however, lower compared to the current study. Al and Ca in the current study were 41 and 23 times higher than the values reported by Artaxo et al., 1992.

Smolik et al., 2003, analyzed air particulate samples by PIXE giving the elemental size distributions and concentrations of of Al, Si, K, Ca, Ti, Mn, Fe, Sr, S, Cl, Ni, V, Cu, Cr, Zn, and Pb. The results of the study to a large extent are comparable to those of the current study. They recorded 0.0870 $\mu g/m^3$ and 0.2190 $\mu g/m^3$ for Al and Si, respectively in the fine mode while in the current study; the measured values were 0.1257 $\mu g/m^3$ and 0.3020 $\mu g/m^3$, respectively. Again, in the fine fraction, Calcium and anthropogenic mixed-source elements (Cr, Zn, Cu and Fe) were relatively lower in Smolik's than the current study; Calcium was 10 times lower while Cr, Zn, Cu and Fe were 3-4 times lower. Similar trend of variation was observed with the coarse fraction.

Begum et al., 2005, also analyzed fine and coarse fractions (0–2.2 μm and 2.2 –10 μm sizes) of airborne particulate samples at a hot spot area of Dhaka using PIXE. Values measured by

this study were very high; higher than all the other studies listed along with the current study. Values recorded for Pb (0.2540 µg/m^3) was striking despite the ban of leaded gasoline in Bangladesh since 1999. This value is about 42 times higher than what was measured by the current study. The authors concluded that, there could be fugitive Pb emissions from battery and other industries. Crustal elements (Al, Si, Fe and K) except Ca were 3-8 times higher, marine (Cl and Na) were 12 and 40 times higher and anthropogenic elements (S, V, Ni, Cu, Zn and Cr) were 3-14 times higher in Begum et al., than the current study. Calcium values were comparable; 0.3010 µg/m^3 for Begum et al and 0.3817 µg/m^3 for the current study. It should be noted that soil im most part of Turkey (current study area) is reported to be calcareous (Tuncel et al., 1997; Al-Momani et al., 1995; Meester, 1971).

Rogula-Kozlowska et al., 2013, investigated the chemical composition of fine particulate matter (PM2.5) in Poland ICP-AES. The mean concentrations of anthropogenic species (As, Ni, Fe, Ti and Pb) measured by Rogula-Kozlowska et al., 2013 in the summer were higher than those of the current study. Lead, Ni and As were 27, 76 and 229 times higher than values measured in the current study. Al concentration from both studies were comparable; 0.1600 µg/m^3 for Rogula-Kozlowska and 0.1257 µg/m^3 for the current study. Marine species (Cl and Na) were however; higher (10 and 30 times, respectively) in Rogula-Kozlowska than the current study. An overview of the variations in the observed elemental concentrations the comparable studies is given in Figure 4.10 below.

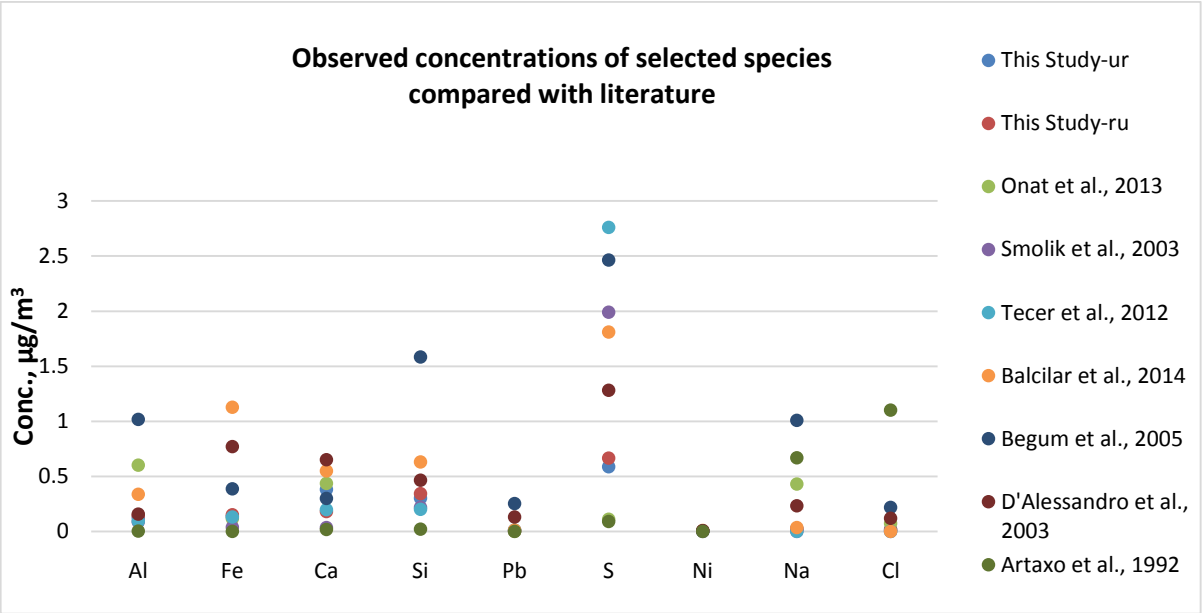

Figure 4.10. *Observed concentrations of selected species compared with other studies; ur and ru represent urban and rural, respectively*

4.2. Source Apportionment

4.2.1. Geoaccumulation index (Igeo)

In Table 4.8 are the calculated Igeo values for each element of $PM_{2.5}$ and $PM_{2.5\text{-}10}$. At both stations and in both fractions of PM, there was no element with Igeo value < 1, which implies there was no deficiency or depletion of any of the measured elements in the study backgrounds. In other words, there were contaminations to certain degrees by the PM elements. At the urban station, only Y and Mo, out of the 26 measured elements had Igeo values < 3, implying they were moderate contaminants. This is understandable as these two trace elements are rarely measured in high concentration in aerosol studies. Elements with Igeo value < 4 were classified as moderate-to-heavy contaminants. These include As, Se, Rb, Sr and Zr, which are clearly anthropogenic species associated with fuel combustion. Vanadium, Cr, Ni, Cu and Br had Igeo value < 5 and therefore classified as heavy contaminants. Thus, being classified as heavy contaminants in urban fine aerosols suggests fuel combustion and traffic emission sources for these elements. Enrichment in the fine fraction may also be related to coal burning as the source for these elements (EPA

SPECIATE, 2014). The last group of elements was those whose Igeo values were ≥ 5. These were extreme contaminants and they include Na, Mg, Al, Si, P, S, Cl, K, Ca, Ti, Mn, Fe, Zn and Pb. These elements are predominantly lithophilic and crustal source. It can be seen in Figure 4.11, that the calculated crustal and marine source enrichments ($Igeo_{crust}$ and $Igeo_{mar}$) distributed the measured PM species into 3 major groups as anthropogenic, crustal and mixed origin sources. A more detailed source apportionment method, PMF, is discussed in the next section.

As stated earlier, Igeo is used as an indicator for determining whether a medium is polluted or depleted of a given pollutant and therefore does not differ in principle from Enrichment Factor application. Due to the common factor of 1.5 in the Igeo formulation, variations in Igeo values of species depends largely on the observed concentration of the species and its background reference concentration. From the results of this study, method of Geoaccumulation index can be said to becomplementary (preliminary) for source apportionment analysis.

Table 4.8. *Calculated Crustal and Marine Geoaccumulation Indices ($Igeo_{crust}$ and $Igeo_{mar}$) for Urban and Rural PM Elements and their Reference Element Concentrations in the Crust, (Mason B. 1966)*

	Urban Station	**Rural Station**

		$PM_{2.5}$		$PM_{2.5-10}$		$PM_{2.5}$		$PM_{2.5-10}$	
Element	**Conc.Ref.**	**$Igeo_{crust}$**	**$Igeo_{mar}$**	**$Igeo_{crust}$**	**$Igeo_{mar}$**	**$Igeo_{crust}$**	**$Igeo_{mar}$**	**$Igeo_{crust}$**	**$Igeo_{mar}$**
Na	28000	7.22	6.16	7.99	6.92	7.10	6.03	7.62	6.55
Mg	20900	7.82	6.75	9.13	8.07	7.64	6.57	8.29	7.23
Al	81300	8.83	7.76	9.93	8.87	8.98	7.91	9.35	8.28
Si	277200	9.70	8.64	10.87	9.81	9.83	8.77	10.27	9.21
P	700	6.03	4.97	6.68	5.61	6.18	5.11	6.14	5.08
S	260	10.37	9.30	9.61	8.54	10.49	9.43	8.85	7.78
Cl	130	6.94	5.87	8.69	7.63	6.71	5.64	8.20	7.14
K	25900	8.51	7.45	9.31	8.25	8.43	7.36	8.57	7.51
Ca	36300	9.94	8.87	11.55	10.49	9.19	8.12	10.37	9.30
Ti	4400	6.52	5.45	7.58	6.52	6.56	5.49	7.15	6.08
V	135	4.73	3.67	5.27	4.21	4.09	3.02	4.26	3.19
Cr	100	4.73	3.67	5.35	4.29	4.87	3.80	5.33	4.26
Mn	950	5.06	3.99	6.05	4.98	5.47	4.41	5.72	4.65
Fe	50000	8.92	7.86	9.95	8.89	9.01	7.95	9.58	8.51
Ni	75	4.73	3.67	5.40	4.34	4.99	3.92	5.50	4.43
Cu	55	4.46	3.40	5.02	3.96	4.09	3.02	4.33	3.26
Zn	70	6.91	5.84	7.11	6.04	6.92	5.86	6.67	5.61
As	1.8	3.64	2.57	3.48	2.42	3.30	2.23	3.08	2.01
Se	0.05	3.08	2.01	2.38	1.32	2.38	1.32	1.69	0.62
Br	2.5	4.95	3.88	4.33	3.26	4.69	3.62	3.30	2.23
Rb	90	3.08	2.01	3.64	2.57	2.79	1.72	3.48	2.42
Sr	375	3.48	2.42	4.69	3.62	3.48	2.42	3.99	2.93
Y	33	2.38	1.32	3.08	2.01	2.38	1.32	2.38	1.32
Zr	165	3.64	2.57	4.18	3.11	3.08	2.01	3.48	2.42
Mo	1.5	2.38	1.32	2.38	1.32	1.69	0.62	2.38	1.32
Pb	13	5.78	4.72	5.78	4.72	4.83	3.76	4.52	3.46

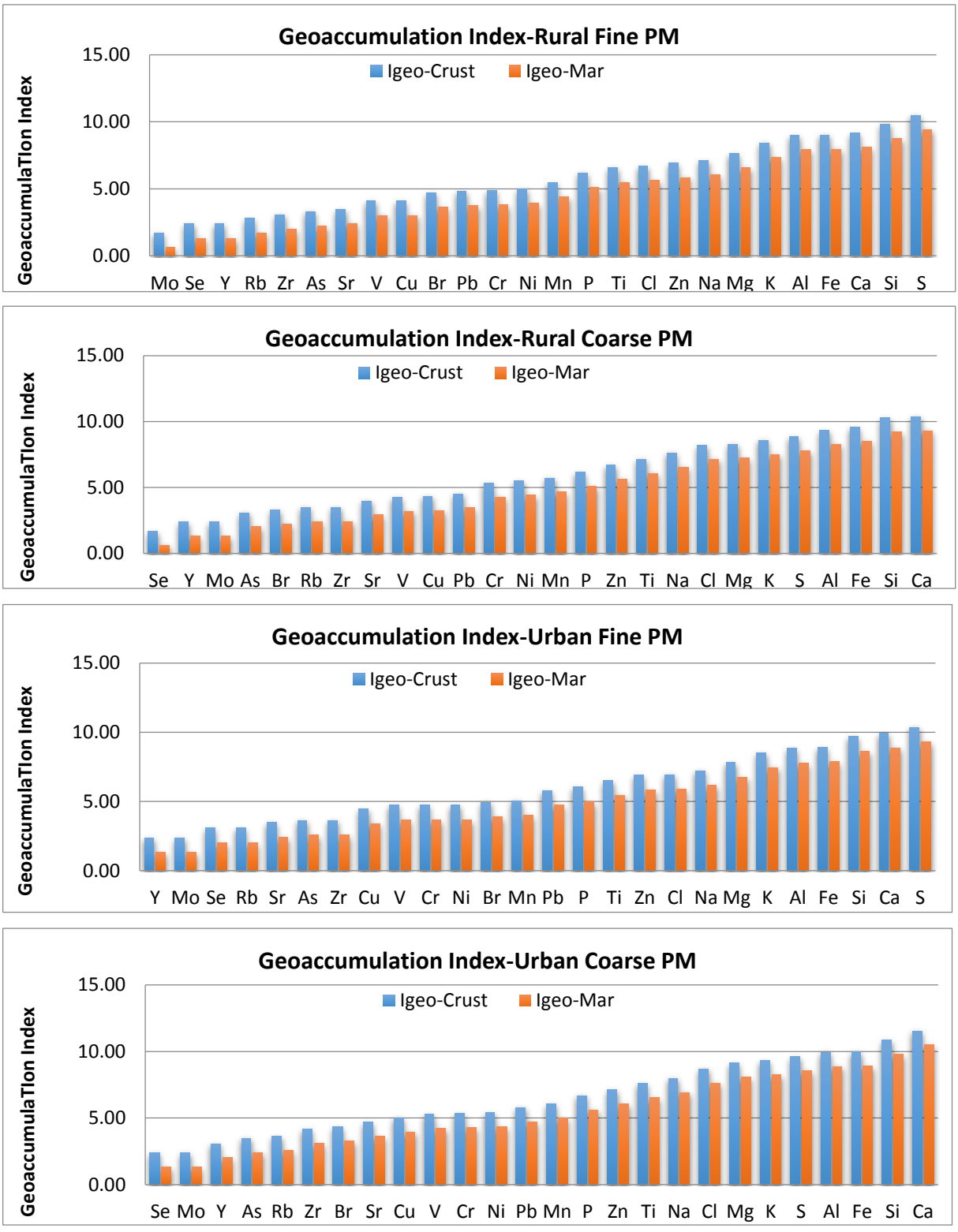

Figure 4.11. *Geoaccumulation indexes for fine and coarse PM metals*.

4.2.2. PMF analysis

4.2.2.1. Identified sources; urban $PM_{2.5}$

Version 5 of EPA's PMF model was used to identify and apportion potential sources of the measured urban and rural $PM_{2.5}$ species. Even though PMF is usually performed on urban fine aerosols, this study considered both rural and urban fine aerosols because of the nature of the rural background of this study; itsclose proximity to theTunçbilek Thermal Power Plant and other industrial facilities (within 5-30 km^2). The study was therefore interested to know the impact of these facilities and also compare with the output of the urban dataset.

Having run PMF model successfully, the generated Base Model Results were carefully analyzed to obtain the final PMF results herein discussed. Parameters such as Residuals, Coefficient of Determination (r^2), Q_{robust}-to-$Q_{theoretical}$ ratio, Factor Contribution (Profiles) and G-score values were the focal points in this analysis and based upon which the factors generated were assigned physical meanings. In this analysis, species missing in more than 25% of samples were categorized as 'bad' and hence excluded for further analysis. However, species with missing values less than 25% were replaced with geometric mean value and 4 times the geometric mean was used as the corresponding uncertainty value for that datum. For species with BDL values, their concentrations were replaced with DL/2 and uncertainties assigned as 5/6xDL. Residuals in the range of ± 3 were regarded as good, residuals greater than ±3 but less than ±5 were labelled as 'bad' whilst those greater than ± 5 were regarded as poor and therefore extracted from the data.

Fpeak effect was controlled by checking the G score correlations between the factors. Fpeak range set for this study was ±1.0. Q was found to be stable at 0.2and therefore the Fpeak value was finally set to 0.2. $Q_{theoritical}$ value obtained was 16194.8 which was close to Q-value of 19192.8 from the model.

Signal-to-noise ratio (S/N) which indicates whether the variation in the measurements was real or within the noise of the data was calculated based on Eq. 4.1. Species with low S/N ratio and/or high percentage of data below detection will likely not provide enough variability in concentrations to meaningfully contribute to factor identification but rather

contribute to the noise in the results (EPA/600/R-14/108). In this study, species were categorized according to Paatero and Hopke

(2003). Species were categorized as 'bad' if the S/N ratio was< 0.2 and 'weak' if S/N ratio was > 0.2 but < 2.

$$(\frac{S}{N})_j = \sqrt{\frac{\sum_{i=1}^{n}(X_{ij}-S_{ij})}{\sum_{i=1}^{n} S^2{}_{ij}}} \quad (4.1)$$

Where Xij is the jth species measured concentration of the *ith* sample and *Sij* is the species corresponding uncertainty. Species with concentrations constantly below their uncertainty are known to have an S/N ratio of 0 while those with concentrations that are twice the uncertainty value have an S/N ratio of 1. S/N ratio greater than 1 often indicates a species with "good" signal, though this depends on how uncertainties were determined (EPA/600/R-14/108).

Seven factors were finally considered after carefully examining the base model results with emphasis on goodness of fit of the model to the original data. As shown Figure 4.12, the average source contribution to the elemental concentration (µg/m^3) are shown on the left y-axis (blue column) whiles the percentages of the elements shown on the right y-axis (red squares). The seven generated factors were categorized into three group sources.

Group 1:

Group 1 identified as crustal/dust source group was driven mainly by litophilic species. It comprises 2 factors; factor 1 and 2. Factor 1 is dominated by Al (48.4%), Si (46.4%), Ti (45.3) and Rb (45.7%). To a less extent, Fe (37.6 %) and Sr (35.7%) were also explained in this profile. Factor 1 is therefore described by this study as a 'soil dust' (S.D) source. A profile similar to factor 1 was observed by Dall'Osto et al., 2012, in which the profile was attributed to the Saharan dust due to North African Tropical air masses. Factor 2 of group 1 was dominated by Ca (51.1%), Ti (30.2%), Sr (37.7%), Fe (30.9%) and Mn

(30.1%). These species are typical of urban fine aerosol components from soil re-suspension, erosive processesand civil constructions. It was thus, called ‘urban dust’ (U.D) source.

Group 2:

Group 2 was called regional/local source group. This group is made up of 2 factors; factor 3 and 4. Factor 3 was dominated by Mg (62.4%) and Na (55.3%), which are typical sea salt species. It is quite doubtful factor 3 is a sea salt profile since either of the receptors of this study is located anywhere near the sea. It is important to note that fertilisers and liming are anthropogenic sources of Mg (Reimann and de Caritat, 1998) and in many industrial productions, Mg is used as a reducing agent. Also, Mgis a lithophile and a major constituent of many mineral groups, including silicates, carbonates, sulphates, phosphates and borates (Wedepohl, 1978).

Based on this background, factor 3 was identified as ‘industrial source’ (I.S.). Chlorine was deficient in terms of factor loading (15.4%) despite its appreciable concentration in this component; likewise, its presence was suspected to be due to industrial emission due to potential anthropogenic sources including human sewage, livestock wasteand synthetic fertilizer, primarily KCl (Schlesinger, 2004), refer also to Group 3 factor 7. It is worth noting that air masses passing over the sea or advecting below the boundary layer pick up sea salt more effectively and transfer to a receptor location. Thus, a possibility of observing a typical marine component at a receptor located far away from the sea; proximity is, however, essencial.

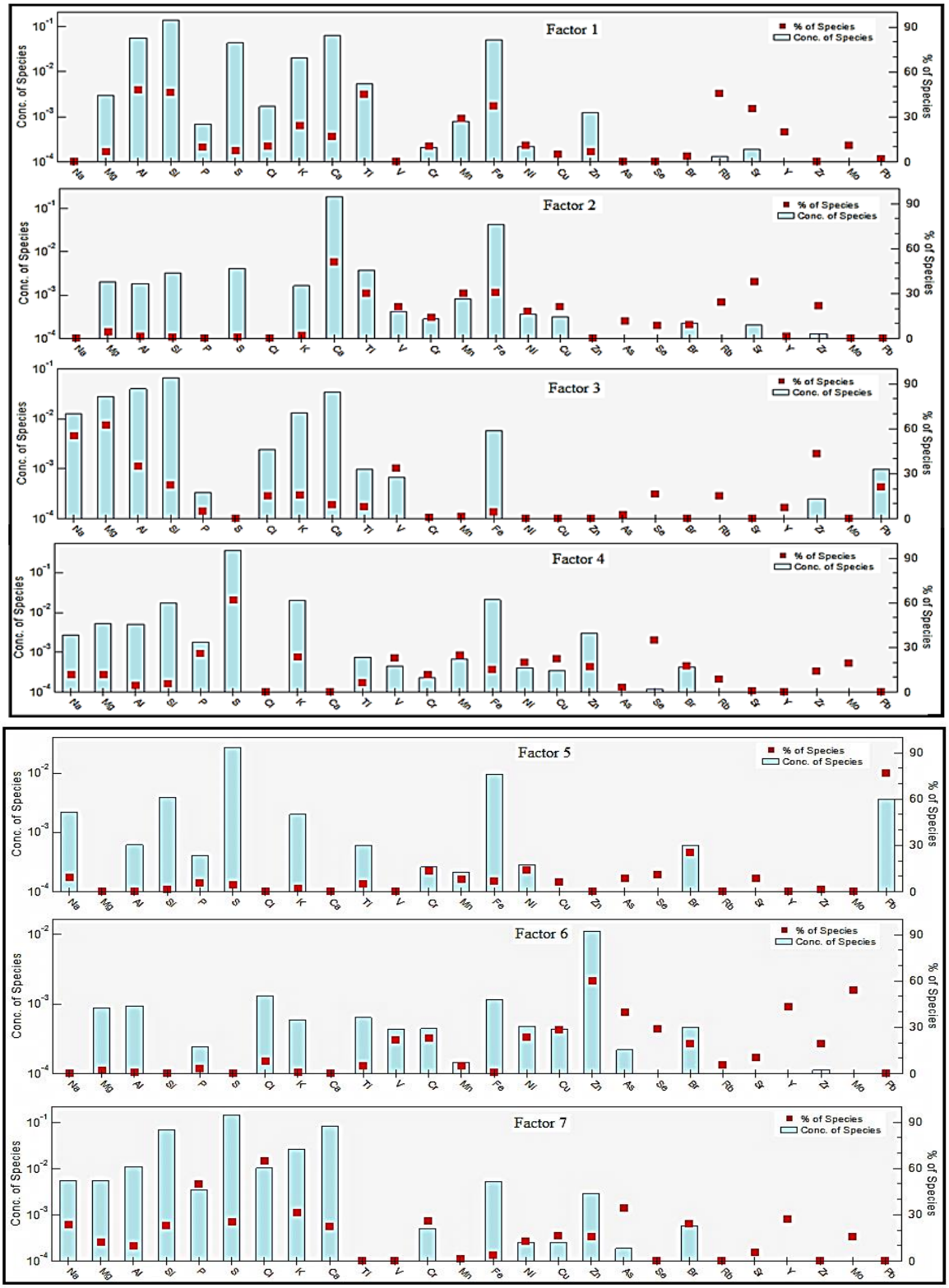

Figure 4.12. *Resolved PMF factors and their elemental compositions (concentration in μg/m^3)*

Factor 4 was characterized by sulfur (61.8%) attributed mainly to aged/secondary sulfates in the atmosphere due to coal combustion. The factor was thus, described as 'local sulfate' (L.S.). Though most part of the region by way of energy policy have switched from the use of coal source fuel to natural gas for space heating during the winter season (November-April), continual operation of the 3 coal-fired thermal power plants in the region make it as a sulfur–polluted region. This assertion is supported by various analysis of the current study including, measured mass concentration, crustal enrichment factor based onGeoaccumulation index, all of which recorded highest Sulfur concentration in the fine PM fraction.

Group 3:

The third and final group was called anthropogenic source group. The group was driven mainly by industrial emissions; fuel and heavy oil combustion. It comprises 3 factors; factor 5, 6 and 7. Factor 5 was dominated by Pb (76.9%) and to a less extent Br (25.4%). Although Pb is no longer a component of gasoline for over 2 decades in Turkey, the presence of Pb in road dust is well documented in Turkey and abroad (Hosiokangas et al., 1995; Z Zhou et al., 2013; Soylak and Turkoglu, 1999; Arslan, 2001; Aksoy et al., 2005 and Ozkan et al., 2005). Other sources of Pb in the atmosphere include non-exhaust vehicular sources such as Pb battery and and the brake system. Bromine is known to be associated with biomass and solid waste burning (Z Zhou et al., 2013) and has been found to correlate; strongly (Paciga et al., 1975) and moderately (Vehlow et al., 2003; Apeagyei et al., 2011 and Zhou et al., 2013) with Pb from automobile emissions. Given the huge percentage difference between these two species explained by factor 2, it can be said Bromine's presence in this profile is due to combination of mixing and transport from elsewhere to the receptor. Factor 5 was therefore called 'residual lead' (R.L.) by this study.

Factor 6 was dominated by Zn (60.2%) along with As (39.6%), Cu (28.7%), Ni (23.8), Cr (22.7%) and V (21.7%). Zinc is associated with vehicular traffic with its main sources from tire and brake ware, industrial and biomass burning. It is also well documented as a mixed-source element. Being profiled along with oil combustion markers (V and Ni) as well as crustal markers (Cr and Cu) and the fact that their emissions accumulate onto dust surfaces

make their presence in the atmosphere linked to road dust (Amato et al., 2009, Sternbeck et al., 2002, Thorpe and Harrison, 2008). This qualifies factor 6 as being a re-suspended dust source and therefore called 'roadside dust' (R.D.) source.

The third factor of group 3, factor 7, was characterized by Cl (65.2%), P (50.3) and As (34.3%). Again, Cl in this profile is believed to be anthropogenic due to the location our receptors. It has been reported in relation to nonferrous smelters that, fine aerosols in industrial atmospheres are quite enriched in Cl, (Tan et al., 2002). Lead Chloride, due to its relatively low boiling point, is preferably emitted in the gas phase of high temperature combustion sources such as waste incinerators (Hu et al., 2003). Furthermore, man-made organic chlorine compounds, such as carbon tetrachloride and methyl chloroform are some major sources of Cl in the atmosphere. Also, Cl is present in many industrially produced volatile organic compounds and bleach, but most of which are decomposed by the natural oxidants in the troposphere, and the chlorine atoms in those compounds eventually become HCl or other soluble species. Industrial emission is therefore suspected to be the main contributor to factor 7 and thus identified as 'industrial source' (I.S.). Factor 7 also explained to a lesser extent some litophilic (Na-23.4% and Si-23.2%) and anthropogenic (S-25.4%, Cr-26.1% and Br-24.2%) species which are all associated to combustion activities. Concentrations of the litophilic species explained were appreciably high and therefore can be said to have some physical impact on this factor. In contrast, concentrations of the anthropogenic species in this profile were negligibly low, suggesting their non-impact on the factor even though they were detected in the aerosol component. The presenceof crustal and anthropogenic species together in an industrial profile is an evidence of the interaction between aerosol components during their transport to the receptor.

4.2.2.2. Identified sources; rural $PM_{2.5}$

PMF analysis of the rural $PM_{2.5}$ data was done using the same criteria as in Section 4.2.2.1 for the urban $PM_{2.5}$ data. Likewise, seven factors were finally resolved by PMF and subsequently classified into 3 main groups.

Group 1:

Group 1, made up of factors 1, 2 and 3 was identified as 'crustal group' due to dominance of crustal species in the three resolved factors. Factor 1 was dominated by Al (75.2%), Si (67.5%), Mg (61.1%) and Sr (51.7%). Based on this profile, factor 1 was described as soil dust (S.D) source. Factor 2 was dominated by Zn (59.2%) and Cu (30%) which are related to non-exhaust vehicular emission and crustal source, respectively. Geoaccumulation index (Igeo) value for Cu was found to be > 4 which signifies a heavy contamination in the soil/dust sources. Igeo value for Zn was > 5 which signifies extreme contamination in the soil/dust sources. On the basis of this, factor 2 was described as roadside dust (R.D1) source. Factor 3 which was also described as roadside dust (R.D2) source was characterized by Ca (45.8%), Mn (37.4%), V (27.9) and Ti (27.4).

Group 2:

Group 2, identified as 'mixed-source group' comprises only factor 4. Nickel (52.1%), Cr (39.5%), As (33.7%) and Se (32.9%) were the dominant species in this factor. These species are well related to both oil and coal combustion and therefore the factor was referred to as fuel combustion (F.C) source.

Group 3:

The third and final group of the rural background data was identified as 'anthropogenic group'. It comprises three factors, factors 5, 6 and 7. Factor 5 was dominated by Pb (68.4%) and to a lesser extent K (28.8%). This factor was duly described as a residual lead (R.L) source. Factor 6 was dominated by sulfur (57.6%) believed to be generated locally by coal-fired power plants located in the region and from domestic space heating. This factor is named 'local sulfur' (L.S) source. Factor 7 was characterized by anthropogenic species including As (63.5%), Cl (50.7%), Br (45.1%) and P (37.7%). These species are suspected to originate from various anthropogenic activities in the region; Arsenic is associated with coal combustion, Cl and P are both related to fertilizer production while Br is from biomass burning. Factor 7 was therefore identified as industrial source (I.S.).

4.2.2.3. Factor contribution and inter-site comparison

Contribution of resolved PMF factors to the mass concentration of fine PM constituents in the urban and rural stations are summarized in Table 4.9 and graphically in Figure 4.13. The highest contributing factor to PM mass concentration at the urban area was factor 4 (25.3%), also known as 'local sulfate' source. This same factor resolved at the rural area was however, the third highest contributor (12.2%) to PM mass concentration. Roadside dust was found to be the second highest contributor to PM concentration at both the rural (28.7%) and the urban (22.4%) areas. The third highest factor at the urban station called 'industrial source' contributed 21.6% to PM mass concentration and was dominated by Cl (65.2%), P (50.3%) and As (34.4%). At the rural area, however, 'local sulfate' was the third highest contributor to PM mass concentration. It contributed 12.2% with S (57.6%) as the dominant species. Factor 4, characterized by fuel and heavy oil combustion markers was the highest factor contributing to PM mass concentration at the rural station. Arsenic is documented as a tracer for fossil fuel combustion (Morawski and Zhang, 2002); coal and oil combustion are known to be important anthropogenic sources of Se in the atmosphere (Mosher and Duce, 1987; Lantzy and Mackenzie, 1979; Nriagu and Pacyna, 1988). Selenium in $PM_{2.5}$ is typically associated with combustion of coal; a primary pollutant released from burning coal (Pekney et al., 2006). Being a member of the Sulfur group (the Chalcogens), Se is expected to follow similar chemical pathways as Sulfur makingfactor 4a fossil fuel combustion source. It should be noted that, factors F1, F2 and F6 of the urban PM profile are all crustal origin and therefore when summed up together contribute 26.56% to PM mass concentration. Likewise, in the rural PM profile F1, F2 and F3 are all of crustal origin; all together contribute 40.97% to PM mass concentration whilst industrial sources in the urban profile, F3 and F7 together contribute 33.6%.

Table 4.9. *Resolved PMF factors and their contributions to PM mass concentrations at the two sampling stations.*

Factor	Factor Name		Factor Contribution (%)	
	URBAN	**RURAL**	**URBAN**	**RURAL**
F1	Soil Dust (S.D)	Soil Dust (S.D)	1.14	7.25
F2	Urban Dust (U.D)	Roadside Dust (R.D1)	2.98	5.07
F3	Industrial Source (I.S2)	Roadside Dust (R.D2)	12.04	28.65
F4	Local Sulfate (L.S)	Fuel Combustion (F.C)	25.34	35.31
F5	Residual Lead (R.L)	Residual Lead (R.L)	14.51	3.14
F6	Roadside Dust (R.D)	Local Sulfate (L.S)	22.44	12.25
F7	Industrial Source (I.S2)	Industrial Source (I.S)	21.56	8.33

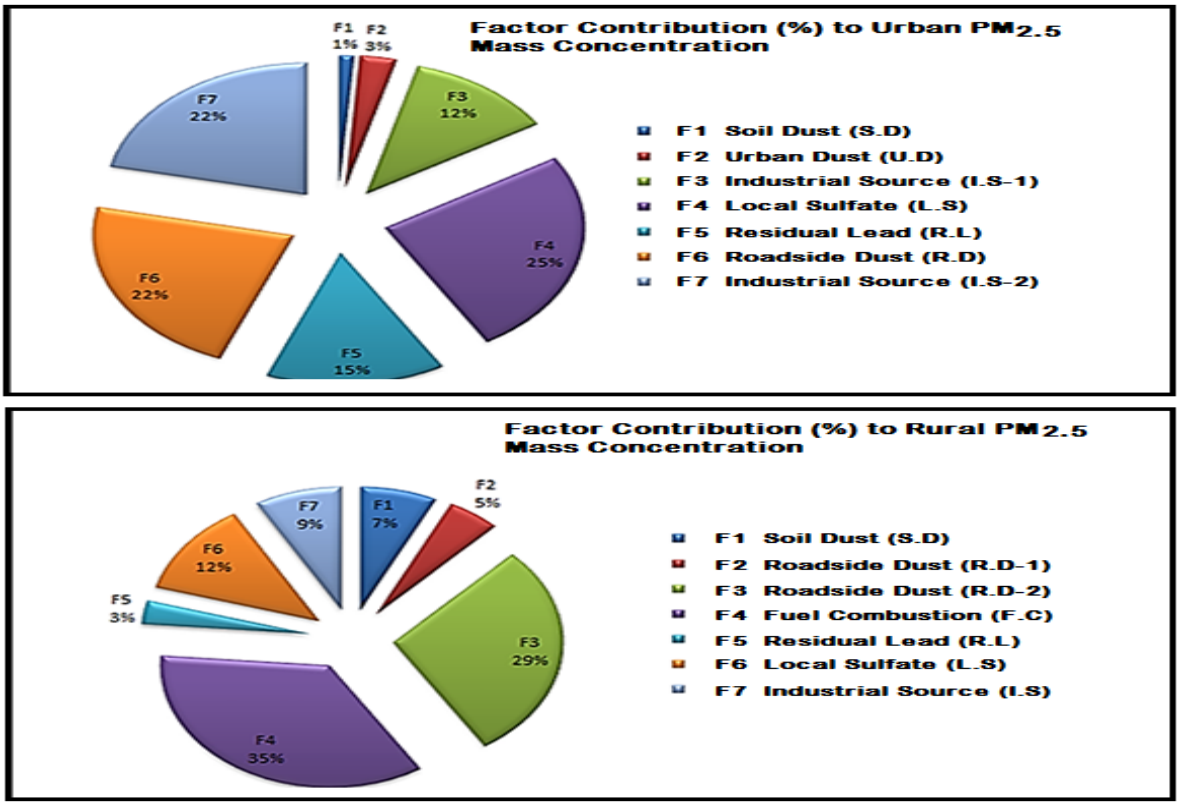

Figure 4.13. *Factor contribution to urban and rural PM mass concentration*

4.3. Potential Source Location

Back trajectories of the air masses arriving at the rural and urban stations were obtained for each day of the campaign period. Five-day archived back trajectories were run using HYSPLIT, modulated by the on-line Real-time Environmental Applications and Display sYstem, (READY). Air mass trajectories that follow the movement of the wind patterns defined by the meteorological models can be produced (READY, 2017).

Three different air mass altitudes representing the transport layer and arrival heights of the trajectories were selected for this study. The lowest and highest altitudes were 100 m and 1400 m, respectively above ground level (AGL). 700m was chosen as the intermediate altitude. It is assumed that 700 m is an average mixed layer depth at which the potential temperature starts to increase. In Figure 4.14, the red, blue and green lines represent the lowest, intermediate and the highest trajectories, respectively. As can be seen, the highest altitude trajectory (1400 m) is the air mass that travelled the farthest from the north-western neighborhood of Turkey – from Romania through Bulgaria to Greece before reaching the receptor locations. The lowest (100 m) and intermediate (700 m) trajectories reaching the stations, however, travelled relatively shorter distances and were found to becoming from the north-east and south-east across the Caspian Sea. All trajectories at both stations showed similar patterns atthe starting altitudes. It can be confirmed that the 100 m and 700 m trajectories reaching the rural stations have a common source; traversing together from Azerbaijan, Georgia and perhaps from the Central Asian countries of Uzbekistan and Turkmenistan before reaching the receptor. At the urban station, these trajectories (100 m and 700 m) were seen as local air masses from the south-west and north-east of Turkey. Thus, pollution due these air masses is locally generated. Earlier studies hypothesized that sources affecting chemical composition of particles in the Eastern Mediterranean atmosphere are traced back to neighboring countries, particularly the Balkans and Ukraine (Dogan et al., 2010, Gullu et al., 2005).

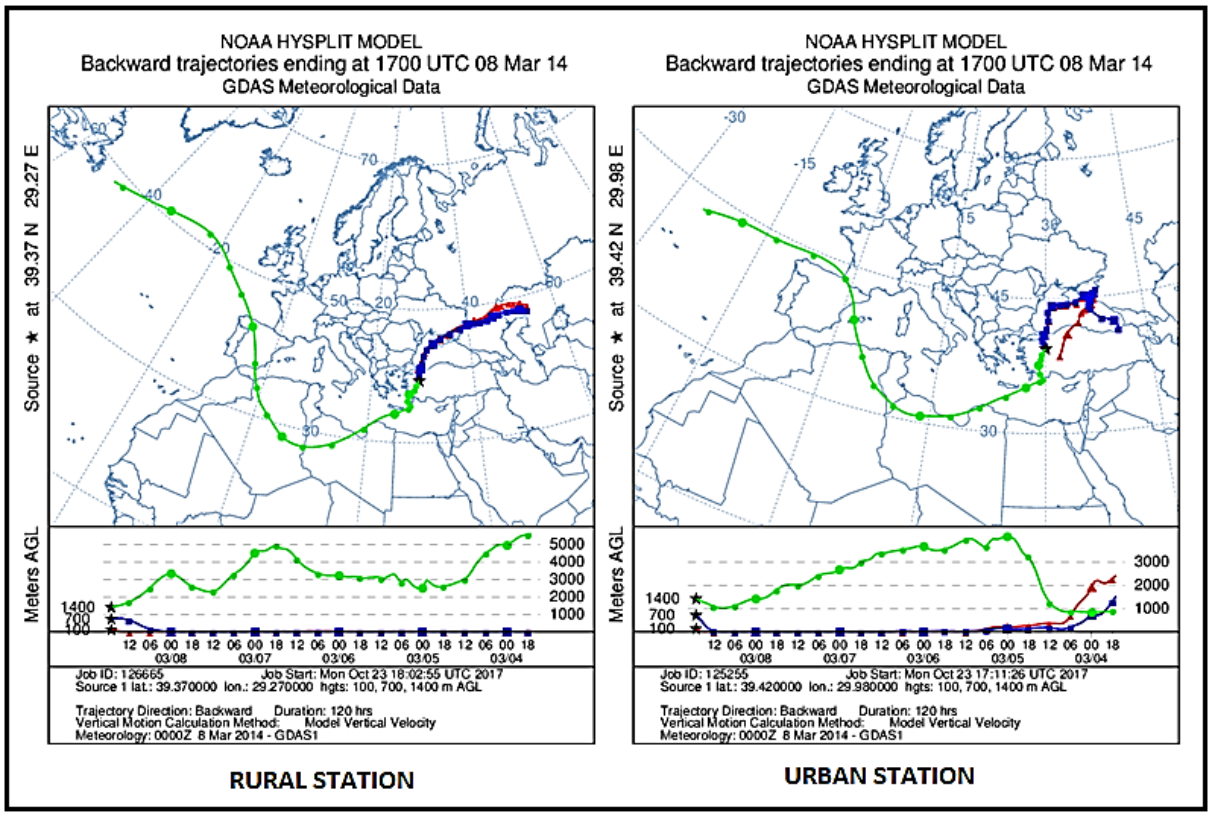

Figure 4.14. *Back trajectory of air masses reaching our rural and urban stations at 100m, 700m and 1400m*

Trajectory frequencies:

Due to 'industrial nature' of the study location, this study did not apply potential source contribution function (PSCF) but rather used trajectory frequencies from the HYSPLIT model to explain the air mass volume and pollution density over domains the trajectories traversed. This method also enables us to differentiate locally generated pollution from those generated from outside the boarders of Turkey.

Trajectory frequencies were generated by the HYSPLIT model with same meteorological inputs except that the highest trajectory height was changed from 1400 m to 1500 m. For each altitude, four trajectory frequency charts were generated, in 0, 1, 2 and 3 minutes of trajectory frequencies.

Trajectory frequencies for 0, 1, 2 and 3 minutes were calculated by the model using the following Eq. 4.2-5, with frequency grid resolution of 1.0 x 1.0 degrees.

$$Trajectory\ Freq.0 = \frac{n_j}{N_j}.100 \quad (4.2)$$

$$Trajectory\ Freq.1 = \frac{e_n}{N_j}.100 \quad (4.3)$$

$$Trajectory\ Freq.2 = \frac{e_n}{E_n}.100 \quad (4.4)$$

$$Trajectory\ Freq.3 = \frac{e_n}{e_{max}}.100 \quad (4.5)$$

Where n_j, is the number of trajectories passing through each grid square, N_j is the total number of trajectories, e_n is number of endpoints per grid square, E_n is total number of endpoints and e_{max} is maximum number of endpoints in any grid square. It is worth noting that there was no residence time in grid cell and that each trajectory was only counted once per grid cell.

The generated trajectory frequency charts are given in Figure 4.15-20. It was observed that, air masses closer to the ground were more polluted than those far away. No major variation was observed between the trajectory frequencies of the rural station and those of the urban station. The most polluted air mass (between 70% and 90% or greater) in the yellow to the red bandswere those of 0 and 1-minute trajectory frequencies. As can be seen from these charts, the most densely polluted air masses (>70% - >90%) are locally generated, i.e. from within the study region. Although air masses carried pollutant materials from outside the boarders of Turkey; mainly from the north-eastern neighborhood across the Black Sea – from Romania, Bulgaria, Macedonia, Albania to Greece and from the western side of the Black Sea, Georgia and south of Russia. Contributions fromcountries in the east i.e. Bulgaria, Macedonia and Albania are in the range of 1%-10%in the purple to the blue bands whilst contribution from Greece, the closest country is in the range of 10% to 20%. An important observation was about the effect of trajectory height (altitude) on pollution density.

Volume of air masses as well as the distances covered by trajectories was found to increase as altitude increases. Thus, the volume of air masses and the distance covered by their trajectories at 1500 m was greater than those of 700 m and 100 m. This actually explains why pollution density (concentration) from the farthest countries are are less compared to the nearby countries and at the receptor locations. It can also be seen from the frequency charts that contributions from Middle Eastern countries like Syria and Iraq are quite significant, being in the range of 20% and 30%. Contribution from western neighboring countries like Georgia, Armenia and Azerbaijan are also in the low range of 1%-10%.

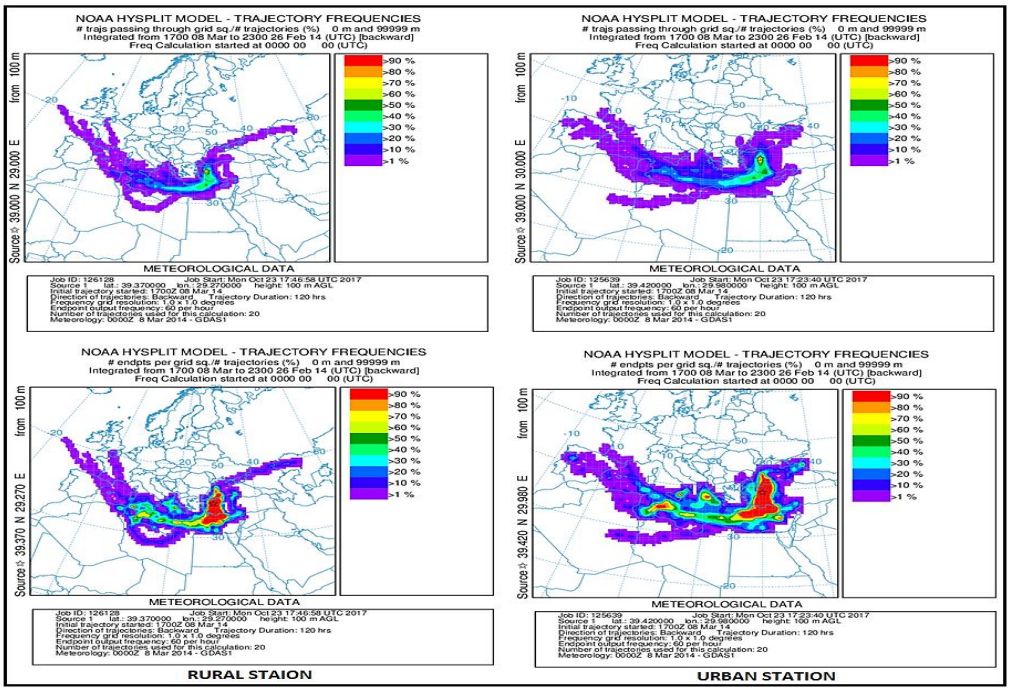

Figure 4.15. *Trajectory frequencies (0 and 1 minute) at 100 m altitude for rural and urban stations*

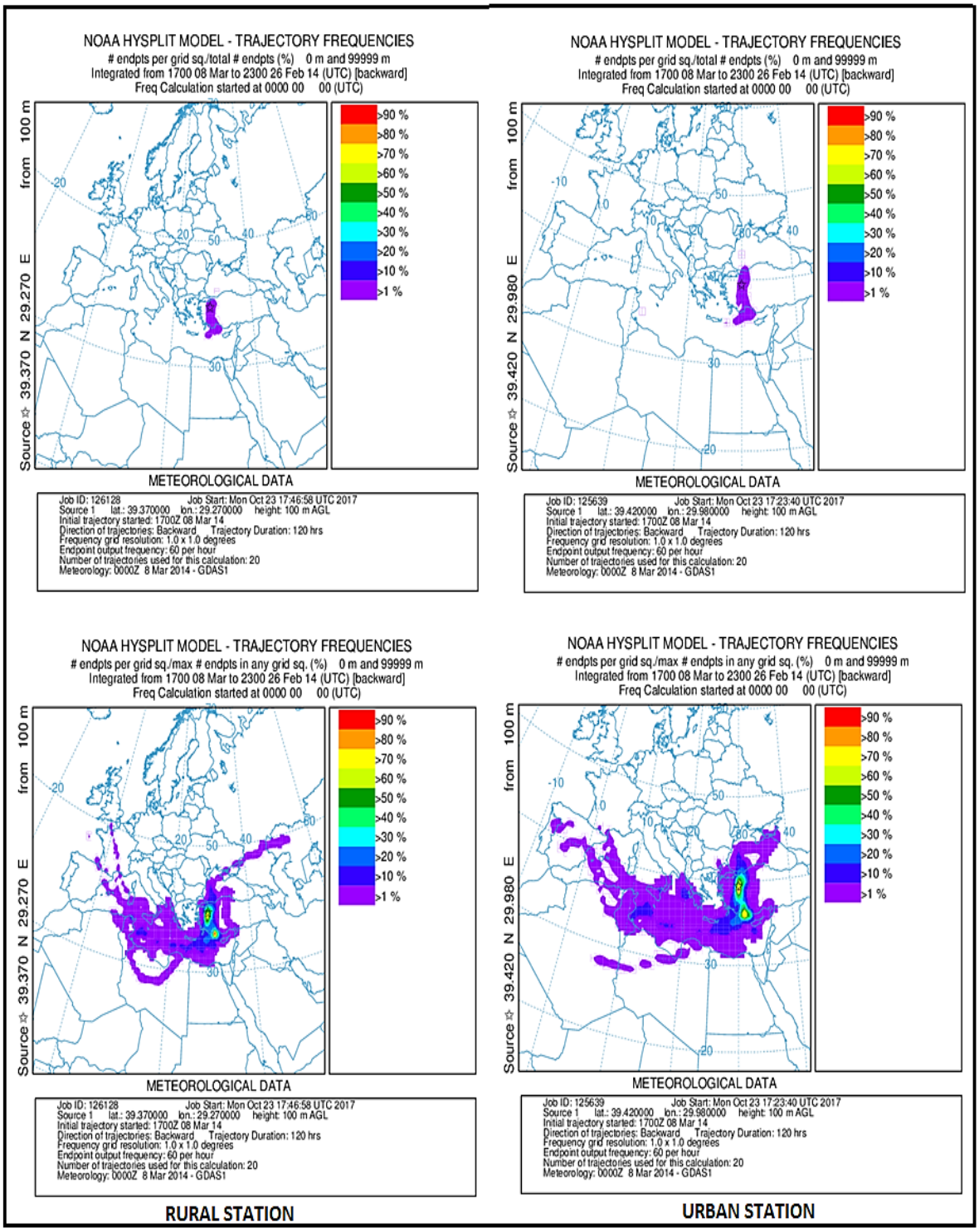

Figure 4.16. *Trajectory frequencies (2 and 3 minutes) at 100 m altitude for rural and urban stations*

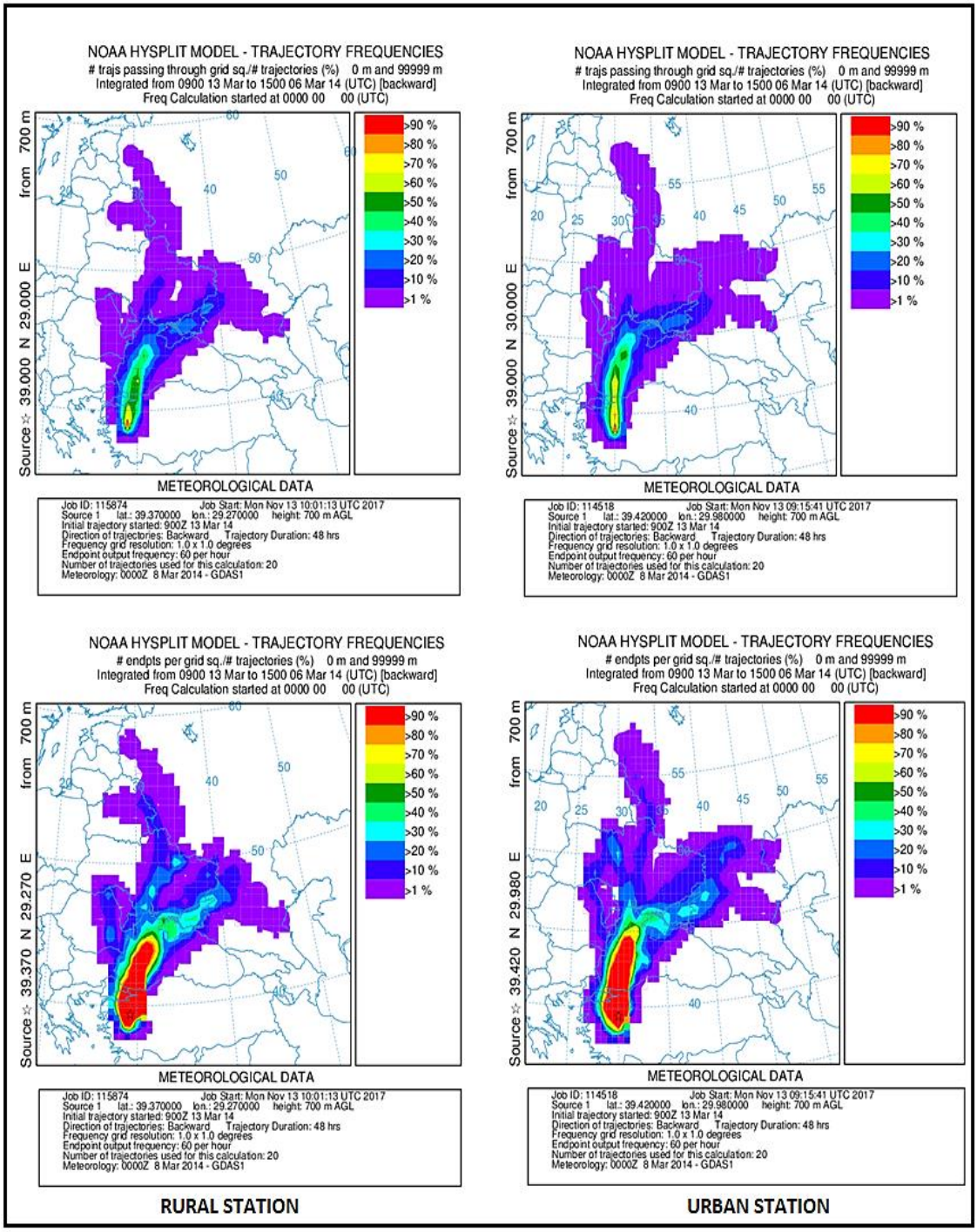

Figure 4.17. *Trajectory frequencies (0 and 1 minute) at 700 m altitude for rural and urban stations*

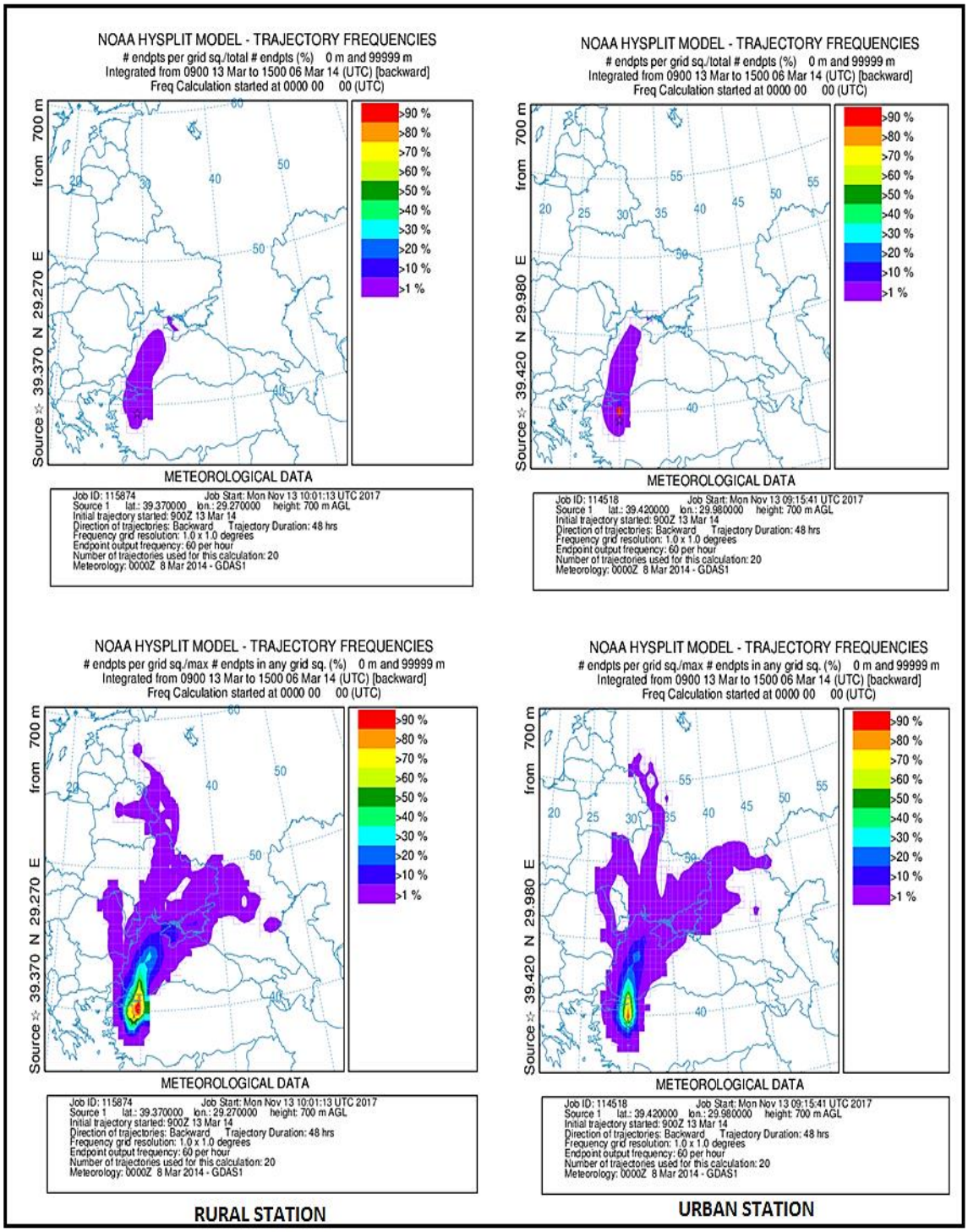

Figure 4.18. *Trajectory frequencies (2 and 3 minutes) at 700 m altitude for rural and urban stations*

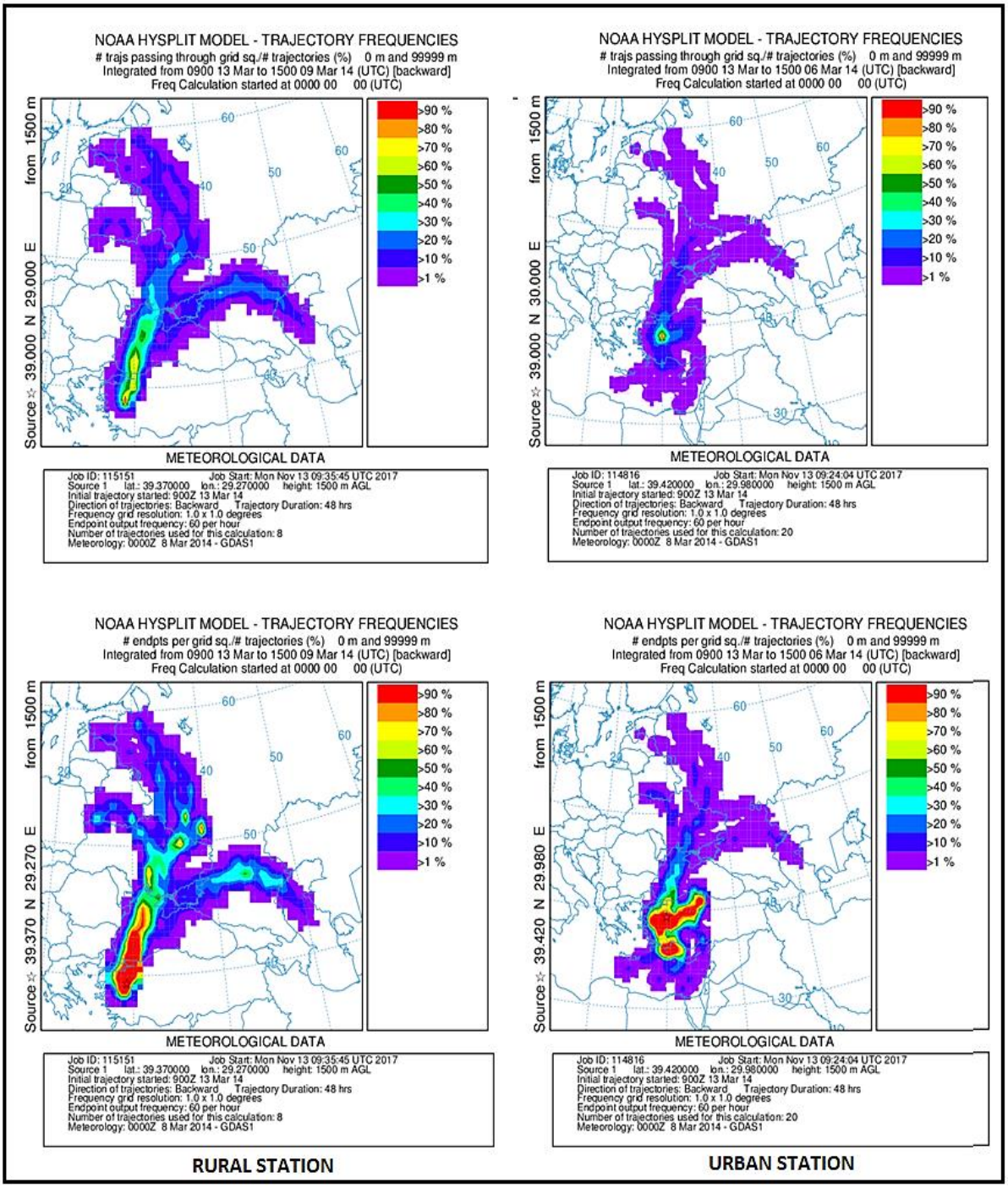

Figure 4.19. *Trajectory frequencies (0 and 1 minute) at 1500 m altitude for rural and urban stations*

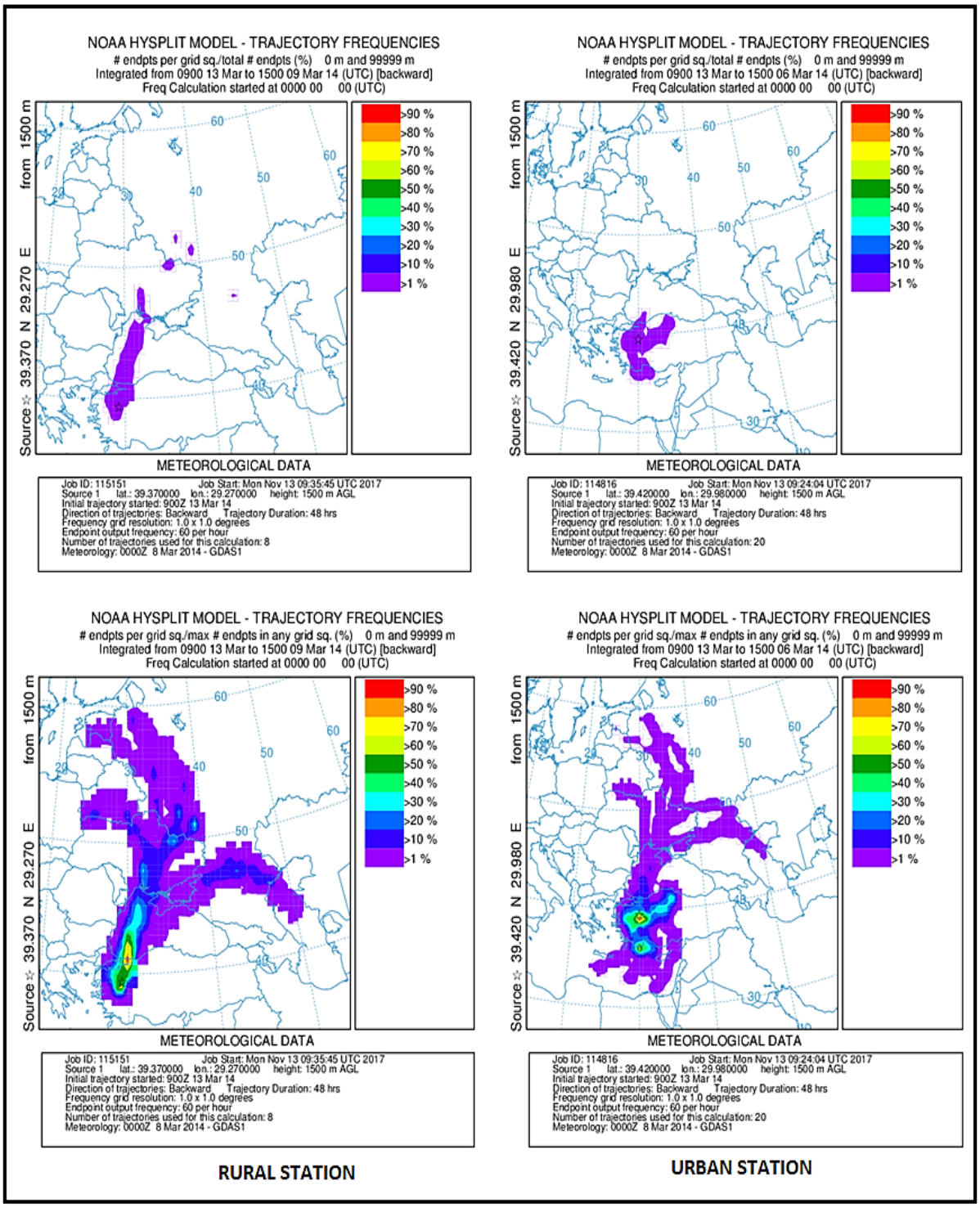

Figure 4.20. *Trajectory frequencies (2 and 3 minutes) at 1500 m altitude for rural and urban stations*

Source contributions:

Air mass trajectories and wind directions observed at the rural station during the study period were further investigated to ascertain source contributions to observed concentrations of anthropogenic species. Thus, contributions by short distance sources i.e. locally generated pollutants via wind roses and long distance sources i.e. sources transported to the receptor from elsewhere beyond the borders of Turkey were determined and analyzed. In the wind rose approach, sampling days were sorted from the highest to the lowest observed concentration days for anthropogenic species including S, As, V and Se; all of which are related to coal and oil combustion. Based on Hopke et al., 2004, 25% of the data comprising highest observed concentrations and corresponding wind directions for each day were used to generate wind roses. 24 hr. wind direction data were obtained from the Kutahya meteorological station based close to the rural monitoring station at Tuncbilek. The resultant vector was calculated in the WRPLOT program and 16 daily wind directional sectors were obtained. Given in Table 4.10 and Figure 4.21 are the summary results for wind directions obtained per day for the selected elements and their corresponding wind rose charts, respectively.

Table 4.10. *Wind directions during sampling days and corresponding 25% highest anthropogenic species concentration*

		S		As		V		Se	
Wind direction	**Total wind count**	**25% wind count**	**25%/total ratio**	**25% wind count**	**25%/total ratio**	**25% wind count**	**25%/total ratio**	**25% wind count**	**25%/total ratio**
N	72	23	0.32	11	0.15	18	0.25	18	0.25
NNE	57	24	0.42	13	0.23	13	0.23	16	0.28
NE	81	17	0.21	34	0.42	19	0.23	29	0.36
ENE	114	21	0.18	42	0.37	25	0.22	26	0.23
E	196	59	0.30	65	0.33	39	0.20	55	0.28
ESE	264	75	0.28	63	0.24	76	0.29	72	0.27
SE	147	44	0.30	28	0.19	42	0.29	53	0.36
SSE	49	11	0.22	9	0.18	15	0.31	13	0.27
S	58	6	0.10	14	0.24	14	0.24	8	0.14
SSW	50	7	0.14	11	0.22	17	0.34	16	0.32
SW	158	33	0.21	39	0.25	37	0.23	41	0.26

Table 4.10 (Continued). *Wind directions during sampling days and corresponding 25% highest anthropogenic species concentration*

		S		As		V		Se	
Wind direction	**Total wind count**	**25% wind count**	**25%/total ratio**	**25% wind count**	**25%/total ratio**	**25% wind count**	**25%/total ratio**	**25% wind count**	**25%/total ratio**
WSW	276	64	0.23	66	0.24	74	0.27	55	0.20
W	316	74	0.23	95	0.30	86	0.27	61	0.19
WNW	252	74	0.29	53	0.21	67	0.27	63	0.25
NW	127	47	0.37	29	0.23	34	0.27	35	0.28
NNW	80	25	0.31	8	0.10	11	0.14	25	0.31

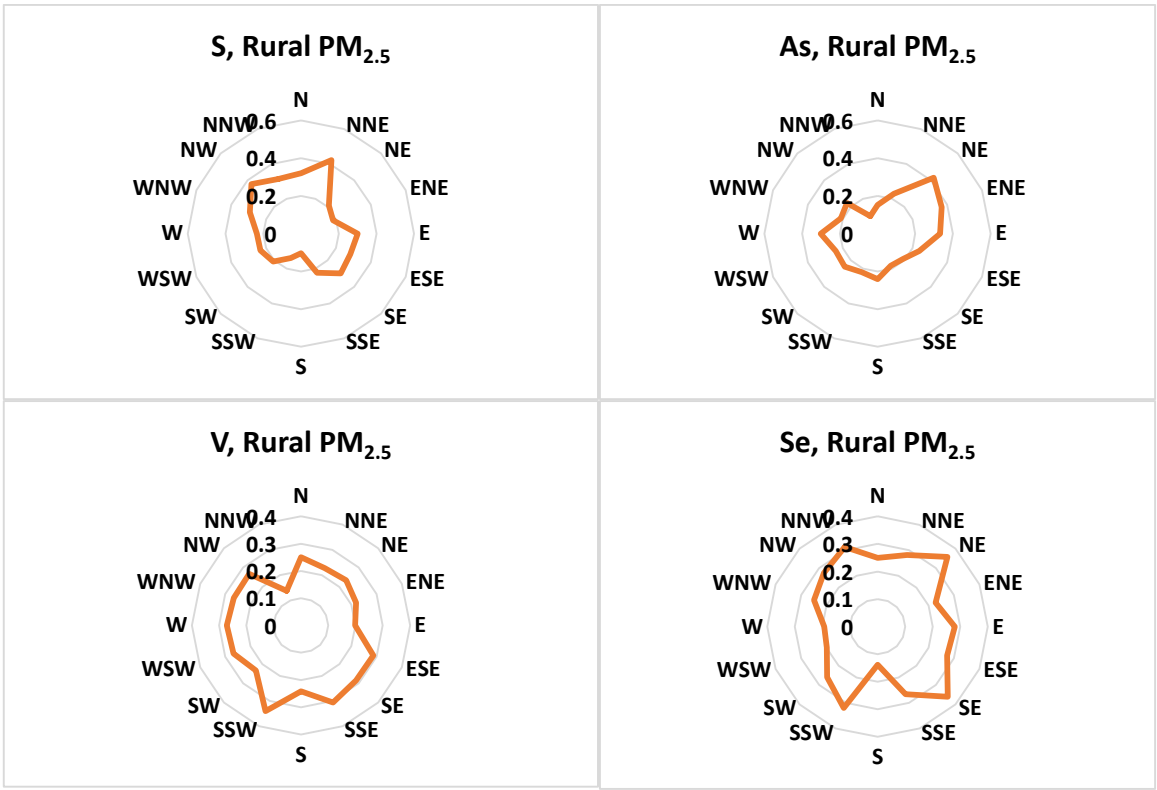

Figure 4.21. *Wind rose charts for the highest 25% observed mass concentrations of anthropogenic species in the rural $PM_{2.5}$*

As can be seen from the wind rose charts above, the highest concentrations of S, As and Se corresponded to NNE, NE and NE wind directions, respectively. These results are quite the expected given the locations of industries with respect to the two monitoring

stations. Approximately 15 km north of the rural station is Tuncbilek Coal-fuelled Power Plant, Gumus Mining is ~12 km north-east and Bor Mining is ~8 km south-west. Interestingly, these three species are coal combustion related species. In a related study (Can et al., 2016), anthropogenic species including As, S and Se had their highest 25% observed concentrations in the ENE, NE and N sectors, respectively. These outlooks are actually similar to those of this study and they both confirms the effects of local sources especially the thermal power plants on air quality in the region. For V, its highest observed concentration in this study corresponded with SSW followed by ESE wind directions. Being a major heavy fuel source species, V concentration might be due to mobile sources such as diesel engine vehicles from the neighboring industrial operatives.

For long range transport, trajectories of air masses at 100 m, 700 m and 1500 m altitudes arriving at the receptor were obtained after running HYSPLIT for four different days of each month of the study period (March 2014-February 2015). Using ArcGIS, the domain of the receptor was gridded into a 5º x 5 º cells and subsequently zoned into 8 directional sectors as north (N), north-east (NE), east (E), south-east (SE), south (S), south-west (SW), west (W) and north-west (NW) shown in Figure 4.22. Source contribution was determined by first determining the number of times an air mass traversed a sector before being intercepted.

Divisions of the receptor domain placed countries like Bulgaria, Romania and Serbia in the NW sector; Greece, Albania and Macedonia in the W sector; the Saharan African Region in the S sector; Syria, Iraq and Iran in the SE sector; Armenia and Azerbaijan in the E sector and Georgia south of Russia in the NE sector. Since the rural monitoring station of this study was located in the western region of Turkey, it fairly fair to assume that it can be influenced by both western and north-western air masses. With 20% and 17% of intercepted air masses (of all trajectory heights) from the western and north-western sectors, respectively, it can be concluded that about 15% of anthropogenic pollution at the rural station is as a result of long range transport from countries within the W and NW sectors. Earlier studies (Karaca et al., 2009; Karaca and Camci, 2010) have underscored that western and north western cities of Turkey are under the influence of pollution from North Africa and the Balkan region; Greece, Bulgaria, Serbia and Croatia. Furthermore, observations of this study support an

earlier hypothesis that sources affecting chemical composition of particles in the Eastern Mediterranean atmosphere are located in neighboring countries, particularly the Balkan countries and Ukraine (Dogan et al., 2010, Gullu et al., 2005).

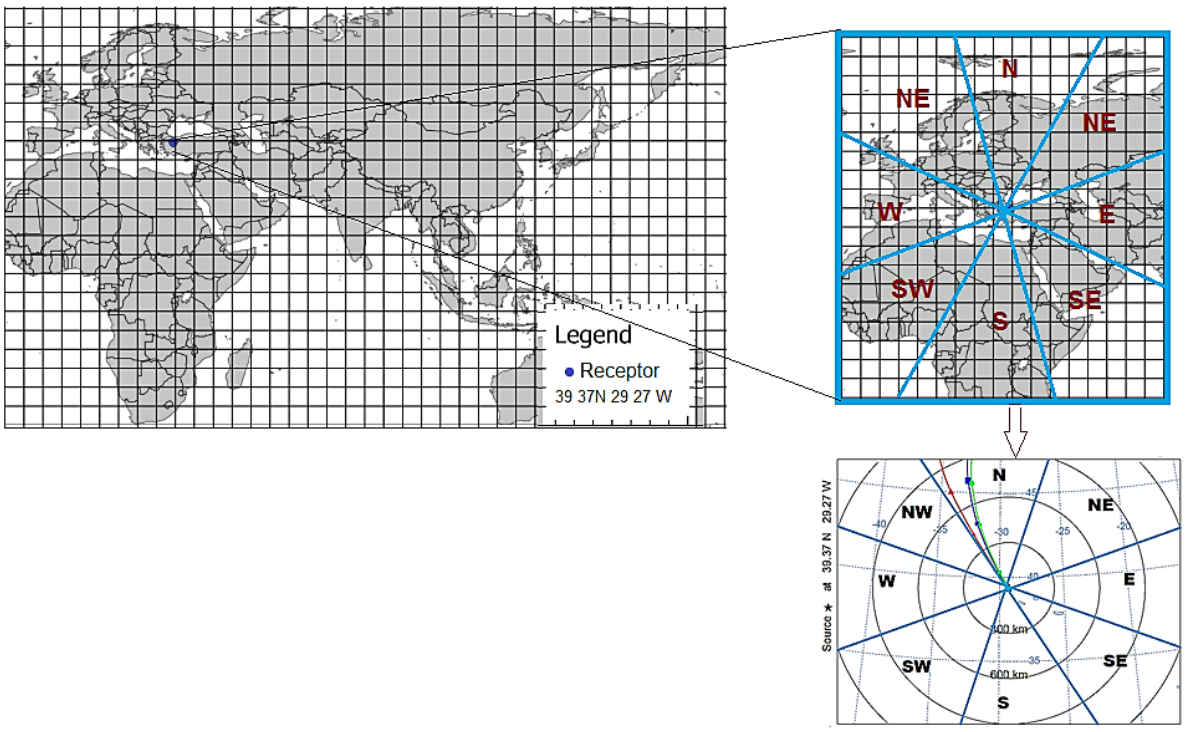

Figure 4.22. *5º x 5 º grid cells of the receptor domain along with zoned directional sectors*

Day by day HYSPLIT generated outputs are given in Figure 4.23-28. The general observed pattern of all air masses i.e. 100 m, 700 m and 1500 m arrival heights was that the northern sector i.e. N, NE and NW together contributed the most air mass arriving at the receptor. They contributed 54% while the southern sector i.e. S+SE+SW contributed 21%. Interestingly, the W sector alone contributed 20%.

For the 100 m trajectory, the highest contributing sector was NE with 21% followed by N, W and NW each contributing 16%. For the 700 m trajectory, N was the highest contributor with 26% of the air masses followed by W and NW contributing 21% and 16%,

respectively. Finally, the highest trajectory altitude, 1500 m had the N sector as its highest contributor with 24% of the air masses followed by the W sector, 22% and NW, 17%.

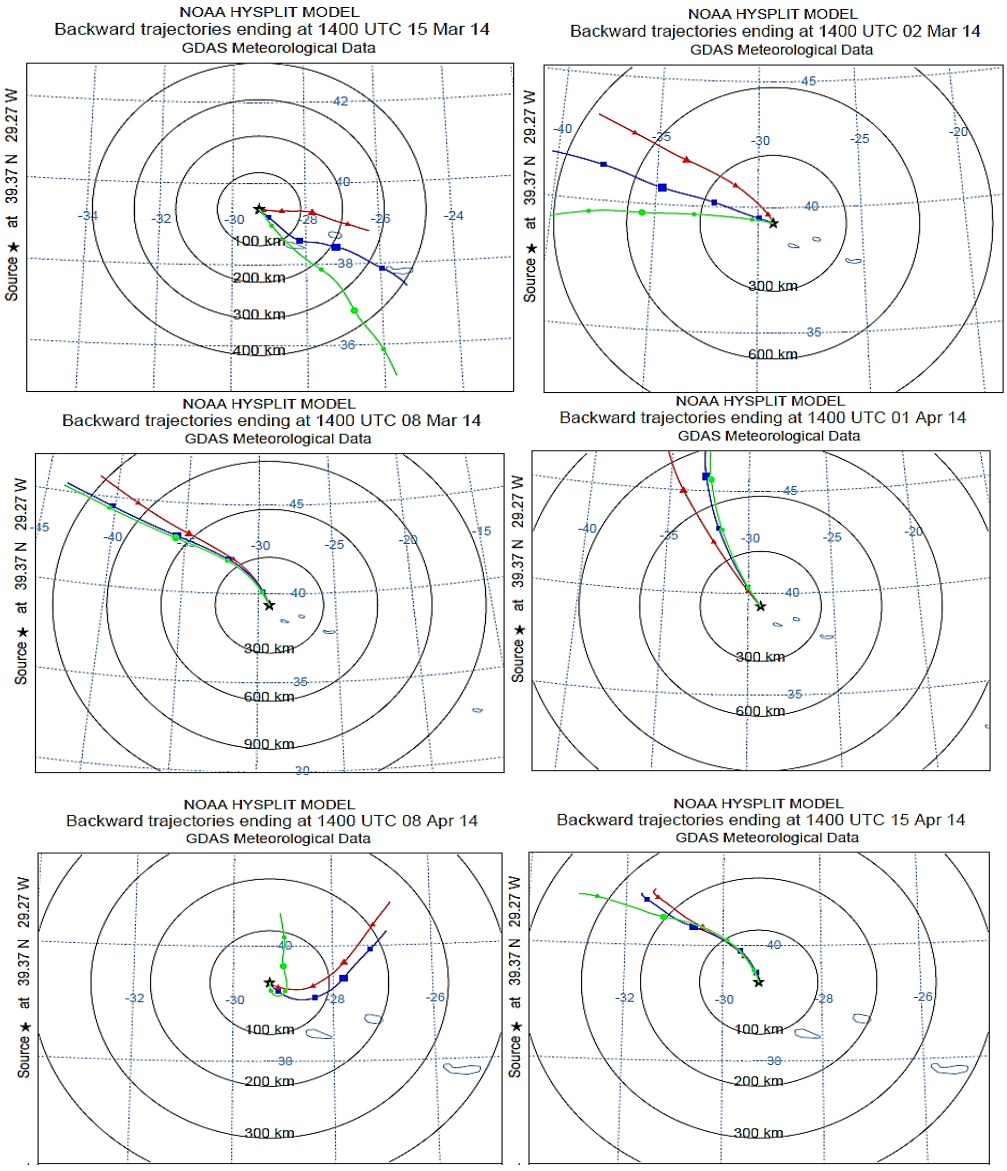

Figure 4.23. *Air mass trajectories of selected sampling days in March and April 2014*

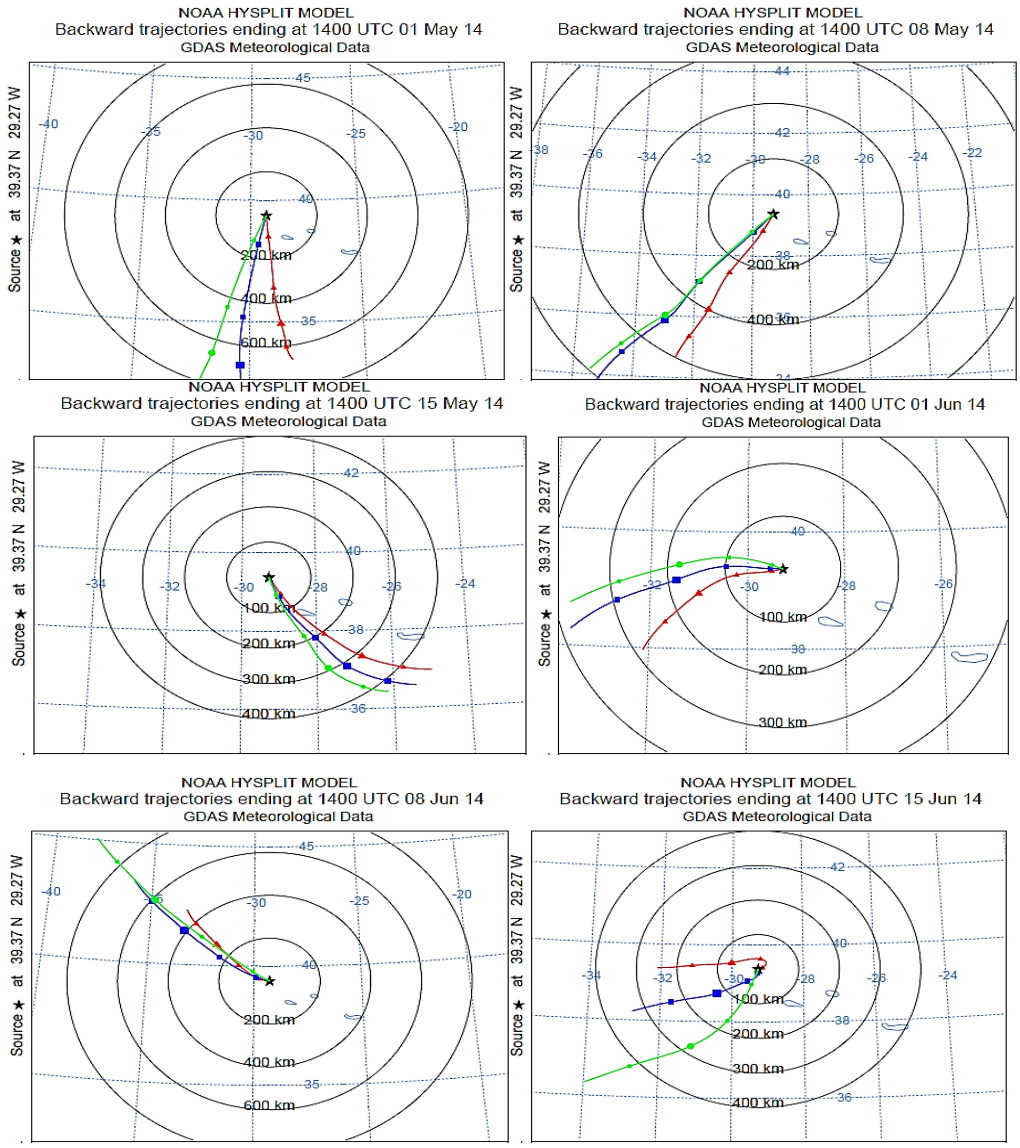

Figure 4.24. *Air mass trajectories of selected sampling days in May and June 2014*

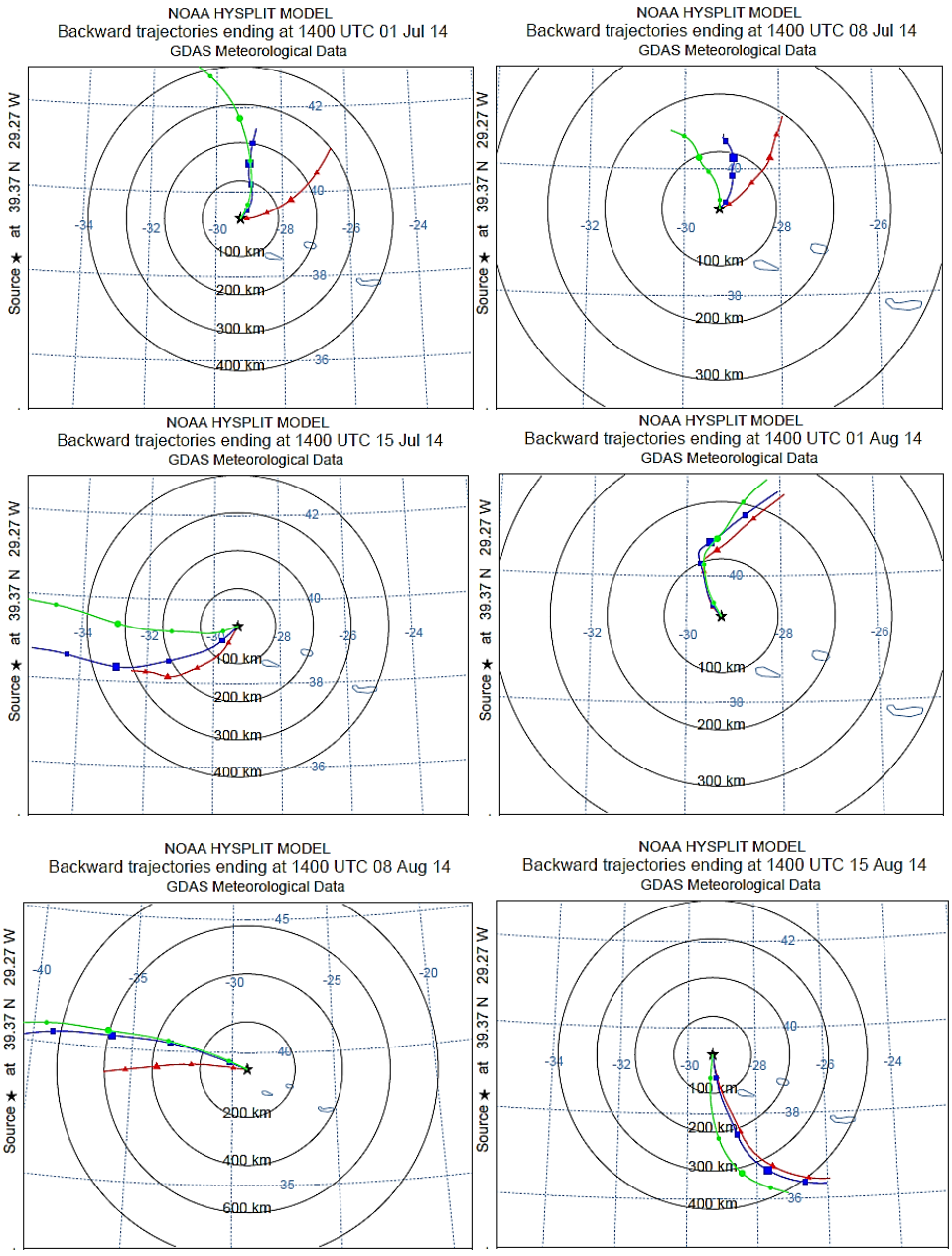

Figure 4.25. *Air mass trajectories of selected sampling days in July and August 2014*

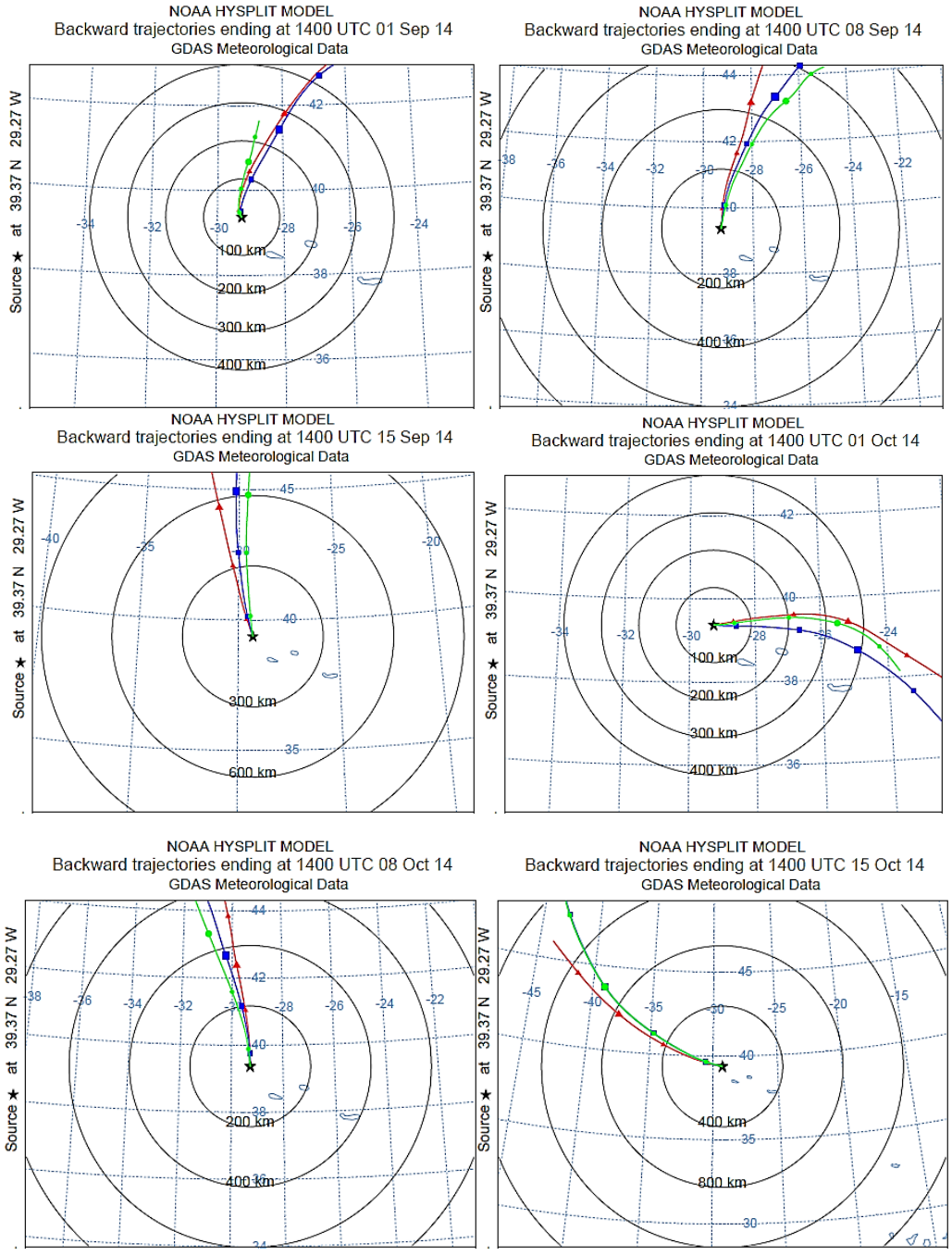

Figure 4.26. *Air mass trajectories of selected sampling days in September and October 2014*

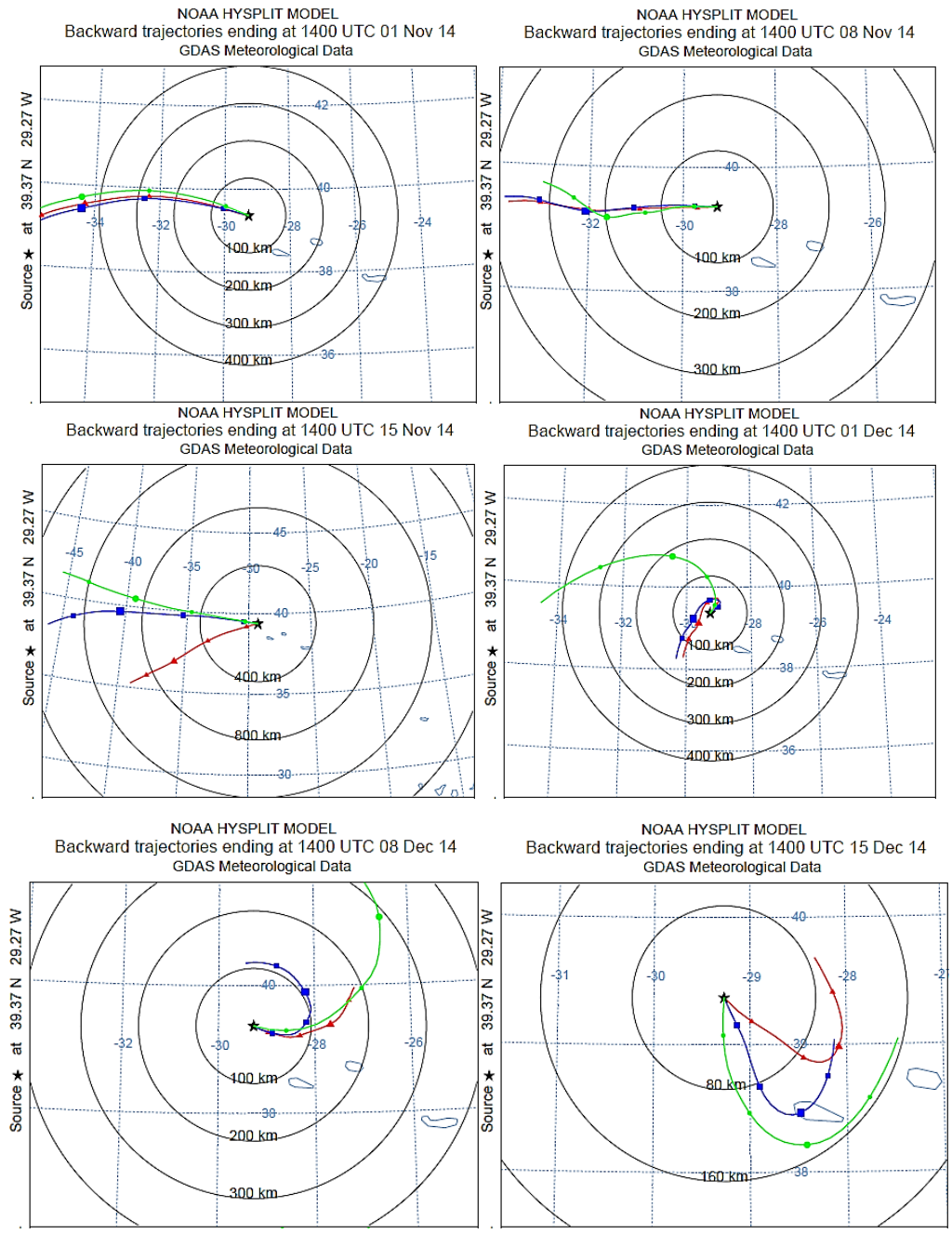

Figure 4.27. *Air mass trajectories of selected sampling days in November and December 2014*

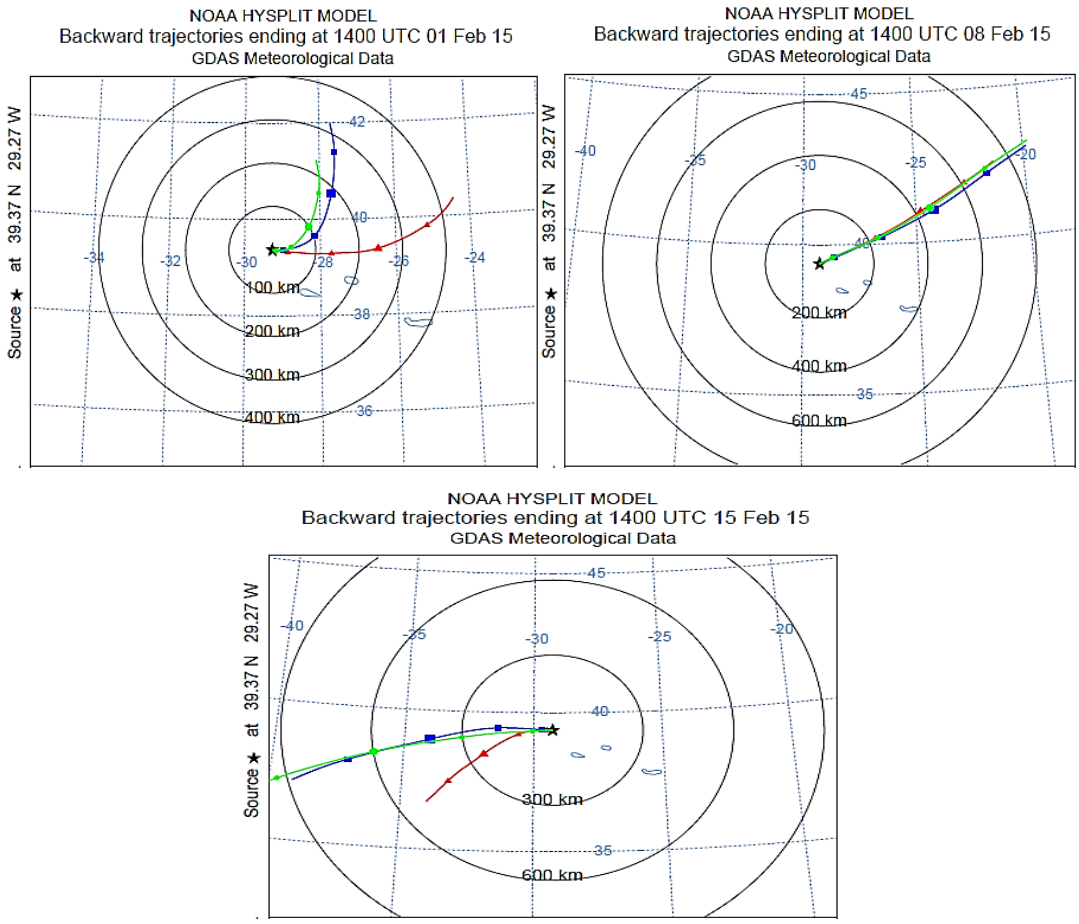

Figure 4.28. *Air mass trajectories of selected sampling days in February 2015*

A sector by sector contribution by all three trajectory heights are summarized in Table 4.11. As can be seen from the radar charts shown in Figure 4.29, the dominant source contributions were all from the north and north-east sectors as observed in the case of the short distance/local sources. This is quite interesting as there is no established relationship between very low (ground level) and high-altitude air masses. Another interesting observation made is that air mass trajectories viewed from sector to sector under same trajectory height or when viewed across as combined trajectories seem to yield similar pattern with order of contribution as N>W>NW>NE>SW>SE>E>S. In terms of volume, the 1500 m trajectory contributed the most with value of 46 while 100 m and 700 m trajectories both contributed 43 each. These observations quite agree with the trajectory frequencies earlier discussed.

Table 4.11. *Air mass contribution to sectors based on trajectory heights*

Wind Sector	100 m	700 m	1500 m	% sector by sector	TOTAL
N	7	11	11	22	29
NE	9	5	6	15	20
E	3	2	2	5	7
SE	3	4	4	8	11
S	1	2	2	4	5
SW	6	3	3	9	12
W	7	9	10	20	26
NW	7	7	8	17	22
TOTAL	**43**	**43**	**46**	**100**	**132**

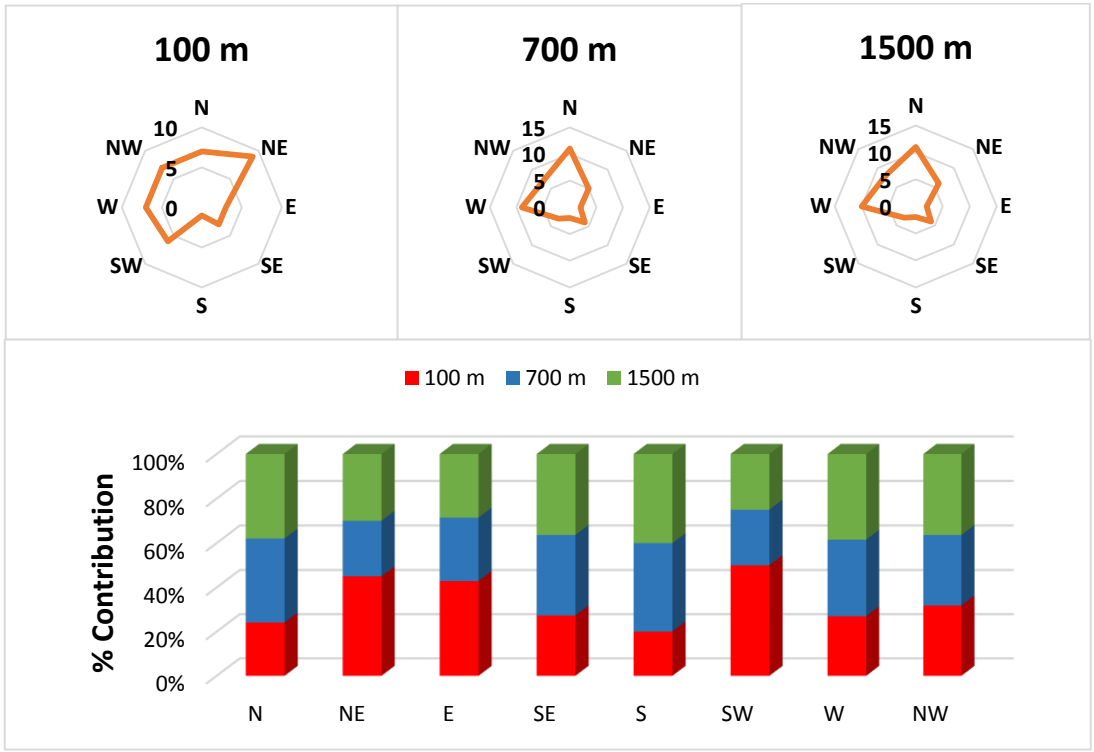

Figure 4.29. *Sector by sector airmass contributions to receptor, (top) wind directional view and (bottom) bar chart view*

4.4. Saharan Dust Intrusion

Satellite observation of air mass advection from the Sahara was done using the Barcelona Dust Forecast Center's model, NMMB/BSC-dust model to assess dust transport to Turkey. The system consists of numerical weather prediction model incorporated with an on-line parameterization of all the major phases of the atmospheric dust cycle. Variables of interest were daily and monthly averages of dust surface Concentration (DSC), aerosol optical depth (AOD) and dust loadings (DL) for the entire sampling campaign period from March 9, 2014 to February 28, 2015. The months of March, July, August and November which represent the coldest but mostly wet and the warmest but mostly dry periods in Turkey were selected as representative months for the entire study period.

4.4.1. Dust loadings

The dust flowconcentrically from the highly loaded countries such as Chad through Niger, Mali, Algeria, Libya and over the Mediterranean into Western Turkey. The highest dust loadings from the source regions were observed in the months of July and August whereas relatively lower loadings were observed in March and November. Dust loads reaching Western Turkey were, however, low, 0.1 – 0.4 g/m^2 in the green color band of 492-550 nm wavelength compared to the loads from the source countries which was in the range 1.2 – 6.4 g/m^2, extending from the yellow (577 nm) to dark brown ($\geq$ 800 nm) aerosol bands. Order of dust loading in Turkey was March>July>November>August. Aerosols affect climate by scattering sunlight back into space and cooling the surface. Since Saharan dust are coarser and therefore have greater light scattering potential than anthropogenic dust, the climate in Western Turkey can be said to be influenced by the Saharan dust intrusion. Figure 4.30, is the generated model charts of dust loadings for the selected periods.

4.4.2. Dust surface concentration

Dust surface concentration is dependent on the aerosol mass/dust loadings at an area. Daily average dust concentration from the dust model ranged between 5 and 20,000 µg/m^3 and that of the monthly average ranged between 5 and 5000 µg/m^3. The highest daily dust surface concentration (> 5000 µg/m^3) was observed particularly in Chad and Niger in Saharan Africa and Iraq and Iran in the Middle East. Incidentally, the highest daily concentration for Turkey (50-200 µg/m^3) was observed in the central and south-west in the month of March; the rest of the months recorded between 5 and > 20 µg/m^3.Thus, the order of surface dust concentration in the year is March>July>November>August. It is important to mention that despite recording the highest dust surface concentration in the month of March, this did not reflect in the elemental concentrations of PM sampled at the receptor locations. Elemental concentration observed in March was relatively lower than July and August. This unusual observation can be attributed to inhibition or lack of re-suspension of dust by precipitation as March is a winter month with a lot of snow or dampy surfaces. Figure 4.31, are model charts illustrating daily (average) dust surface concentrations (µg/m3) over the selected periods of consideration.

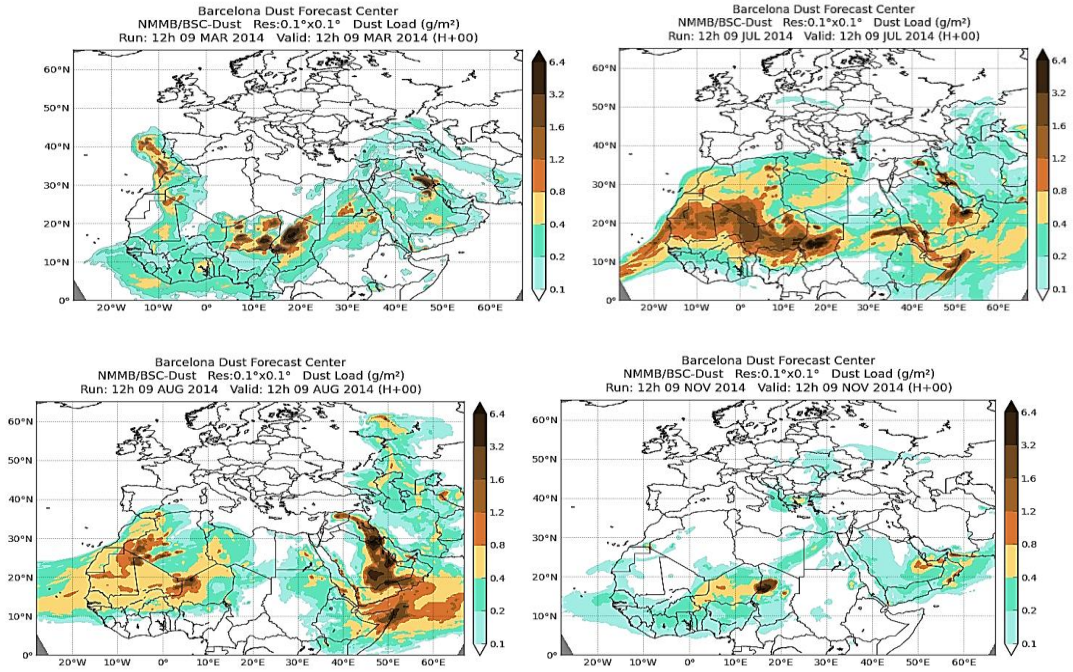

Figure 4.30. *Dust loadings on selected months during sampling campaigns*

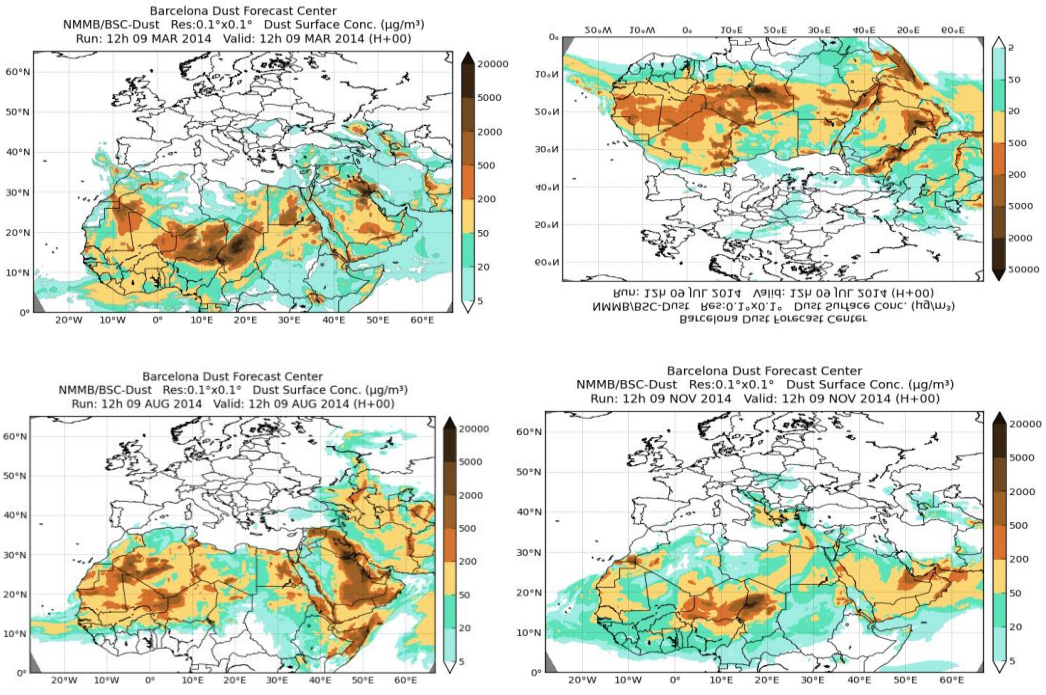

Figure 4.31. *Daily dust surface concentrations (µg/m^3) over the selected periods*

4.4.3. Aerosol Optical Depth

Aerosol Optical Depth (AOD) is the measure of aerosols distributed within a column of air from the Earth's surface to the top of the atmosphere (Holben et al., 1998; Smirnov et al., 2004). The measurement includes variables such as urban haze, smoke, particles, desert dust, sea salt etc. This parameter gives us an insight on the visual outlook of the atmosphere. For example, an optical depth of less than 0.1 (plain band) is an indication of a crystal-clear sky with maximum visibility, whereas an optical depth value of 1 or greater (red to reddish-brown) indicates a very hazy condition with hazicity increasing in that order (Smirnov et al., 2004; NASA Earth Observation). AOD is related to the amount of aerosols in the vertical column of atmosphere over the observed location (NOAA; Accessed online, May 2018). In line with dust loading and dust surface concentration observed earlier, aerosol optical depth was observed in the same order; March>July>November>August making the months of August and November the clearest atmosphere in Turkey in the study year. The maximum optical depth of 0.1-0.2 m was observed in the entire central to south-west and part of north-east regions of Turkey in March whereas in the month of July, same optical depth of aerosols was observed in west-most of the country. Figure 4.32, illustrates the variability in optical depths of aerosols in the selected representative months in the study area.

4.4.4. Near-Real-Time Observation

An important step in dust intrusion forecasting is to perform a near-real-time (NRT) evaluation aimed at assessing the relationship between the dust modeland NRT AERONET's observations. In this regard, Angstrom Exponent (AE) and dust optical depth (DOD) as well as aerosol optical depth (AOD) were observed each day of the representative months using a Saharan Aerosol Network Station IMS-METU-ERDEMLI based in Turkey.

The base station output showed generally, a good agreement between the AERONET and NMMB/BSC dust model values of AOD and DOD in all the selected months. Such agreement also authenticates the model's integrity and reliability for regional and local dust flow analyses. As can be seen in Figure 4.33, both the dust model and NRT AERONET recorded the highest AOD and DOD values around 17thin Mach;

around 13thin July and in August around 26th. In November, however, there was a little deviation, the highest AOD was observed around 15th whilst DOD was observed around 17th.

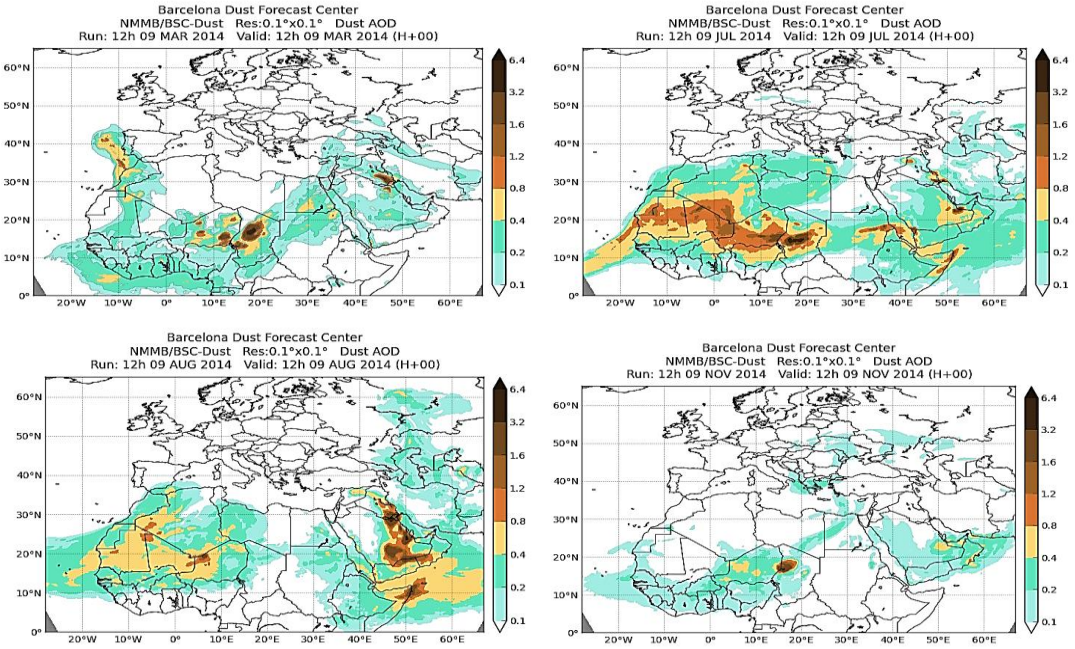

Figure 4.32. *Optical depths of aerosols in the selected representative months*

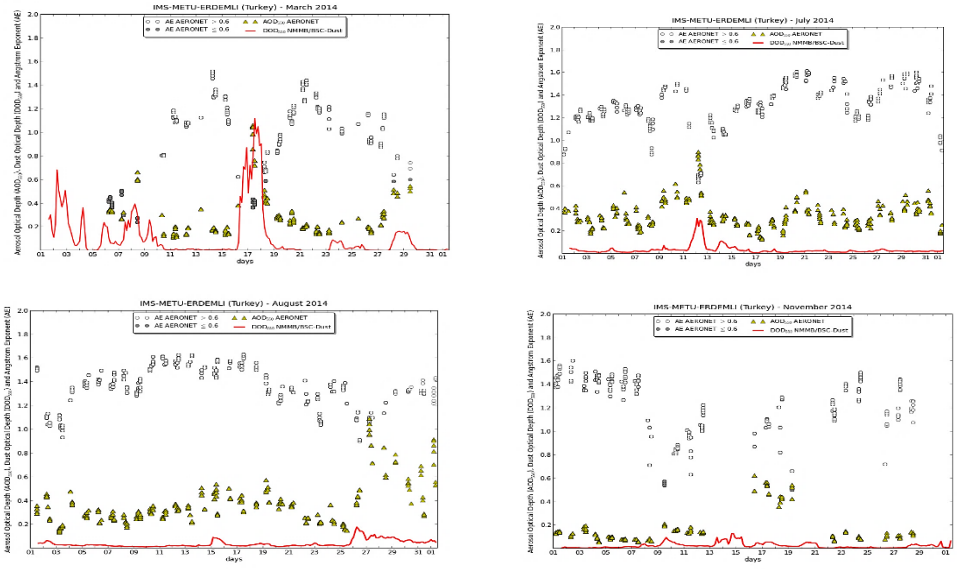

Figure 4.33. *IMS-METU-ERDEMLI station observation of Angstrom Exponent (AE); dust optical depth and aerosol optical depth at 550 nm.*

4.5. Mineral Dust Episodes

As stated previously, mineral dust tracers like Al, Fe, Ca and Ti can be used to investigate and identify Saharan/mineral dust episodes. The most important source regions of dust are all in the Northern Hemispheric region including North Africa, the Middle East, the northwestern Indian subcontinent, central Asia, and northwestern China (Engelbrecht et al., 2010). Therefore, to identify an event as a mineral dust episode at least one of its air mass back trajectory must be traced to one of the above stated regions.

In the air mass back trajectory analysis of this study, it was observed that the 100 and 700 meters trajectories, reproduced in Figure 4.34, reaching both the rural and urban receptors had travelled across the Caspian Sea and therefore believed to have their sources from Central Asia. Thus, making the event a mineral dust episode. Also, dust intrusion analysis as discussed in the previous section of this thesis, it has been demonstrated from the dust flow system that dust reaching Western Turkey (the location of the receptor) comes from the Sahara (North Africa) whereas dust reaching Central Turkey comes from the Middle East.

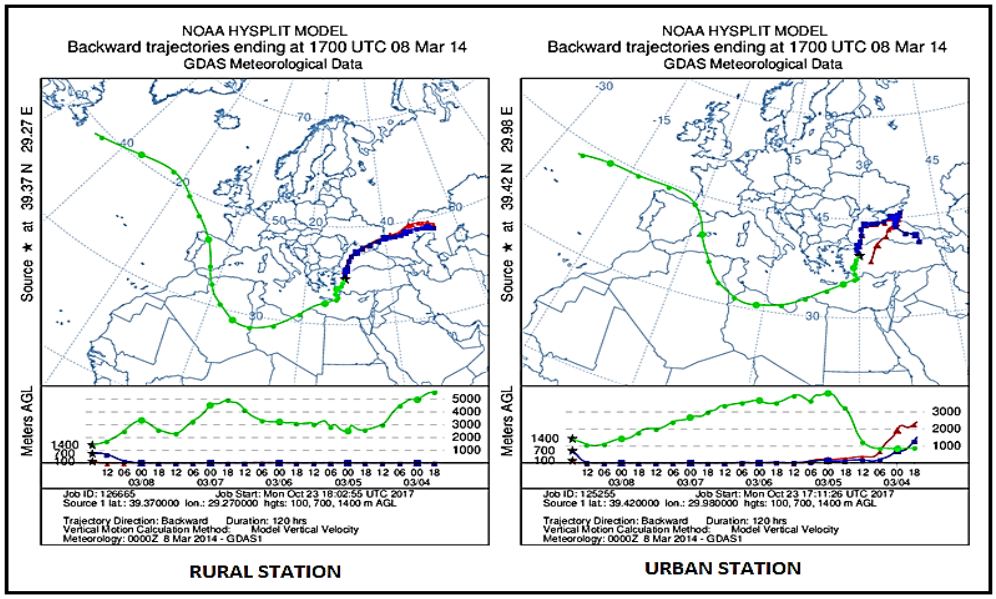

Figure 4.34. *Air mass back trajectories reaching receptor locations in Western Turkey*

Dust-to-non-dust day ratios:

Another approach used to unravel whether the dust episode is a mineral dust and of the above stated origins was to observe the concentrations of mineral dust species relative to dust and non-dust days. Previous studies have reported using this approach to investigate dust intrusion phenomenon (Borbely-Kiss et al., 1999 and 2004; Marcazzan et al., 1993). By this approach the high concentration of mineral dust markers is identified and used as indicators of dust intrusion as well as mineral dust episodes. To achieve this objective, the sampling period was first grouped as dust and non-dust days and ratio of dust-to-non-dust days were determined for all PM species. It was assumed that a rainy day constituted a non-dust day whilst a non-rainy day constituted a dust day. By this approach, episodes with higher concentrations of dust tracers, higher dust-to-non-dust ratios and significant difference (sample t-test) between dust and non-dust events signified mineral dust episodes.

Statistical difference between the median concentration of species on dust and non-dust days was tested using Mann-Whitney U test. According to the test results, there was a significant difference in the median values at the 95% CL between dust and non-dust days of mainly crustal (Al, Ca, Mg, Ti, Na, Fe, Si, K, and Cr) and anthropogenic species (S and P). As can be seen in Figure 4.35, these species obtained dust-to-nondust ratio values ranging between 1.50 and 2.50 in the two PM fractions across the two monitoring stations. The high ratio values obtained mainly by these litophilic species signified higher PM mass loadings and hence higher concentrations of these species during the dry period than the wet period. Such observation on one hand is due to re-suspension of soil and dust particles during the dry period and on the other hand due to inhibition of soil and dust re-suspension due to dumpy and covered surfaces by precipitations during the nondust period. This in effect establishes the mineral dust episodes of PM investigated. Species which did not show significant difference between dust and nondust day median values were mainly anthropogenic mixed-source (Zn, Cu, Ni, V, Br, Mn and As) and marine source (Cl) species. Their ratio values were relatively lower (0.40 – 1.45) compared to those of the crustal species. Marine and anthropogenic species are mostly water-soluble due to their soluble salts and labile nature and are therefore easily removed from the atmosphere by wet deposition processes. Nonetheless, anthropogenic species belonging to the mixed-source group like Cu, Se, Rb, Sr,

Pb and Mn recorded appreciable concentration on dry days yielding dust-to-non-dust day rattios between 1 and 1.4. Several aerosol studies including Kocak et al., 2012 have reported high concentrations of anthropogenic species on dust days yielding ratio values of dust/non-dust day similar to those obtained by this study.

High concentrations of anthropogenic species have been attributed to high surface area of dust particles acting as reaction surfaces for PM precursor gases (SO_2) and chemical components. Also, mixing between anthropogenic species and local sources during transport by air mass to the receptor is another phenomenon contributing to high concentrations of anthropogenic species on a dust day. Species like Mo, Y, Se and Rb were poorly detected by PIXE and therefore were not considered for further analysis and discussion. It has, however, been reported that low concentrations of anthropogenic species, Zn, Pb, Mo and Sb are due to transport from elsewhere to the receptor (Tokgoz, published PhD thesis). Given in Table 4.12, is the summary statistics and ratio values for species on dust and non-dust days.

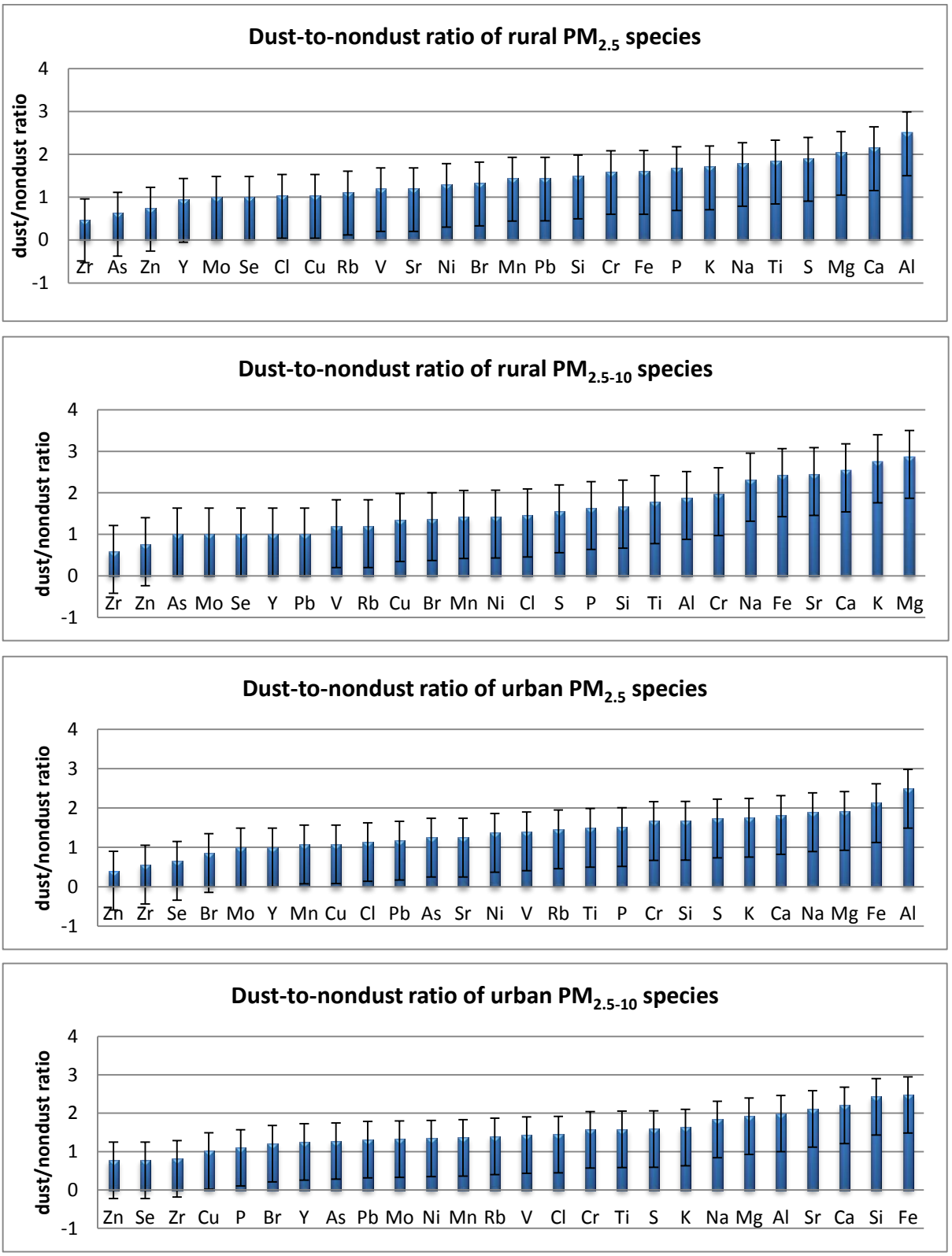

Figure 4.35. *Dust-to-non-dust days ratios of fine and coarse PM species of rural and urban backgrounds*

Table 4.12. *Median concentration (µg/m^3) of species on dust and non-dust days*

	RURAL FINE			RURAL COARSE			URBAN FINE			URBAN COARSE		
Element	Dust day	Non-dust day	Dust/Non-dust	Dust day	Non-dust day	Dust/Non-dust	Dust day	Non-dust day	Dust/Non-dust	Dust day	Non-dust day	Dust/Non-dust
Na	0.133	0.075	1.788	0.150	0.065	2.318	0.146	0.077	1.896	0.245	0.133	1.842
Mg	0.432	0.205	2.047	0.388	0.135	2.868	0.487	0.253	1.925	0.683	0.355	1.925
Al	2.174	0.868	2.504	1.528	0.968	1.578	2.240	0.899	2.491	2.979	1.493	1.995
Si	0.208	0.139	1.495	0.340	0.219	1.551	0.434	0.259	1.678	0.534	0.320	1.668
P	0.025	0.015	1.690	0.028	0.017	1.637	0.029	0.019	1.519	0.034	0.031	1.102
S	0.523	0.274	1.908	0.473	0.344	1.376	0.373	0.215	1.735	0.355	0.223	1.591
Cl	0.060	0.057	1.043	1.103	0.665	1.458	0.064	0.056	1.135	0.513	0.331	1.447
K	0.530	0.308	1.709	0.609	0.421	1.560	0.752	0.429	1.753	0.857	0.526	1.629
Ca	1.695	0.786	2.157	2.178	0.856	2.544	2.060	1.128	1.826	2.212	1.001	2.210
Ti	0.144	0.078	1.846	0.122	0.069	1.779	0.081	0.054	1.500	0.149	0.094	1.585
V	0.006	0.005	1.200	0.006	0.005	1.200	0.052	0.037	1.405	0.033	0.023	1.435
Cr	0.084	0.070	1.600	0.051	0.026	1.970	0.071	0.061	1.670	0.010	0.009	1.557
Mn	0.063	0.041	1.526	0.014	0.010	1.420	0.009	0.008	1.073	0.034	0.025	1.361
Fe	1.262	0.787	1.603	1.113	0.459	2.427	0.683	0.321	2.125	1.238	0.499	2.481
Ni	0.012	0.008	1.500	0.023	0.014	1.643	0.007	0.005	1.400	0.017	0.011	1.545
Cu	0.041	0.039	1.043	0.052	0.039	1.349	0.027	0.025	1.078	0.024	0.024	1.021
Zn	0.061	0.082	0.743	0.039	0.051	0.764	0.045	0.077	0.584	0.075	0.097	0.777
As	0.001	0.002	0.628	0.001	0.001	1.000	0.005	0.004	1.250	0.004	0.003	1.280
Se	0.001	0.001	1.000	0.001	0.001	1.000	0.001	0.002	0.658	0.001	0.001	0.779
Br	0.004	0.003	1.333	0.003	0.002	1.370	0.010	0.012	0.858	0.023	0.019	1.211
Rb	0.003	0.002	1.119	0.006	0.005	1.200	0.003	0.002	1.458	0.003	0.002	1.440
Sr	0.006	0.005	1.200	0.006	0.002	2.455	0.004	0.003	1.250	0.006	0.005	1.200
Y	0.001	0.001	0.951	0.001	0.001	1.000	0.003	0.003	1.000	0.002	0.001	1.256
Zr	0.002	0.004	0.476	0.003	0.003	0.980	0.006	0.007	0.563	0.005	0.006	0.818
Mo	0.001	0.001	1.000	0.001	0.001	1.000	0.001	0.001	1.000	0.001	0.000	1.330
Pb	0.016	0.011	1.447	0.001	0.001	1.000	0.101	0.086	1.171	0.118	0.089	1.318

Variation in dust tracer enrichment:

The study was curious to know how the enrichment of the selected dust tracers varied. As a result, elemental ratios of these tracers i.e. Al/Ca, Si/Al, Ti/Fe, Ti/Ca, Si/Fe and Ca/Fe were observed to assess variability in their enrichment relative to dust and non-dust event days. As can be seen in Figure 4.36, elemental ratios for the dust days were found to be quite similar to those of the non-dust daysfor all the species considered. The ratio values for non-dust days ranged between 0.04 for Ti/Ca and 3.02 for Ca/Fe. Ti/Fe, Si/Al, Si/Fe and Al/Ca obtained 0.14, 0.29, 0.81 and 1.09, respectively. On dust days, the ratios ranged between 0.04 for Ti/Ca and 3.51 for Ca/Fe. Ti/Fe, Si/Al, Si/Fe and Al/Ca had ratio values of 0.12, 0.19, 0.64 and 0.80, respectively.

With the exception of Ca-to-Fe ratio in this study, concentrations of Ca, Fe and Al were found to be relatively higher in the dust days than the non-dust days. It was found that between Ca and Fe enrichment, Ca concentration was relatively higher than Fe on a dust day and conversely on a non-dust day Fe concentration was higher. Such observation can be attributed to some physicochemical properties of these metals i.e. atomic size/surface area and water-solubility. The sizes of atoms are of importance in the determination of coordination number i.e. the number of groups attached to the central atom in a compound and hence in the composition of compounds (Encyclopedia Britannica, accessed online, April 2018).

Both elemental Fe and Ca occur naturally and they both dissolve or react with water under normal condition. Their reaction with atmospheric SO_2 leads to the formation of iron sulfate and calcium sulfate with solubility of 0.288g/L and 2.7-8.8 g/L, respectively (LENNTECH, accessed online, April 2018). This makes solubility of Cagreater than Fe and therefore reduction in its enrichment and concentration on a non-dust day – a typical precipitation day. On a dust day, however, determining factor for enrichment depends on the surface area of the species. The larger the surface area, the more space is available for reaction between species and precursor gases. It is important to state that, surface area in this regard refers to the outer surface commonly referred to as atomic size/radius. It has been reported that the alkali and alkaline earth metals have a linear relationship between their atomic and

ionic radii (Somayajulu et al., 1957) and based on the periodic law; atomic radius or atomic size decreases across the period due to increase in effective nuclear charge and attraction of electrons to the nucleus. This favors Ca, making Ca enricher and higher in concentration than Fe on a dust day.

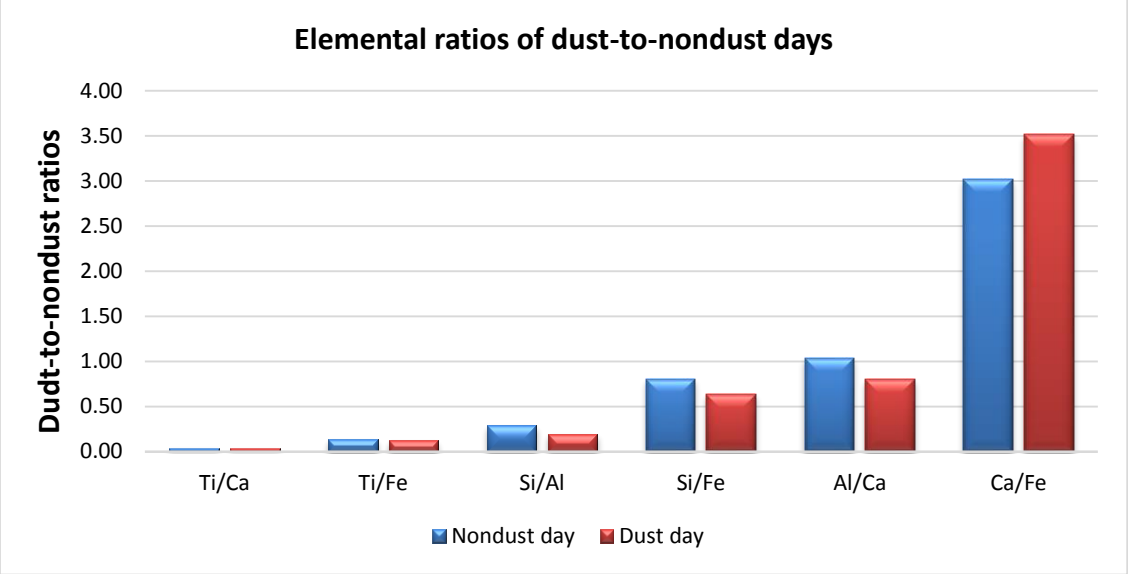

Figure 4.36. *Elemental ratios for dust and non-dust days*

Impact of local meteorology:

Rainfall is an important meteorological parameter that can have an important impact on both composition and concentration of PM species. Also, rainfall can cause generation of episodes in concentration data of species. To assess species relation with rainfall, the measured species concentrations were plotted against observed maximum rainfall (mm) during the sampling campaign.

The major rain events recorded during this study occurred in February (~ 6mm), April (~ 10mm), May (~ 9mm) and November (~ 11mm) at the rural station while at the urban station, the major rains were recorded in April (~ 5mm), May (~ 9mm), June (~ 8mm),

September (~ 18mm) and November (~ 21mm). It should be noted that, the peak rain event (22 mm) occurred at the rural station on 16th November while at the urban station, the peak rainfall occurred on 3rd February (42 mm) and 14th September (39 mm). A general inverse relation was observed between concentration and; rainfall.

As can be seen in Figures 4.37-44, the minimum total rainfall was recorded in July and February whereas the highest observed concentration of crustal (dust tracer) species, Al, Fe, Si and Ca was obtained in July and August which coincided with the period of highest dust loadings in the Sahara as discussed earlier. Thus, it was found that when dust loading was higher in the Sahara, dust flow to the receptor location in Western Turkey was higher and concentrations of mineral dust tracers were also higher. However, it was observed that when rainfall events were higher, concentrations of these species were relatively lower. This implies washout by rain as a removal mechanism was effective even though dry deposition is reported to be the better removal mechanism of crustal aerosols.

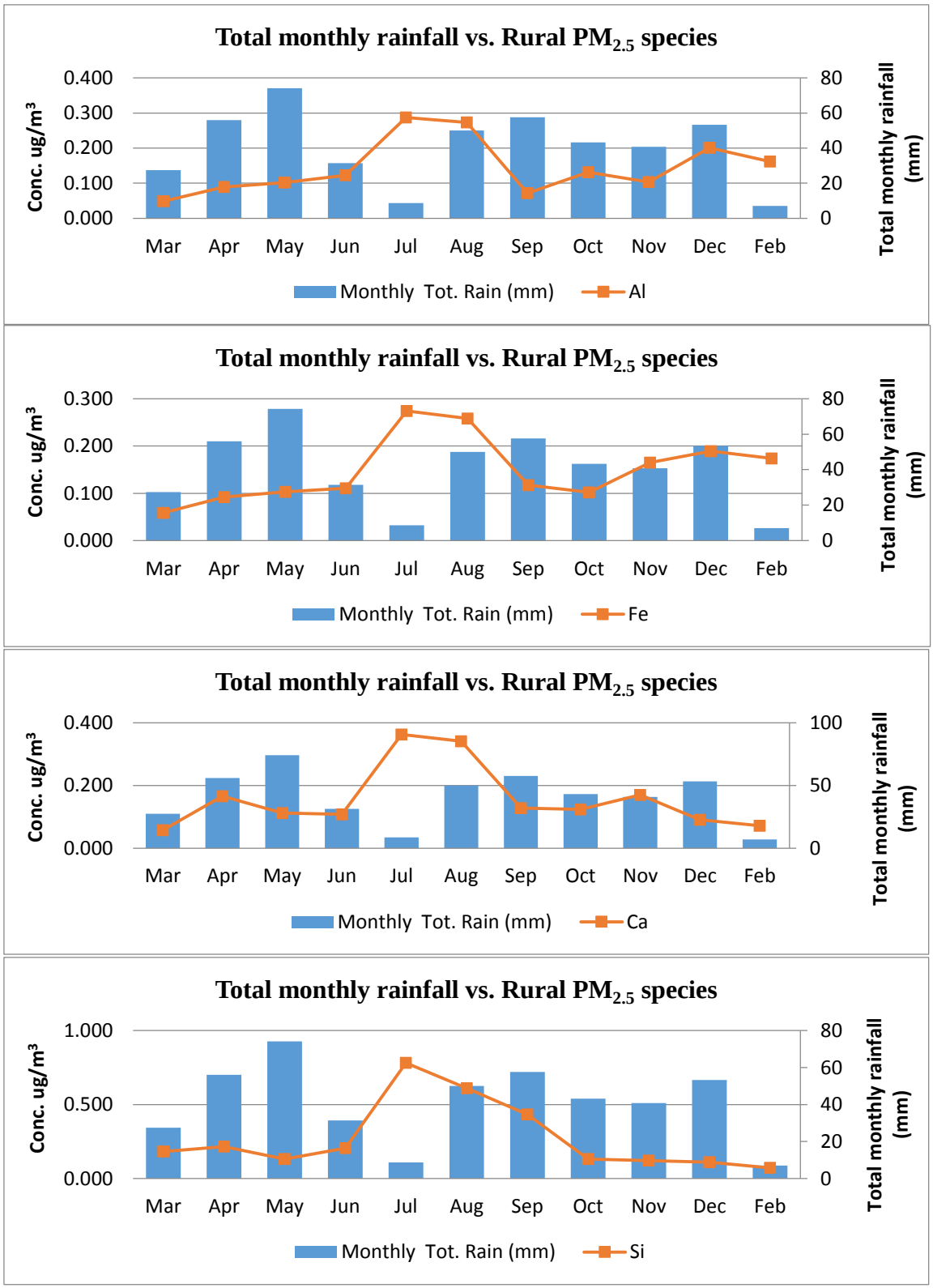

Figure 4.37. *Variation of dust tracer concentration in rural $PM_{2.5}$ with rainfall*

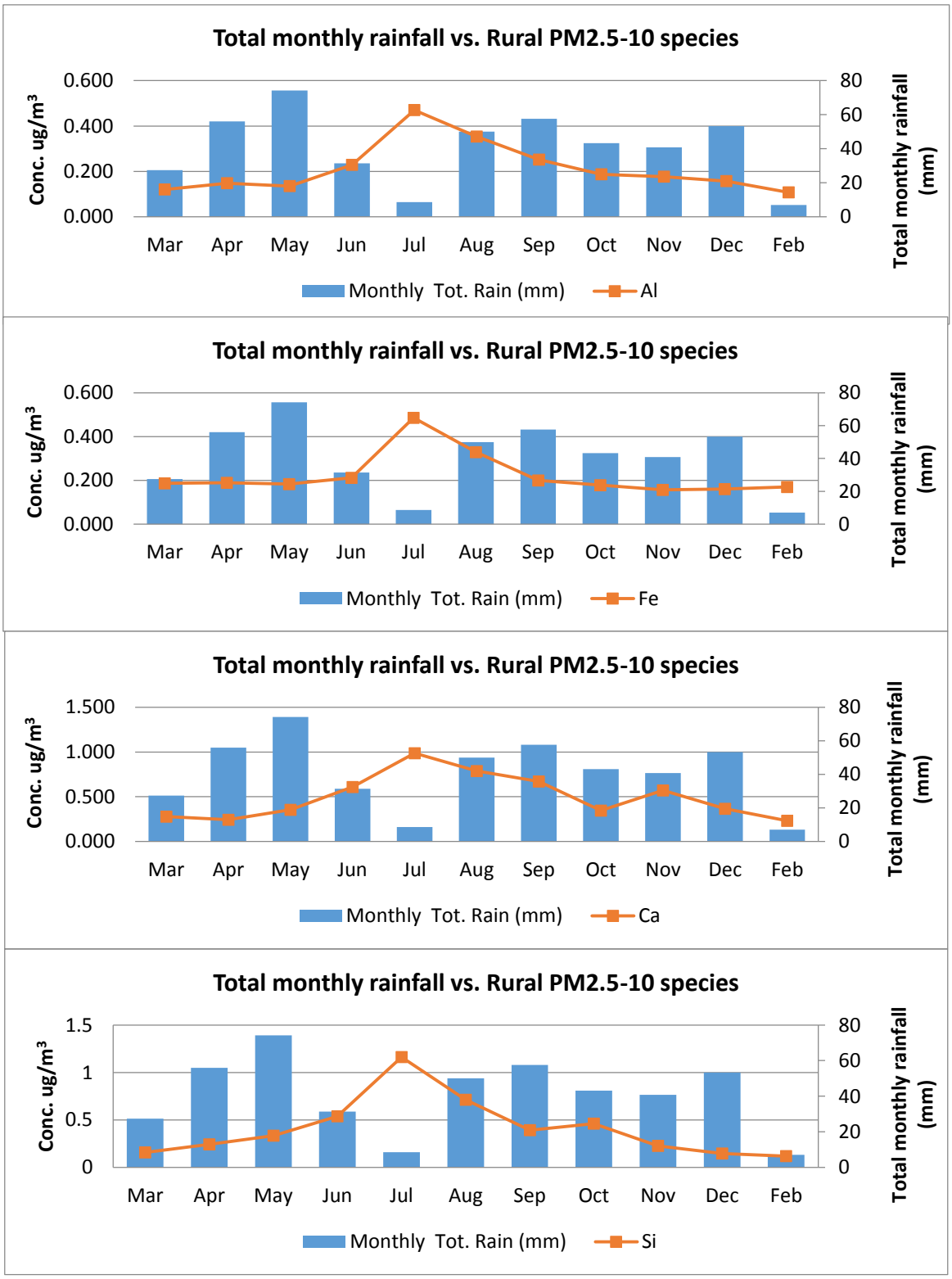

Figure 4.38. *Variation of dust tracer concentration in rural PM2.5-10 with rainfall*

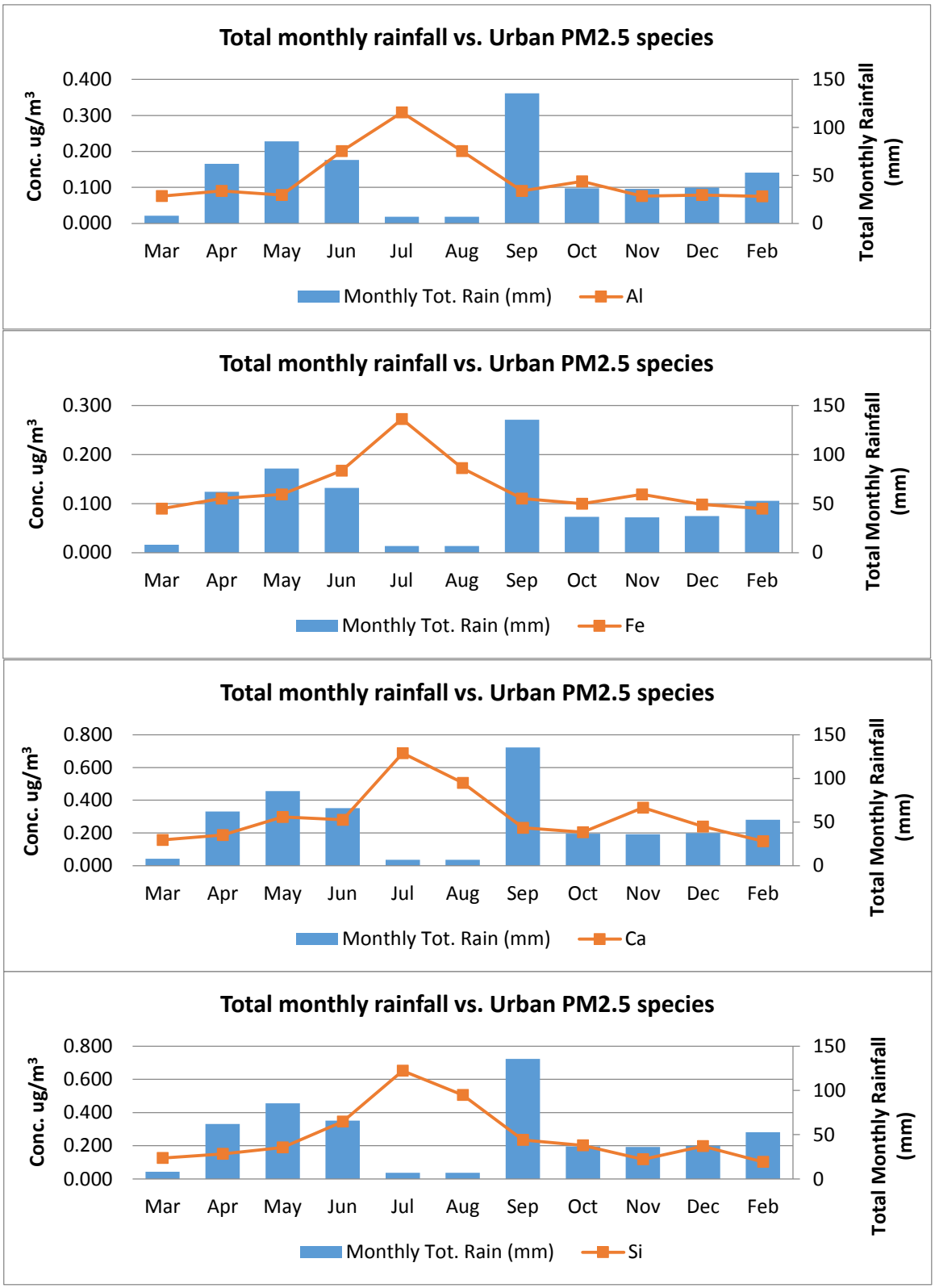

Figure 4.39. *Variation of dust tracer concentration in urban PM2.5 with rainfall*

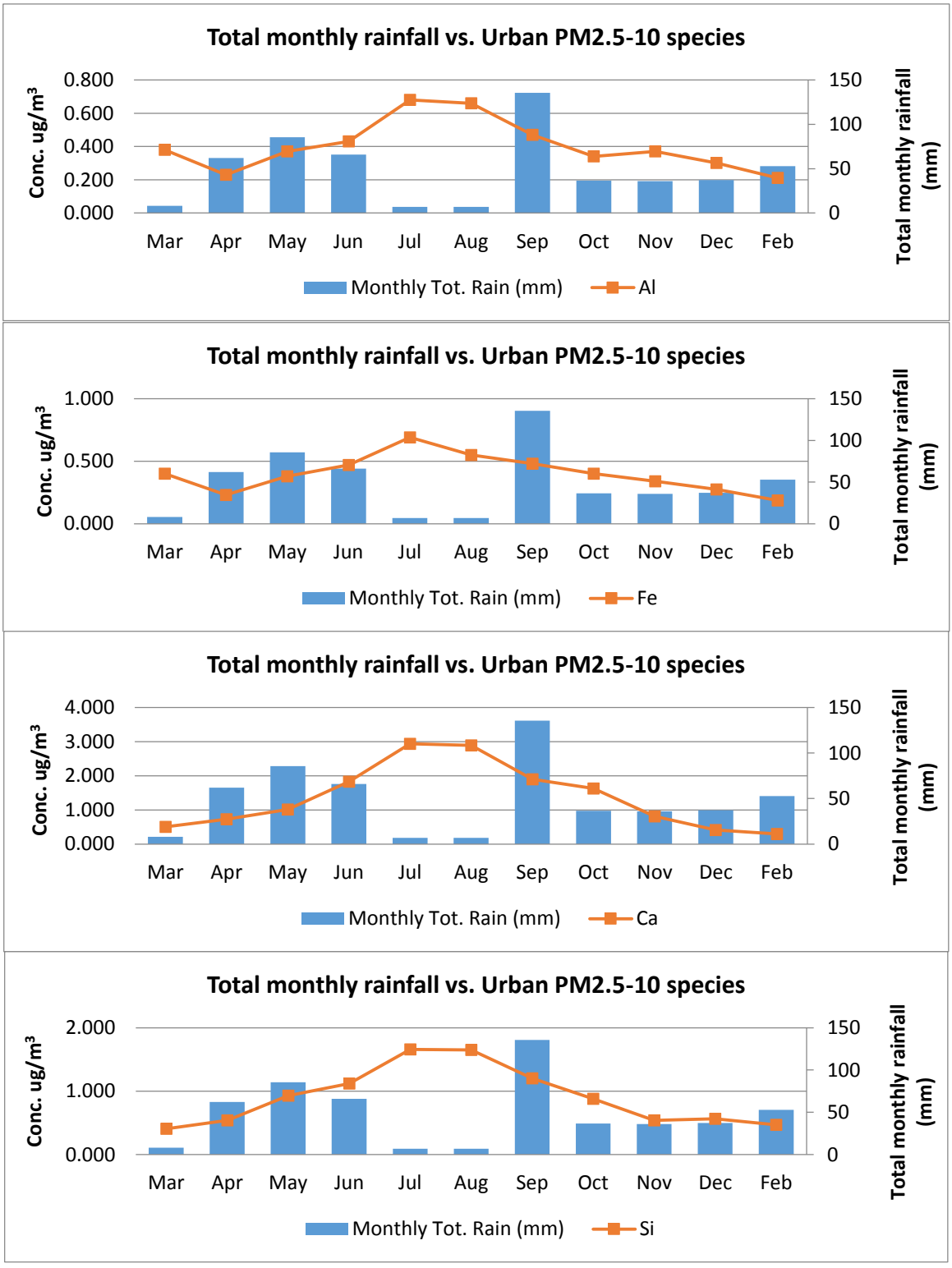

Figure 4.40. *Variation of dust tracer concentration in urban $PM_{2.5-10}$ with rainfall*

Variation of (selected anthropogenic and marine source) species with rainfall events are given the following charts, Figure 4.41-44. Anthropogenic species, V recorded its lowest monthly average of 0.0017 μg/m^3 in December of which only few rain events (2 mm) was recorded. Zn, however, recorded its monthly lowest in February which recorded the highest rainfall event. All the species in the coarse fraction recorded their lowest monthly average in September, the month with the most rain events.

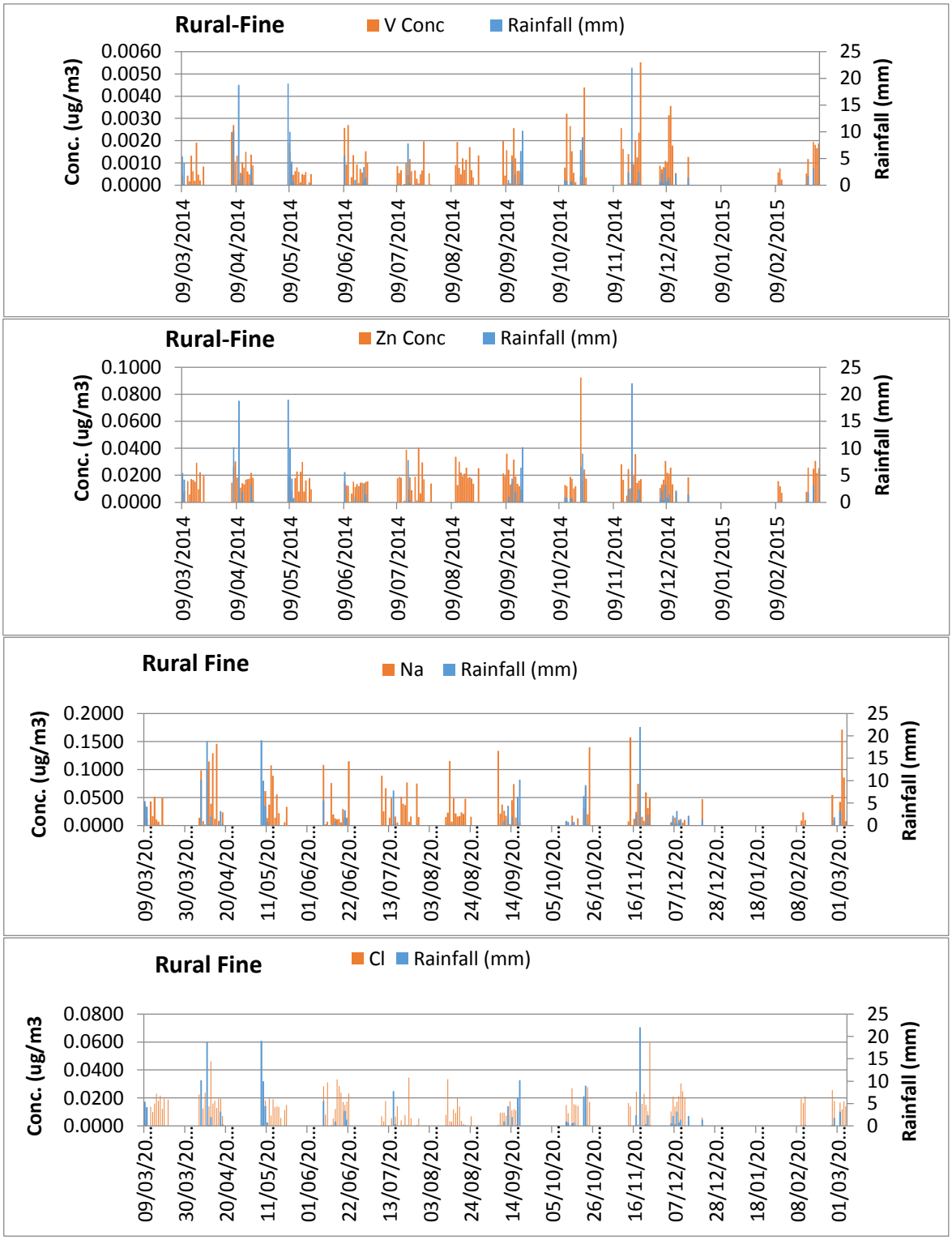

Figure 4.41. *Variation of anthropogenic and 'marine source' species concentration in rural $PM_{2.5}$ with rainfall*

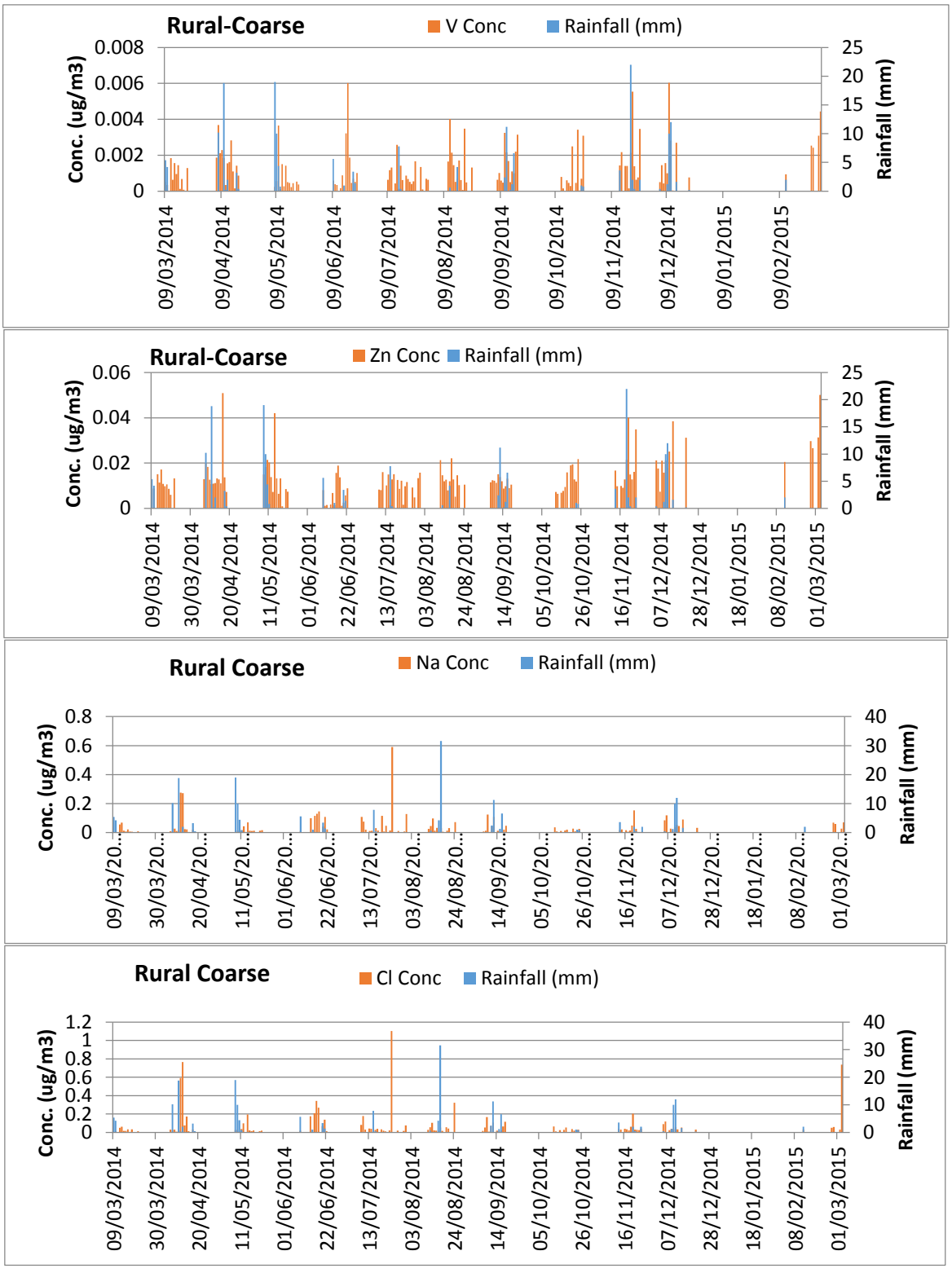

Figure 4.42. *Variation of anthropogenic and marine source species concentration in rural $PM_{2.5-10}$ with rainfall*

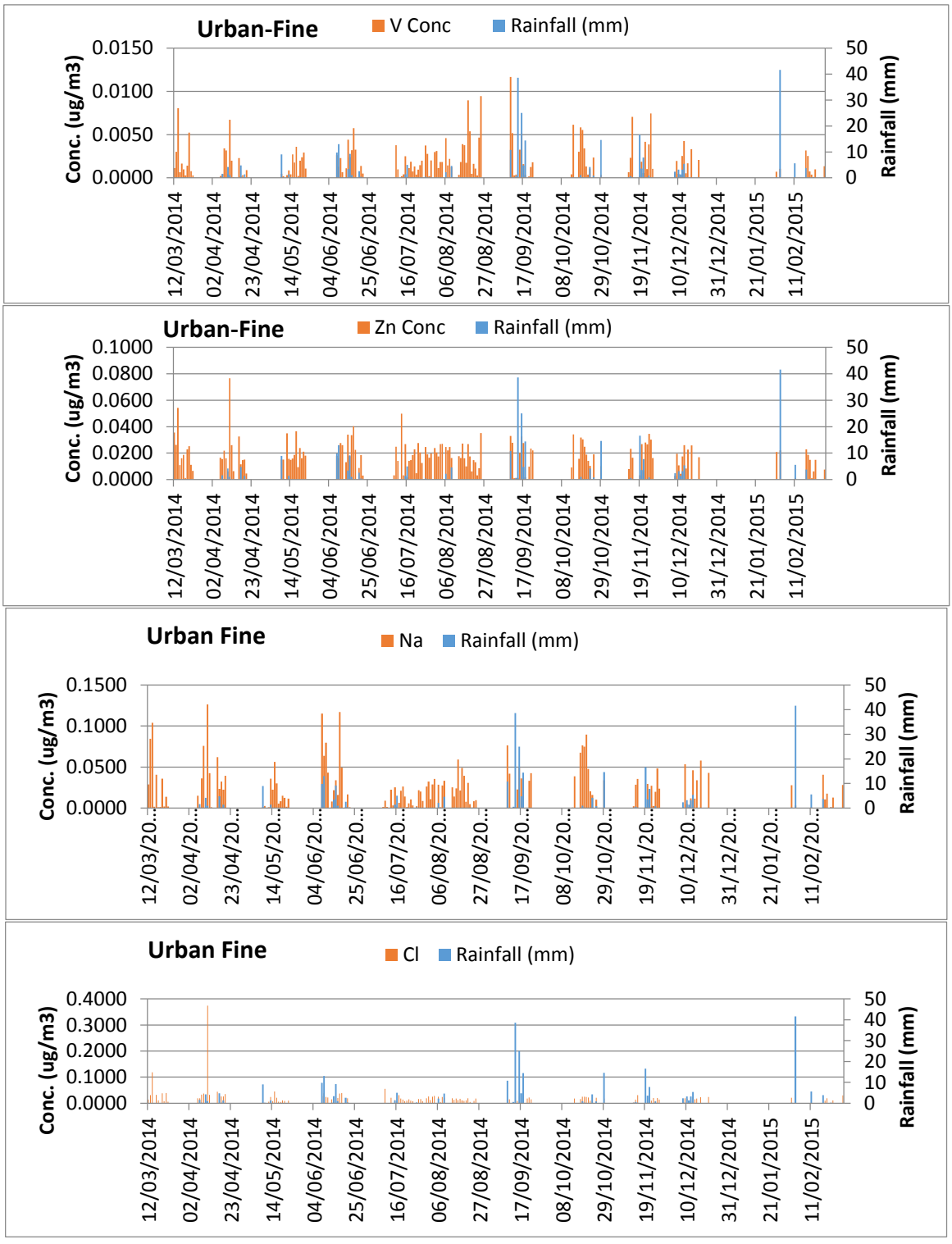

Figure 4.43. *Variation of anthropogenic and marine source species concentration in urban $PM_{2.5}$ with rainfall*

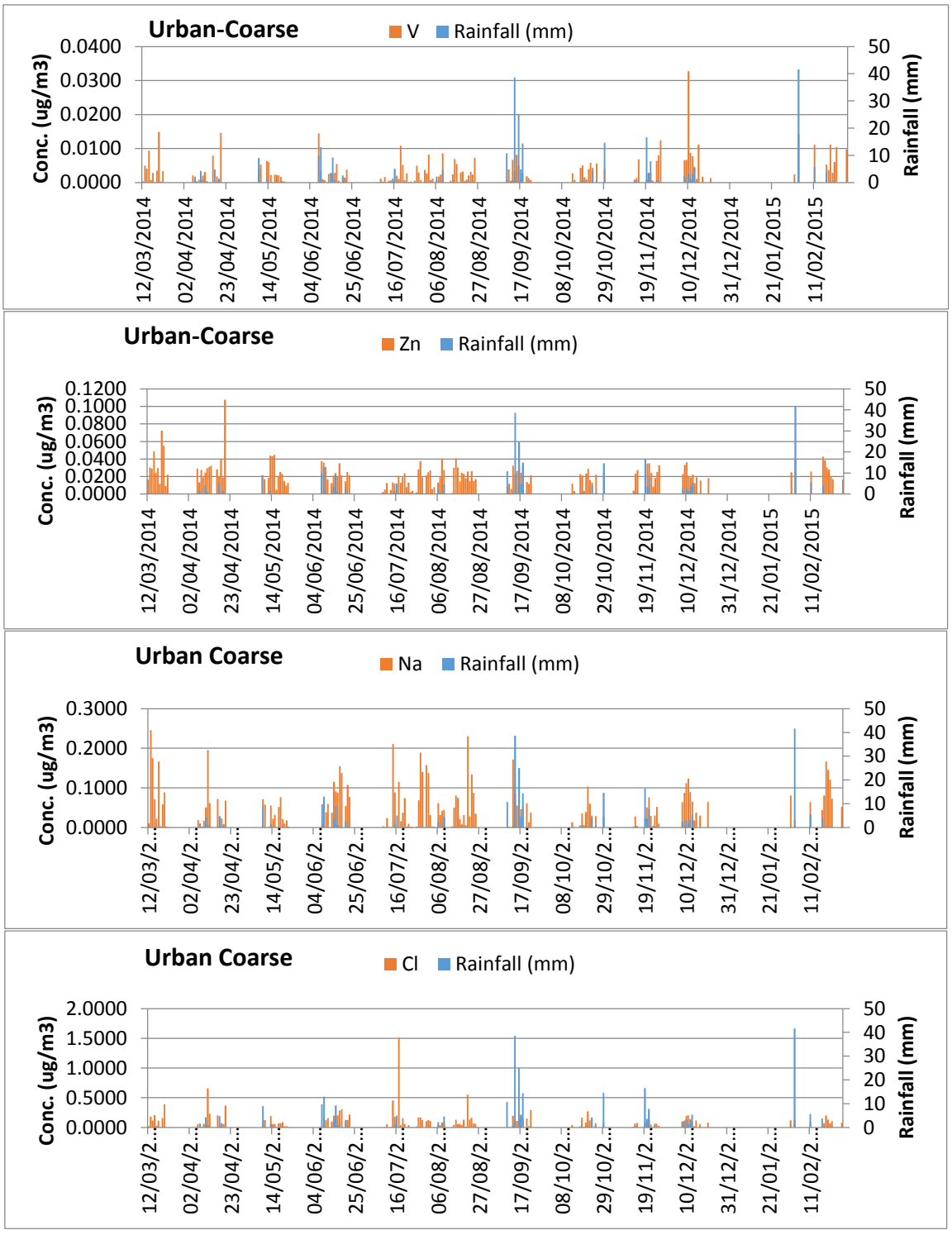

Figure 4.44. *Variation of anthropogenic and marine source species concentration in urban $PM_{2.5-10}$ with rainfall*

Since temperature is a local meteorological parameter which has a direct impact on atmospheric dryness, mineral dust episode can be investigated by looking at the relationship between temperature and concentrations of the dust tracers on one hand and on the other hand temperature relation with anthropogenic and marine source species. The result as can be seen in Figure 4.45-47, shows that concentrations of the dust species generally increased steadily as temperature increased. The peak monthly average temperature at both rural and urban stations corresponded with the highest monthly average concentrations of Al, Fe, Ca and Si. As primary and non-reactive species, effect of temperature on these species is therefore described as indirect rather than direct.

In contrast, anthropogenic (V and Zn) source species recorded their lowest concentrations at the highest temperature period with relatively higher concentrations at the low temperature periods. Chromium, though classified as anthropogenic, was found to show a positive relationship with temperature, thus, exhibiting a crustal characteristic. As indicated earlier, Cr is well documented as a mixed source species – either as crustal or non-crustal (steel and metallurgical industries). Öztürk and Tuncel, 2009 reported higher concentrations of Cr in the rural southeastern Turkey, attributed to high content of Cr in the local soil mineralogy.

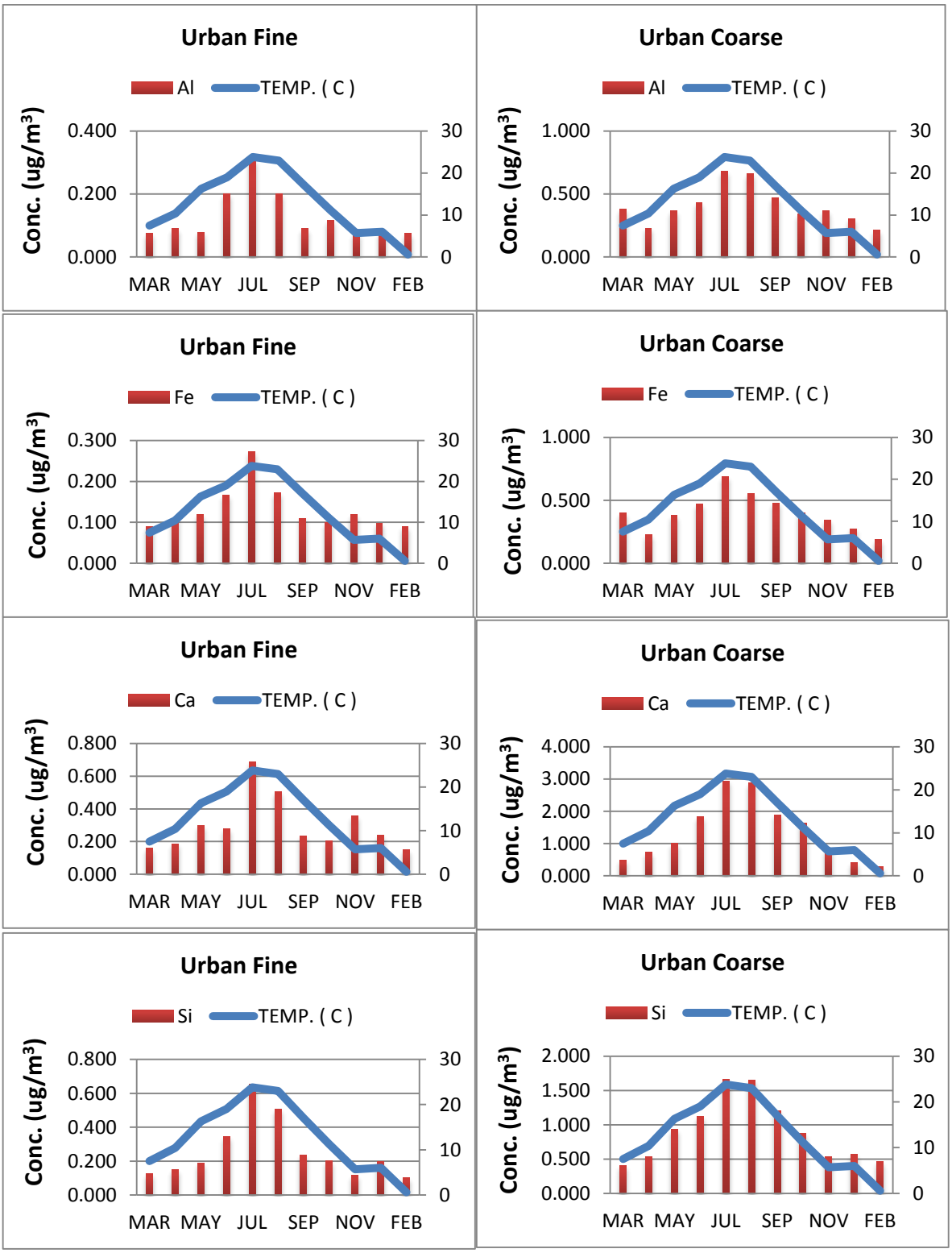

Figure 4.45. *Relationship between monthly average concentration of dust tracer species and temperature*

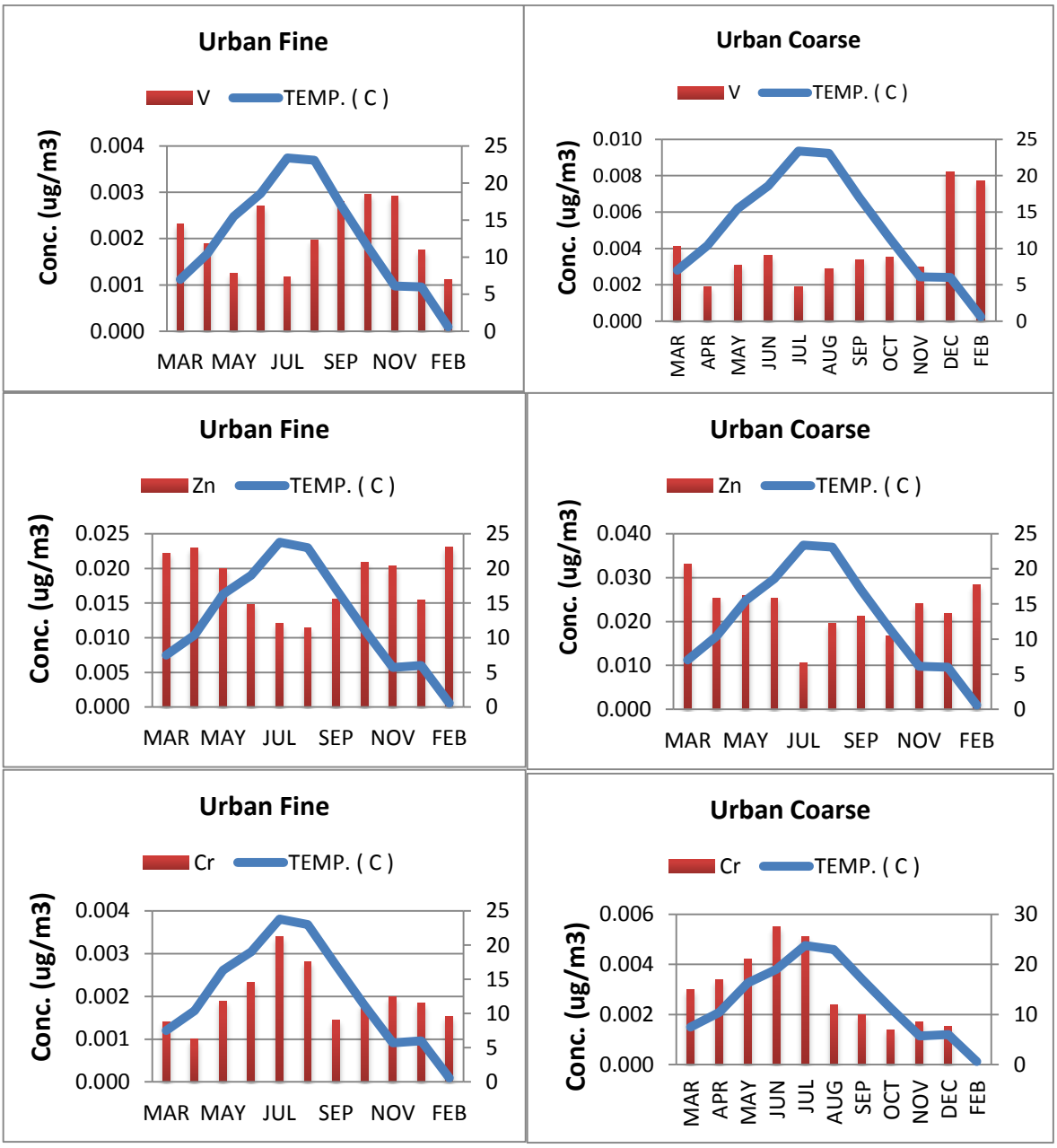

Figure 4.46. *Relationship between monthly average concentrations of species with temperature*

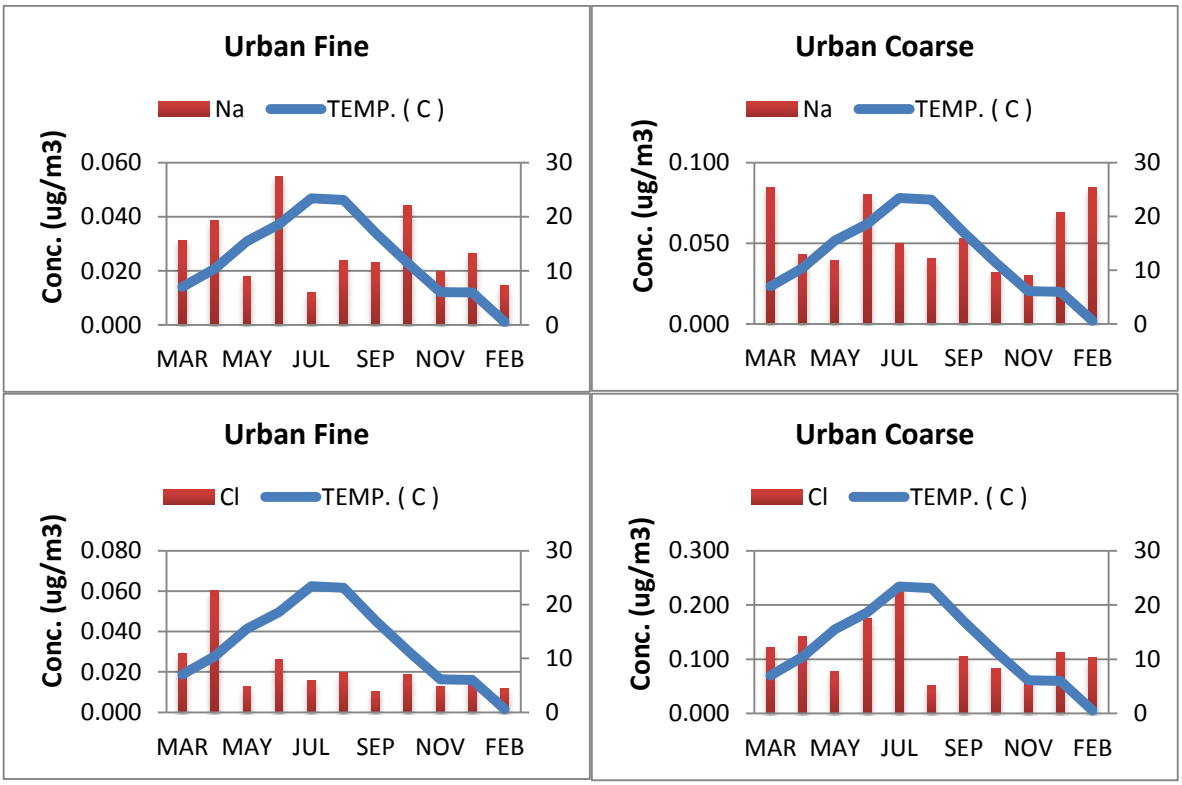

Figure 4.47. *Relationship between monthly average concentrations of marine source species with temperature*

Daily variations:

Time series plots of daily variation inspecies concentrations for selected species are given in Figure 4.48-51. Daily variation was determined by first permutating all the sampling days and finding the difference in the measured concenration. It was observed that, most of the species especially the crustal ones showed more variations even though the magnitude of variation was negligible than the anthropogenic species. Species like Na, Al, Mg and Si in fine PM fraction of the rural station; P, S, K, Si and Ca in the coarse fraction at both the rural and the urban stations varied between 2 and 7 µg units. For Na the highest episodic concentrations were observed on 25 November 2014, recording 0.1800 µg/m^3 in the rural fine PM whilst in the urban fine PM fraction the highest episode was observed on 19 April 2014 with 0.300 µg/m^3 observed concentration. It is quite normal recording high concentrations of Na for stations located far away from the sea as episodes of crustal

materials can be responsible for high Na concentration. Furthermore, the earth's crust can be a minor source of Na.

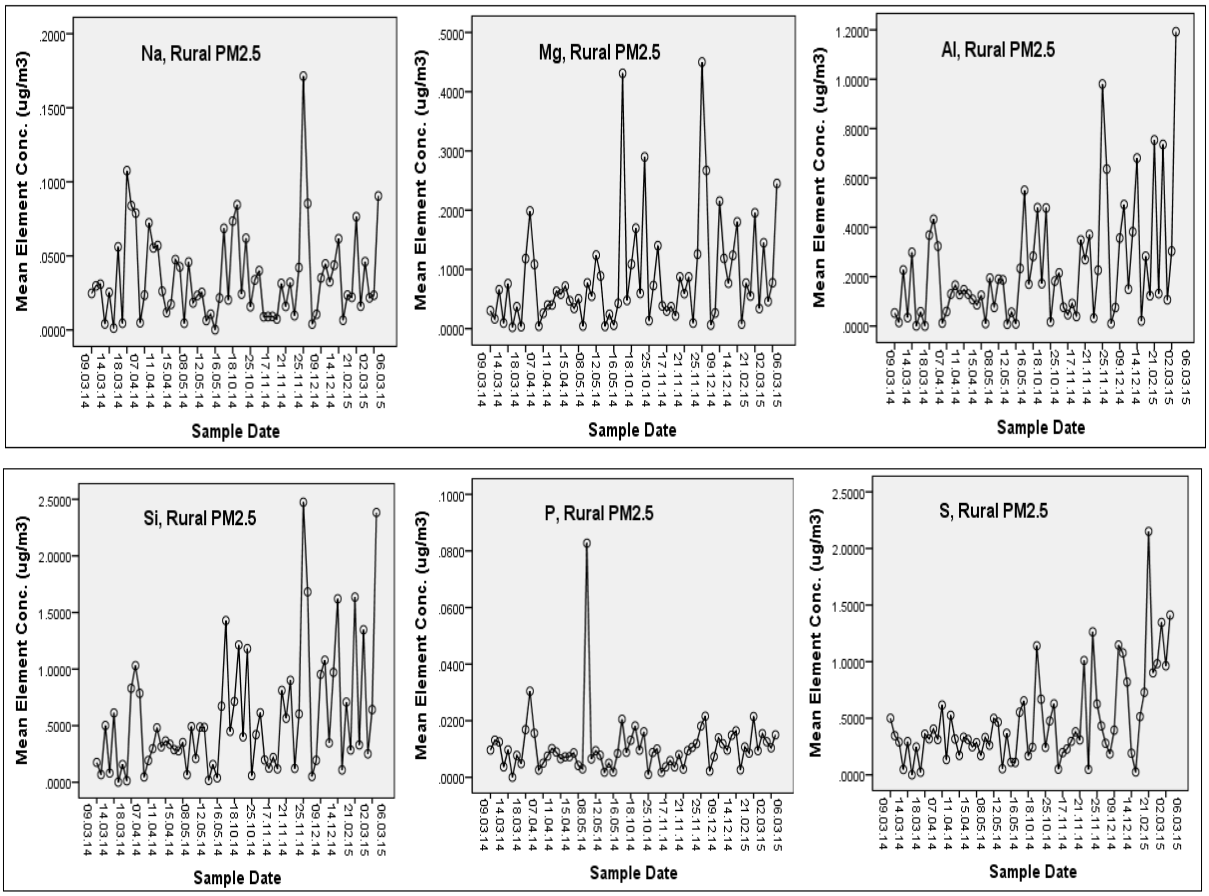

Figure 4.48. *Daily average concentrations (µg/m3) of selected rural-fine PM species.*

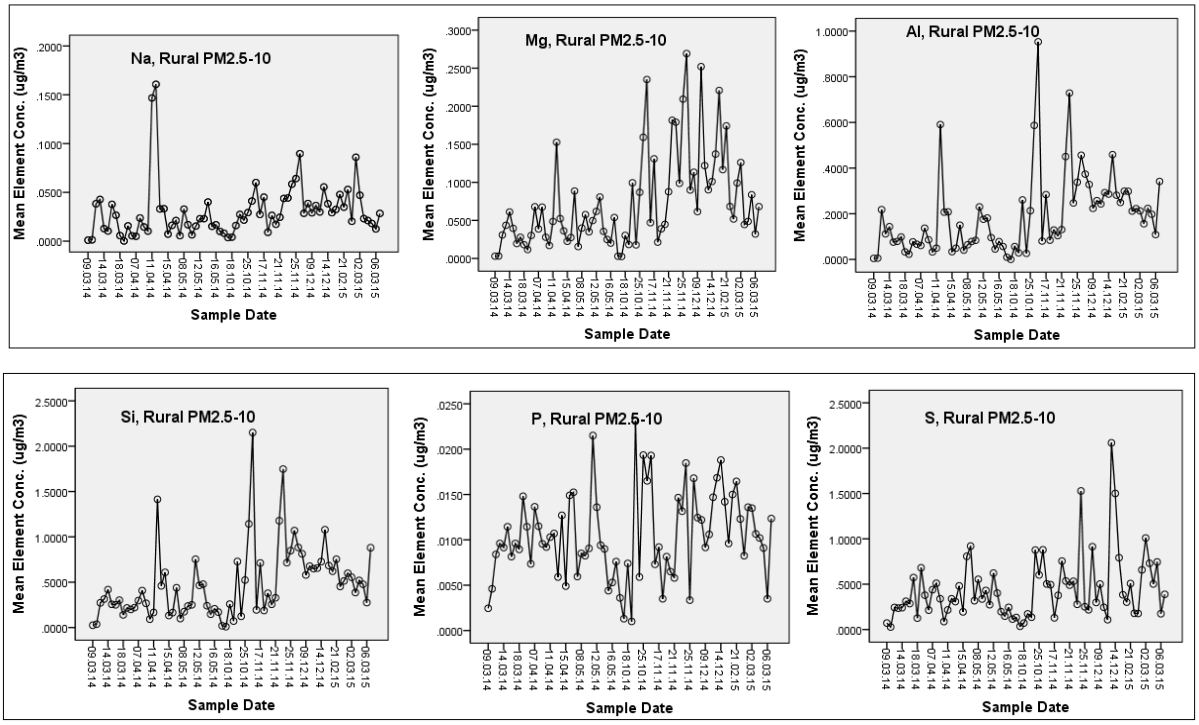

Figure 4.49. *Daily average concentrations (µg/m3) of selected rural-coarse PM species*

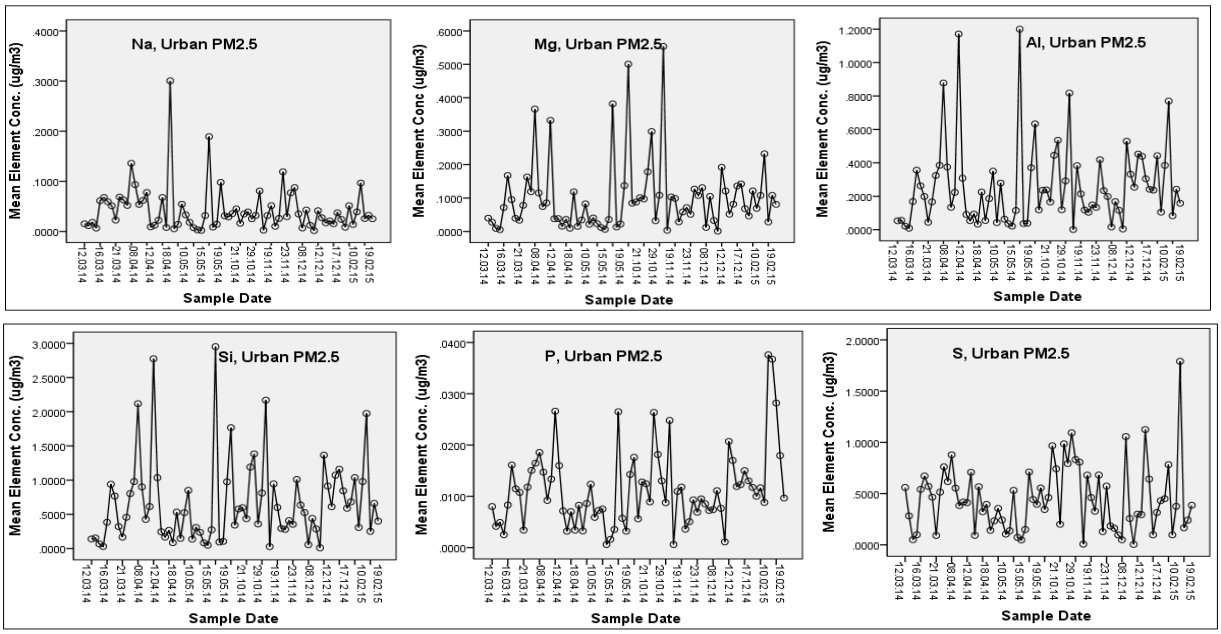

Figure 4.50. *Daily average concentrations (µg/m^3) of selected urban-fine PM species*

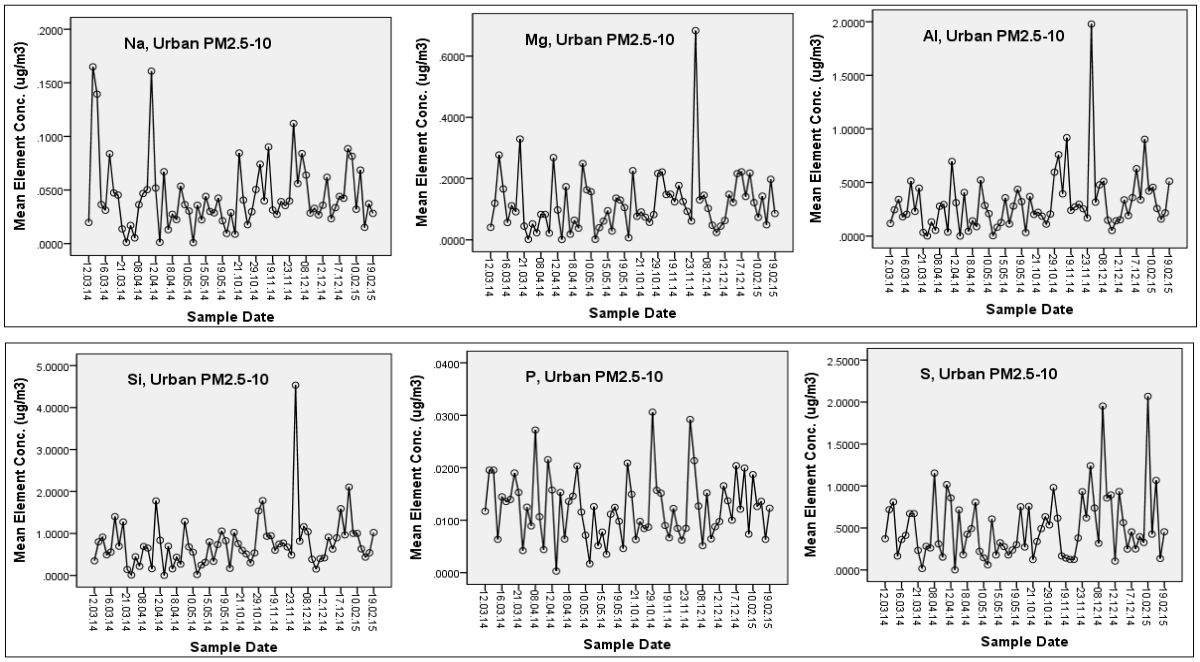

Figure 4.51. *Daily average concentrations (µg/m^3) of selected urban-coarse PM species*

As can also be seen in the time series charts, there were episodic concentrations on certain days by mostly litophilic species. Such episodic variations in aerosols species are reported in the literature (Bergametti et al., 1992, Kocak et al., 2004, Öztürk and Tuncel, 2009) and attributed mainly to variations in emission strength, transport pathways and local meteorological conditions. As indicated earlier in the PMF factor analysis, Na enrichment is attributed to crustal rather than marine source. Anthropogenic species like S and P were also found with episodes. The highest episode for S for e.g. was observed during the heating period on 02 March 2015 in the rural fine PM (2.200 µg/m^3) whilst in the urban fine PM the episode was recorded on 15 February 2015 (1.800 µg/m^3).

4.6. Health Risk Assessment

The health risk assessment commenced with determination of exposure doses of trace metals of fine PM via inhalation, ingestion and dermal absorption. This was followed by cancer risk assessment and sensitivity analysis using Crystal Ball's probabilistic approach. It is important to note that Crystal Ball's applications are based on Monte Carlo Simulation model. Because the computed inhalation data based upon which risk was estimated exhibited right skewed/lognormal distribution (as shown in Figure 4.52), median value of the estimated ILCR was used to generate random variables as well as define the forecast (output) in the model run.

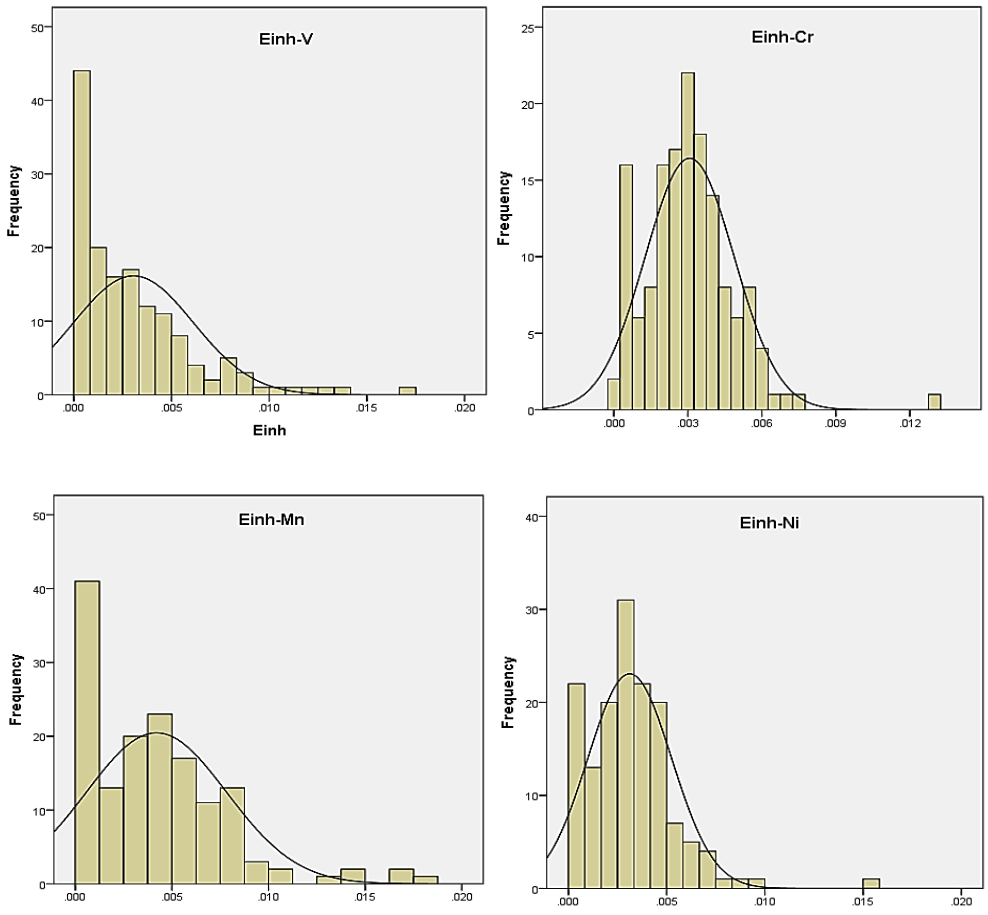

Figure 4.52. *Distribution of $PM_{2.5}$ trace metals over inhalation doses*

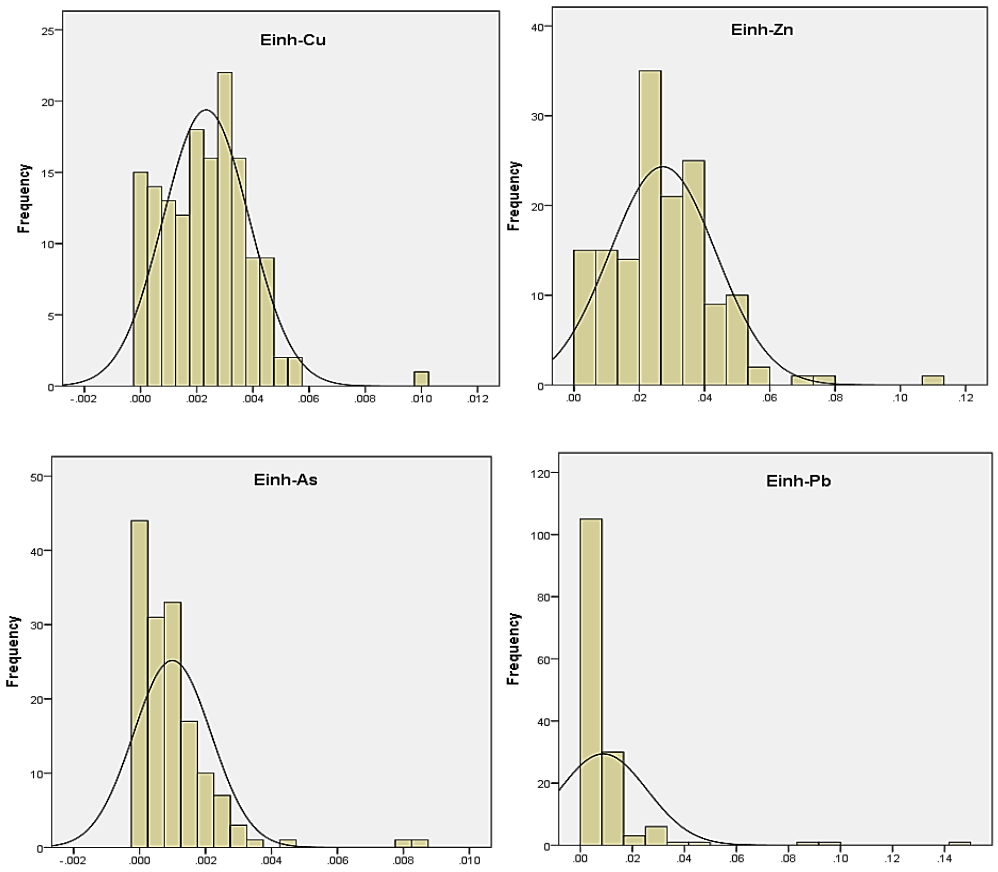

Figure 4.52 (Continued). *Distribution of $PM_{2.5}$ trace metals over inhalation doses*

4.6.1. Cancer risk simulation

As indicated earlier, quantitative assessment of cancer risk estimated as ILCR was simulated using a probabilistic approach of the Crystal Ball model in which 2000 iterations were finally carried out to obtain the risk distributions shown in Figure 4.53 and 4.54, respectively for adult and child age groups. Though cancer risk was simulated for both carcinogenic and non-carcinogenic species, only simulationoutputs for Cr, one of the potential carcinogenic species analyzed is shown for illustrative purposes.

Shown in the risk distribution charts are the mean, median, 5^{th} and 95^{th} percentile values of cancer risk for both adult and child age groups. The median for adult and child age groups were 1.99E-08 and 5.25E-08, respectively. These values are 50 and 19 times, respectively less than the cancer risk limit value of 1.00E-6. At the 5^{th} and 95^{th} percentile the estimated cancer risk were 54 and 46 times, respectively less than the cancer risk limit

in the adult age group whilst in the child age group, the 5th and 95th percentiles were 20 and 17 times less than the risk limit.

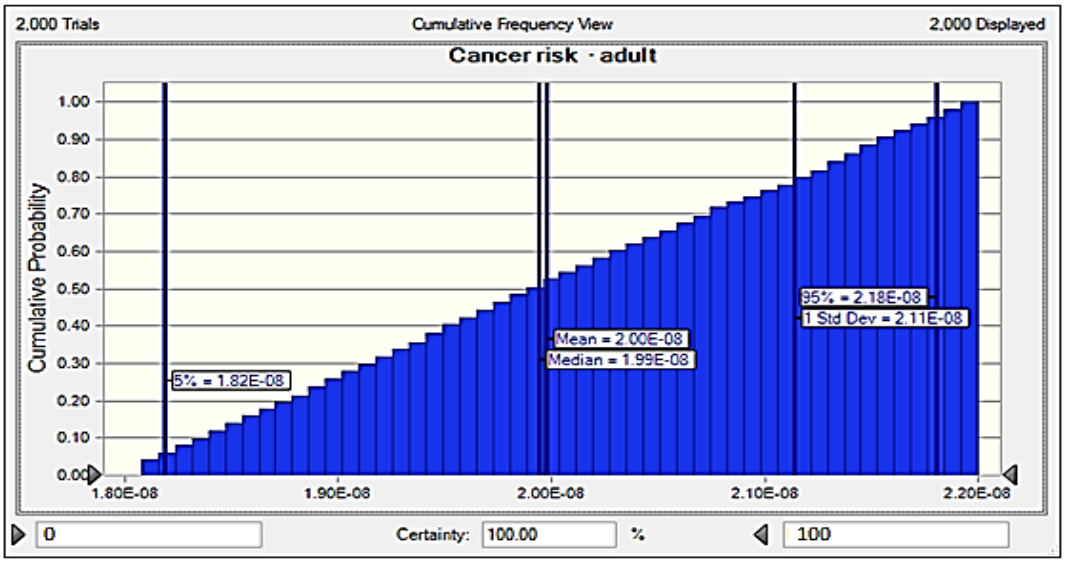

Figure 4.53. *Cumulative probability distribution of the cancer risk (ILCR, for adult age group) of Cr based on inhalation dose by means of a Monte Carlo simulation of the Crystal Ball software for 2000 iterations*

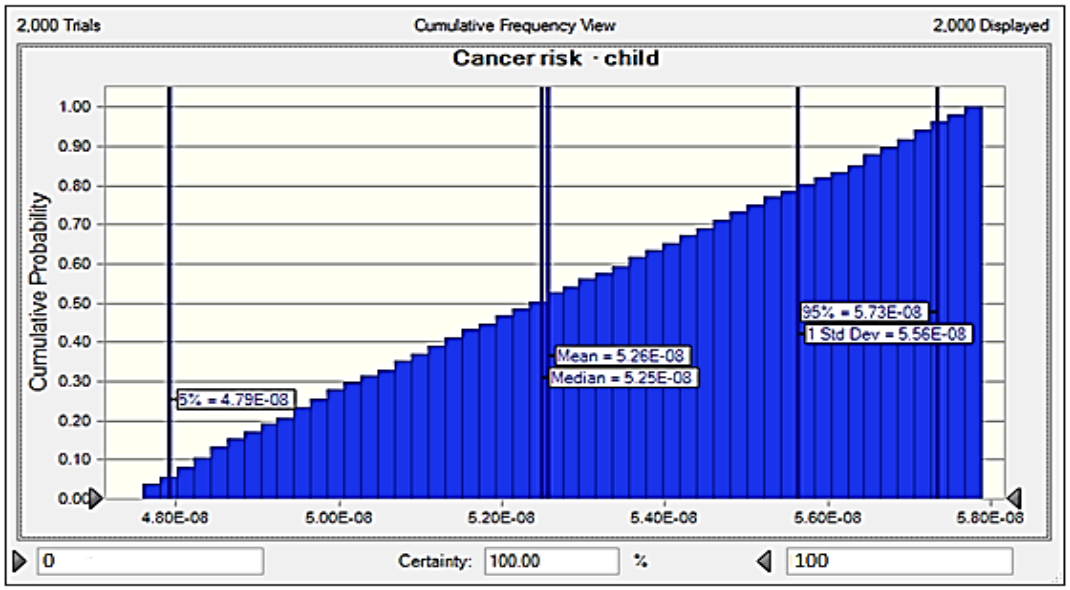

Figure 4.54. *Cumulative probability distribution of the cancer risk (ILCR, for child age group) of Cr based on inhalation dose by means of a Monte Carlo simulation of the Crystal Ball software for 2000 iterations*

The procedure for the risk assessmentin Crystal Ball is summarized in Figure 4.55. There are three main components in the crystal Ball system for simulation; input/assumption, decision and output components. For this study, only the input/assumption and output components were used to simulate cancer risk.

'Assumption' is the probabilistic input which defines the range of the input variable. It can be referred to as the simulation input or simply input variable. In this component, the input variable was defined based on the distribution of the input dataset. Lognormal distribution as indicated earlier was used to define the input variable. After defining the input variable, the simulation output also known as 'forecast' was defined by setting the number of trials i.e. iterations. A couple of trials were selected to run trial simulation in order to choose the best iteration number for the simulation.

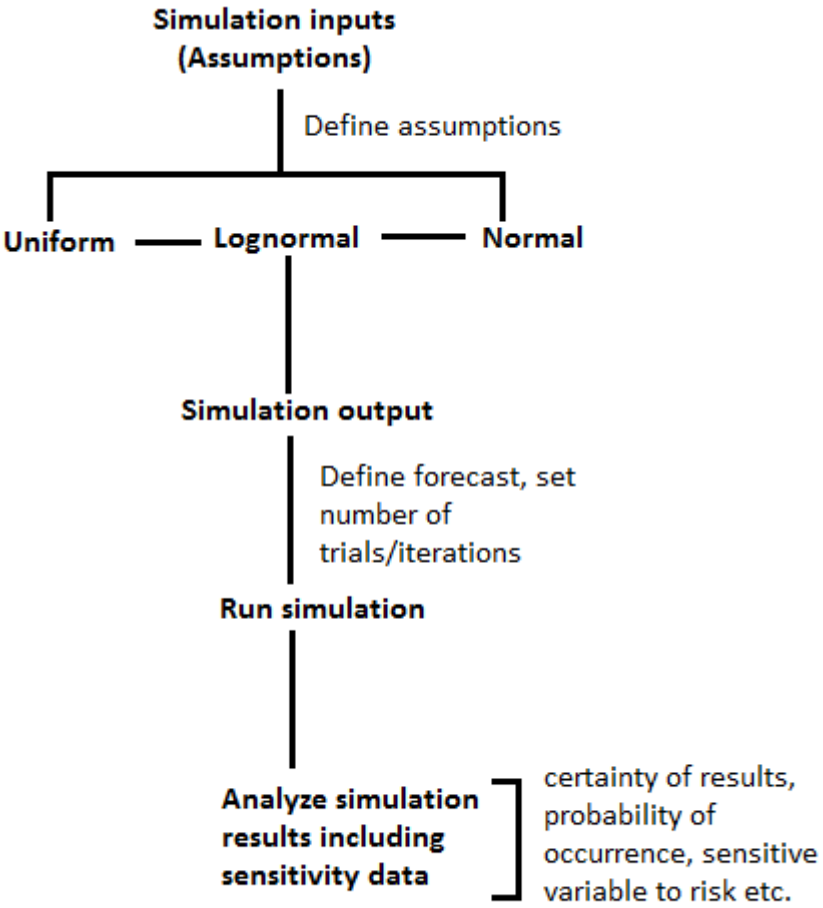

CRYSTAL BALL SIMULATION & SENSITIVITY			
	Simulation	child	adult
	Body weight (BW)	6.25E+01	1.60E+01
	Average time (AT)	2.59E+04	2.56E+04
	Exp. Duration (ED)	5.68E+00	2.48E+01
	Exp.frequency (EF)	3.07E+02	3.61E+02
	CSF	8.83E+00	1.30E+01
	InhR/day	7.00E+00	2.25E+01
	IngR/day	8.26E+01	1.74E+02
	Med. Conc.	5.83E-04	6.40E-04
	Cancer risk limit	1.08E-06	9.00E-07
	Cancer risk	5.68E-08	1.80E-08

Input variables also known as 'assumptions' in Crystal Ball model.

Output variables also known as 'forecast' in Crystal Ball model.

Figure 4.55. *Risk assessment procedure (top) and cancer risk simulation and sensitivity variables (bottom)*

4.6.2. Daily exposure doses

Given in Table 4.13 are the medians of estimated cancer risk, calculated exposure doses of the three pathways with their corresponding reference dose values. As can be seen, for adult and child age groups, ingestion doses of all the metals (V, Cr, Mn, Ni, Cu, Zn, As and Pb) were higher than both inhalation and dermal absorption doses, i.e. $E_{ing}>E_{inh}>E_{derm}$. For adult age group, ingestion contributed 85% of the intake whilst inhalation and dermal absorption contributed 12% and 3%, respectively. The intake distribution was similar for the child age group; 94% by ingestion, 4% by inhalation and 2% by dermal absorption.

Table 4.13. *Calculated exposure doses, cancer risk and reference doses*

	Median values-child					**Reference Doses**		
	E_{inh}	**E_{ing}**	**E_{derm}**	**ILCR**	$\sum R_I/19$	**RfD_{inh}**	**RfD_{ing}**	**RfD_{derm}**
V	2.10E-03	5.49E-02	1.27E-10	6.31E-11	7.23E-10	7.00E-03	7.00E-3	7.00E-5
Cr	3.00E-03	7.85E-02	1.82E-10	9.02E-11	7.28E-10	1.00E-04	3.00E-3	2.50E-2
Mn	3.70E-03	9.76E-02	2.27E-10	1.12E-10	9.95E-10	5.00E-05	1.40E-1	1.84E-3
Ni	3.00E-03	7.94E-02	1.84E-10	9.12E-11	7.35E-10	5.00E-05	5.00E-2	4.00E-2
Cu	2.40E-03	6.22E-02	1.44E-10	7.15E-11	5.53E-10	4.02E-02	4.00E-2	1.20E-02
Zn	2.57E-02	6.76E-01	1.57E-09	7.77E-10	6.45E-09	3.00E-01	3.00E-1	6.00E-2
As	7.00E-04	1.90E-02	4.41E-11	2.18E-11	2.34E-10	1.50E-05	3.00E-4	6.65E-07
Pb	5.00E-03	1.33E-01	3.08E-10	1.52E-10	2.09E-09	3.52E-03	3.50E-3	5.25E-4
	Median values-adult					**Reference Doses**		
	E_{inh}	**E_{ing}**	**E_{derm}**	**ILCR**	$\sum R_I/56$	**RfD_{inh}**	**RfD_{ing}**	**RfD_{derm}**
V	4.12E-03	3.51E-02	1.62E-10	1.01E-10	4.42E-10	7.00E-03	7.00E-3	7.00E-5
Cr	5.90E-03	5.38E-02	2.49E-10	1.45E-10	4.45E-10	1.00E-04	3.00E-3	2.50E-2
Mn	7.30E-03	9.72E-02	4.50E-10	1.80E-10	6.09E-10	5.00E-05	1.40E-1	1.84E-3
Ni	5.95E-03	5.75E-02	2.66E-10	1.47E-10	4.49E-10	5.00E-05	5.00E-2	4.00E-2
Cu	4.70E-03	3.62E-02	1.67E-10	1.15E-10	3.38E-10	4.02E-02	4.00E-2	1.20E-02
Zn	5.07E-02	3.15E-01	1.46E-09	1.25E-09	3.94E-09	3.00E-01	3.00E-1	6.00E-2
As	1.40E-03	6.30E-03	2.90E-11	3.51E-11	1.43E-10	1.50E-05	3.00E-4	6.65E-07
Pb	9.90E-03	5.11E-02	2.36E-10	2.45E-10	1.28E-09	3.52E-03	3.50E-3	5.25E-4

E_{inh}, is exposure dose via inhalation, E_{ing}, is exposure dose via ingestion, E_{derm}, is exposure dose via dermal absorption, ILCR, is incremental cancer risk factor, R_I, is individual lifetime cancer risk, RfD_{inh}, is reference dose for inhalation, RfD_{ing}, is reference dose for ingestion and $RfD_{derm,}$ is reference dose for dermal absorption.

High ingestion doses can well be attributed to food especially fruits and vegetables on whose surfaces fine particulates are adsorbed and eventually ingested. Drinking water can be implicated but to a lesser extent as most part of Turkey including the study area drink treated bottled water. Dermal absorption recorded the least dose level perhaps due to covering of the skin by clothing; according to reports in the literature, only about 5–25% of the human body gets exposed during winter. Inhalation dose was expected to be higher than observed since the fraction of PM ($PM_{2.5}$) being considered is both inhalable and respirable. Low level of inhalation dose can, however, be attributed to low infiltration/air exchange rate between indoor and outdoor environments limiting the effects of outdoor air quality on the indoor. It is worth noting that all the metals except Zn and Mn recorded higher ingestion doses than their reference doses for both age groups. Though both Zn and Mn have been classified by IARC as being non-carcinogenic (IARC, 2011), they are, however, known to be toxic and therefore could pose a health threat to the population of the study area.

In general, the result suggests exposure to toxic metals of PM are potentially higher in food and water than inhaling and dermally absorbing them directly from indoor environment. In a similar study conducted in China, (Cao et al., 2014) the results indicated that food ingestion played an important role in the total average daily dose of children for most metals/metalloids, especially Cu, Ni and Mn. For the child age group, ingestion dose for Zn was found to be approximately 4 times higher than its reference dose. In the adult age group, however, the ingestion and reference doses of Zn were of the same order of magnitude. This result implies ingestion of trace metals of PM among adult age group is about 4 times lower than the child age group. In contrast, inhalation and dermal absorption doses (E_{inh} and E_{derm}, respectively) were 2 orders of magnitude lower than their respective reference doses (RfD_{inh} and RfD_{derm}, respectively). The result also indicates high risk of exposure to toxic metals by the child age group compared to the adult age group. Elementally, the order of increasing level of exposure is: Zn>Pb>Mn>Ni>Cr>Cu>V>As. Whilst the inhalation doses of V, Cu, Zn and Pb were 2-5 orders of magnitude lower than their corresponding reference doses; Cr, Mn, Ni and As were 2-3 orders of magnitude higher than their corresponding reference doses. It is important to note that these elements have been identified as either carcinogenic, agents of carcinogen or toxic (Dragovic et al., 2013). IARC has classified Mn as toxic element having no carcinogenicity to humans whilst As, Cr and Ni are carcinogenic to humans (Manousakas et al., 2013). Dose

relationship among the three pathways and their reference doses is shown graphically in Figure 4.56.

It is important to note that as emissions are affected by variability of meteorological parameters so do exposure doses vary seasonaly and hence cancer risk. Typically, seasonal pollutant like S and other coal combustion species like As are expected to be high in winter. It will therefore be prudent to conduct further study in the near future to determine seasonal variation in exposure and cancer risk.

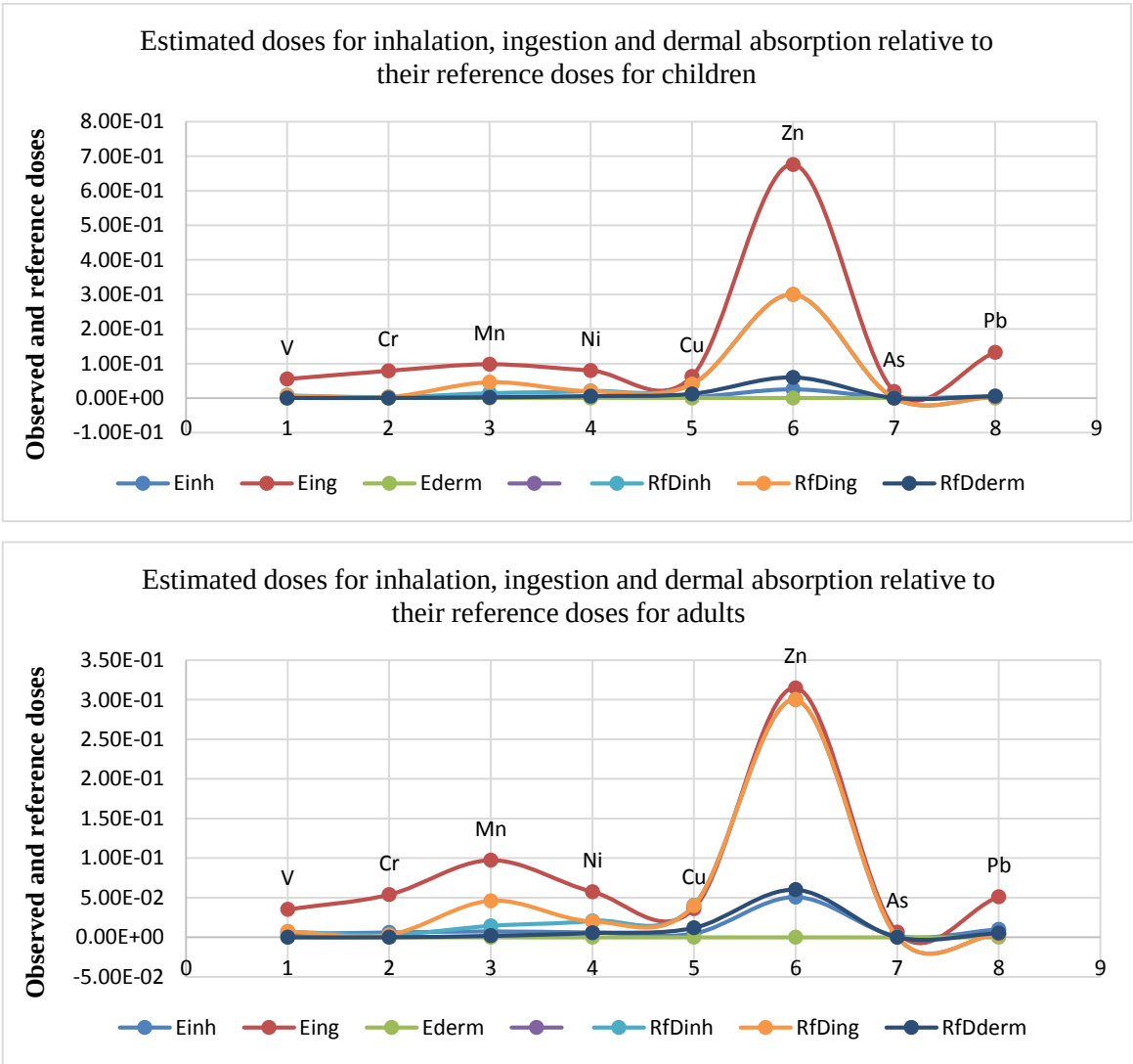

Figure 4.56. *Observed inhalation, ingestion and dermal absorption doses relative to their reference doses for both child (top) and adult (bottom) age groups. E_{inh}, is inhalation exposure dose, E_{ing}, is ingestion exposure dose, Ederm, is dermal exposure dose, RfDinh, RfDing and RfDderm are reference doses for inhalation, ingestion and dermal absorption, respectively*

4.6.3. Cancer risk levels

Cancer risk i.e. sum of hazards ($\sum_{2}^{20} {R_I}/_{19}$ and$\sum_{21}^{76} {R_I}/_{56}$) ranged between 9.95E-10 and 2.09E-09 for the child age group and between 6.09E-10 and 1.28E-09 forthe adult age group. Figure 4.57 illustrates estimated individual risks relative to the risk threshold. The maximum cancer risk for child and adult age groups were found to be 450 and 750 times less than the risk limit. Lonati et al., 2012, reported median risk level of 10^{-8} – 10^{-10} being ten-fold lower than the deterministic estimate. They underscored that the estimated risk was almost entirely determined by Cd exposure through diet. Incidentally, the highest exposure dose in this study was recorded by Zn with ingestion being the highest contributing intake pathway. It is important to note that Zn and Cd belong to the same group of transition metals and therefore share some common properties; having same affinity and susceptibility to food surface adherence. Other transition metals, Ni and Cr and metalloid, As, have been found to be leading carcinogens, 30 – 200 times higher than the safe limit through food ingestion (Cao et al., 2013).

In this study, estimated risk for all the metals were below the cancer threshold value of 1.00E-06. While this indicates acceptable probability distribution and that there is no cause for carcinogenesis by these metals to the population of the study area, there is however, a concern regarding Zn whose level in the child age group was very close to the threshold value. Thus, a non-carcinogenic effect of Zn could be a threat especially to children in the study area. Based on this inference, hazard quotient (non-carcinogenic risk) was calculated for Zn. The results obtained were 2.15 for child age group and 1.31 for adult age group. These figures are higher than the non-carcinogenic safe limit of 1. In general, the cancer risk assessment well reflects the daily exposure doses earlier discussed. The child age group recorded approximately 24% higher values for both carcinogenic (As, Cr and Ni) and non-carcinogenic (Mn, Zn and Pb) species than the adult age group.

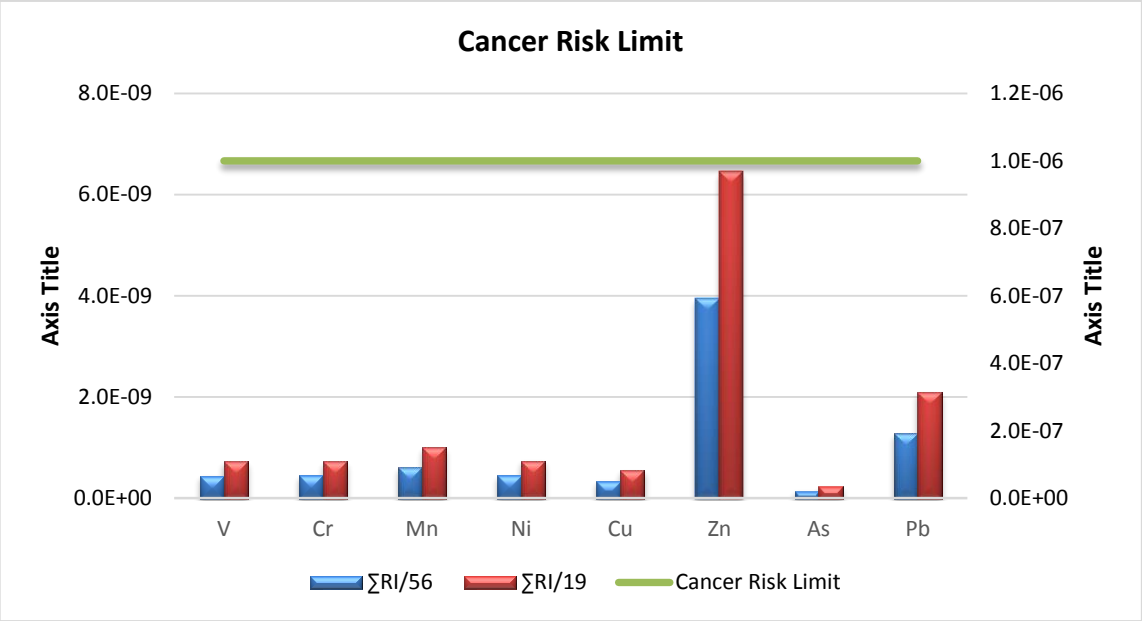

Figure 4.57. *Cancer risk (sum of hazards) for adult and child age groups with the cancer threshold*

4.6.4. Sensitivity analysis

Sensitivity analysis was performed to determine the contributions/impacts of uncertain variables to the output i.e. cancer risk. Principally, the objective was to find which factor is most sensitive and therefore drives the cancer risk. In other studies, including Widziewicz et al., 2016 and Lonati et al., 2012, parameters such as body weight (BW), exposure frequency (EF), exposure duration (ED) and averaging time (AT) have been used in testing sensitivity to cancer risk. In addition to these parameters, this study considered cancer slope factor (CSF) and observed metal concentration (C), both of which are directly related to the estimated ILCR.

Results of the sensitivity test is graphically illustrated in Figure 4.58. Contributions of these variables in percentage terms ranged between 1.0% and 44% for AT and ED, respectively for the child age group whilst in the adult age group contribution ranged between 3% and 61% again for AT and ED, respectively. In the child age group, ED, was found to be the major driving force (44%) to cancer risk followed by BW (36%), EF (9%), C (7%), CSF (3%) and AT (1%). In the adult age group, however, the order of impact to cancer risk was ED (61%), EF (17%), BW (8%), C (6%), CSF (5%) and AT (3%).

Dynamics of BW relative to cancer risk was well pronounced in this study. Whilst it rated the second highest impact in the child age group with a percentage of 36, in the adult age group it rated third with only 8%. This implies as one ages, BW, as cancer risk factor dwindles and replaced by EF. Metal concentration had almost the same impact on risk between the two age groups, lagging BW and EF.

Though physiological parameters i.e. body weight, age etc. are well documented in the literature as being significant to cancer hazards (Widziewicz et al., 2016; Kumar et al., 2009; Mari et al., 2009; Schuhmacher et al., 2001), cancer slope factor is also documented as highly significant and yet highly uncertain parameter (Chen and Liao, 2006) for cancer risk assessment. The sensitivity result of this study, however, shows that the contribution of CSF to risk was quite low, about 3-5% across the two age groups. CSF was initially treated as a uniform distributed (UN) data in the Monte Carlo simulation, it was changed to a normal distribution (NR) and finally to a lognormal distribution (LN). In all these forms the impact did not change significantly; 2-5% for UN, 1-4% for N and 3-5% for LN.

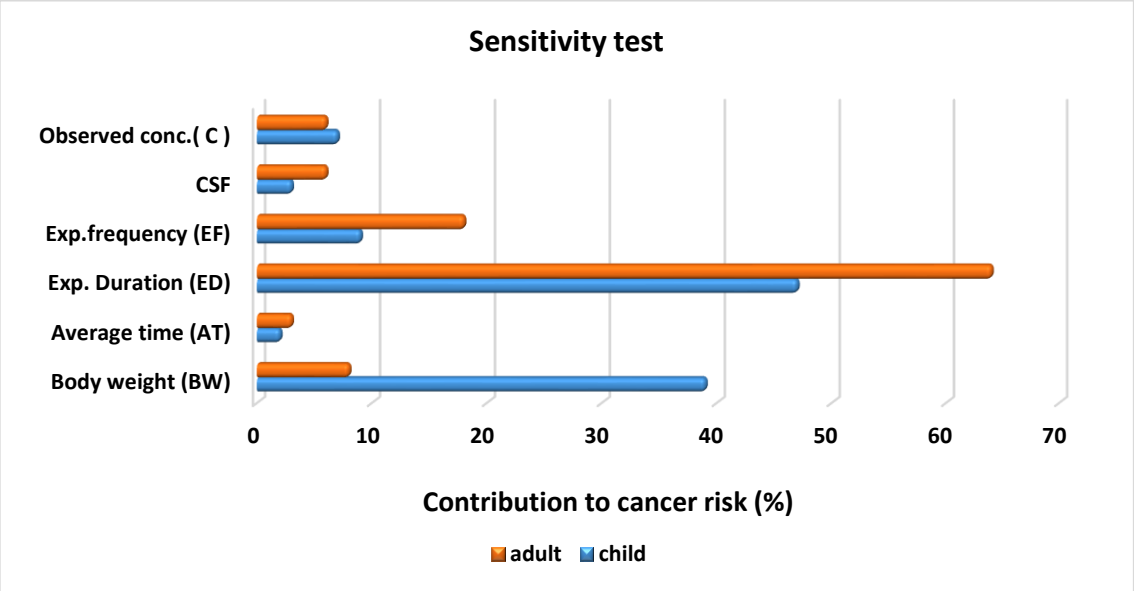

Figure 4.58. *Contribution to cancer risk by risk assessment parameters*

4.6.5. Daily exposure dose vs. cancer risk (Spearman's correlation)

To measure the strength and direction of relationship between daily exposure dose and cancer risk, the Spearman's correlation was used. Results of the correlation tests are summarized in Table 4.14. For both child and adult age groups, a strong positive relationship was observed with correlation coefficients of 0.98 (98%) at the 0.01 level. This implies as exposure dose increasesso does cancer risk. Figure 4.59, illustrates graphically the bivariate relationship between exposure dose and cancer risk.

Table 4.14. *Relationship between exposure dose and cancer risk-Spearman's correlation*

		Sum of Hazard-child	Exposure dose-child	Sum of hazard-adult	Exposure dose-adult
Sum of Hazard-child	Correlation Coefficient	1.000	.970**	1.000**	.976**
	Sig. (2-tailed)	.	.000	.	.000
	N	8	8	8	8
Exposure dose-child	Correlation Coefficient	.970**	1.000	.970**	.994**
	Sig. (2-tailed)	.000	.	.000	.000
	N	8	8	8	8
Sum of hazard-adult	Correlation Coefficient	1.000**	.970**	1.000	.976**
	Sig. (2-tailed)	.	.000	.	.000
	N	8	8	8	8
Exposure dose-adult	Correlation Coefficient	.976**	.994**	.976**	1.000
	Sig. (2-tailed)	.000	.000	.000	.
	N	8	8	8	8
**. Correlation is significant at the 0.01 level (2-tailed).					

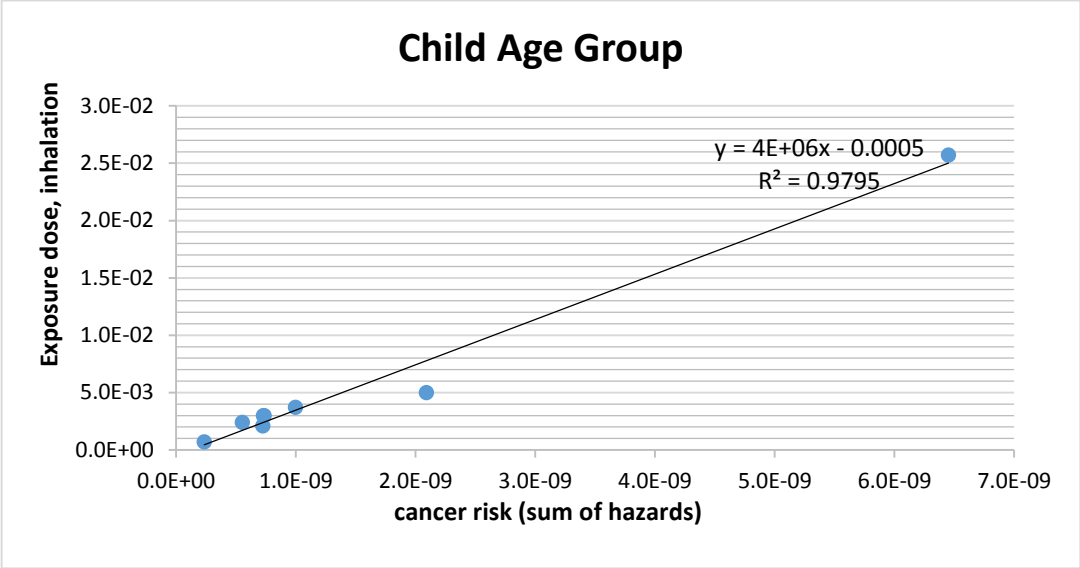

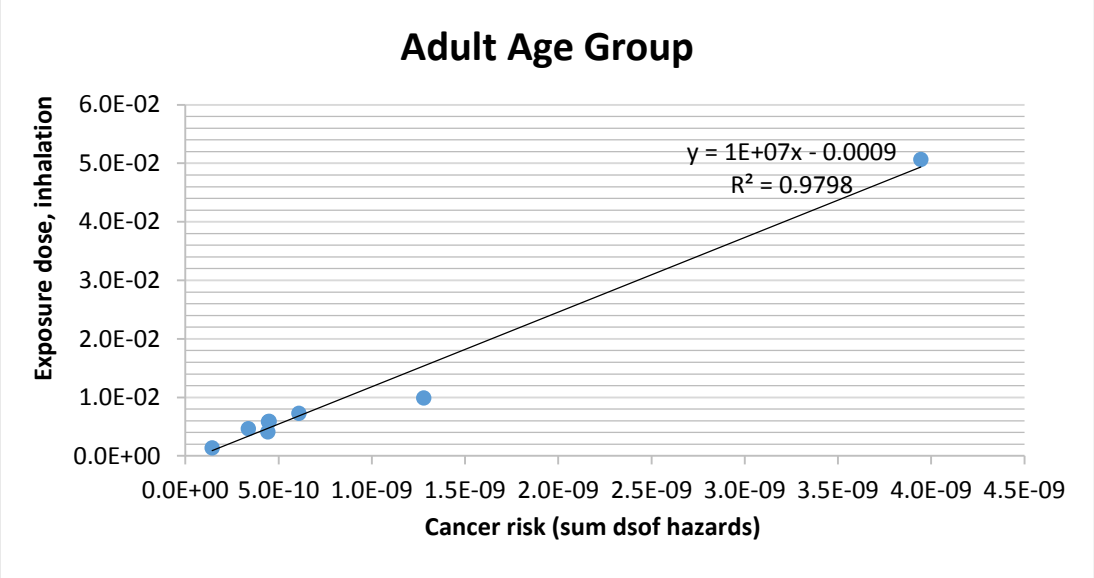

Figure 4.59. *Relationship between inhalation exposure dose and cancer risk for child and adult age groups – Spearman's correlation*

5. CONCLUSIONS AND RECOMMENDATIONS

5.1. General and Specific Findings

General outcome and specific findings of this study as well recommendations for future considerations are summarized as follows:

General outcome:

Fine ($PM_{2.5}$) and coarse ($PM_{2.5-10}$) aerosols collected from rural and urban monitoring stations located in an industrial region of western Turkey were analyzed by both Inductively Coupled Plasma-Tandem Mass Spectrometer (ICP-MSMS) and Particle Induced X-ray Emission (PIXE) techniques. A comparative analysis between the results of the two techniques based on their resolvation for 21 elements including Na, Mg, Al, S, Ca, Ti, V, Cr, Mn, Fe, Ni, Cu, Zn, As, Se, Br, Rb, Sr, Zr, Mo and Pb was investigated.

Percent below detection limit (%BDL) for PIXE, varied between 0% (for Zn) and 83% (for Mo) with important marker elements such as Ca, S, K, Cl and Na being 4%, 8%, 11%, 12% and 21% respectively. For ICP-MSMS, %BDL varied between 0% (for Mg) and 98% (for Se); important markers such as Na, Al, Ca, Cr, V and S were between 0% and 1% below detection. Ratio values (ICP-MSMS/PIXE ratio) for most elements excluding Na, Mg, Al, Br and Zr were ~1, suggesting a good relation between the two techniques. In terms of measured concentration, the two techniques yielded almost the same concentration amounts for the elements Ti, V, Cr, Mn, Fe, As, Se, Br, Rb, Sr, Zn, Mo and Pb – hence they were found to be equally competitive for measurement of these elements. Detection and/or recovery of species was generally better by ICP-MSMS than PIXE. Low recovery (or high %BDL by PIXE was attributed to attenuation of low energy x-rays from lighter elements and peak overlap, continuous background due to bremsstrahlung and also, the effects of matrix factors which decreases the limit of detection of the element and consequently affect the observed concentration in PIXE.

PIXE has added advantage over ICP-MSMS for analysis of species found to be comparable between the two methods (Ti, V, Cr, Mn, Fe, As, Se, Br, Rb, Sr, Zn, Mo and Pb) due to its ability to analyze without sample dissolutionwhich in most cases are a source of contamination in ICP-MS analysis. The use of catalyzers such as $LaNO_3$ prior to ICP-MSMS analysis to increase solubility for partially dissolved species during

digestion is an important set-backin ICP-MSMS. Also, species with very high ionization energy may not be excited in the plasma flame and will therefore not be detected by ICP-MSMS.Furthermore, PIXE measurement takes far shorter time than ICP-MSMS.

Back trajectory analysis for source location and positive matrix factorization for source apportionment were conducted using HYSPLIT and PMF V5 models, respectively. Back trajectories of the air masses arriving at the monitoring stations each day of the sampling campaign of this study were analyzed. Five-day archived back trajectories were run using the on-line HYSPLIT model. Similar patterns were observed for all trajectories at the starting altitudes in the HYSPLIT model's output of back trajectories. The highest altitude (1400 m) of air masses reaching our stations was found to come from the north-western neighborhood of Turkey (Ukraine, Romania, Bulgaria and Greece). The lowest (100 m) and intermediate (700 m) arrival heights of air masses, however, travelled relatively shorter distances and were found to come from the north-east and south-east regions. At the rural station, the 100 m and 700 m trajectories were found to have a common source; traversing together from Azerbaijan and Georgia before reaching the receptor. At the urban station, however, these same trajectories, (100 m and 700 m) were seen as local air masses from the south-west and north-east of Turkey; suggesting pollution due to these air masses are locally generated. Pollution due to neighboring countries were low (1%-30%) compared to locally generated pollution (70% - 90%).

EPA's PMF (version 5) model was run and based on goodness of fit of the model to the original data and by careful examination of the base model results; seven factors were finally considered for analysis at both stations. The seven generated factors were categorized into three group sources at each station. At the urban station, group 1 was called crustal/dust group; comprises 2 factors dominated by Al, Si, Ti, Rb, Ca, Sr, Fe and Mn. Group 2 was called local source group; comprises 2 factors driven mainly by typical sea salt species (Na, Mg and Cl) and Sulfate. The third group called anthropogenic group, driven mainly by industrial emissions; fuel and heavy oil combustion. Group 1 at the rural station had 3 factors and was called 'crustal group' due to dominance of crustal species in the three resolved factors. Group 2, called 'mixed-source group' comprises only 1 factor characterized by oil and coal combustion species and the third group was called 'anthropogenic group'; comprises 3 factors, dominated by Pb.

Elements including Na, Mg, Al, Si, K, Ti, Mn, Fe, Rb, Sr and Zr had EFc value < 3 and were therefore considered to be originating from crustal sources. Elements referred to as highly enrich were those having EFc values between 30 and above 1000. These include S, Cl, Zn, As, Se, Br, Mo and Pb. This category of elements is anthropogenic source mainly from fuel combustion. The pattern of the calculated Geoaccumulation index (Igeo) values did not deviate from that of enrichment factor values making the two methods a good complement to each other as preliminary source apportionment technique. No element recorded Igeo value < 1, implying non-deficiency or depletion of any of the measured elements in the study backgrounds.

Dust intrusion from the Sahara was studied using NMMB/BSC-dust model of the Barcelona Dust Forecast Center to assess dust transport to Western Turkey in particular. The highest dust loads were observed in the months of July and August whereas relatively lower loadings were observed in March and November. Dust loads reaching Western Turkey were, however, low, 0.1 – 0.4 g/m^2 compared to the loads from the source countries which ranged between 1.2 and 6.4 g/m^2. Incidentally, the highest daily surface dust concentration for Turkey (50-200 $\mu g/m^3$) was observed in the central and south-west of the country in the month of March corresponding with the peak period of Saharan dust transport to the Eastern Mediterranean.

Mineral dust episodes were observed using dust tracers; dust-to-nondust day ratios and back trajectory results. The trace of the 100 and 700 meters trajectories arriving at the two receptor locations across the Caspian Sea into the Central Asian country of Azerbaijan signified a mineral dust episode at the receptors. Also, higher concentrations of dust tracers, higher dust-to-nondust ratios of dust tracer species (Al, Fe, Ca and Ti) signified mineral dust episodes.

Health risk assessment was conducted by determining daily exposure doses of V, Cr, Mn, Ni, Cu, Zn, As and Pb via inhalation, ingestion and dermal absorption for both adult and child age groups. Using Monte Carlo's probabilistic approach, lifetime cancer risk factors (ILCR) were then determined for the two age groups.

Sensitivity analysis was performed to determine the contributions/impacts of uncertain variables to the output i.e. cancer risk in the two age groups. Six parameters including body weight (BW), exposure frequency (EF), exposure duration (ED),

averaging time (AT), cancer slope factor (CSF) and observed metal concentration (C) were considered in the sensitivity analysis.

Specific findings include:

I. Species including Ca, Al, Mg and Na were better detected by ICP-MSMS than PIXE – making ICP a better method for characterizing these species.

II. In terms of measured concentration, the two methods yielded similar concentration amounts for species Ti, V, Cr, Mn, Fe, As, Si, Br, Rb, Sr, Zn, Mo and Pb – making the two methods equally competitive for characterizing these species.

III. A good positive relationship ($R^2 = 0.7 – 0.9$) between the two methods elementally and generally for PM measurements at the 95% CL.

IV. Recovery of species was generally better (~ 30%) by ICP-MS than PIXE.

V. According to back trajectory analysis, pollutant materials measured at the receptor was traced back as far as Azerbaijan and Georgia to the east of Turkey.

VI. According to the dust model (NMMB/BSC dust model), dust flow into Western Turkey originate from the Sahara across the Mediterranean whereas dust flow into Central Turkey originate from the Middle East.

VII. The highest daily surface dust concentration in Turkey was observed in the Central and South-west of the country in the month of March coinciding with the peak period of Saharan dust transport to the Eastern Mediterranean.

VIII. Observation of mineral dust episodes at the two receptor locations using combination of mineral dust tracers concentration ratios, back trajectories and satellite observations.

IX. Health risk assessment including daily exposure doses and cancer risk was conducted using Monte Carlo probabilistic approach. Ingestion dose was found to be the highest followed by inhalation and lastly dermal absorption. Ingestion contributed 85% of the dose in the adult age group and 94%, in the child age group. Inhalation contributed 12% and 4% in the adult and child age groups, respectively. Dermal absorption contributed 3% and 2% in the adult and child age groups.

X. Estimated risk i.e. incremental lifetime cancer risk (ILCR) for all the metals were below the cancer threshold value of 1.00E-06. Zn and Mn were the only species whose ingestion doses were found to be higher than their corresponding reference doses in both age groups. A non-carcinogenic effect of Zn as a threat especially to children in the study area was expressed by this study.

XI. Hazard quotient (non-carcinogenic risk) determined for Zn was greater than 1 in both adult and child age groups – an indication of non-carcinogenesis of Zn.

XII. Based on sensitivity analysis, the least and highest impacting parameters on cancer risk in both the child and adult age groups were averaging time (AT) and exposure duration (ED), respectively.

XIII. In the child age group, ED, the major driving force to cancer risk contributed 44% followed by body weight, BW (36%), exposure frequency, EF (9%), observed metal concentration, C (7%), cancer slope factor, CSF (3%) and averaging time, AT (1%).

XIV. In the adult age group the major driving force to cancer risk, ED, contributed 61%, followed by exposure frequency, EF (17%), body weight, BW (8%), observed metal concentration, C (6%), cancer slope factor, CSF (5%) and averaging time, AT (3%).

XV. The sensitivity test also reveals that, as one ages, BW, as cancer risk factor dwindles and replaced/taken over by EF.

5.2. Recommendations

Having used air mass back trajectory for PM source location, further studies to evaluate trajectory frequencies for effective pollution density analysis is highly recommended. Also recommended for further studies is the effect of trajectory (of air mass) arrival heights on observed concentration at the receptor. Detail dust flow climatology and satellite observation of dust flow pattern vis-à-vis the use of statistical tool like trajstat will be conducted in the near future. Determine seasonal variations in exposure doses and cancer risk will be conducted.

REFERENCES

Adams, Peter J., John H. Seinfeld, and Dorothy M. Koch. 1999. “Global Concentrations of Tropospheric Sulfate, Nitrate, and Ammonium Aerosol Simulated in a General Circulation Model.” *Journal of Geophysical Research Atmospheres*.

Adamson, Ian Y.R., Heather Prieditis, and Renaud Vincent. 1999. “Pulmonary Toxicity of an Atmospheric Particulate Sample Is Due to the Soluble Fraction.” *Toxicology and Applied Pharmacology*.

Air, Clean et al. 2012. “EPA Finalizes 2012 Renewable Fuel Standards.” *Clean Air*.

Al-Shayeb, S. M., and M. R D Seaward. 2001. “Heavy Metal Content of Roadside Soils along Ring Road in Riyadh (Saudi Arabia).” *Asian Journal of Chemistry*.

Alpert, P., and B. Ziv. 1989. “The Sharav Cyclone: Observations and Some Theoretical Considerations.” *Journal of Geophysical Research*.

Andersen, Helle Vibeke, and Mads F. Hovmand. 1999. “Review of Dry Deposition Measurements of Ammonia and Nitric Acid to Forest.” In *Forest Ecology and Management*,.

Anderson, Kelsy A., and John A. Downing. 2006. “Dry and Wet Atmospheric Deposition of Nitrogen, Phosphorus and Silicon in an Agricultural Region.” *Water, Air, and Soil Pollution*.

Arimoto, R., R. A. Duce, B. J. Ray, and U. Tomza. 2003. “Dry Deposition of Trace Elements to the Western North Atlantic.” *Global Biogeochemical Cycles*.

Artaxo, Paulo et al. 1999. “Analysis of Atmospheric Aerosols by PIXE: The Importance of Real Time and Complementary Measurements.” *Nuclear Instruments and Methods in Physics Research, Section B: Beam Interactions with Materials and Atoms*.

Arunraj, N. S., Saptarshi Mandal, and J. Maiti. 2013. “Modeling Uncertainty in Risk Assessment: An Integrated Approach with Fuzzy Set Theory and Monte Carlo Simulation.” *Accident Analysis and Prevention*.

Ban-Weiss, G. A., and W. D. Collins. 2014. “Aerosols: Role in Radiative Transfer.” In

Encyclopedia of Atmospheric Sciences: Second Edition,.

Barbieri, Maurizio. 2016. "The Importance of Enrichment Factor (EF) and Geoaccumulation Index (Igeo) to Evaluate the Soil Contamination." *Journal of Geology & Geophysics*.

Begum, Bilkis a, Swapan K Biswas, and Philip K Hopke. 2007. "Source Apportionment of Air Particulate Matter by Chemical Mass Balance (CMB) and Comparison with Positive Matrix Factorization (PMF) Model." *Aerosol and Air Quality Research*.

Bell, Michelle L., Jonathan M. Samet, and Francesca Dominici. 2004. "Time-Series Studies of Particulate Matter." *Annual Review of Public Health*.

Van Den Berg, Martin et al. 1998. "Toxic Equivalency Factors (TEFs) for PCBs, PCDDs, PCDFs for Humans and Wildlife." *Environmental Health Perspectives*.

Brauer, Michael et al. 2012. "Exposure Assessment for Estimation of the Global Burden of Disease Attributable to Outdoor Air Pollution." *Environmental Science & Technology*.

Burnett, Richard T. et al. 2014. "An Integrated Risk Function for Estimating the Global Burden of Disease Attributable to Ambient Fine Particulate Matter Exposure." *Environmental Health Perspectives*.

Calvert, Jack G., Fu Su, Jan W. Bottenheim, and Otto P. Strausz. 1978. "Mechanism of the Homogeneous Oxidation of Sulfur Dioxide in the Troposphere." *Atmospheric Environment (1967)*.

Calzolai, Giulia et al. 2008. "PIXE and XRF Analysis of Particulate Matter Samples: An Inter-Laboratory Comparison." *Nuclear Instruments and Methods in Physics Research, Section B: Beam Interactions with Materials and Atoms*.

Campbell, J. L. et al. 2010. "The Guelph PIXE Software Package IV." *Nuclear Instruments and Methods in Physics Research, Section B: Beam Interactions with Materials and Atoms*.

Cao, Zhi Guo et al. 2012. "Particle Size: A Missing Factor in Risk Assessment of Human Exposure to Toxic Chemicals in Settled Indoor Dust." *Environment*

International.

Chen, Tze-Ming, Janaki Gokhale, Scott Shofer, and Ware G Kuschner. 2007. "Outdoor Air Pollution: Nitrogen Dioxide, Sulfur Dioxide, and Carbon Monoxide Health Effects." *The American journal of the medical sciences*.

Chiari, M. et al. 2005. "Characterization of Airborne Particulate Matter in an Industrial District near Florence by PIXE and PESA." In *X-Ray Spectrometry,*.

Chiari, Massimo et al. 2015. "Use of Proton Elastic Scattering Techniques to Determine Carbonaceous Fractions in Atmospheric Aerosols Collected on Teflon Filters." *Journal of Aerosol Science*.

Chin, Mian, T. Diehl, P. Ginoux, and W. Malm. 2007. "Intercontinental Transport of Pollution and Dust Aerosols: Implications for Regional Air Quality." *Atmospheric Chemistry and Physics*.

Chio, Chia Pin et al. 2014. "Health Risk Assessment for Residents Exposed to Atmospheric Diesel Exhaust Particles in Southern Region of Taiwan." *Atmospheric Environment*.

Chueinta, Wanna, Philip K. Hopke, and Pentti Paatero. 2000. "Investigation of Sources of Atmospheric Aerosol at Urban and Suburban Residential Areas in Thailand by Positive Matrix Factorization." *Atmospheric Environment*.

Di Ciaula, Agostino. 2012. "Emergency Visits and Hospital Admissions in Aged People Living Close to a Gas-Fired Power Plant." *European Journal of Internal Medicine*.

Coffee, Peter. 2005. "Crystal Ball 7.1 Reins in Uncertainty." *eWeek*.

Cogliano, Vincent James et al. 2010. "Preventable Exposures Associated with Human Cancers." *Journal of the National Cancer Institute*.

Córdoba, Patricia et al. 2012. "The Retention Capacity for Trace Elements by the Flue Gas Desulphurisation System under Operational Conditions of a Co-Combustion Power Plant." *Fuel*.

Cuesta, Juan et al. 2010. "Northward Bursts of the West African Monsoon Leading to Rainfall over the Hoggar Massif, Algeria." *Quarterly Journal of the Royal Meteorological Society*.

D'Alessandro, A. et al. 2003. "Hourly Elemental Composition and Sources Identification of Fine and Coarse PM10 Particulate Matter in Four Italian Towns." *Journal of Aerosol Science*.

Dall'Osto, M. et al. 2013. "On the Spatial Distribution and Evolution of Ultrafine Particles in Barcelona." *Atmospheric Chemistry and Physics*.

Davidson, C. I. et al. 1985. "Dry Deposition of Sulfate onto Surrogate Surfaces." *Journal of Geophysical Research*.

Demirel, Gülçin, Özlem Özden, Tuncay Döğeroğlu, and Eftade O. Gaga. 2014. "Personal Exposure of Primary School Children to BTEX, NO2and Ozone in Eskişehir, Turkey: Relationship with Indoor/Outdoor Concentrations and Risk Assessment." *Science of the Total Environment*.

Department for Environment Food and Rural Affairs (DEFRA). 2010. Environment *Air Pollution: Action in a Changing Climate*.

Dockery, D W et al. 1993. "An Association between Air Pollution and Mortality in Six U.S. Cities." *The New England journal of medicine*.

Draxler, Roland R, and G D Hess. 1998. "An Overview of the HYSPLIT_4 Modelling System for Trajectories, Dispersion, and Deposition." *Australian Meteorological Magazine*.

Duruibe, J O, M O C Ogwuegbu, and J N Egwurugwu. 2007. "Heavy Metal Pollution and Human Biotoxic Effects." *International Journal of Physical Sciences*.

Dutta, Palash. 2015. "Uncertainty Modeling in Risk Assessment Based on Dempster–Shafer Theory of Evidence with Generalized Fuzzy Focal Elements." *Fuzzy Information and Engineering*.

Dutta, Palash, and Tazid Ali. 2012. "A Hybrid Method to Deal with Aleatory and Epistemic Uncertainty in Risk Assessment." *International Journal of Computer Applications*.

Eck, T. F. et al. 1999. "Wavelength Dependence of the Optical Depth of Biomass Burning, Urban, and Desert Dust Aerosols." *Journal of Geophysical Research*.

Engel-Cox, Jill et al. 2013. "Toward the next Generation of Air Quality Monitoring:

Particulate Matter." *Atmospheric Environment*.

Engelstaedter, Sebastian, Ina Tegen, and Richard Washington. 2006. "North African Dust Emissions and Transport." *Earth-Science Reviews*.

EPA. 2006. "Air Quality Criteria for Ozone and Related Photochemical Oxidants." *Molecular and cellular biochemistry*.

EU. 2008. "Directive 2008/50/EC of the European Parliament and of the Council of 21 May 2008 on Ambient Air Quality and Cleaner Air for Europe." *Official Journal of the European Communities*.

European Parliament, and Council of the European Union. 2008. "Directive 2008/50/EC on Ambient Air Quality and Cleaner Air for Europe." *Official Journal of the European Union*.

Feng, Huan et al. 2011. "Metal Contamination in Sediments of the Western Bohai Bay and Adjacent Estuaries, China." *Journal of Environmental Management*.

Ferrario, E, N Pedroni, and E Zio. 2014. "Line Sampling and Fuzzy Interval Analysis for the Propagation of Aleatory and Epistemic Uncertainties in Risk Models." In *Safety, Reliability and Risk Analysis: Beyond the Horizon - Proceedings of the European Safety and Reliability Conference, ESREL 2013,*.

Ferreira-Baptista, L., and E. De Miguel. 2005. "Geochemistry and Risk Assessment of Street Dust in Luanda, Angola: A Tropical Urban Environment." *Atmospheric Environment*.

Flage, Roger, Piero Baraldi, Enrico Zio, and Terje Aven. 2013. "Probability and Possibility-Based Representations of Uncertainty in Fault Tree Analysis." *Risk Analysis*.

Fleming, Zoë L., Paul S. Monks, and Alistair J. Manning. 2012. "Review: Untangling the Influence of Air-Mass History in Interpreting Observed Atmospheric Composition." *Atmospheric Research*.

Ginoux, Paul et al. 2001. "Sources and Distributions of Dust Aerosols Simulated with the GOCART Model." *Journal of Geophysical Research Atmospheres*.

———. 2012. "Global-Scale Attribution of Anthropogenic and Natural Dust Sources

and Their Emission Rates Based on MODIS Deep Blue Aerosol Products." *Reviews of Geophysics*.

Giuntini, L., M. Massi, and S. Calusi. 2007. "The External Scanning Proton Microprobe of Firenze: A Comprehensive Description." *Nuclear Instruments and Methods in Physics Research, Section A: Accelerators, Spectrometers, Detectors and Associated Equipment*.

Goudie, A. S., and N. J. Middleton. 2001. "Saharan Dust Storms: Nature and Consequences." *Earth-Science Reviews*.

Granero, S, and J L Domingo. 2002. "Levels of Metals in Soils of Alcala de Henares, Spain: Human Health Risks." *Environment International*.

Grantz, D A, J H B Garner, and D W Johnson. 2003. "Ecological Effects of Particulate Matter." *Environment international*.

Hacıoğlu, H.İ. et al. 2016. "A New Approach for Site Selection of Air Quality Monitoring Stations: Multi-Criteria Decision-Making." *Aerosol and Air Quality Research*.

Haustein, K. et al. 2012. "Atmospheric Dust Modeling from Meso to Global Scales with the Online NMMB/BSC-Dust Model - Part 2: Experimental Campaigns in Northern Africa." *Atmospheric Chemistry and Physics*.

Haywood, James, and Olivier Boucher. 2000. "Estimates of the Direct and Indirect Radiative Forcing Due to Tropospheric Aerosols: A Review." *Reviews of Geophysics*.

Haywood, Jim. 2003. "Radiative Properties and Direct Radiative Effect of Saharan Dust Measured by the C-130 Aircraft during SHADE: 1. Solar Spectrum." *Journal of Geophysical Research*.

Haywood, James, and Olivier Boucher. 2000. "Estimates of the Direct and Indirect Radiative Forcing Due to Tropospheric Aerosols: A Review." *Reviews of Geophysics*.

Heintzenberg, Jost. 1989. "Fine Particles in the Global Troposphere A Review." *Tellus B*.

Hemond, Harold F., and Elizabeth J. Fechner. 2015. Chemical Fate and Transport in the Environment *Chemical Fate and Transport in the Environment*.

Holben, B.N. et al. 1998. "AERONET—A Federated Instrument Network and Data Archive for Aerosol Characterization." *Remote Sensing of Environment*.

Huang, J., C. Zhang, and J. M. Prospero. 2009. "Large-Scale Effect of Aerosols on Precipitation in the West African Monsoon Region." *Quarterly Journal of the Royal Meteorological Society*.

IARC. 2016. "Agents Classified by the IARC Monographs." *IARC Monographs*.

IARC Working Group on the Evaluation of Carcinogenic Risks to Humans. 2012. "Chemical Agents and Related Occupations." *IARC monographs on the evaluation of carcinogenic risks to humans / World Health Organization, International Agency for Research on Cancer*.

International Energy Agency. 2016. "World Energy Outlook 2016." *International Energy Agency*.

Ishii, K. et al. 2005. "Contribution of Atomic Bremsstrahlung in PIXE Spectra and Screening Effect in Atomic Bremsstrahlung." In *X-Ray Spectrometry*,.

Jacob, Daniel J. 1999. "Chapter 1. Measures of Atmospheric Composition." *Introduction to Atmospheric Chemistry*.

Jacob, Daniel J., and Darrell A. Winner. 2009. "Effect of Climate Change on Air Quality." *Atmospheric Environment*.

Jacobson, M. Z. 2013. Journal of Chemical Information and Modeling *Fundamentals of Atmospheric Modeling*.

Johansson, Sven A.E. 1989. "PIXE: A Novel Technique for Elemental Analysis." *Endeavour*.

Johansson, Sven, John Campbell, and Klas Malmqvist. 1997. "Particle-Induced X-Ray Emission Spectrometry (PIXE)." *X-ray Spectrometry*.

K., Widziewicz. 2016. "Metal Induced Inhalation Exposure in Urban Population: A Probabilistic Approach." *Atmospheric Environment*.

Kallos, G, A Papadopoulos, P Katsafados, and S Nickovic. 2006. “Transatlantic Saharan Dust Transport: Model Simulation and Results.” *Journal of Geophysical Research-Atmospheres*.

Kemp, Kare. 2002. “Trends and Sources for Heavy Metals in Urban Atmosphere.” *Nuclear Instruments and Methods in Physics Research B*.

Kim, Eugene, David Kalman, and Timothy Larson. 2000. “Dry Deposition of Large, Airborne Particles onto a Surrogate Surface.” *Atmospheric Environment*.

Kim, Jong Yeop, and John J. Sansalone. 2008. “Event-Based Size Distributions of Particulate Matter Transported during Urban Rainfall-Runoff Events.” *Water Research*.

Knafl, George J., and Margaret Grey. 2007. “Factor Analysis Model Evaluation through Likelihood Cross-Validation.” *Statistical Methods in Medical Research*.

Koçak, Mustafa, Nilgün Kubilay, and Nikos Mihalopoulos. 2004. “Ionic Composition of Lower Tropospheric Aerosols at a Northeastern Mediterranean Site: Implications Regarding Sources and Long-Range Transport.” *Atmospheric Environment*.

Koçak, Mustafa, Nikos Mihalopoulos, and Nilgün Kubilay. 2007. “Chemical Composition of the Fine and Coarse Fraction of Aerosols in the Northeastern Mediterranean.” *Atmospheric Environment*.

Laden, F, L M Neas, D W Dockery, and J Schwartz. 2000. “Association of Fine Particulate Matter from Different Sources with Daily Mortality in Six U.S. Cities.” *Environmental health perspectives*.

Laden, Francine, Lucas M. Neas, Douglas W. Dockery, and Joel Schwartz. 2000. “Association of Fine Particulate Matter from Different Sources with Daily Mortality in Six U.S. Cities.” *Environmental Health Perspectives*.

Larssen, Thorjørn, Lei Duan, and Jan Mulder. 2011. “Deposition and Leaching of Sulfur, Nitrogen and Calcium in Four Forested Catchments in China: Implications for Acidification.” *Environmental Science and Technology*.

Lave, L. B., and E. P. Seskin. 1972. “Air Pollution, Climate, and Home Heating: Their

Effects on U.S. Mortality Rates." *American journal of public health*.

Lefohn, Allen S., William Jackson, Douglas S. Shadwick, and H. Peter Knudsen. 1997. "Effect of Surface Ozone Exposures on Vegetation Grown in the Southern Appalachian Mountains: Identification of Possible Areas of Concern." *Atmospheric Environment*.

Léon, Jean François, and Michel Legrand. 2003. "Mineral Dust Sources in the Surroundings of the North Indian Ocean." *Geophysical Research Letters*.

Lestari, Puji, Ali K. Oskouie, and Kenneth E. Noll. 2003. "Size Distribution and Dry Deposition of Particulate Mass, Sulfate and Nitrate in an Urban Area." *Atmospheric Environment*.

Li, Jianbing, Lei Liu, Guohe Huang, and Guangming Zeng. 2006. "A Fuzzy-Set Approach for Addressing Uncertainties in Risk Assessment of Hydrocarbon-Contaminated Site." *Water, Air, and Soil Pollution*.

Li, Zhanqing et al. 2017. "Aerosol and Boundary-Layer Interactions and Impact on Air Quality." *National Science Review*.

Liang, Jinyou, and Mark Z. Jacobson. 1999. "A Study of Sulfur Dioxide Oxidation Pathways over a Range of Liquid Water Contents, PH Values, and Temperatures." *Journal of Geophysical Research Atmospheres*.

Lin, Jim J., Kenneth E. Noll, and Thomas M. Holsen. 1994. "Dry Deposition Velocities as a Function of Particle Size in the Ambient Atmosphere." *Aerosol Science and Technology*.

Lipfert, F W, J Zhang, and R E Wyzga. 2000. "Infant Mortality and Air Pollution: A Comprehensive Analysis of US Data for 1990." *JOURNAL OF THE AIR & WASTE MANAGEMENT ASSOCIATION*.

Lippmann, M., and R. B. Schlesinger. 2000. "Toxicological Bases for the Setting of Health-Related Air Pollution Standards." *Annual Review of Public Health*.

Lucarelli, F. et al. 2011. "Is PIXE Still a Useful Technique for the Analysis of Atmospheric Aerosols? The LABEC Experience." *X-Ray Spectrometry*.

Luo, Chao. 2003. "Sensitivity Study of Meteorological Parameters on Mineral Aerosol

Mobilization, Transport, and Distribution." *Journal of Geophysical Research*.

Luo, Xiao San et al. 2012. "Incorporating Bioaccessibility into Human Health Risk Assessments of Heavy Metals in Urban Park Soils." *Science of the Total Environment*.

Manousakas, M., K. Eleftheriadis, and H. Papaefthymiou. 2013. "Characterization of PM10 Sources and Ambient Air Concentration Levels at Megalopolis City (Southern Greece) Located in the Vicinity of Lignite-Fired Plants." *Aerosol and Air Quality Research*.

Massi, M. et al. 2002. "The External Beam Microprobe Facility in Florence: Set-up and Performance." In *Nuclear Instruments and Methods in Physics Research, Section B: Beam Interactions with Materials and Atoms*,.

Megaritis, A. G. et al. 2014. "Linking Climate and Air Quality over Europe: Effects of Meteorology on PM2.5concentrations." *Atmospheric Chemistry and Physics*.

Mkoma, Stelyus L. et al. 2009. "Chemical Composition and Mass Closure for PM10 Aerosols during the 2005 Dry Season at a Rural Site in Morogoro, Tanzania." *X-Ray Spectrometry*.

Mohr, Martin et al. 1996. "Submicron Fly Ash Penetration through Electrostatic Precipitators at Two Coal Power Plants." *Aerosol Science and Technology*.

Muezzinoglu, Aysen, and Sibel Cukurluoglu Cizmecioglu. 2006. "Deposition of Heavy Metals in a Mediterranean Climate Area." *Atmospheric Research*.

Müller, G. 1985. "The Reflectivity Method: A Tutorial." *J Geophys*.

Munro, Rosemary, Richard Siddans, William J. Reburn, and Brian J. Kerridge. 1998. "Direct Measurement of Tropospheric Ozone Distributions from Space." *Nature*.

Murozono, K. et al. 1999. "PIXE Spectrum Analysis Taking into Account Bremsstrahlung Spectra." *Nuclear Instruments and Methods in Physics Research, Section B: Beam Interactions with Materials and Atoms*.

Nava, S. et al. 2010. "An Integrated Approach to Assess Air Pollution Threats to Cultural Heritage in a Semi-Confined Environment: The Case Study of Michelozzo's Courtyard in Florence (Italy)." *Science of the Total Environment*.

Nejedlý, Z., J. L. Campbell, W. J. Teesdale, and C. Gielen. 1997. "PIXE and PESA Aspects of the Guelph Visibility and Fine Particulate Monitoring Program." *Nuclear Instruments and Methods in Physics Research, Section B: Beam Interactions with Materials and Atoms*.

Neyzi, Olcay et al. 2006. "Growth References for Turkish Children Aged 6 to 18 Years." *Acta paediatrica (Oslo, Norway : 1992)*.

Neyzi, Olcay, H Nurçin Saka, and Selim Kurtoğlu. 2013. "Anthropometric Studies on the Turkish Population--a Historical Review." *Journal of clinical research in pediatric endocrinology*.

Nieto-Morote, A., and F. Ruz-Vila. 2011. "A Fuzzy Approach to Construction Project Risk Assessment." *International Journal of Project Management*.

Nriagu, Jerome O. 1979. "Global Inventory of Natural and Anthropogenic Emissions of Trace Metals to the Atmosphere [7]." *Nature*.

Ohlström, Mikael O., Kari E.J. Lehtinen, Mikko Moisio, and Jorma K. Jokiniemi. 2000. "Fine-Particle Emissions of Energy Production in Finland." *Atmospheric Environment*.

Organization, World Health. 2014. "Media Centre 7 Million Premature Deaths Annually Linked to Air Pollution." *World Health Organization*.

Paatero, P, and U Tapper. 1994. "Positive Matrix Factorization - A Nonnegative Factor Model With Optimal Utilization of Error-Estimates of Data Values." *Environmetrics*.

Pacyna, J.M., and E.G. Pacyna. 2001. "An Assessment of Global and Regional Emissions of Trace Metals to the Atmosphere from Anthropogenic Sources Worldwide." *Environmental Reviews*.

Pan, Y. P., and Y. S. Wang. 2015. "Atmospheric Wet and Dry Deposition of Trace Elements at 10 Sites in Northern China." *Atmospheric Chemistry and Physics*.

Pastoor, Timothy P. et al. 2014. "A 21st Century Roadmap for Human Health Risk Assessment." *Critical Reviews in Toxicology*.

Paté-Cornell, M. Elisabeth. 1996. "Uncertainties in Risk Analysis: Six Levels of

Treatment.” *Reliability Engineering and System Safety*.

Pedroni, Nicola et al. 2012. “Propagation of Aleatory and Epistemic Uncertainties in the Model for the Design of a Flood Protection Dike.” *PSAM 11 & ESREL 2012*.

Pekney, Natalie J., and Cliff I. Davidson. 2005. “Determination of Trace Elements in Ambient Aerosol Samples.” *Analytica Chimica Acta*.

Peng, Xing et al. 2017. “Source Apportionment and Heavy Metal Health Risk (HMHR) Quantification from Sources in a Southern City in China, Using an ME2-HMHR Model.” *Environmental Pollution*.

Pérez, C. et al. 2011. “Atmospheric Dust Modeling from Meso to Global Scales with the Online NMMB/BSC-Dust Model – Part 1: Model Description, Annual Simulations and Evaluation.” *Atmospheric Chemistry and Physics*.

Perkin Elmer. 2001. “The 30-Minute Guide to ICP-MS.” *Technical Note: ICP-Mass Spectrometry*.

Pöschl, Ulrich. 2005. “Atmospheric Aerosols: Composition, Transformation, Climate and Health Effects.” *Angewandte Chemie - International Edition*.

Prasad, Anup K., and Ramesh P. Singh. 2007. “Changes in Aerosol Parameters during Major Dust Storm Events (2001-2005) over the Indo-Gangetic Plains Using AERONET and MODIS Data.” *Journal of Geophysical Research Atmospheres*.

Prieditis, H., and I. Y R Adamson. 2002. “Comparative Pulmonary Toxicity of Various Soluble Metals Found in Urban Particulate Dusts.” *Experimental Lung Research*.

Pröfrock, Daniel, and Andreas Prange. 2012. “Inductively Coupled Plasma-Mass Spectrometry (ICP-MS) for Quantitative Analysis in Environmental and Life Sciences: A Review of Challenges, Solutions, and Trends.” *Applied Spectroscopy*.

Prospero, J M, and R Arimoto. 2009. “Atmospheric Transport and Deposition of Particulate Material to the Oceans.” In *Encyclopedia of Ocean Sciences*,.

Qu, Chang Sheng et al. 2012. “Human Exposure Pathways of Heavy Metals in a Lead-Zinc Mining Area, Jiangsu Province, China.” *PLoS ONE*.

Quincey, Paul, and David Butterfield. 2009. “Ambient Air Particulate Matter PM10 and

PM2.5: Developments in European Measurement Methods and Legislation." *Biomarkers*.

Quiterio, Simone Lorena, Célia Regina Sousa da Silva, Graciela Arbilla, and Viviane Escaleira. 2004. "Metals in Airborne Particulate Matter in the Industrial District of Santa Cruz, Rio de Janeiro, in an Annual Period." *Atmospheric Environment*.

Radojević, M., and R. M. Harrison. 1992. Atmospheric acidity: sources, consequences and abatement. *Atmospheric Acidity: Sources, Consequences and Abatement.*

Reimann, Clemens, and Patrice De Caritat. 2005. "Distinguishing between Natural and Anthropogenic Sources for Elements in the Environment: Regional Geochemical Surveys versus Enrichment Factors." *Science of the Total Environment*.

Renan, M. J. 1980. "Optimization of Trace Analysis by Pixe: Angular Dependence of the Background Continuum." *X???Ray Spectrometry*.

Rodríguez, S. et al. 2011. "Transport of Desert Dust Mixed with North African Industrial Pollutants in the Subtropical Saharan Air Layer." *Atmospheric Chemistry and Physics*.

Salim Akhter, M., and Ismail M. Madany. 1993. "Heavy Metals in Street and House Dust in Bahrain." *Water, Air, & Soil Pollution*.

San José, R. et al. 2005. "A Modelling Study of an Extraordinary Night Time Ozone Episode over Madrid Domain." *Environmental Modelling and Software*.

Sandroni, V. et al. 2007. "Dry Atmospheric Deposition and Diazotrophy as Sources of New Nitrogen to Northwestern Mediterranean Oligotrophic Surface Waters." *Deep-Sea Research Part I: Oceanographic Research Papers*.

Schmidt, Bernd, and Klaus Wetzig. 2013. Journal of Chemical Information and Modeling *Ion Beams in Materials Processing and Analysis: Ion Beam Technology*.

See, S. W., R. Balasubramanian, and W. Wang. 2006. "A Study of the Physical, Chemical, and Optical Properties of Ambient Aerosol Particles in Southeast Asia during Hazy and Nonhazy Days." *Journal of Geophysical Research Atmospheres*.

Sehmel, George A. 1980. "Particle and Gas Dry Deposition: A Review." *Atmospheric Environment (1967)*.

Seinfeld, J. H. 2014. “Tropospheric Chemistry and Composition: Aerosols/Particles.” In *Encyclopedia of Atmospheric Sciences: Second Edition*,.

Seinfeld, J H, and S N Pandis. 1998. “Atmospheric Chemistry and Physics: From Air Pollution to Climate Change.” *Atmospheric chemistry and physics from air pollution to climate change Publisher New York NY Wiley 1998 Physical description xxvii 1326 p A WileyInterscience Publication ISBN 0471178152*.

Seinfeld, John H, and Spyros N Pandis. 2006. Atmospheric Chemistry and Physics *Atmospheric Chemistry and Physics: From Air Pollution to Climate Change*.

Shah, Munir H. et al. 2006. “Spatial Variations in Selected Metal Contents and Particle Size Distribution in an Urban and Rural Atmosphere of Islamabad, Pakistan.” *Journal of Environmental Management*.

Shah, Munir H., and Nazia Shaheen. 2010. “Seasonal Behaviours in Elemental Composition of Atmospheric Aerosols Collected in Islamabad, Pakistan.” *Atmospheric Research*.

Shao, Lin, Y. Q. Wang, and M. Nastasi. 2006. “A New Iterative Process for Accurate Analysis of Displaced Atoms from Channeling Rutherford Backscattering Spectrometry.” *Nuclear Instruments and Methods in Physics Research, Section B: Beam Interactions with Materials and Atoms*.

Shukla, J. B., A. K. Misra, Shyam Sundar, and Ram Naresh. 2008. “Effect of Rain on Removal of a Gaseous Pollutant and Two Different Particulate Matters from the Atmosphere of a City.” *Mathematical and Computer Modelling*.

Signorell, Ruth, and A. Bertram. 2009. “Physical Chemistry of Aerosols.” *Physical Chemistry Chemical Physics*.

Singh, Anita, Rajesh Kumar Sharma, Madhoolika Agrawal, and Fiona M. Marshall. 2010. “Health Risk Assessment of Heavy Metals via Dietary Intake of Foodstuffs from the Wastewater Irrigated Site of a Dry Tropical Area of India.” *Food and Chemical Toxicology*.

Singh, Aprajita et al. 2015. “Release of Heavy Metals from Industrial Waste and E-Waste Burning and Its Effect on Human Health and Environment.” *International*

Journal of Emerging Research in Management &Technology.

Skoog, D.A., F.J. Holler, and T.A. Nieman. 1997. "Thermal Methods." *Principles of Instrumental Analysis*.

Slinn, S. A., and W. G N Slinn. 1980. "Predictions for Particle Deposition on Natural Waters." *Atmospheric Environment (1967)*.

Slinn, W. G.N. 1982. "Predictions for Particle Deposition to Vegetative Canopies." *Atmospheric Environment (1967)*.

Srivastava, Ravi K., Wojciech Jozewicz, and Carl Singer. 2001. "SO2 Scrubbing Technologies: A Review." *Environmental Progress*.

Stockwell, William R. 1994. "The Effect of Gas-Phase Chemistry on Aqueous-Phase Sulfur Dioxide Oxidation Rates." *Journal of Atmospheric Chemistry*.

Tanimizu, Masaharu, Naoki Sugiyama, Emmanuel Ponzevera, and Germain Bayon. 2013. "Determination of Ultra-Low 236U/238U Isotope Ratios by Tandem Quadrupole ICP-MS/MS." *Journal of Analytical Atomic Spectrometry*.

Tessier, A., P. G.C. Campbell, and M. Bisson. 1979. "Sequential Extraction Procedure for the Speciation of Particulate Trace Metals." *Analytical Chemistry*.

Thorpe, Alistair, and Roy M. Harrison. 2008. "Sources and Properties of Non-Exhaust Particulate Matter from Road Traffic: A Review." *Science of the Total Environment*.

Traversi, R. et al. 2014. "A Comparison between PIXE and ICP-AES Measurements of Metals in Aerosol Particulate Collected in Urban and Marine Sites in Italy." *Nuclear Instruments and Methods in Physics Research, Section B: Beam Interactions with Materials and Atoms*.

US EPA. 2009. "Risk Assessment Guidance for Superfund Volume I: Human Health Evaluation Manual (Part F, Supplemental Guidance for Inhalation Risk Assessment)." *Office of Superfund Remediation and Technology Innovation Environmental Protection Agency*.

USEPA. 2003. "Air Pollution Control Fact Sheet." *EPA-CICA Fact Sheet: Flue Gas Desulfurization*.

———. 2004a. “Air Quality Criteria for Particulate Matter.” *Air Quality Criteria for Particulate Matter*.

———. 2004b. “Risk Assessment Guidance for Superfund (RAGS). Volume I. Human Health Evaluation Manual (HHEM). Part E. Supplemental Guidance for Dermal Risk Assessment.” *US Epa*.

USEPA, United States Environmental Protection Agency. 2004c. “Air Quality Criteria for Particulate Matter October 2004, Volume 2.” *Air Quality Criteria for Particulate Matter*.

Vallius, Marko et al. 2003. “Source Apportionment of Urban Ambient PM2.5in Two Successive Measurement Campaigns in Helsinki, Finland.” *Atmospheric Environment*.

Wagstrom, Kristina M., and Spyros N. Pandis. 2011. “Source-Receptor Relationships for Fine Particulate Matter Concentrations in the Eastern United States.” *Atmospheric Environment*.

Wang, Han, Man He, Beibei Chen, and Bin Hu. 2017. “Advances in ICP-MS-Based Techniques for Trace Elements and Their Species Analysis in Cells.” *Journal of Analytical Atomic Spectrometry*.

Wang, Y. Q., X. Y. Zhang, and Roland R. Draxler. 2009. “TrajStat: GIS-Based Software That Uses Various Trajectory Statistical Analysis Methods to Identify Potential Sources from Long-Term Air Pollution Measurement Data.” *Environmental Modelling and Software*.

Ward, Elizabeth M. et al. 2010. “Research Recommendations for Selected IARC-Classified Agents.” *Environmental Health Perspectives*.

Watson, John G. 2002. “Visibility: Science and Regulation.” *Journal of the Air and Waste Management Association*.

Westphal, D L, C A Curtis, M Liu, and A L Walker. 2009. “Operational Aerosol and Dust Storm Forecasting.” *IOP Conference Series: Earth and Environmental Science*.

WHO. 2003. “Health Aspects of Air Pollution with Particulate Matter, Ozone and

Nitrogen Dioxide." *Report on a WHO Working Group Bonn, Germany 13–15 January 2003*.

———. 2012. World health statistics 2012 *Part III: Global Health Indicators*.

Widziewicz, Kamila, and Krzysztof Loska. 2016. "Metal Induced Inhalation Exposure in Urban Population: A Probabilistic Approach." *Atmospheric Environment*.

Wilcke, Wolfgang et al. 2006. "Polychlorinated Biphenyls (PCBs) in Soils of the Moscow Region: Concentrations and Small-Scale Distribution along an Urban-Rural Transect." *Environmental Pollution*.

Wogan, Gerald N. et al. 2004. "Environmental and Chemical Carcinogenesis." *Seminars in Cancer Biology*.

Woodruff, Tracey J., Jeanne Grillo, and Kenneth C. Schoendorf. 1997. "The Relationship between Selected Causes of Postneonatal Infant Mortality and Particulate Air Pollution in the United States." *Environmental Health Perspectives*.

Woodruff, Tracey J., Jennifer D. Parker, and Kenneth C. Schoendorf. 2006. "Fine Particulate Matter (PM2.5) Air Pollution and Selected Causes of Postneonatal Infant Mortality in California." *Environmental Health Perspectives*.

World Health Organization. 2006. "WHO Air Quality Guidelines for Particulate Matter, Ozone, Nitrogen Dioxide and Sulfur Dioxide: Global Update 2005: Summary of Risk Assessment." *Geneva: World Health Organization*.

World Health Organization (WHO). 2000. "Chapter 7.1 Nitrogen Dioxide." In *Air Quality Guidelines for Europe-Second Edition*,.

Xu, Xue, Xinwei Lu, Xiufeng Han, and Ni Zhao. 2015. "Ecological and Health Risk Assessment of Metal in Resuspended Particles of Urban Street Dust from an Industrial City in China." *Current Science*.

Zender, Charles S. 2003. "Mineral Dust Entrainment and Deposition (DEAD) Model: Description and 1990s Dust Climatology." *Journal of Geophysical Research*.

Zhang, Leiming, Sunling Gong, Jacob Padro, and Len Barrie. 2001. "A Size-Segregated Particle Dry Deposition Scheme for an Atmospheric Aerosol Module." *Atmospheric Environment*.

Zhu, Aihua, V. Ramanathan, Fang Li, and Dohyeong Kim. 2007. “Dust Plumes over the Pacific, Indian, and Atlantic Oceans: Climatology and Radiative Impact.” *Journal of Geophysical Research Atmospheres*.

Zhu, Xiaoxia et al. 2015. “Maternal Exposure to Fine Particulate Matter (PM2.5) and Pregnancy Outcomes: A Meta-Analysis.” *Environmental science and pollution research international*.